

Relaxation oscillations in slow-fast systems beyond the standard form

Von der Fakultät für Mathematik und Informatik
der Universität Leipzig
angenommene

D I S S E R T A T I O N

zur Erlangung des akademischen Grades

DOCTOR RERUM NATURALIUM
(Dr.rer.nat.)

im Fachgebiet

MATHEMATIK

vorgelegt

von Diplommathematikerin ILONA KOSIUK

geboren am 11.08.1983 in Bielsko-Biala (Polen)

Die Annahme der Dissertation haben empfohlen:

1. Prof. Dr. Freddy Dumortier (Hasselt University, Belgien)
2. Prof. Dr. Jürgen Jost (MPI-MiS, Leipzig, Deutschland)

Die Verleihung des akademischen Grades erfolgt auf Beschluss des Rates der Fakultät für Mathematik und Informatik vom 14.11.2012 mit dem Gesamtprädikat magna cum laude.

Leipzig, den 14.11.2012.

Erklärungen

- Ich erkenne die Promotionsordnung der Fakultät für Mathematik und Informatik der Universität Leipzig vom 25.2.2002 an.
- Die eingereichte Arbeit wurde nicht in gleicher oder ähnlicher Form einer anderen Prüfungsbehörde zum Zwecke einer Promotion oder eines anderen Prüfungsverfahrens vorgelegt.
- Es haben keine früheren erfolglosen Promotionsversuche stattgefunden.

.....
(Ilona Kosiuk)

ACKNOWLEDGEMENT

Writing a PhD thesis is a great example of a process with slow-fast dynamics. At the beginning you are very excited, full of energy and you want to be FAST in finding a topic and solving great difficult problems you will be famous for someday. You are so attracted to it! Unfortunately, after some time you realize it is not so easy, your enthusiasm decreases and you are pretty SLOW in what you do, everything is overwhelming and you feel lost. But not for too long, life is good again when you obtain some first results. And then the expiration date of your contract is approaching and you are SUPER FAST with preparing everything on time. I have experienced all the SLOW-FAST phases during my PhD years. All these years were exciting and wonderful, and there are several people responsible for this whom I want to thank.

To my supervisor Jürgen Jost at the Max Planck Institute for Mathematics in the Sciences (MPI MiS) in Leipzig, I thank you for showing me what the research is by giving me the opportunity to be a member in your group. Thank you for much freedom, which allowed me to develop my research direction. Thank you for joint discussions, interesting lectures and seminars organized for us at the MPI, which encouraged me to learn different dynamical systems approaches. For providing fantastic facilities, which make us all feel at home.

To my friend and external supervisor Peter Szmolyan from Vienna University of Technology, you guided my research from the very first day and introduced me to the fascinating world of singular perturbations. I thank you for your excellent supervision balanced with our friendship. Thank you for your patience, hours spent on interesting discussions and for the fruitful long-distance collaboration in the last three years. You have been a real teacher to me.

The International Max Planck Research School, MPI MiS, and the Research Academy of Leipzig generously awarded me with travel funding to attend eleven international conferences and workshops. My participation in these conferences has had a significant impact on my research: it not only allowed me to present and receive feedback on my work, but most importantly allowed me to meet interesting scientists and the singular perturbation community experts, whose works I admire. Thank you very much for giving me the opportunity to travel and visit so many interesting places.

At one of those conferences I have had a chance to personally meet Albert Goldbeter, undoubtedly a leading expert in the modelling and analysis of oscillations in biological systems. Goldbeter's work has been a real inspiration and a great source of challenging mathematical problems. I thank you particularly for suggesting that I study the mitotic oscillator, which turned out to exhibit even more interesting oscillatory behavior than we thought. This unexpected novel type of dynamics directed our attention towards another class of dynamical systems and inspired us to start a new research direction.

I thank Antje Vandenberg for helping me to organize all the conference trips and to deal with all the paperwork after each of the trips.

I thank Hayk Mikayelyan, the IMPRS scientific coordinator, for his help and support during my stay at MPI.

I thank the library team at the Max Planck Institute for satisfying all finding-paper-caprice I had.

Many thanks go to the computer group for their technical support and solving all my weird computer problems.

To my MPI friends Danijela Horak, Frank Bauer, Hedi Wilhelm, I do not know guys, if I can find the words to describe how happy I am that I have met you. We have shared all the ups and downs together over hundreds cups of tea and coffee. We have had so many good laughs that even now when I recall certain situations I smile. It is really the end of an era and it is so emotional! Danijela, thank you for your positive energy, wonderful friendship and enormous support. I could not do it without you. For all the fabulous moments we have had together, Namaste. Frank, thanks for your friendship and applying the Friday rule to your life, which made my pangs of conscience disappear – I knew I can count on you. And of course, I could not forget, thanks for inventing the S-number (mine is pretty poor though). Hedi, thank you for not only being a great friend and officemate, but also the best hand-crafting teacher ever! Thank you for our sewing sessions, where I have learned so much from you. Our Sunday hand-crafting meetings brought me so much joy and helped to go through a stressful time during my PhD.

I have met many fantastic people during my stay at MPI. The time we were all at the institute was legen – wait for it – dary:). I thank Joe, Lily, Nils, Wiktor, Lorenzo, Martin and Yang among the others from jj-all for interesting discussions and sharing delicious sweets during the tea break.

I thank Martin Kell, Danijela Horak, Frank Bauer, for their careful proofreading my thesis.

To my friend Ewa Weinmüller, who always had time for me and taught me so much. Thank you for our inspiring skyping sessions, joint travels and showing me how exciting life can be.

I thank Agnieszka Daniel for each of 587 wonderful emails she wrote me during last three years. You are the best example that a real friendship is not diminished by distance and you can be close even if you are far away.

My enormous gratitude goes to my parents along with my brother for their love and always believing that I am “the smart one”.

Last, but not least to my beloved husband Jędrzej, who knows me better than I know myself. I thank you for your love, support and for keeping reminding me that “*By day and by night we are being prospered in all of our interests*”. Thank you for making me laugh everyday, and for making our dreams come true.

Contents

Chapter 1. Introduction	3
Chapter 2. Introduction to geometric methods of singular perturbation theory	14
2.1. Regularly vs. singularly perturbed systems	14
2.2. Slow-fast systems in standard form	15
2.3. Fenichel theory – basis theorems	17
2.4. Blow-up method	19
2.5. Background on singularly perturbed planar folds	21
Chapter 3. Geometric singular perturbation analysis of an autocatalator model	24
3.1. Slow-fast analysis of the autocatalator	24
3.1.1. Regime 1: $b = O(1)$	25
3.1.2. Regime 2: $b = O(1/\varepsilon)$	27
3.2. Blow-up analysis	30
3.2.1. Dynamics in charts	31
3.2.2. Dynamics of the blown-up system	33
3.3. Construction of the Poincaré map	34
3.3.1. Analysis of Π_1 – passage of the fold point	35
3.3.2. Analysis of Π_2 – passage of the hyperbolic line L_A	35
3.3.3. Analysis of Π_3 – contraction towards the vertical slow manifold M	37
3.3.4. Analysis of Π_4 – passage of the nilpotent point q	38
3.3.5. Analysis of Π_5 – transition towards the attracting slow manifold S_a	38
3.3.6. Proof of Theorem 3.4	38
3.4. Canard cycles	39
3.5. Passage of the nilpotent point q	40
Chapter 4. Blowing-up the glycolytic oscillator	46
4.1. Scaling properties and singular limits	46
4.1.1. Basic properties and scaling	46
4.1.2. Slow-fast analysis of classical relaxation oscillations for fixed $\delta > 0$	48
4.1.3. The case ε, δ small	49
4.2. Scaling regimes	50
4.2.1. Regime 1, $a = O(1), b = O(\delta^2)$	51
4.2.2. Regime 2, $a = O(1), b = O(1)$	53
4.2.3. Regime 3, $a = O(\delta), b = O(1)$	54
4.2.4. Singular cycles	55
4.3. Blow-up analysis	56

4.3.1.	Blow-up of the non-hyperbolic line $l_b \times \{0\}$	57
4.3.2.	Blow-up of the non-hyperbolic line $l_{a,4}$	61
4.3.3.	Properties of the blown-up system	66
4.3.4.	Poincaré map and existence of limit cycles	68
Chapter 5.	A new type of relaxation oscillations in a model of the mitotic oscillator	73
5.1.	Slow-fast analysis of the mitotic oscillator	73
5.1.1.	Basic properties and sustained oscillations	73
5.1.2.	Slow-fast structure	75
5.1.3.	Fast dynamics	76
5.1.4.	Slow dynamics	78
5.1.5.	Singular cycle	81
5.2.	Blow-up analysis	84
5.2.1.	Local analysis close to the non-hyperbolic edge l_e	85
5.2.2.	Local analysis close to the non-hyperbolic line l_M	106
5.3.	Proof of the main result	113
5.4.	Dynamics near the exit point $q_{e,3}$	115
	Bibliography	119

CHAPTER 1

Introduction

Biological complexity is one of the most striking feature of the world we live in [64], [84]. There are none more complicated systems than biological living organisms. How much do we know about our bodies and how they are meant to function? How much do we know about biochemical processes occurring in our cells? How much do we know about the molecular machinery of networks in cells, such as gene regulatory networks and protein-protein interactions controlling cell growth? The truth is that in the 21st century we are only beginning to understand the true complexity of the biological world. But what has been known for many years now is that periodic oscillations are central in a variety of biological systems [40], [84]. They play important physiological roles at all biological organization levels and are present at each scale of biological complexity. Important examples include oscillatory enzyme reactions, breathing, pulsatile hormone secretion, neural and cardiac rhythms [38], [40], [83]. Hence, understanding the mechanisms underlying these phenomena is a key to a global understanding of biological complexity.

Often a starting point for modelling biological phenomena are *ordinary differential equations (ODEs)* [3], [16], [54], [76], [103]. ODE models have proved to be particularly useful for describing different oscillatory processes and have the form

$$(1.1) \quad \frac{dx}{dt} = F(x),$$

where $x \in \mathbb{R}^n$ represents some vector state variable and F is the nonlinear rate function describing the underlying biological mechanism. An oscillatory time series of the model corresponds to a *periodic solution* of (1.1) with the period T , i.e.,

$$(1.2) \quad x(t + T) = x(t),$$

which in turn corresponds in the phase space to a closed curve called a *limit cycle* [92]. Typically, realistic biological models involve many parameters. In this case the behaviour of the solution $x(t, \lambda)$ varies accordingly to the parameter values. Mostly we are interested in *the bifurcations* of a system, i.e., whether a small parameter change of a system causes a sudden qualitative change in its behaviour [18], [46], [116]. One example of a local bifurcation is *the Hopf bifurcation*, i.e., the appearance or the disappearance of a limit cycle through a local change in the stability properties of a steady point [104]. Thus, some oscillations in the model can be controlled, i.e., either induced or suppressed via Hopf bifurcation.

One interesting type of periodic solutions are *relaxation oscillations* [42], [73], [81], [111]. These highly non-linear oscillations characterized by repeated switching of slow and fast motions appear frequently in applications of biological nature. A prototypical system where they occur is the van der Pol equation of a triode circuit [118], [119]. Oscillations observed by van der Pol were quickly recognized as having a lot of similarities to biological oscillations. Indeed, relaxation oscillators appear

to characterize many important biological phenomena such as heartbeat (van der Mark and van der Pol model [120]), neuronal activity (the Fitz-Hugh-Nagumo model and the Morris-Lecar model [60]), and population cycles of predator-prey type [58]. Based on a detailed stylistic and linguistic analysis of the Petrarch's poems, a relaxation oscillator was proposed to model the dynamics of love between Petrarch and his beloved Laura [96]. In Petrarch's emotional cycle slow change phases interrupted by sudden and fast transitions can be observed. Those slow-fast transitions are another key to the understanding of a wide range of biological problems.

The uniqueness and specificity of different phenomena in chemistry and biology is due to the interplay between the time scales. To ensure the correct timing and ordering of important biological processes such as cell division, metabolism, food digestion, biochemical phenomena involved in these processes occur at different time scales. For instance, many important chemical reactions proceed with time scales of 10^{-9} to 10^{-12} s. In enzyme kinetics the binding of the substrate to the active site on the enzyme occurs in a few nano-seconds, while enzymatic reactions last up to a few seconds. This mix of various time scales appears to give rise to the presence of sudden (often surprising) jumps in the state of biological systems.

Mathematical models contributed greatly to uncovering of the mechanisms of oscillatory multiple time scale phenomena. In particular, processes evolving on different time scales have been successfully modeled by singularly perturbed ordinary differential equations [90] of the form

$$(1.3) \quad \begin{aligned} \varepsilon \dot{x} &= f(x, y, \varepsilon), \\ \dot{y} &= g(x, y, \varepsilon) \end{aligned}$$

with $(x, y) \in \mathbb{R}^n \times \mathbb{R}^m$, smooth functions f and g , and a small parameter $\varepsilon > 0$. The derivative in system (1.3) is with respect to the slow time scale t . On the fast time scale $\tau = t/\varepsilon$ the governing equations are

$$(1.4) \quad \begin{aligned} x' &= f(x, y, \varepsilon), \\ y' &= \varepsilon g(x, y, \varepsilon). \end{aligned}$$

Traditionally, slow-fast systems and the related oscillatory phenomena have been studied by the method of the matched asymptotic expansions, see e.g. [42], [71] [74], and also [81], [121]. Techniques from non-standard analysis [26] have been employed in the study of slow-fast systems as well. Recently, a more qualitative approach based on the methods from dynamical systems theory known as *geometric singular perturbation theory* has been developed [34], [61], [62]. Its foundation goes back to Fenichel [34] and the basic reasoning is the following.

The dynamics of system (1.3) for $\varepsilon > 0$, or of the equivalent fast system (1.4), is studied by analyzing and suitably combining the dynamics of *the reduced problem*

$$(1.5) \quad \begin{aligned} 0 &= f(x, y, 0), \\ \dot{y} &= g(x, y, 0), \end{aligned}$$

and the dynamics of *the layer problem*

$$(1.6) \quad \begin{aligned} x' &= f(x, y, 0), \\ y' &= 0, \end{aligned}$$

which are the $\varepsilon = 0$ limiting problems on the slow and fast time scale, respectively. The equation $f(x, y, 0) = 0$ defines *the critical manifold* S on which the reduced

problem (1.5) acts as a dynamical system. On the other hand, the critical manifold S is a manifold of equilibria of the layer problem (1.6). Due to results by Fenichel [34], normally hyperbolic pieces of critical manifolds perturb smoothly to locally invariant *slow manifolds* for ε sufficiently small. While in systems (1.3) – (1.4) slow and fast processes are combined, it is beneficial and much easier to study slow and fast processes separately. Thus, we can concentrate on the slow dynamics and analyze the algebraic-differential problem (1.5), in which the fast variables are entrained by the slow ones. On the other hand, focusing on the layer problem (1.6), we simplify the study by considering the slow variables fixed. The essence of the geometric approach is to obtain (under suitable assumptions) orbits of a singularly perturbed system (1.3) as perturbations of *singular orbits* consisting of pieces of orbits of the reduced problem (1.5) and of the layer problem (1.6).

Interesting phenomena take place when the critical manifold S has a folded structure, i.e., attracting and repelling parts of the critical manifold are separated by *fold points*, which are singularities of the reduced system (1.5). Under certain assumptions, such folded structures of critical manifolds give rise to the *jumping behavior* for solutions, i.e., reaching a fold point in finite forward time, the solutions jump from one attracting part following approximately the dynamics of the layer problem (1.6). Such jump points explain the fast transitions described above and are an ingredient of relaxation orbits. Namely, a limit cycle of a relaxation type is formed when solutions after following the slow flow along one attracting branch jump at a fold point to another stable branch of the critical manifold, follow the slow flow along it until a second fold point is reached. From there the final jump occurs, back to the first attracting branch possibly forming a closed loop.

The above described scenario with S-shaped critical manifolds is the prototypical situation to obtain classical relaxation oscillations. A substantial difficulty in the analysis of these oscillations are the fold points of the critical manifold and other points, where normal hyperbolicity of the critical manifold is lost. At these points Fenichel theory fails, i.e., the existence of slow manifolds under ε -perturbations is not guaranteed. Recently, it has become clear how to extend geometric singular perturbation theory beyond non-hyperbolic points. The answer came with the pioneering work by Dumortier and Roussarie [28], in which *the blow-up method* has proven to be an effective tool in the geometric analysis of singularly perturbed equations near non-hyperbolic points [10], [21], [22], [27], [30], [31], [56], [69], [71], [73], [95]. Thus, classical relaxation oscillations have been analyzed by combining Fenichel theory and the blow-up method, and are well-understood phenomena [73], [111].

However, relaxation oscillations can be found in a more general setting; in particular, in slow-fast systems, which are not written in the standard form (1.4). Systems in which separation into slow and fast variables is not given a priori, arise frequently in applications [23], [50], [51], [56], [68], [79]. Many of these systems include additionally various parameters of different orders of magnitude and complicated (non-polynomial) nonlinearities. This poses several mathematical challenges, since the application of singular perturbation arguments is not at all straightforward. As a result it is hard to seek for locally attracting and repelling slow manifolds that organize phase space and extract the geometry that for example organizes the oscillations. Obviously, it is hard to deal with problems in which disjoint time scales cannot be used to our advantage. For that reason most of such systems have been

studied only numerically guided by phase-space analysis arguments or analyzed in a rather non-rigorous way. It turns out that the main idea of the singular perturbation approach can also be applied in such non-standard cases.

This thesis is concerned with the application of concepts from geometric singular perturbation theory and geometric desingularization based on the blow-up method to the study of relaxation oscillations in slow-fast systems beyond the standard form. We present a detailed geometric analysis of oscillatory mechanisms in three mathematical models describing biochemical processes. Our work shows – in the context of non-trivial applications – that the geometric approach, in particular the blow-up method, is valuable for the understanding of the dynamics of systems with no explicit splitting into slow and fast variables, and for systems depending singularly on several parameters.

First we present the study of a two-variable chemical oscillator called the autocatalator. We explain in detail the dynamics and the asymptotic dependence on the parameter ε of the model. In this work we demonstrate that to understand the dynamics of even a rather simple system a careful singular perturbation analysis is needed. An interesting phenomenon occurs in the model due to a folded critical manifold with an unbounded branch, i.e., the orbits of the autocatalator jump at the fold point and come back to the attracting slow manifold after a large excursion. In order to find a limit cycle of a relaxation type, the variables of the autocatalator model are rescaled such that the resulting equations are no longer in the standard form (1.3). This renders the analysis more complex as there is no global separation of slow-fast variables; however, it allows to capture the full dynamics of the model and explain large oscillations related to *mixed-mode oscillations* [10], [69], [70], [79], [80], [93].

The second and the third problem under consideration arise from biochemistry. We consider two models from enzyme kinetics, i.e., an ODE system describing glycolytic oscillations and a three-dimensional model for the mitotic oscillator, both models proposed by Albert Goldbeter [40]. The glycolytic oscillator is a slow-fast system; however, it is a two-parameter singular perturbation problem. The corresponding critical manifold has a folded-structure and its geometry depends singularly on one of the parameters. Thus, we again deal with the interaction between slow and fast processes in a model beyond the standard form. A comprehensive and clear picture of the oscillatory dynamics of the model is given.

The mitotic oscillator displays also interesting non-linear dynamics, which can be studied in the GSPT spirit. More precisely, we transform the mitotic oscillator into a system that exhibits dynamics of slow-fast character, but lacks a global separation of slow-fast variables. We have found that the dynamics of cyclin (one of the variables of the mitotic oscillator) plays an essential role in the generation of relaxation oscillations of a new type. They arise from the phenomenon of a *delayed exchange of stability*, which occurs at non-hyperbolic lines along which branches of the two-dimensional critical manifold intersect. This novel phenomenon is analyzed and explained by means of the blow-up method.

In addition to the intrinsic interest in these models, there are several other motivations for their analysis. We believe that the first two problems under consideration are well-suited to serve as an introduction to the blow-up method in the context of non-trivial applications. In particular, the potential of iterating several blow-ups becomes clearly visible. One of the motivations of these works is

to exemplarily show how geometric constructions (especially blow-up) can handle complicated singular perturbation problems with a variety of scaling regimes.

Another central message of our work is that the novel blow-up construction and the original two-parameter character of the problem presented in Chapter 4 could be useful in other problems depending singularly on several parameters. It will turn out that one parameter mainly affects the slow-fast structure, while the second parameter mainly influences the geometry and the singularities of the critical manifold. We will show that the blow-up method leads to a clear geometric picture of this fairly complicated two-parameter multi-scale problem. There is a strong need for a more general framework for slow-fast systems with several singular perturbation parameters and we believe our work is a starting point for further development.

Last, but not least, our analysis of the mitotic oscillator in Chapter 5 shows that the hidden slow-fast nature of the dynamics of the "regularized"/rescaled mitotic oscillator can be used to obtain insight into the understanding of the original model, which so far has been obtained by numerical simulations guided by phase-plane arguments. Due to the occurrence of non-polynomial nonlinearities, it is not immediately obvious from the governing equations that the slow-fast nature of the rescaled problem can be helpful. One message of this work is that the combination of geometric singular perturbation theory with the blow-up method is a powerful and systematic tool for the analysis of oscillatory multiple time scale phenomena.

This thesis consists of five chapters. In Chapter 2, which has a theoretical character, we recall basic results in Fenichel theory covering slow-fast systems with compact critical manifolds. Furthermore, a brief review of the extension of Fenichel theory beyond normal hyperbolicity is given. In Chapter 3 – 5 we present a detailed geometric singular perturbation analysis of the autocatalator model, the glycolytic oscillator, and the mitotic oscillator, respectively. The results presented in Chapter 3 and Chapter 4 led to the publications [50], [67], and [68], respectively, which are joint work with Peter Szmolyan (Vienna University of Technology).

We now turn to the description of the background and the specifics of the problems presented in each of the chapters, and summarize our main results.

Main results

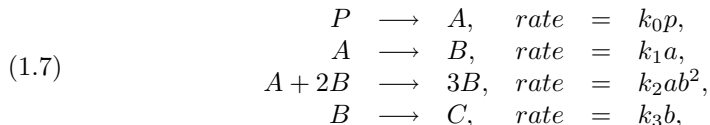
CHAPTER 3: AUTOCATALATOR MODEL

*The secret of life is autocatalysis*¹

Oscillatory chemical reactions are fundamental in biology. They provide a mechanism for the biological processes, for instance ageing, the heart beat or the development of cardiac arrhythmias [98]. *The autocatalator model* was originally proposed

¹Review by Gert Korthof of "At Home in the Universe. The Search for Laws of Self-Organization and Complexity" by Stuart Kauffman.

by P. Gray and S. Scott [45] to model the following hypothetical chemical reaction



where P, A, B , and C are certain chemical species with concentrations p, a, b , and c , respectively, and constants $k_i, i = 0, \dots, 3$. Thus, the scheme (1.7) considers the conversion of chemical precursor P to a final product C via two reactive intermediates A and B through the above sequence of steps. The third step in (1.7) is autocatalytic (hence the name of the model), i.e., in the autocatalytic reaction the product of the reaction is the catalyst. Consequently, the rate of reaction increases and the reaction accelerates as the reaction progresses. Mathematically speaking, this happens due to the cubic term $k_2 ab^2$ in the autocatalytic step, which is quadratic in b , i.e., for small values of b this term is small, but for large values of b it is large. Autocatalytic reactions are present in important biological processes such as the initial transcripts of rRNA and glycolysis (see Chapter 4). Recently, Kauffman has emphasized the role of autocatalysis in processes of life [64].

The autocatalator model and its extensions have been used to reproduce many typical features of chemical oscillations [43], [44], [98]. In this work we consider the rate equations describing the progress of reaction (1.7) in the following dimensionless form

$$(1.8) \quad \begin{aligned} \dot{a} &= \mu - a - ab^2, \\ \varepsilon \dot{b} &= -b + a + ab^2, \end{aligned}$$

where $(a, b) \in \mathbb{R}^2$, $\mu \in \mathbb{R}$ and $\varepsilon > 0$. Thus, the autocatalator model (1.8) has two parameters μ and ε , which enter the model due to the dimensionlessness procedure. While the parameter μ is not interesting in itself, the occurrence of the parameter ε will have a consequence for the nature of the dynamics of the model, i.e., small values for ε will make typically b a fast variable. In other words, due to the occurrence of the small parameter ε solutions evolve on several time scales. Thus, system (1.8) with $\varepsilon > 0$ small is written in the standard form of slow-fast systems with the slow variable a and the fast variable b . The derivative in (1.8) is with respect to slow time scale t . For certain parameter values a limit cycle exists. Geometric singular perturbation theory is used to prove the existence of this limit cycle. A central tool in the analysis is the blow-up method, which allows the identification of a complicated singular cycle, which is shown to persist.

More precisely, in our analysis of system (1.8) we will encounter a fold point, but also other non-hyperbolic points, which will be treated by suitable blow-ups. We will show that for $\mu > 1$ and ε sufficiently small system (1.8) has a globally attracting limit cycle of relaxation type. However, the asymptotic behavior and the global structure of the limit cycle is considerably more complicated than that for the van der Pol oscillator. It will turn out that additional scalings are needed to capture the full dynamics, since for $b = O(1/\varepsilon)$ the dynamics and limiting behavior are not captured by the corresponding reduced and layer problems. In the regime $b = O(1/\varepsilon)$ the cubic terms in system (1.8) dominate and a different slow-fast structure emerges. Thus, it is necessary to match the regime $b = O(1)$ with the regime $b = O(1/\varepsilon)$. We demonstrate that the blow-up method is a convenient tool for geometric matching of these two regimes. It will turn out that several iterated

blow-ups have to be used to obtain a complete desingularization of the problem. In fact, this novel feature motivated much of our interest in the problem.

The complicated dynamics of a related three-dimensional system, where roughly speaking μ becomes a dynamic variable, has been studied numerically and analytically in [78], [79], [80], [93]. The main feature of that system is the occurrence of *mixed-mode oscillations*, which consist of periodic or chaotic sequences of small and large oscillations. Mixed-mode oscillations have been related to certain types of canards, which generate the small oscillations while the large oscillations are often of relaxation type [10], [69], [78], [79], [80]. In [79] a mechanism for the occurring large relaxation oscillations was proposed. In Chapter 3 we will give a detailed analysis of this mechanism in the context of the planar system (1.8).

CHAPTER 4: GLYCOLYTIC OSCILLATOR

Glycolysis is a cellular process that occurs in almost every living organism. It involves a complex chain of enzyme reactions and results in the release of free energy, which is then used in other processes. An interesting feature of this important bioenergetic process is that the concentrations of the glycolytic intermediates oscillate under certain conditions. Such oscillations have been observed in yeast cells [15], muscle cells [37], tumor cells [59], pancreatic beta-cells [17], and heart cells [91]. Whereas the molecular basis of glycolytic oscillations is known, their biological significance and function are still unclear [40], [52].

Several — slightly different — planar ODE models have been proposed [41], [53], [102], which reproduce these oscillations. An important feature of all these models is their ability to capture the autocatalytic nature of the glycolysis reaction. In the first two models, however, the allosteric nature of the enzyme kinetics is not considered. In contrast, the Goldbeter-Lefever model is based on allosteric regulation² with positive feedback. Later this basic model has been extended by including a larger number of enzymes of the glycolytic chain; see, e.g. [106]. Nevertheless, the two-variable Goldbeter-Lefever model still serves as a starting point for modern theoretical and experimental studies as it reflects the core of the oscillatory mechanism. More recently various two- and three-dimensional models of glycolytic oscillations have been used as parts of larger systems modeling the production of insulin in pancreatic beta-cells; see, e.g. [8].

Understanding of these models has been mostly obtained by numerical simulations guided by phase-plane arguments. The slow-fast nature of the dynamics has also been frequently used to obtain insight into the dynamics. Due to the occurrence of various parameters of very different orders of magnitude and complicated (non-polynomial) nonlinearities, the application of singular perturbation arguments is not at all straightforward.

We will be concerned exclusively with the Goldbeter-Lefever model [41], written in the form (1.9). In [101] Segel and Goldbeter gave a fairly detailed — but still non-rigorous — analysis of the Goldbeter-Lefever model. In dimensionless variables

²Allosteric control is one means of regulating enzyme action, i.e., a molecule binds to an enzyme at a site other than the active site and changes the activity of the enzyme. A reader interested in enzyme kinetics is referred to [65]. A detailed description of the allosteric model for glycolytic oscillations can be found in [40], [41].

the governing equations have the form

$$(1.9) \quad \begin{aligned} \rho\alpha' &= \mu - \phi(\alpha, \gamma), \\ \gamma' &= \lambda\phi(\alpha, \gamma) - \gamma, \end{aligned}$$

where α and γ denote certain substrate and product concentrations and

$$\phi(\alpha, \gamma) = \frac{\alpha^2(\gamma + 1)^2}{L + \alpha^2(\gamma + 1)^2}.$$

The equations contain four positive parameters λ, L, μ and ρ , where L and λ turn out to be large³ and satisfy $\lambda \ll L$, while μ and ρ are of moderate size.

In their analysis of system (1.9) Segel and Goldbeter applied what they call the method of scaling. In particular, they identified a small parameter

$$(1.10) \quad \varepsilon := \sqrt{\frac{\lambda}{L}},$$

which causes the slow-fast structure of system (1.9). It turns out that system (1.9) exhibits classical relaxation oscillations in the limit of large L and fixed λ . However, the main interest in [101] lies in the situation where L and λ are both large. In this case, the asymptotics of system (1.9) become more complicated. By considering several different scaling regimes, Segel and Goldbeter argued that the condition

$$(1.11) \quad \sqrt{\frac{\lambda}{L}} \ll \frac{1}{\sqrt{\lambda}} \ll 1$$

implies the existence of a relaxation cycle.

In this work we complement the reasoning given in [101] by proving that condition (1.11) indeed implies the existence of a relaxation cycle of system (1.9). We will rewrite system (1.9) in the standard form (2.6) of singularly perturbed problems, which we then examine geometrically in the spirit described above. By a suitable scaling of the variables α and γ , we rewrite system (1.9) in the form

$$(1.12) \quad \begin{aligned} a' &= \varepsilon(a^2b^2(\mu - 1) + \mu\delta^2), \\ b' &= a^2b^2(1 - b) + \delta^2(a^2b^2 - b + \delta^2), \end{aligned}$$

where (a, b) correspond to (α, γ) , ε is given by (1.10), and

$$(1.13) \quad \delta := \lambda^{-1/2}.$$

Hence, a is the slow variable and b is the fast variable with respect to ε . In our notation condition (1.11) has the form

$$(1.14) \quad \varepsilon \ll \delta \ll 1.$$

We now briefly outline our approach to the analysis of system (1.12). Setting $\varepsilon = 0$ and $\delta = 0$ in system (1.12) gives the layer problem

$$(1.15) \quad \begin{aligned} a' &= 0, \\ b' &= a^2b^2(1 - b). \end{aligned}$$

The corresponding critical manifold S^0 , defined by $a^2b^2(1 - b) = 0$, consists of the lines $a = 0$, $b = 0$, and $b = 1$, which we denote by l_b , l_a , and l_h , respectively. Since the zeros $a = 0$ and $b = 0$ have multiplicity two, the lines l_a and l_b are non-hyperbolic lines of equilibria, whereas the line l_h corresponding to the simple zero $b = 1$ is

³ L is the allosteric constant influencing the degree of the cooperativity of the enzyme, see [40] and [41] for a detailed biochemical explanation.

normally hyperbolic. Hence, this limiting problem is degenerate and the structure of the relaxation oscillations is not visible at all. We introduce three scaling regimes in which parts of the relaxation cycle become visible again by partially undoing the scaling leading to system (1.12). Not surprisingly, these scaling regimes are closely related to the scaling regimes of Segel and Goldbeter. However, the three scaling regimes do not overlap and matching these regimes is a difficult problem.

The main goal of this work is to show that the blow-up method is well suited to overcome these difficulties. It turns out that two blow-ups of the degenerate critical manifold S^0 (with respect to δ) lead to a complete desingularization of the problem such that uniform results in ε become possible. In this approach the degenerate lines $a = 0$ and $b = 0$ are blown-up to cylinders by rewriting the original (a, b, δ) variables in suitable cylindrical variables. In the blown-up geometry the existence of the relaxation cycle can be proved. Matching of the scaling regimes now takes place in additional charts covering parts of the cylinders not covered by the scaling regimes.

CHAPTER 5: MITOTIC OSCILLATOR

While you are reading this text dramatic events occur in your body: every second millions of your cells divide. Each of them divides in half coping itself to maintain your body healthy. Each of them goes through several phases of the *cell division cycle*, the last of which is called *mitosis*. What drives the cell through the cell cycle? What controls it and how does the cell know what to do in each of the phases? When and how does the cell know it is ready to divide? As simple as the cell division story sounded in the biology class, the cell division is a complex fundamental process of life, which at the molecular level has been understood just recently.

The key regulators of the cell cycle control system have been found by the Nobel Prize Laureates: Paul Nurse and Tim Hunt [57], [88], [89]. They discovered two classes of proteins, *cyclin dependent kinases* (*cdks*) and *cyclins*, which are responsible for the timing and ordering of the cell cycle transitions. Their experiments showed that the binding of cyclin and cdk results in a formation of an enzyme in which cdk plays the role of a molecular engine driving the cell forward from one stage to another. This engine is switched on and off by cyclin, which regulates the function of cdk. Furthermore, it has been discovered that cyclin levels go up before the division and go down after the cell divided.

It is this cyclin periodic oscillatory behavior feature among the others, which motivated Albert Goldbeter that the cell cycle could be driven by a continuous biochemical oscillator [39]. Taking into account the fact that the activation of *cdc2* kinase (a type of kinase involved in mitosis) is driven by accumulation of cyclin while the former promotes cyclin degradation, Goldbeter developed a minimal model of the mitotic oscillator based on a negative feedback [39]. The model involves the Michaelis-Menten type kinetics and therefore the dynamics of the model is described by highly non-linear ordinary differential equations.

Namely, the model consisting of three coupled ordinary differential equations for the fraction of active cyclin protease X , the fraction of active *cdc2* kinase M ,

and the cyclin concentration C , has the form

$$\begin{aligned}
 \frac{dX}{d\tau} &= V_3(M) \frac{1-X}{k_3+1-X} - V_4 \frac{X}{k_4+X}, \\
 \frac{dM}{d\tau} &= V_1(C) \frac{1-M}{k_1+1-M} - V_2 \frac{M}{k_2+M}, \\
 \frac{dC}{d\tau} &= v_i - v_d X \frac{C}{K_d+C} - k_d C,
 \end{aligned}
 \tag{1.16}$$

with the effective maximum rates $V_1(C)$ and $V_3(M)$ given by

$$V_1(C) = V_{M1}C/(K_c + C), \quad V_3(M) = V_{M3}M.$$

The parameter v_d denotes the maximum rate of cyclin degradation by protease X , v_i is the constant rate of cyclin synthesis. K_d and K_c denote the Michaelis constants for cyclin degradation and for cyclin activation of the *cdc25* phosphatase acting on the phosphorylated form of the *cdc2* kinase, respectively. k_d represents an apparent first-order rate constant related to non-specific degradation of cyclin. Parameters V_i and $k_i, i = 1, \dots, 4$ denote the effective maximum rates and the Michaelis constants, respectively, for each of the enzymes E_i involved in the two cycles of phosphorylation-dephosphorylation.

For certain parameter values and Michaelis constants small the qualitative features of the cell-cycle are captured, i.e., switching behavior of cyclin and *cdk2* kinase emerges. More explicitly, Goldbeter and Erneux [33] showed that under certain conditions the model exhibits sustained oscillations in all mitotic intermediates. From the molecular point of view the mechanism how oscillations are generated has been understood; however, from the mathematical point of view the pattern of the oscillations observed in system (1.16) remained mysterious, i.e., the existence of periodic orbits in (1.16) was too difficult to prove. To overcome this difficulty, Goldbeter and Erneux simplified the problem by applying the *quasi-steady-state approximation (QSSA)* for one of the dependent variables. In particular, assuming that the enzyme reacts so fast with the substrate that it can be taken as being in equilibrium, i.e., $\frac{dM}{dt} = 0$, they eliminated M and analyzed the reduced two-variable system. The QSSA is commonly used tool in modelling of biochemical networks and has been employed in chemical kinetics for more than 80 years. However, the main disadvantage of this approach is that the resulting simplified systems may be qualitatively different from the original ones, which was illustrated and emphasised by the authors in the case of the mitotic oscillator. More precisely, the traditional approach to explain oscillations based on the QSSA showed that the resulting two-dimensional problem exhibits no oscillations. Then, to improve the QSSA approach, a rather complicated rescaling was introduced. In spite of the fact that a new QSSA reduced two-dimensional problem exhibited some oscillatory behavior, the obtained oscillations did not explain the time series of the full model (1.16).

In this work we analyze the mitotic oscillator (1.16) in the spirit of geometric singular perturbation theory. This approach due to complicated non-polynomial non-linearities is not straightforward at all. Our results show that by introducing a suitable time change, the mitotic oscillator can be reformulated into a singular perturbation problem with respect to small Michaelis constants. Due to the occurrence of these small parameters solutions of the rescaled problem evolve on different time scales. However, the resulting equations are not in the standard form of slow-fast

systems. Nevertheless, we will demonstrate that the hidden slow-fast nature of the dynamics of the rescaled system can be used to obtain new insights into the understanding of the mitotic oscillator, which so far has been obtained by numerical simulations guided by phase-plane arguments.

Our main results are that for certain parameter values the model exhibits a novel type of relaxation oscillations, and the concepts from Fenichel theory and geometric desingularization based on the blow-up method are the right tools for their description. Our approach is the following.

We rewrite the model as a three-dimensional singularly perturbed system in the variables (X, M, C) . The equations are, however, not in standard form, i.e., away from the critical manifold all variables are fast. The critical manifold consists of four planes $M = 0$, $X = 0$, $M = 1$, and $X = 1$. Each of these planes changes its stability at non-hyperbolic line given by $C = C_{crit}$, $M = M_{crit}$, $C = C_{crit}$, and $M = M_{crit}$, respectively. In addition, the planes intersect along another four non-hyperbolic lines, where the phenomenon of *delayed exchange of stability* occurs resulting in the generation of relaxation oscillations of a new type. More precisely, within the geometric singular perturbation approach we are able to identify a singular periodic orbit the first half of which consists of

- (1) slow motion in the attracting part of the plane $M = 0$ towards the (non-hyperbolic) edge $(X, M) = (0, 0)$,
- (2) very slow drift along the edge $(X, M) = (0, 0)$,
- (3) slow motion in the attracting part of the plane $X = 0$ to a point p on the non-hyperbolic line $M = M_{crit}$,
- (4) and a fast jump from p to the attracting part of the plane $M = 1$.

The second half of the cycle is generated in a similar manner. This novel type of relaxation oscillations is studied by means of several blow-up transformations. In this approach the degenerate lines $M = M_{crit}$ and the edges are blown-up to cylinders by rewriting the original (X, M, C) variables in suitable cylindrical variables. In the blown-up geometry the existence of the relaxation cycle is proven. Our geometric study provides new insight into the nature of the oscillations and the dynamics of proteins related to mitosis of the cell division cycle. It naturally leads to a number of question for future research.

CHAPTER 2

Introduction to geometric methods of singular perturbation theory

In this chapter we give a brief guide to recently developed geometric methods for the analysis of systems of singularly perturbed ordinary differential equations. We provide some introductory definitions, introduce slow-fast systems, and present a collection of fundamental results in Fenichel theory [34]. Furthermore, we introduce the blow-up method [28] and recall the results by Szmolyan and Krupa [71] on slow manifolds of slow-fast systems with critical manifolds containing non-degenerate folds.

All the definitions and theorems collected in this chapter are based on [27], [34], [61], [62], [66], [82], [90], [110]. The techniques presented here are a basic part of the toolbox from geometric singular perturbation theory. A non-trivial application of some of these concepts to different biochemical oscillations models are in detail presented in Chapter 3 – 5.

2.1. Regularly vs. singularly perturbed systems

Perturbation problems are characterized by the presence of a small parameter $\varepsilon > 0$. We distinguish two types of perturbations: *regular* and *singular* [82], [90]. The purpose of this section is to recall some basic notions and properties of regularly and singularly perturbed ordinary differential equations.

Consider an autonomous system of ODEs of the form

$$(2.1) \quad \dot{x} = F(x, \varepsilon),$$

where $x \in \mathbb{R}^n$, $F(x, \varepsilon) = (F_1(x, \varepsilon), \dots, F_n(x, \varepsilon))$ is an n -dimensional vector function of the arguments x and a small parameter $\varepsilon > 0$, with all F_j , $j = 1, \dots, n$, defined and continuous at all points of a certain domain $\Omega \subset \mathbb{R}^{n+1}$. The derivative in (2.1) is with respect to $t \in \mathbb{R}$. Setting $\varepsilon = 0$ in (2.1) defines the unperturbed problem

$$(2.2) \quad \dot{x} = F(x, 0).$$

Let $x_\varepsilon(t)$ and $x_0(t)$ denote solutions of (2.1) and (2.2), respectively, defined on some finite time interval $t_0 \leq t \leq T$, and with the same initial condition $x_0 = x_\varepsilon(t_0) = x_0(t_0)$, $(x_0, \varepsilon) \in \Omega$.

Suppose the functions F_j are continuously differentiable with respect to x and continuous in ε in the domain Ω , then for a sufficiently small ε , solution $x_\varepsilon(t)$ is defined on the same interval $t_0 \leq t \leq T$ as solution $x_0(t)$ and can be represented as

$$(2.3) \quad x_\varepsilon(t) = x_0(t) + R_0(t, \varepsilon),$$

where $R_0(t, \varepsilon) \rightarrow 0$ as $\varepsilon \rightarrow 0$ uniformly with respect to t on the interval $t_0 \leq t \leq T$.

If, in the domain Ω , the right hand side of (2.1) is continuously differentiable $m \geq 1$ times with respect to all the variables x and ε , then for a sufficiently small

ε , solution $x_\varepsilon(t)$ can be represented as

$$(2.4) \quad x_\varepsilon(t) = x_0(t) + \varepsilon x_1(t) + \dots + \varepsilon^{m-1} x_{m-1}(t) + R_m(t, \varepsilon),$$

where, as $\varepsilon \rightarrow 0$, $R_0(t, \varepsilon) \rightarrow 0$ as a quantity of order ε^m uniformly with respect to t on the interval $t_0 \leq t \leq T$.

If, in the domain Ω , the right hand side of (2.1) is an analytic function of its arguments, then for a sufficiently small ε , solution $x_\varepsilon(t)$ can be represented as a series

$$(2.5) \quad x_\varepsilon(t) = x_0(t) + \sum_{m=1}^{\infty} \varepsilon^m x_m(t)$$

converging uniformly on the interval $t_0 \leq t \leq T$.

In all these cases, system (2.1) is called *regularly perturbed* or a *regular perturbation* of the system (2.2). In contrast to these systems, the nature of expansions for *singular perturbation problems* is much more complex and unexpected, i.e., in the asymptotic expansions for singular perturbation problems more complicated terms can occur, such as logarithmic terms $\varepsilon^{m/k} \log^l \varepsilon$ or $\varepsilon^{m/k}$, $m, k, l \in \mathbb{N}$; see e.g. [94]. Thus, one defines *singular perturbation problems*, in an informal way, as problems in which a breakdown of the regular perturbation limit $x_\varepsilon(t) \rightarrow x_0(t)$ occurs.

In this thesis we deal with singular perturbation problems, which describe processes evolving on time scales with different orders of magnitude. Such processes arise frequently in applications ranging from physics to biochemistry. In the following section we will see that these singularly perturbed equations frequently have a specific structure, i.e., a small parameter $\varepsilon > 0$ multiplies one of the derivatives, which makes the standard regular perturbation theory inapplicable. The parameter ε is called the *singular perturbation parameter* and measures the separation between time scales.

In the following we present *slow-fast systems*, which may be employed in the case of processes occurring at two different time scales, i.e., when the dynamics of some variables is much faster than the dynamics of the other variables. Moreover, we present an overview of geometric methods to study such systems.

2.2. Slow-fast systems in standard form

The equations we consider are of the form

$$(2.6) \quad \begin{aligned} x' &= f(x, y, \varepsilon), \\ y' &= \varepsilon g(x, y, \varepsilon) \end{aligned}$$

with a small parameter $\varepsilon > 0$, $(x, y) \in \mathbb{R}^n \times \mathbb{R}^m$ for $n, m \in \mathbb{N}$, and smooth functions f and g (in all three arguments). The derivative in (2.6) is with respect to the time variable τ . By introducing a change of time scales $t = \tau\varepsilon$, system (2.6) can be reformulated as

$$(2.7) \quad \begin{aligned} \varepsilon \dot{x} &= f(x, y, \varepsilon), \\ \dot{y} &= g(x, y, \varepsilon). \end{aligned}$$

The overdot differentiation in (2.7) is with respect to the slow time scale t . Hence, near points where $f(x, y, \varepsilon)$ is $O(1)$ the variable x varies on the fast scale τ , while near points where $f(x, y, \varepsilon)$ is $O(\varepsilon)$ solutions vary on the slow time scale $t = \tau\varepsilon$. Thus, we call system (2.6) and (2.7) the *fast system* and the *slow system*, respectively. For $\varepsilon > 0$ these two systems are equivalent, i.e., the phase portrait remains

unchanged, only the speed of propagation along the orbit changes. The parameter ε varies in a small interval around zero and measures the ratio between the time scales. Note that for $\varepsilon > 0$ fast and slow processes are combined in (2.6) (equivalently in (2.7)).

To study fast and slow processes separately, but simultaneously, we analyze the dynamics of two limiting problems obtained by taking the limit $\varepsilon \rightarrow 0$ in (2.6) and (2.7), respectively. Namely, setting $\varepsilon = 0$ in (2.6) defines *the layer problem*

$$(2.8) \quad \begin{aligned} x' &= f(x, y, 0), \\ y' &= 0. \end{aligned}$$

The corresponding *reduced problem* on the slow time scale t , obtained by setting $\varepsilon = 0$ in (2.7), is given by

$$(2.9) \quad \begin{aligned} 0 &= f(x, y, 0), \\ \dot{y} &= g(x, y, 0). \end{aligned}$$

Note that the reduced problem (2.9) is an algebraic-differential equation, i.e., (2.9) is considered as a dynamical system for y , however, only on the set

$$S := \{(x, y) \in \mathbb{R}^{n+m} : f(x, y, 0) = 0\}.$$

called the *critical manifold*. In contrast to (2.9), in the analysis of the layer problem (2.8) one studies the dynamics of the fast variables x , while keeping the slow components y frozen. This is closely related to a bifurcation analysis, i.e., the asymptotic behavior of the layer problem, its attractors and repellers are analyzed for all possible values of y treated as parameters. In particular, the critical manifold S is a set of equilibria of the layer problem (2.8), and therefore strongly influences also the fast dynamics.

The linearized stability of points in S as the steady states of the layer problem (2.8) is determined by the Jacobian $\frac{\partial f}{\partial x}$. We call the critical manifold S *normally hyperbolic*¹, when the Jacobian $\frac{\partial f}{\partial x}|_S$ is uniformly hyperbolic, i.e., its spectrum is uniformly bounded away from the imaginary axis. A normally hyperbolic connected compact subset $S_0 \subset S$ is called *attracting (repelling)*, if all eigenvalues of $\frac{\partial f}{\partial x}|_p$ have negative (positive) real parts for $p \in S_0$. If S_0 is normally hyperbolic and neither attracting nor repelling, we call it *saddle-type*.

The critical manifold S is not always a manifold in the strict sense, since points of self-intersection or other singularities may arise. In a neighborhood of any point in S , where the Jacobian $\frac{\partial f}{\partial x}$ is nonsingular the equation $f(x, y, 0) = 0$ can be solved for $x = h_0(y)$ by the implicit function theorem. In this situation the reduced problem (2.9) is described by the equation

$$(2.10) \quad \dot{y} = g(h_0(y), y, 0).$$

In many problems valuable information on the dynamics of system (2.6) with ε small can be obtained by analyzing and suitably combining the dynamics of the layer problem (2.8) and the reduced problem (2.9). It is natural to expect that the layer problem is an approximation of the fast dynamics and that the reduced problem is an approximation of the slow dynamics. In many situations higher order

¹The notion of normal hyperbolicity is defined for invariant manifolds more generally. It states that the attraction to and/or repulsion from the manifold is stronger than the dynamics on the manifold itself; the exact definition can be found in [116].

approximations are obtained by the method of matched asymptotic expansions [42], [66], [81], [90].

REMARK 2.1. *In the figures of this thesis the dynamics of reduced problems and corresponding layer problems are shown simultaneously, in blue and green, respectively. Hyperbolic behavior of the layer problem is indicated by double arrows, while a single arrow indicates non-hyperbolic behavior of the layer problem, see e.g. Figure 2.5.*

2.3. Fenichel theory – basis theorems

During the last twenty years, in addition to the method of matched asymptotic expansions, a more qualitative approach based on methods from dynamical systems theory known as *geometric singular perturbation theory* has been developed. This approach goes back to Fenichel [34], and in this section we recall some of the basic results of his pioneering work. As a more detailed introduction to the theory we recommend the survey [61], where also references to numerous applications can be found. For a thorough discussion including proofs we refer to the original work by Fenichel [34]. An interesting explanation of geometric singular perturbation theory and its use in biological practice can be found in [51].

The two theorems cited below and illustrated in Figure 2.1 and Figure 2.2 describe precisely the relation between the dynamics of system (2.6) and the combined dynamics of the layer problem (2.8) and the reduced problem (2.9).

THEOREM 2.1. (Fenichel, [34]) *For $f, g \in C^k$ in (x, y, ε) and S_0 a normally hyperbolic compact subset of the critical manifold S given by $S_0 = \{(h_0(y), y) : y \in U\}$ with U compact², there exists $\varepsilon_0 > 0$ such that for $\varepsilon \in (0, \varepsilon_0]$ there exists a locally invariant n -dimensional C^k manifold S_ε given as a graph $S_\varepsilon = \{(h(y, \varepsilon), y)\}$, where h is C^k in x and ε , and $h(y, 0) = h_0(y)$.*

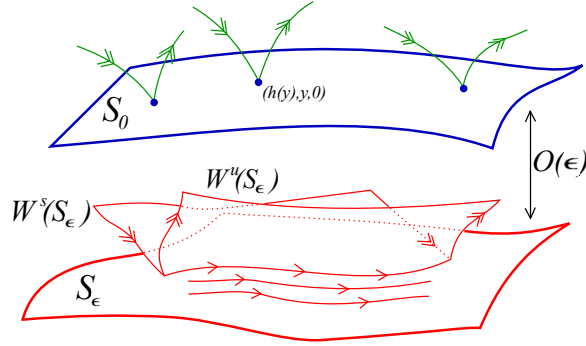


FIGURE 2.1. Illustration of Fenichel theorems: persistence of a slow manifold S_ε .

The manifold S_ε is called a *slow manifold*. Note that local invariance of S_ε means that trajectories enter or leave through boundaries of S_ε . Moreover, S_0 perturbs to

²Fenichel theory for non-compact manifolds has been developed as well [32].

S_ε , which has a distance $O(\varepsilon)$ from S_0 and the flow on S_ε converges to the slow flow as $\varepsilon \rightarrow 0$, i.e., the slow flow on S_ε can be described as

$$\dot{y} = g(h(y, \varepsilon), y, \varepsilon).$$

For a given critical manifold S_0 , let n_s and n_u denote the number of negative and positive eigenvalues, respectively. Close to S_0 the layer problem (2.8) has two manifolds, which intersect in S_0 , i.e., the $(m + n_s)$ -dimensional stable manifold $W^s(S_0)$ and the $(m + n_u)$ -dimensional unstable manifold $W^u(S_0)$, where m is the dimension of the slow variables (for the planar case $m = 1$). The characterization of the slow flow on S_ε in terms of its stable and unstable manifolds $W^s(S_\varepsilon)$ and $W^u(S_\varepsilon)$ is given in the following theorem

THEOREM 2.2. (Fenichel, [34]) *Let $\alpha > 0$ and $\beta > 0$ be such that $\operatorname{Re}(\lambda_s) < -\alpha < 0$ and $\operatorname{Re}(\lambda_u) > \beta > 0$, then there exists ε_0 such that for $\varepsilon \in (0, \varepsilon_0]$ the following holds.*

- (1) *There exists a stable $(m + n_s)$ -dimensional C^k -manifold $W^s(S_\varepsilon)$ and an unstable $(m + n_u)$ -dimensional C^k -manifold $W^u(S_\varepsilon)$, which are both locally invariant and C^k -close to $W^s(S_0)$ and $W^u(S_0)$, respectively.*
- (2) *The dynamics in $W^s(S_\varepsilon)$ ($W^u(S_\varepsilon)$) is described by stable (unstable) invariant C^k -foliation \mathcal{F}^s (\mathcal{F}^u) of $W^s(S_\varepsilon)$ ($W^u(S_\varepsilon)$) such that the distance between orbits, which start in the same leaf of \mathcal{F}^s (\mathcal{F}^u) is decaying (growing) exponentially fast with rate $e^{-\alpha t}$ ($e^{\beta t}$).*
- (3) *The leaves of \mathcal{F}^s (\mathcal{F}^u) are invariant under the flow, i.e., each leaf $\mathcal{F}^s(x, y)$ ($\mathcal{F}^u(x, y)$) is mapped to another leaf $\mathcal{F}^s(x(t), y(t))$ ($\mathcal{F}^u(x(t), y(t))$) by flow in forward (backward) time t .*

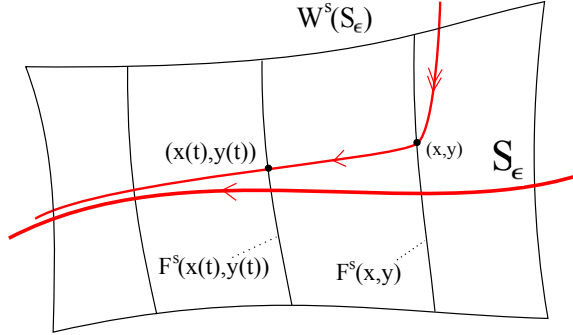


FIGURE 2.2. Behavior near a slow manifold S_ε .

The slow manifold S_ε has the same stability properties with respect to the fast variables as S_0 , i.e., the attracting and repelling manifolds S_a and S_r perturb smoothly to locally invariant manifolds $S_{a,\varepsilon}$ and $S_{r,\varepsilon}$, respectively, for sufficiently small $\varepsilon \neq 0$.

To obtain $S_{a,\varepsilon}$ (respec. $S_{r,\varepsilon}$) the center-manifold theory can be used in an elegant manner [13]. Consider the following extended system

$$(2.11) \quad \begin{aligned} x' &= f(x, y, \varepsilon), \\ y' &= \varepsilon g(x, y, \varepsilon), \\ \varepsilon' &= 0 \end{aligned}$$

in the extended phase space \mathbb{R}^3 . Note that the planes $\varepsilon = \text{const.}$ are invariant for (2.11). Moreover, on the plane $\varepsilon = 0$ the dynamics is governed by the layer problem (2.8). Thus, $S \times \{0\}$ is a manifold of equilibria for the extended system (2.11). Assume that S is normally hyperbolic and fully attracting, i.e., $S = S_a$. Then, the linearization of system (2.11) at points $S_a \times \{0\}$ has a double zero eigenvalue and one uniformly hyperbolic stable eigenvalue. From the center manifold theorem we conclude that there exists an attracting two-dimensional center-like manifold M_a . The slow manifold $S_{a,\varepsilon}$ is then obtained as sections $\varepsilon = \text{const.}$ of M_a . Since the slow manifold M_a is not unique, neither is S_a . However, all manifolds lie exponentially close to each other, i.e., lie at a Hausdorff distance $O(e^{-K/\varepsilon})$ from each other for some constant $K > 0$.

Similarly, we can obtain the repelling manifold M_r . Note that this construction breaks down when the linearization of system (2.11) has a triple zero eigenvalue. More precisely, the critical manifold S contains then points where the Jacobian $\frac{\partial f}{\partial x}$ is non-hyperbolic, i.e., $\frac{\partial f}{\partial x}$ has a zero eigenvalue or a purely imaginary eigenvalue. A zero eigenvalue of the Jacobian $\frac{\partial f}{\partial x}$ at a point in S is typically related to a singularity of the critical manifold S . The most common singularity in that context are *fold points* corresponding to a saddle-node bifurcation of the layer problem. In the method of matched asymptotic expansions these singularities of S lead to complicated asymptotic expansions containing fractional powers and logarithms of ε , see e.g. [42], [81], and also [71], [121].

Hence, such non-hyperbolic points are a major source of difficulties in all approaches and it is of great interest to study how $S_{a,\varepsilon}$ as well as nearby solutions behave as they pass near non-hyperbolic points.

2.4. Blow-up method

For a long time it was unclear how to extend geometric singular perturbation theory to fold points and other non-hyperbolic points of the critical manifold S . After the pioneering work of Dumortier and Roussarie [28] it turned out that *the blow-up method* is a powerful tool in the analysis of singular perturbation problems with non-hyperbolic points. Here we closely follow [71] and [110], and present the blow-up of a non-hyperbolic point. See also [29], where the blow-up technique is presented on different interesting examples in the plane and 3d-space.

Consider a planar singularly perturbed system augmented by a trivial equation $\varepsilon' = 0$, i.e.,

$$(2.12) \quad \begin{aligned} x' &= f(x, y, \varepsilon), \\ y' &= \varepsilon g(x, y, \varepsilon), \\ \varepsilon' &= 0 \end{aligned}$$

and suppose that an equilibrium located at the origin is such that

$$f(0, 0, 0) = 0, \quad \frac{\partial f}{\partial x}(0, 0, 0) = 0.$$

Note that the linearization of system (2.12) at the origin has a triple zero eigenvalue; thus, the origin is a very degenerate equilibrium of the extended system (2.12). To overcome this degeneracy, we apply the blow-up method, i.e., a suitably weighted spherical coordinates transformation by which the degenerate equilibrium is blown-up to a sphere. More precisely, the blow-up transformation is defined as a

mapping $\Phi : \mathbb{S}^2 \times [0, r_0] \rightarrow \mathbb{R}^3$

$$(2.13) \quad \begin{aligned} x &= r^\alpha \bar{x}, \\ y &= r^\beta \bar{y}, \\ \varepsilon &= r^\gamma \bar{\varepsilon} \end{aligned}$$

with $r_0 > 0$, the weights $(\alpha, \beta, \gamma) \in \mathbb{Z}^3$, and $\mathbb{S}^2 = \{(\bar{x}, \bar{y}, \bar{\varepsilon}) : \bar{x}^2 + \bar{y}^2 + \bar{\varepsilon}^2 = 1\}$.

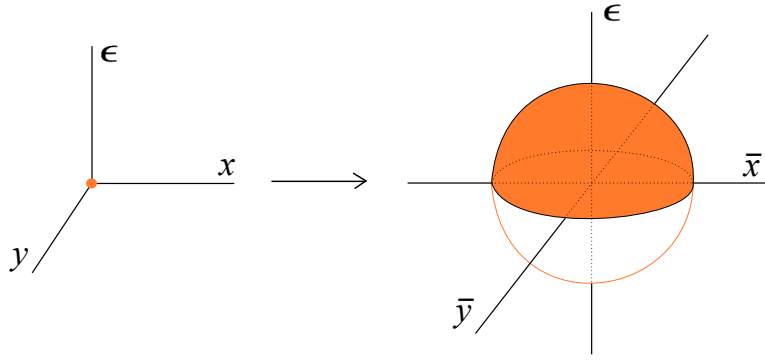


FIGURE 2.3. Blow-up of a point to the two-sphere.

The map Φ is a diffeomorphism for $r > 0$ and for $r = 0$ is singular, i.e., it maps the two-sphere $Z = \mathbb{S}^2 \times \{0\}$ to the origin, see Figure 2.3. The map Φ induces the blown-up vector field \bar{X} such that the diagram in Figure 2.4 commutes. Since an equilibrium is blown-up, the blown-up vector field vanishes on the sphere. After dividing out a suitable power of the radial variable r , a sufficiently non-degenerate flow on the sphere is obtained to allow a complete analysis.

REMARK 2.2. *In other words, after the blow-up and local division one obtains a non-trivial rescaled version of the blown-up vector field on the sphere $\mathbb{S}^2 \times \{0\}$, which contains vital information about the flow of the vector field X corresponding to (2.12). This procedure of a local division by r called desingularization will be explained in more detail in Chapter 3 – 5.*

$$\begin{array}{ccc} B & \xrightarrow{\Phi} & \mathbb{R}^3 \\ \bar{X} \downarrow & & \downarrow X \\ TB & \xrightarrow{\Phi_*} & T\mathbb{R}^3 \end{array}$$

FIGURE 2.4. Commutative diagram for the induced vector field, where $B = \mathbb{S} \times [0, r_0]$.

The blown-up vector field is analyzed in local charts, which are obtained by setting one blown-up variable on \mathbb{S}^2 equal to ± 1 in the definition of the blow-up transformation (2.13). Thus, the charts cover the two-sphere by planes perpendicular to the axes. The most important chart in the blown-up analysis is the chart

corresponding to $\bar{\varepsilon} = 1$ in (2.13). The corresponding blow-up transformation is simply an ε -rescaling of the original variables (x, y) , since $r = \varepsilon^{-\gamma}$. Thus, it is called *the rescaling chart* or *the classical chart* to emphasize its importance. Due to the equation $\varepsilon' = 0$, which implies $r' = 0$, r acts as a parameter in the rescaling chart. However, in other charts the radial variable r becomes dynamic, and thus, the blown-up systems are not a family of planar vector fields. These additional charts are needed to capture the dynamics on unbounded domains in the classical chart, i.e., points at the infinity correspond to points on the "equator" on the sphere.

By now the blow-up method has found numerous applications in the analysis of the dynamics associated with non-hyperbolic points of singularly perturbed differential equations, see e.g. [21], [28], [30], [31], [69], [73], [95], [110], [111]. In many of these applications degenerate points are blown-up to spheres, however in our works, presented in Chapter 3–5, higher dimensional degenerate objects are blown-up, e.g. non-hyperbolic curves are blown-up to cylinders (see also [56], [95], [100], [111] for other applications). Moreover, the blow-up method applied to our problems has to be used iteratively, i.e., several consecutive blow-ups have to be used to obtain a complete desingularization. More explicitly, this means that if a certain blow-up leads to a less degenerate problem, which still has degenerate points, these points can be treated by additional blow-ups [50].

How to determine the proper weights for each specific problem to obtain a complete desingularization is the most subtle part of the blow-up method. A general method for finding suitable weights does not exist, however, in certain singular perturbation problems the theory of Newton polyhedra of polynomial vector fields can be useful (see [11] for the existing theory).

A more detailed and excellent exposition of the blow-up method in the context of singular perturbation can be found in [110]. For a more general background on dynamical systems, we refer to [46].

2.5. Background on singularly perturbed planar folds

In this section we briefly describe results from [71] on slow manifolds of planar singularly perturbed systems with critical manifolds containing non-degenerate fold points.

We consider planar systems of the form (2.6). Assume that the critical manifold S is a folded curve with a non-degenerate fold point at the origin, i.e.,

$$\begin{aligned} f(0, 0, 0) &= 0, & f_x(0, 0, 0) &= 0, \\ f_{xx}(0, 0, 0) &\neq 0, & f_y(0, 0, 0) &\neq 0, & g(0, 0, 0) &\neq 0. \end{aligned}$$

Thus, the critical manifold S consists of an attracting branch S_a and a repelling branch S_r with $f_x(x, y, 0) < 0$ on S_a and $f_x(x, y, 0) > 0$ on S_r .

Without a loss of generality we assume that the position of the critical manifold S is as shown in Figure 2.5. We assume further that the reduced flow on S is downwards, i.e., $g(x, y, 0)$ is strictly negative on S . The dynamics of the layer problem and the reduced problem are as shown in Figure 2.5. Thus, we have the typical behavior of a *jump point*. Solutions starting between S_a and S_r are attracted by S_a , then follow the reduced flow until the fold point from where they jump to the right along the weakly unstable fiber of the fold point.

Compact parts of S_a and S_r are normally hyperbolic. Fenichel theory [34], [61] implies that S_a and S_r perturb smoothly to locally invariant slow manifolds $S_{a,\varepsilon}$

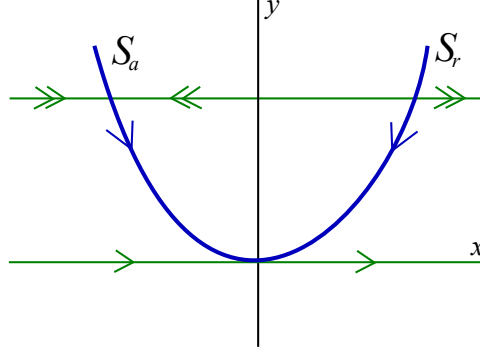


FIGURE 2.5. Jump point and dynamics of the layer and the reduced problems.

and $S_{r,\varepsilon}$ for ε small. The slow manifold $S_{a,\varepsilon}$ ($S_{r,\varepsilon}$) is attracting (repelling) and has an invariant stable (unstable) foliation with fibers close to the horizontal orbits of the layer problem. The slow flow on $S_{a,\varepsilon}$ and $S_{r,\varepsilon}$ is a smooth perturbation of the reduced flow on S_a and S_r , and hence is still directed downwards; see Figure 2.6.

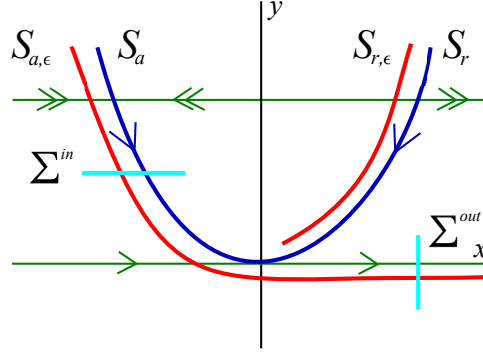


FIGURE 2.6. Slow manifolds and sections.

These results are valid outside any fixed small neighborhood of the fold point. The analysis of the asymptotic behavior of solutions close to the fold point has been the central problem in the analysis of relaxation oscillations [42], [81] by the method of matched asymptotic expansions. A more recent approach in the analysis of critical manifolds with non-hyperbolic points based on the blow-up method is introduced in [28]. A detailed geometric analysis of the dynamics and asymptotics close to the fold point based on the blow-up method is given in [71]. There it is shown that the dynamics close to the fold point is governed by equations of the form

$$\begin{aligned}
 x' &= x^2 - y + O(\varepsilon, xy, y^2, x^3), \\
 y' &= \varepsilon(-1 + O(x, y, \varepsilon)), \\
 \varepsilon' &= 0.
 \end{aligned}
 \tag{2.14}$$

The degenerate equilibrium $(0, 0, 0)$ of system (2.14) is blown-up to a sphere by the transformation

$$(2.15) \quad x = r\bar{x}, \quad y = r^2\bar{y}, \quad \varepsilon = r^3\bar{\varepsilon}$$

with $(\bar{x}, \bar{y}, \bar{\varepsilon}) \in \mathbb{S}^2$ and $r \in \mathbb{R}$. After dividing out a suitable power of the radial variable r , a nontrivial flow on the sphere is obtained. The resulting flow on the sphere is sufficiently non-degenerate to allow a complete analysis. For details we refer to [71].

In order to describe the behavior of the attracting slow manifold $S_{a,\varepsilon}$ beyond the fold point, we consider a section Σ^{in} transverse to S_a defined by $y = y_0, y_0 > 0$ and a section Σ^{out} transverse to the unstable fiber of the fold point defined by $x = x_0, x_0 > 0$. The following result has been proved as Theorem 2.1 in [71].

THEOREM 2.3. *Under the assumptions made in this section there exists $\varepsilon_0 > 0$ such that the following assertions hold for $\varepsilon \in (0, \varepsilon_0]$*

- (1) *The manifold $S_{a,\varepsilon}$ passes through Σ^{out} at a point $(x_0, h(\varepsilon))$, where*

$$h(\varepsilon) = O(\varepsilon^{2/3}).$$

- (2) *Under the flow of system (2.6) the section Σ^{in} is mapped to an interval around $S_{a,\varepsilon} \cap \Sigma^{out}$. The transition map from Σ^{in} to Σ^{out} is a contraction with contraction rate $e^{-c/\varepsilon}$, where c is a positive constant.*

We conclude that for ε small, solutions starting between $S_{a,\varepsilon}$ and $S_{r,\varepsilon}$ are exponentially contracted onto $S_{a,\varepsilon}$, follow the slow flow on $S_{a,\varepsilon}$ downwards, and jump almost horizontally to the right after passing the fold point.

CHAPTER 3

Geometric singular perturbation analysis of an autocatalator model

We consider the planar system of differential equations

$$(3.1) \quad \begin{aligned} \dot{a} &= \mu - a - ab^2, \\ \varepsilon \dot{b} &= -b + a + ab^2, \end{aligned}$$

where $(a, b) \in \mathbb{R}^2$, $\mu \in \mathbb{R}$ and the parameter $\varepsilon > 0$ varies in a small interval around zero. As explained in the introduction, system (3.1) is a model for an autocatalytic chemical process with the variables a and b being scaled concentrations. The autocatalytic nature of the process is modeled by the ab^2 term, i.e., the production rate of b increases linearly with the concentration of b , see e.g. [93], [98]. Naturally the physically meaningful range of the variables is $a, b \geq 0$. Our main result is that for $\mu > 1$ and ε sufficiently small system (3.1) has a globally attracting limit cycle of relaxation type.

This chapter is organized as follows. In Section 3.1 we analyze the dynamics and asymptotic behavior of the autocatalator in the regimes $b = O(1)$ and $b = O(1/\varepsilon)$. Section 3.2 presents the blow-up analysis. In Section 3.3 we prove the existence of a periodic orbit of relaxation type for the blown-up system. Section 3.4 contains some remarks about canard cycles of system (3.1), which occur for $\mu \approx 1$. In order not to interrupt the main argument and to avoid confusing notation the proof of Theorem 3.8 based on a second blow-up procedure is given in Section 3.5.

3.1. Slow-fast analysis of the autocatalator

Due to the occurrence of the small parameter ε solutions evolve on several time scales. System (3.1) is written in the standard form of slow-fast systems with the slow variable a and the fast variable b . The derivative in (3.1) is with respect to slow time scale t . By transforming to the fast variable $\tau := t/\varepsilon$ we obtain the equivalent fast system

$$(3.2) \quad \begin{aligned} a' &= \varepsilon(\mu - a - ab^2), \\ b' &= -b + a + ab^2, \end{aligned}$$

where $'$ denotes differentiation with respect to τ . Setting $\varepsilon = 0$ defines two limiting systems: *the reduced system* (obtained from (3.1))

$$(3.3) \quad \begin{aligned} \dot{a} &= \mu - a - ab^2, \\ 0 &= -b + a + ab^2, \end{aligned}$$

and *the layer problem* (obtained from (3.2))

$$(3.4) \quad \begin{aligned} a' &= 0, \\ b' &= -b + a + ab^2. \end{aligned}$$

In problems of this type the reduced problem captures essentially the slow dynamics and the layer problem captures the fast dynamics.

3.1.1. Regime 1: $b = O(1)$. We begin by discussing some of the basic properties of the layer problem (3.4) and the reduced problem (3.3). The layer problem is a one-dimensional dynamical system in the fast variable b with the slow variable a acting as a parameter. The critical manifold S

$$(3.5) \quad S = \{(a, b) : a - b + ab^2 = 0\}$$

is the manifold of steady states of the layer problem. S is a graph $a = \frac{b}{1+b^2}$, $b \geq 0$, see Figure 3.1. The linearized stability of points in S as the steady states of the layer problem (3.4) is determined by the sign of $\frac{b^2-1}{1+b^2}$; thus, the manifold S consists of an attracting branch S_a with $b < 1$, a repelling branch S_r with $b > 1$, and a non-hyperbolic fold point $p_f = (1/2, 1)$.

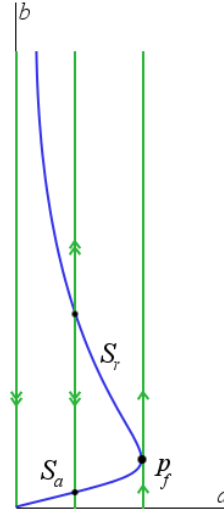


FIGURE 3.1. Critical manifold S and fast flow of the layer problem (3.4).

The slow dynamics of the reduced problem (3.3) on the critical manifold S is obtained by differentiating equation $a = \frac{b}{1+b^2}$ with respect to time t and substituting this expression into $\dot{a} = \mu - a - ab^2$, which gives

$$(3.6) \quad \dot{b} = \frac{1+b^2}{1-b^2}(\mu - b).$$

This system is singular at $b = 1$ and has a steady state for $b = \mu$. Three different cases can be distinguished (depicted in Figure 3.2):

- (1) For $\mu < 1$ the steady state is stable and lies on the attracting critical manifold S_a . All solutions corresponding to $b > \mu$ approach the fold in finite backward time.
- (2) For $\mu = 1$ there is no equilibrium since the singularity in (3.6) at $b = 1$ cancels and the reduced flow passes through the fold point.

- (3) For $\mu > 1$ the steady state is unstable and lies on the repelling manifold S_r . All solutions corresponding to $b < \mu$ approach the fold in finite forward time.

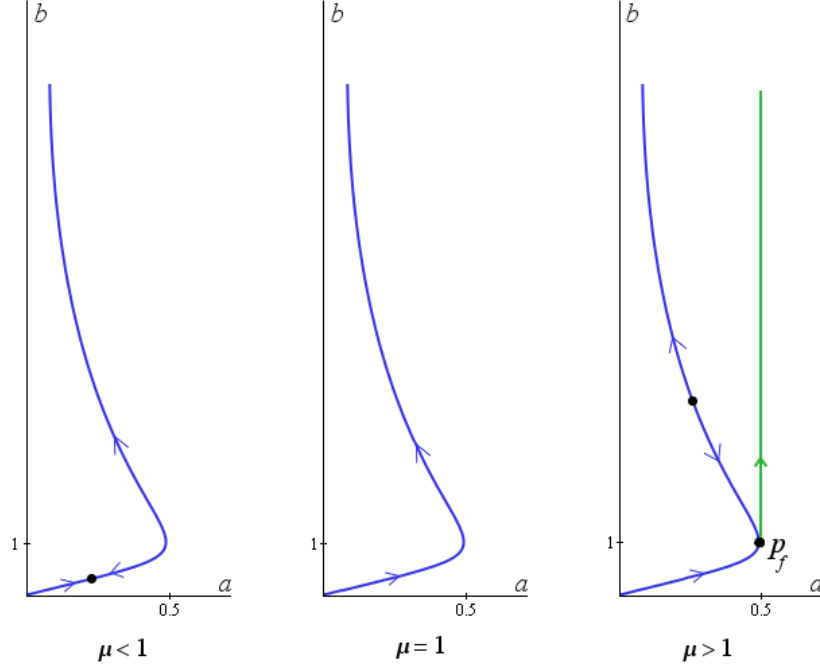


FIGURE 3.2. Dynamics of the reduced problem (3.6) depending on parameter μ .

In this work we focus on the case $\mu > 1$. In the singular limit solutions starting on the left side of S are rapidly attracted to S_a , follow the reduced dynamics until they reach the fold point and then jump up vertically along the orbit $a = \frac{1}{2}$ of the layer problem. Thus, we have the familiar phenomenon of a jump point in Regime 1, see the $\mu > 1$ case in Figure 3.2.

A precise description of the dynamics for $0 < \varepsilon \ll 1$ can be given by combining standard Fenichel theory [34] with the blow-up analysis of planar fold points given in [71]. We conclude from [34] that outside a small neighborhood of the fold point p_f , the manifolds S_a and S_r persist as nearby invariant slow manifolds $S_{a,\varepsilon}$, $S_{r,\varepsilon}$, respectively for ε small, i.e.,

THEOREM 3.1. *For small $\delta > 0$ there exist $\varepsilon_0 > 0$ and smooth functions $b = h_{a,\varepsilon}(a)$ and $b = h_{r,\varepsilon}(a)$ defined on $I_a := [-\delta, \frac{1}{2} - \delta]$ and $I_r := [\delta, \frac{1}{2} - \delta]$, respectively, such that the graphs*

$$S_{a,\varepsilon} = \{(a, b) : b = h_{a,\varepsilon}(a), a \in I_a\}, \quad S_{r,\varepsilon} = \{(a, b) : b = h_{r,\varepsilon}(a), a \in I_r\}$$

are locally invariant attracting, respectively repelling slow manifolds of system (3.1) for $\varepsilon \in (0, \varepsilon_0]$.

At the fold point p_f , where normal hyperbolicity fails, Fenichel theory does not apply. Nevertheless, the description of the dynamics near p_f for $\varepsilon \neq 0$ by using blow-up techniques has been given in [28], [71]. In particular, the asymptotic behavior of the continuation of $S_{a,\varepsilon}$ beyond the fold point has been studied in [71], see Section 3.3.1 for details. Hence, the singular limit behavior described above persists for small ε , i.e. all orbits starting between $S_{a,\varepsilon}$ and $S_{r,\varepsilon}$ are rapidly attracted by $S_{a,\varepsilon}$, follow the slow flow to the right and jump almost vertically to large values of b after passing the fold point, see Sections 3.3.5 and 3.3.1 for a detailed description based on suitably defined transition maps.

This analysis implies that for $\mu > 1$ limit cycles with $b = O(1)$ do not exist. In order to find a cycle for system (3.1) larger values of b must be taken into account.

3.1.2. Regime 2: $b = O(1/\varepsilon)$. For large values of b the cubic terms in (3.1) become dominant and the asymptotic behavior is not correctly described by the layer equations (3.4), i.e., new scales arise and a different asymptotic analysis is needed. This is best seen if the variables are rescaled according to

$$(3.7) \quad a = A, \quad b = \frac{B}{\varepsilon}, \quad T = t/\varepsilon^2.$$

In these variables the equations have the form

$$(3.8) \quad \begin{aligned} A' &= \mu\varepsilon^2 - A\varepsilon^2 - AB^2, \\ B' &= -B\varepsilon + A\varepsilon^2 + AB^2, \end{aligned}$$

where $'$ denotes differentiation with respect to T .

Setting $\varepsilon = 0$ in (3.8) gives

$$(3.9) \quad \begin{aligned} A' &= -AB^2, \\ B' &= AB^2. \end{aligned}$$

The A -axis and B -axis are two lines of equilibria, denoted by l_A and l_B , respectively, which intersect at the origin. Hence, system (3.8) is a singularly perturbed system which, however, is not in standard form since both variables evolve in the $\varepsilon = 0$ problem. Therefore, system (3.9) will be also called layer problem in the following.

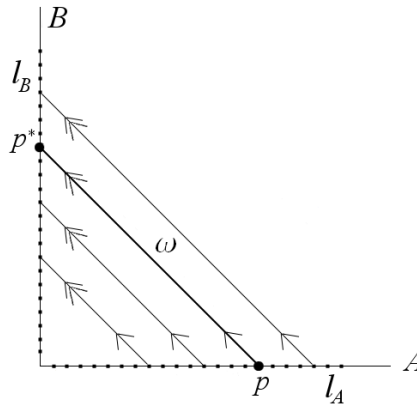


FIGURE 3.3. Dynamics of the layer problem (3.9).

The dynamics of this layer problem is rather simple, see Figure 3.3. The two lines of equilibria are connected by heteroclinic orbits, i.e., an equilibrium $(A_0, 0) \in l_A$ is connected to the equilibrium $(0, A_0) \in l_B$ by an orbit of the layer problem lying on the straight line $B = A_0 - A$.

Outside of a neighborhood of the origin the line l_B is exponentially attracting, whereas the line l_A is non-hyperbolic for the layer problem. Thus, any compact subset of the line l_B that does not contain the origin can be taken as a normally hyperbolic critical manifold M_0 . Then, Fenichel theory [34] implies the existence of a slow manifold M_ε that is a perturbation of M_0 , i.e., lies within $O(\varepsilon)$ of M_0 . More precisely, we have the following result.

THEOREM 3.2. *Let $M_0 = \{(0, B) : B \in [B_0, B_1], B_0 > 0\}$. There exists $\varepsilon_0 > 0$ such that for $\varepsilon \in (0, \varepsilon_0]$ there exists a smooth locally invariant attracting one-dimensional slow manifold M_ε given as a graph*

$$(3.10) \quad M_\varepsilon = \{(A, B) : A = h(B, \varepsilon), B \in [B_0, B_1]\}.$$

The function $h(B, \varepsilon)$ is smooth and has the expansion $h(B, \varepsilon) = \varepsilon^2 \frac{\mu}{B^2} + O(\varepsilon^3)$.

PROOF. The existence of the slow manifold as a graph $A = h(B, \varepsilon)$ follows from Fenichel Theory due to the normal hyperbolicity of M_0 . By plugging the expansion of h in powers of ε into (3.8) and comparing coefficients of powers of ε the expansion (3.10) is easily obtained. \square

The equation governing the slow dynamics on M_ε is found by substituting the function $h(B, \varepsilon)$ into (3.8). Hence, the slow flow on M_ε is governed by the equation

$$(3.11) \quad \frac{dB}{d\tau} = -B + O(\varepsilon),$$

where $\tau = \varepsilon T = t/\varepsilon$. We conclude that B decays exponentially on M_ε .

Thus, Regime 2 provides the following mechanism for obtaining a closed singular cycle. All of Regime 1 is compressed into the non-hyperbolic line of equilibria l_A . In particular, the fold point p_f of the critical manifold S and its fast fiber in Regime 1 collapse into the point $p = (1/2, 0)$. The point p is connected to the point $p^* = (0, 1/2) \in l_B$ by a heteroclinic orbit ω of the layer problem (3.9). From there the singular orbit follows the reduced dynamics (3.11) along the critical manifold M_0 until it reaches the origin. Thus, we introduce the singular cycle $\gamma_0 := S_A \cup \omega \cup S_B$, where S_A is the segment from the origin to p_f on l_A and S_B is the segment from p^* to the origin on l_B .

Note, however, that we have no valid description of the dynamics and asymptotics near the non-hyperbolic line l_A in Regime 2. A full description of the dynamics will be obtained by matching Regime 2 with Regime 1. In fact, we will prove the following theorem.

THEOREM 3.3. *For $\mu > 1$ and ε sufficiently small there exists a unique attracting periodic orbit γ_ε of system (3.8), and hence of the equivalent system (3.1), which tends to the singular cycle γ_0 for $\varepsilon \rightarrow 0$.*

We illustrate these results with numerical simulations obtained by using Mathematica 6. Figure 3.4 shows the limit cycle γ_ε for $\varepsilon = 0.001$ and $\mu = 3$ lying close to the singular cycle γ_0 . In Figure 3.5 the part of γ_ε corresponding to Regime 1 is shown. The solution corresponding to the limit cycle is attracted to the slow manifold, follows the slow manifold and jumps to large values of b after passing the

fold point. The unstable equilibrium is shown in Figure 3.5. Due to the scaling the unstable equilibrium seems to lie on the limit cycle in Figure 3.4.

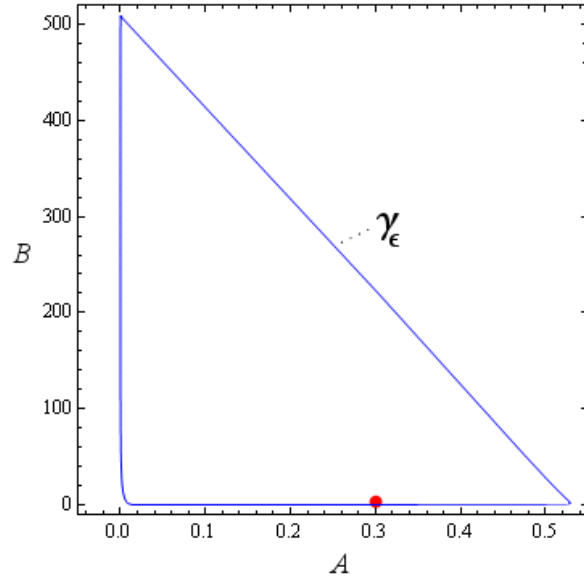


FIGURE 3.4. Limit cycle γ_ϵ for $\epsilon = 0.001$ and $\mu = 3$ of system (3.8).

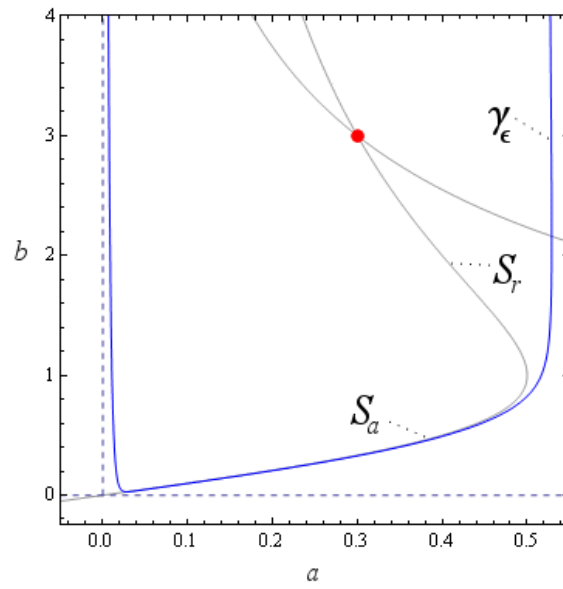


FIGURE 3.5. Part of the limit cycle γ_ϵ for $\epsilon = 0.001$ and $\mu = 3$ in Regime 1.

The matching of Regime 1 with Regime 2 will be done in a geometric way based on the blow-up technique. In the next section, we begin this blow-up analysis by defining a suitable blow-up of the non-hyperbolic line of steady states l_A . We analyze the dynamics of the blown-up system and define a better resolved singular cycle. In Section 3.3 we prove that the singular cycle of the blown-up system persists for $\varepsilon \neq 0$.

3.2. Blow-up analysis

The starting point of our geometric analysis is the rescaled extended system in the form

$$(3.12) \quad \begin{aligned} A' &= \mu\varepsilon^2 - A\varepsilon^2 - AB^2, \\ B' &= -\varepsilon B + A\varepsilon^2 + AB^2, \\ \varepsilon' &= 0. \end{aligned}$$

System (3.12) is viewed as a three dimensional vector field X , i.e., ε is viewed as a variable instead of as a parameter. Note that the planes $\varepsilon = \text{const.}$ are invariant for this three dimensional system. In particular, on the plane $\varepsilon = 0$ the flow is given by the layer problem (3.9). Moreover, $l_A \cup \{0\}$ is a manifold of equilibria for (3.12) and the eigenvalues of the linearization of system (3.12) evaluated at these equilibria are all equal to zero. To overcome this degeneracy we apply the following blow-up transformation

$$(3.13) \quad A = \bar{a}, \quad B = r\bar{b}, \quad \varepsilon = r\bar{\varepsilon}$$

with $\bar{a} \in \mathbb{R}$, $(\bar{b}, \bar{\varepsilon}) \in \mathbb{S}^1 = \{(\bar{b}, \bar{\varepsilon}) \mid \bar{b}^2 + \bar{\varepsilon}^2 = 1\}$, and $r \in \mathbb{R}_0^+$. The blow-up transformation simply introduces polar coordinates in the (B, ε) -plane. For $r > 0$ the blow-up transformation is a diffeomorphism. The preimage of the singular line $l_A \times \{0\}$ is the cylinder $Z = \mathbb{R} \times \mathbb{S}^1 \times \{0\}$, i.e., the singular line $l_A \times \{0\}$ is blown-up to the cylinder Z , see Figure 3.6.

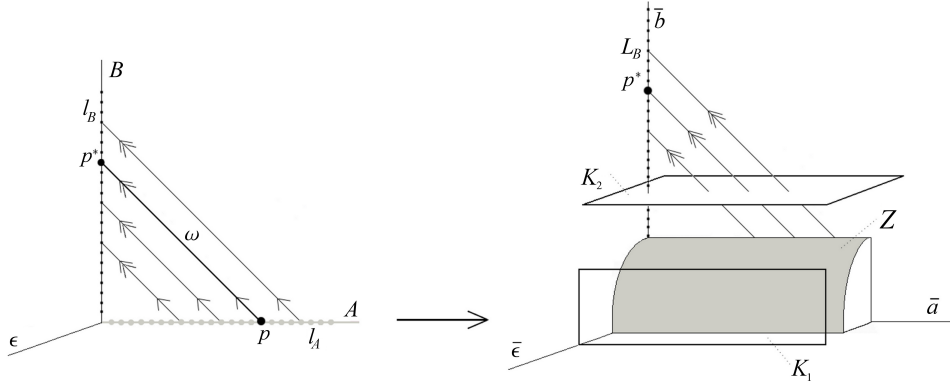


FIGURE 3.6. Blow-up transformation (3.13) for system (3.12) and local charts K_1 and K_2 .

The vector field (3.12) induces a vector field \bar{X} on the blown-up space $\mathbb{R} \times \mathbb{S}^1 \times \mathbb{R}_0^+$. Since the cylinder Z is constructed as the blow-up of a line of equilibria, the blown-up vector field vanishes on the cylinder. To obtain a non-trivial flow on the

cylinder the blown-up vector field must be desingularized by dividing out a factor r .

The blown-up vector field is analyzed in charts K_1 and K_2 defined by setting $\bar{\varepsilon} = 1$ and $\bar{b} = 1$, respectively, in the blow-up transformation (3.13). Thus, chart K_1 covers the front side of the cylinder corresponding to $\bar{\varepsilon} > 0$, while K_2 covers the upper part of the cylinder corresponding to $\bar{b} > 0$, see Figure 3.6. It turns out that after desingularization the blown-up vector field written in chart K_1 is precisely the original system (3.2). Thus, the specific form of the blow-up transformation is directly linked to the form of the rescaling (3.7), see also Remark 3.2 below.

REMARK 3.1. *Intuitively, it is clear that chart K_1 covers Regime 1 and that chart K_2 covers Regime 2. Note, however, that a rigorous perturbation analysis in Regime 1 is only possible for bounded values of b , whereas a rigorous perturbation analysis in Regime 2 is only possible for B bounded away from zero. It is an important property of the blow-up method that these results are recovered in the corresponding charts. In addition, the blow-up method provides a compactification of the region corresponding to unbounded b in Regime 1 and a desingularization of the nonhyperbolic line l_A in Regime 2, which allows to match the two regimes.*

3.2.1. Dynamics in charts. Consider the charts K_1 and K_2 defined by setting $\bar{\varepsilon} = 1$ and $\bar{b} = 1$ respectively, in the blow-up transformation (3.13). Hence, the blow-up transformation in charts K_i , $i = 1, 2$, is given by

$$(3.14) \quad A = a_1, \quad B = r_1 b_1, \quad \varepsilon = r_1,$$

$$(3.15) \quad A = a_2, \quad B = r_2, \quad \varepsilon = r_2 \varepsilon_2.$$

The change of coordinates κ_{12} from K_1 to K_2 is given by

$$(3.16) \quad a_2 = a_1, \quad r_2 = r_1 b_1, \quad \varepsilon_2 = 1/b_1.$$

We denote the inverse transformation of κ_{12} by κ_{21} .

Dynamics in chart K_1 . By inserting (3.14) into system (3.12), we obtain the blown-up system, which is a family of planar vector fields with parameter r_1 , (since $r'_1 = 0$)

$$(3.17) \quad \begin{aligned} a'_1 &= r_1^2(\mu - a_1 - a_1 b_1^2), \\ r_1 b'_1 &= r_1^2(a_1 b_1^2 + a_1 - b_1), \\ r'_1 &= 0. \end{aligned}$$

Now we desingularize the equations by rescaling time $t_1 := r_1 t$, so that the factor r_1 disappears. We obtain

$$(3.18) \quad \begin{aligned} a'_1 &= r_1(\mu - a_1 - a_1 b_1^2), \\ b'_1 &= a_1 - b_1 + a_1 b_1^2, \end{aligned}$$

which is precisely the original system (3.2) with

$$a = a_1, \quad b = b_1, \quad \varepsilon = r_1.$$

Thus, the geometric singular perturbation analysis of Regime 1 is valid on compact regions in chart K_1 .

REMARK 3.2. Writing system (3.12) in chart K_1 corresponds to undoing the scaling (4.3). This explains also the choice of the weights, i.e., the r -factors, in the blow-up transformation (3.13). The blow-up transformation has to be chosen such that the rescaling (4.3) corresponds to the blow-up transformation (3.14) in chart K_1 defined by $\bar{\varepsilon} = 1$.

Dynamics in chart K_2 . Applying transformation (3.15) to system (3.12) and desingularizing by dividing out the factor r_2 , we obtain

$$(3.19) \quad \begin{aligned} a_2' &= -r_2(a_2 + \varepsilon_2^2 a_2 - \varepsilon_2^2 \mu), \\ r_2' &= r_2(a_2 + \varepsilon_2^2 a_2 - \varepsilon_2), \\ \varepsilon_2' &= -\varepsilon_2(a_2 + \varepsilon_2^2 a_2 - \varepsilon_2), \end{aligned}$$

where $'$ denotes differentiation with respect to a rescaled time variable t_2 . System (3.19) has two invariant subspaces, namely the plane $\varepsilon_2 = 0$ and the plane $r_2 = 0$.

The dynamics in the invariant plane $\varepsilon_2 = 0$ is governed by

$$(3.20) \quad \begin{aligned} a_2' &= -a_2 r_2, \\ r_2' &= a_2 r_2. \end{aligned}$$

The r_2 -axis and the a_2 -axis are two lines of equilibria, which we denote by L_B and L_A , respectively. The line L_B corresponds to the normally hyperbolic line l_B . Away from $(a_2, r_2) = (0, 0)$ the line L_B is attracting for the flow in $\varepsilon_2 = 0$. The new line of equilibria L_A is repelling for the flow in $\varepsilon_2 = 0$. Thus, the dynamics in $\varepsilon_2 = 0$ is very similar to the dynamics of the layer problem (3.9), but with the normally hyperbolic line L_A instead of the non-hyperbolic line l_A , see Figure 3.7.

In the invariant plane $r_2 = 0$ system (3.19) reduces to

$$(3.21) \quad \begin{aligned} a_2' &= 0, \\ \varepsilon_2' &= -(a_2 + \varepsilon_2^2 a_2 - \varepsilon_2)\varepsilon_2. \end{aligned}$$

The equilibria of this system are the line L_A and a curve of equilibria corresponding to the critical manifold S from Section 3.1.1. Recall that S consists of an attracting branch S_a and a repelling branch S_r separated by the non-hyperbolic fold point p_f . Within $r_2 = 0$ the line L_A is attracting, i.e., there exist heteroclinic orbits from S_r to L_A in $r_2 = 0$.

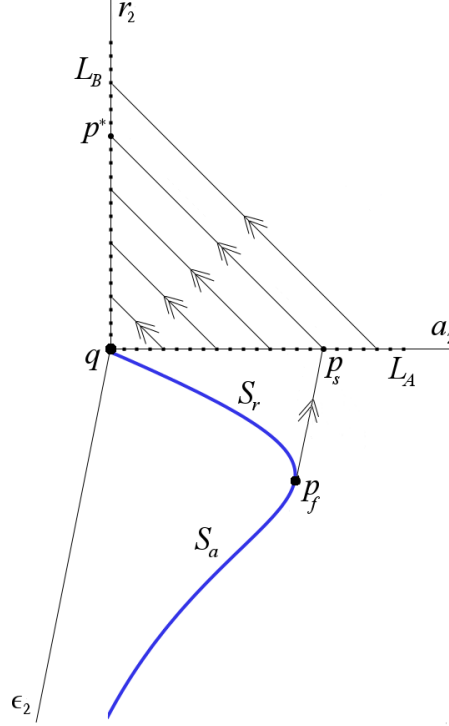
REMARK 3.3. Note that the repelling slow manifold S_r and the unstable fiber of the fold point p_f , which are unbounded in Regime 1, have been compactified in chart K_2 .

LEMMA 3.1. The following assertions hold for system (3.19):

- (1) The linearization at the steady states in L_B has a double zero eigenvalue and a simple eigenvalue $-r_1$ with eigenspaces $\text{span}\{(0, 1, 0)^T, (0, 0, 1)^T\}$ and $\text{span}\{(-1, 1, 0)\}$.
- (2) The line L_A is a line of hyperbolic steady states of saddle type.
- (3) The linearization of the system (3.19) at the origin has a triple zero eigenvalue.

PROOF. Computations. □

Property 1 of the lemma suggests the existence of an attracting two-dimensional invariant manifold containing the line L_B as long as r_2 is bounded away from zero. Since the region $r_2 \geq \delta$ corresponds to $B \geq \delta$, this manifold is precisely the slow manifold described in Theorem 3.2. Thus, we conclude

FIGURE 3.7. Dynamics of system (3.19) in $\varepsilon_2 = 0$ and $r_2 = 0$.

LEMMA 3.2. *Let $\delta > 0$. For $r_2 \geq \delta$ system (3.19) has an exponentially attracting two-dimensional slow manifold M containing the line of equilibria L_B . The manifold M is given as a graph $a_2 = \mu \varepsilon_2^2 + O(r_2^3 \varepsilon_2^3)$. There exists a stable foliation \mathcal{F} with base M and one-dimensional fibers. The contraction along \mathcal{F} in a time interval of length t is stronger than e^{-ct} for any $0 < c < \delta$. For the slow flow on M the variable r_2 is strictly decreasing.*

Note that away from the origin the line L_A has gained hyperbolicity due to the blow up in contrast to the situation for the line l_a for system (3.9). The origin is still a very degenerate equilibrium of system (3.13), which will be studied later by means of further blow-up (Section 3.4).

3.2.2. Dynamics of the blown-up system. The above analysis provides us with the following picture of the dynamics of the blown-up vector field shown in Figure 3.8. We find the critical manifold S with its attracting and repelling branches S_a , S_r on the cylinder and the lines L_B , L_A of equilibria.

There are five particular points, denoted by $p_* \in S_a$, $p_f \in S$, $p_s \in L_A$, $p^* \in L_B$, $q \in L_A \cap L_B \cap S_r$. The point p_f is the fold point of S and the other points are described below. We introduce the following notation: ω_1 is the segment of S_a from p_* to p_f ; ω_2 is the heteroclinic orbit of system (3.20) connecting p_f to p_s ; ω_3 is the union of p_s and the heteroclinic orbit of system (3.21) connecting p_s to p^* ; ω_4 is the segment of L_B connecting p^* to q ; ω_5 is the heteroclinic orbit connecting q with p_* .

on the cylinder $r = 0$, which is described by system (3.20) close to q and by (3.18) close to p_* .

We define the singular cycle $\Gamma_0 = \omega_1 \cup \omega_2 \cup \omega_3 \cup \omega_4 \cup \omega_5$. Note that due to the blow-up the singular cycle γ_0 of Theorem 3.3 has been replaced by the more complicated singular cycle Γ_0 . Due to the improved hyperbolicity properties of Γ_0 we can show that Γ_0 persists as a genuine periodic orbit for ε small. Since $\varepsilon = r\bar{\varepsilon}$ we have to analyze the blown-up vector field for r small or $\bar{\varepsilon}$ small, i.e., close to the cylinder $r = 0$ or close to the invariant plane $\bar{\varepsilon} = 0$, respectively.

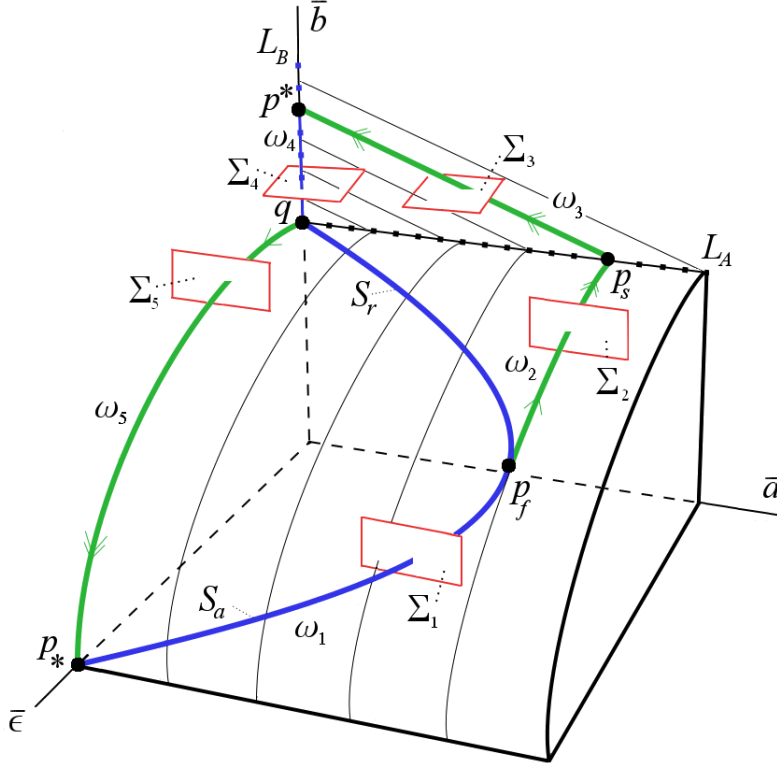


FIGURE 3.8. Dynamics of the blown-up system, singular cycle Γ_0 , and sections.

THEOREM 3.4. *For $\mu > 1$ the blown-up vector field \bar{X} has a family of attracting periodic orbits $\bar{\Gamma}_\varepsilon$ parameterized by $\varepsilon \in (0, \varepsilon_0]$, ε_0 sufficiently small, which for $\varepsilon \rightarrow 0$ tend to the singular cycle $\Gamma_0 = \omega_1 \cup \omega_2 \cup \omega_3 \cup \omega_4 \cup \omega_5$.*

REMARK 3.4. *Theorem 3.3 follows from Theorem 3.4 by applying the blow-up transformation (3.13).*

3.3. Construction of the Poincaré map

In this section we prove Theorem 3.4 by showing that an appropriately defined Poincaré map possesses an attracting fixed point. The Poincaré map will be constructed as the composition of five local transition maps defined in suitable

neighborhoods of the singular cycle Γ_0 . The five local transition maps are discussed in detail in Subsections 3.3.1 – 3.3.5.

We choose sections Σ_i , $i = 1, \dots, 5$ as shown in Figure 3.8, i.e.,
 Σ_1 is transversal to the curve of steady states S_a and close to the fold point p_f ;
 Σ_2 is transversal to the heteroclinic orbit ω_2 and close to p_s ;
 Σ_3 is transversal to the heteroclinic orbit ω_3 and close to the line L_B ;
 Σ_4 is transversal to the line L_B and close to the nilpotent point q ;
 Σ_5 is transversal to the heteroclinic orbit ω_5 and close to q .

The sections Σ_i will be defined more precisely in Subsections 3.3.1 – 3.3.5, where the blown up system is considered in specific charts.

We introduce the following maps defined by the flow of \bar{X} :

$$\begin{aligned} \Pi_1 : \Sigma_1 &\rightarrow \Sigma_2 & - & \text{passage of the fold point } p_f, \\ \Pi_2 : \Sigma_2 &\rightarrow \Sigma_3 & - & \text{passage of the hyperbolic line } L_A, \\ \Pi_3 : \Sigma_3 &\rightarrow \Sigma_4 & - & \text{contraction onto the vertical slow manifold,} \\ \Pi_4 : \Sigma_4 &\rightarrow \Sigma_5 & - & \text{passage of the nilpotent point } q, \\ \Pi_5 : \Sigma_5 &\rightarrow \Sigma_1 & - & \text{contraction onto the attracting slow manifold.} \end{aligned}$$

We will show that the map $\Pi : \Sigma_1 \rightarrow \Sigma_1$ defined as

$$\Pi = \Pi_5 \circ \Pi_4 \circ \Pi_3 \circ \Pi_2 \circ \Pi_1$$

is a contraction with a fixed point.

Let $\delta > 0$, $\beta_1 > 0$, $\beta_2 > 0$ and α_i be fixed small numbers, which will be used in the definition of all sections Σ_i , $i = 1, \dots, 5$.

3.3.1. Analysis of Π_1 – passage of the fold point. The construction of the transition map Π_1 is carried out in chart K_1 , i.e., the dynamics is governed by system (3.18), which is the original system (3.2) with $a = a_1$, $b = b_1$, $\varepsilon = r_1$. We define

$$\Sigma_1 = \{(a_1, b_1, r_1) : a_1 = \tfrac{1}{2} - \delta, b_1 \in [0, \tfrac{1}{2}], r_1 \in [0, \beta_1]\}$$

and

$$\Sigma_2 = \{(a_1, b_1, r_1) : |\tfrac{1}{2} - a_1| \leq \alpha_2, b_1 = 1/\delta, r_1 \in [0, \beta_1]\}.$$

For ε sufficiently small all orbits starting in Σ_1 are rapidly attracted by the slow manifold $S_{a,\varepsilon}$ from Theorem 3.1. The analysis in [71] implies that the continuation of $S_{a,\varepsilon}$ intersects Σ_2 transversally. Hence, the map Π_1 is well defined. By combining the analysis of the generic fold point in [71] with standard Fenichel theory [34] we obtain

THEOREM 3.5. *For fixed $\delta > 0$ there exists $\beta_1 > 0$ such that the transition map*
(3.22)
$$\Pi_1 : \Sigma_1 \rightarrow \Sigma_2$$

is defined. The transition map Π_1 is exponentially contracting, i.e., for r_1 fixed the a_1 component of the map is contracting with rate e^{-c_1/r_1} with a constant $c_1 > 0$.

3.3.2. Analysis of Π_2 – passage of the hyperbolic line L_A . We now analyze the dynamics close to the point $p_s \in L_A$. The construction of the transition map Π_2 is carried out in chart K_2 , i.e., the dynamics is governed by system (3.19).

In K_2 the section Σ_2 is a subset of the plane $\varepsilon_2 = \delta$. We define the section Σ_3 by

$$\Sigma_3 = \{(a_2, r_2, \varepsilon_2) : |\tfrac{1}{2} - a_2| \leq \alpha_3, r_2 = \delta, \varepsilon_2 \in [0, \beta_2]\}.$$

Let $p_0 = (\frac{1}{2}, 0, \delta) \in \Sigma_2$ denote the point, where the singular cycle Γ_0 intersects the section Σ_2 . Let $R_2 \in \Sigma_2$ be an arbitrarily small rectangle centered at p_0 , see Figure 3.9. Recall that the invariant plane $r_2 = 0$ corresponds to the cylinder and that the plane $\varepsilon_2 = 0$ is invariant.

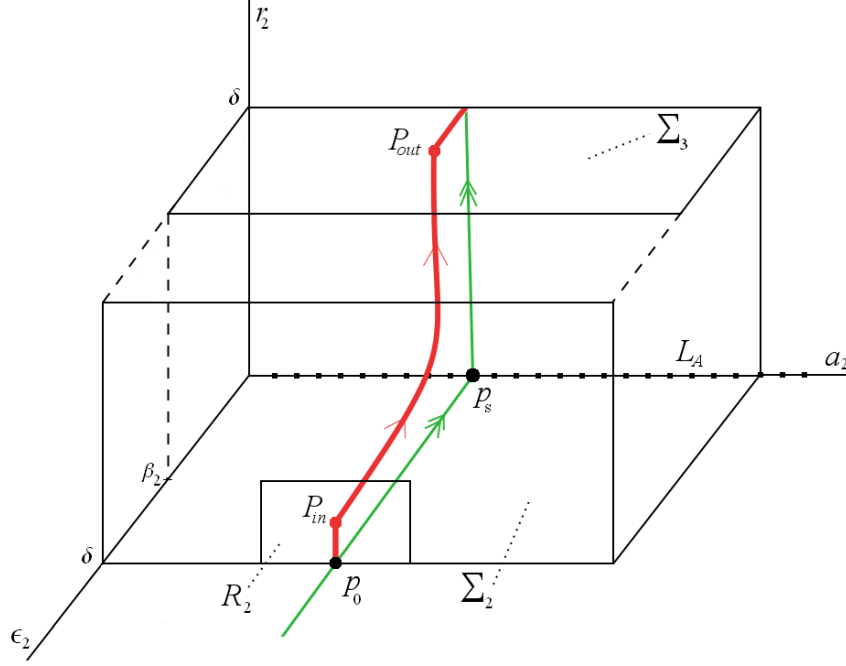


FIGURE 3.9. Passage of the hyperbolic line L_A .

For computational purposes we shift the point p_s to the origin by making the change of coordinates $\tilde{a}_2 = a_2 - \frac{1}{2}$. For the sake of readability we omit the subscript of the variables in this subsection. In these variables the system has the form

$$(3.23) \quad \begin{aligned} \tilde{a}' &= -r - 2r\varepsilon G(\varepsilon, \tilde{a}), \\ r' &= r, \\ \varepsilon' &= -\varepsilon \end{aligned}$$

with

$$G(\tilde{a}, \varepsilon) := \frac{(1 - \mu\varepsilon)}{1 + 2\tilde{a} + 2\varepsilon^2(\tilde{a} + 1/2) - 2\varepsilon},$$

where we have divided the vector field by the factor $F(\tilde{a}, r, \varepsilon) = \tilde{a} + \frac{1}{2} + \varepsilon^2(\tilde{a} + \frac{1}{2}) - \varepsilon$, which does not vanish in a small neighborhood of the origin. For this system the origin is a non-hyperbolic equilibrium whose eigenvalues are $-1, 1, 0$ and are in resonance ($-1 + 1 = 0$). This indicates that the resonant terms in (3.23) cannot be eliminated by a normal form transformation and that the transition map is difficult to compute due to the occurrence of logarithmic terms. However, we are able to show

THEOREM 3.6. *For system (3.19) the transition map*

$$\Pi_2 : R_2 \rightarrow \Sigma_3, \quad (a_{in}, r_{in}, \delta) \mapsto (a_{out}, \delta, r_{in})$$

is well defined for δ small enough and sufficiently small rectangle $R_2 \subset \Sigma_2$, and satisfies

$$(3.24) \quad a_{in} + r_{in} - \delta - 2(1 + c_2)\delta r_{in} \ln r_{in} \leq a_{out} \leq a_{in} + r_{in} - \delta,$$

where the constant $c_2 > 0$ can be made arbitrarily small for δ small. The map Π_2 restricted to the line $r_{in} = \text{const.}$ is at most algebraically expanding.

PROOF. In the proof we use the system (3.23) with the shifted variable $\tilde{a} = a - \frac{1}{2}$. To estimate a_{out} for given $(r_{in}, a_{in}) \in \Sigma_2$ consider a solution $(\tilde{a}, r, \varepsilon)(t)$ of (3.23), which satisfies

$$(3.25) \quad \begin{aligned} \tilde{a}(0) &= \tilde{a}_{in}, & \tilde{a}(T) &= \tilde{a}_{out}, \\ r(0) &= r_{in}, & r(T) &= \delta, \\ \varepsilon(0) &= \delta, & \varepsilon(T) &= \varepsilon_{out}. \end{aligned}$$

The formulas $\varepsilon(t) = \delta e^{-t}$ and $r(t) = r_{in} e^t$ imply that the transition time T is given by

$$(3.26) \quad T = \ln \frac{\delta}{r_{in}}.$$

Since $0 \leq G(\tilde{a}, \varepsilon) \leq 1 + c_2$ with $c_2 > 0$ small for δ small, we obtain the inequality

$$-r_{in} e^t - 2\delta r_{in}(1 + c_2) \leq a' \leq -r_{in} e^t$$

by using the formulas for $r(t)$ and $\varepsilon(t)$. Inequality (3.24) follows by integrating and using the initial conditions and the formula for the transition time.

Since \tilde{a} satisfies the scalar non-autonomous differential equation

$$\tilde{a}' = r_{in} e^t - 2\delta r_{in} G(\delta e^{-t}, \tilde{a}),$$

\tilde{a}_{out} depends Lipschitz continuously on \tilde{a}_{in} on a line $r_{in} = \text{const.}$ with a Lipschitz constant of the order r_{in}^{-L} for some constant L . □

3.3.3. Analysis of Π_3 – contraction towards the vertical slow manifold

M . The construction of the transition map Π_3 is carried out in chart K_2 , i.e., the dynamics is governed by system (3.19) in the variables $(a_2, r_2, \varepsilon_2)$. We define Σ_4 by

$$\Sigma_4 = \{(a_2, r_2, \varepsilon_2) : |a_2| \leq \alpha_4, r_2 = \delta, \varepsilon_2 \in [0, \beta_2]\}$$

with β_2 and $\alpha_4 > 0$ small. For $B = r_2 \geq \delta$ the system is equivalent to system (3.8) and Lemma 3.2 is applicable for $\varepsilon = r_2 \varepsilon_2$ small enough, which can be guaranteed by choosing β_2 small.

We conclude that all orbits starting in Σ_3 are rapidly attracted by the slow manifold M , follow the slow flow downwards, and intersect Σ_4 . More precisely we have

THEOREM 3.7. *For $\delta > 0$ there exists β_2 small enough such that*

(1) *The transition map*

$$\Pi_3 : \Sigma_3 \rightarrow \Sigma_4, \quad (a_{2,in}, \delta, \varepsilon_{2,in}) \mapsto (a_{2,out}, \delta, \varepsilon_{2,in})$$

is well defined. Restricted to lines $\varepsilon_{2,in} = \text{const.}$ in Σ_3 the map Π_3 is contracting with a rate e^{-c_3/ε_2} with $c_3 > 0$ as $\varepsilon_{2,in} \rightarrow 0$.

- (2) The intersection of M with Σ_4 is a smooth curve σ_4 given by $a_2 = \mu\varepsilon_2^2 + O(\varepsilon_2^3\delta^3)$.
- (3) The image $\Pi_3(\Sigma_3)$ is an exponentially thin wedge lying exponentially close to the curve σ_4 .

PROOF. Since $r_{2,in} = r_{2,out} = \delta$ the relation $\varepsilon = r_2\varepsilon_2$ implies $\varepsilon_{2,out} = \varepsilon_{2,in}$. The other assertions of the theorem follow from standard Fenichel theory. \square

3.3.4. Analysis of Π_4 – passage of the nilpotent point q . The construction of the transition map Π_4 is carried out in chart K_2 . We define the section Σ_5

$$\Sigma_5 = \{(a_2, r_2, \varepsilon_2) : |a_2| \leq \alpha_5, r_2 \in [0, \beta_1/\delta], \varepsilon_2 = \delta\}.$$

Let $R_4 \subset \Sigma_4$ be an arbitrarily small rectangle centered at the origin, where the singular cycle Γ_0 intersects Σ_4 .

THEOREM 3.8. *For δ small enough and a sufficiently small rectangle $R_4 \subset \Sigma_4$ the transition map $\Pi_4 : R_4 \rightarrow \Sigma_5$ is a C^1 -map and has the following properties*

- (1) The continuation of M by the flow intersects Σ_5 in a C^1 -curve σ_5 , which is tangent to $r_2 = 0$.
- (2) Restricted to lines $\varepsilon_2 = \text{const.}$ in R_4 the map Π_4 is contracting with a rate e^{-c_4/ε_2} with $c_4 > 0$ as $\varepsilon_{2,in} \rightarrow 0$.
- (3) The image $\Pi_4(R_4)$ is an exponentially thin wedge containing the curve σ_5 .

PROOF. The proof based on blowing up the point q is given in Section 3.5. \square

3.3.5. Analysis of Π_5 – transition towards the attracting slow manifold S_a . We now analyze the transition map from Σ_5 to Σ_1 . This is done in chart K_1 , where the dynamics is described by system (3.18). Recall that system (3.18) is just the original system (3.2), where $\varepsilon = r_1$ is constant along the flow. In K_1 the section Σ_5 is given by

$$\Sigma_5 = \{(a_1, b_1, r_1) : |a_1| \leq \alpha_5, b_1 = 1/\delta, r_1 \in [0, \beta_1]\}.$$

For β_1 small the analysis from Regime 1 implies that all orbits starting from $(a_{in}, \frac{1}{\delta}, \varepsilon) \in \Sigma_5$ are attracted by the slow manifold $S_{a,\varepsilon}$, follow the slow dynamics along $S_{a,\varepsilon}$ and after a while cross the section Σ_1 transversally. More precisely, we have

THEOREM 3.9. *For $\delta > 0$ there exists β_1 small such that*

- (1) The transition map $\Pi_5 : \Sigma_5 \rightarrow \Sigma_1$ is well defined.
- (2) Its restriction to a slice $\varepsilon = \text{const.}$ is a contraction with the contraction rate $O(e^{-c_5/\varepsilon})$, where $c_5 > 0$.
- (3) The image $\Pi_5(\Sigma_5)$ is an exponentially thin wedge lying exponentially close to the smooth curve formed by the intersection of the family $S_{a,\varepsilon}$ with Σ_1 .

3.3.6. Proof of Theorem 3.4.

PROOF. It follows from Theorems 3.5 – 3.9 that for β_1 sufficiently small the transition map $\Pi : \Sigma_1 \rightarrow \Sigma_1$ given by

$$\Pi = \Pi_5 \circ \kappa_{21} \circ \Pi_4 \circ \Pi_3 \circ \Pi_2 \circ \kappa_{12} \circ \Pi_1$$

is well defined. In this formula the coordinate changes are needed because Π_1 and Π_5 have been defined in chart K_1 , while Π_2 , Π_3 and Π_4 have been defined in chart K_2 .

Since ε is a constant of motion for the blown-up system, lines $\varepsilon = \text{const.}$ are invariant under the map Π . Since the maps $\Pi_1, \Pi_3, \Pi_4, \Pi_5$ are exponentially contracting on lines $\varepsilon = \text{const.}$ and Π_2 is at most algebraically expanding, the map Π restricted to $\varepsilon = \text{const.}$ is exponentially contracting. The contraction mapping theorem implies the existence of a unique fixed point corresponding to an exponentially attracting periodic orbit $\bar{\Gamma}_\varepsilon$ of the blown-up vector field close to the singular cycle Γ_0 for ε sufficiently small. \square

3.4. Canard cycles

As the parameter μ passes through $\mu = 1$, the a -nullcline of system (3.1) crosses the fold point p_f of the critical manifold S . According to [71] the non-hyperbolic point p_f is a *canard point* for $\mu = 1$. The corresponding reduced flow on the critical manifold S is smooth at the point p_f and passes through the fold point, see Figure 3.2. It has been shown in [6], [7], [12], [25], [28], and [71] that this configuration implies the existence of canard solutions and the occurrence of a canard explosion for $\mu \approx 1$ and ε small. Canard solutions correspond to situations where the slow manifolds $S_{a,\varepsilon}$ and $S_{r,\varepsilon}$ are exponentially close in a neighborhood of p_f . A canard solution is a solution which is initially attracted by $S_{a,\varepsilon}$, passes the fold point and follows the repelling slow manifold $S_{r,\varepsilon}$ for a while before it is finally repelled from $S_{r,\varepsilon}$. A canard solution which forms a closed cycle is called a canard cycle. Canard explosion is the phenomenon that a small limit cycle is generated in a Hopf-bifurcation at $\mu = \mu_{Hopf}(\varepsilon)$ and grows to a large relaxation cycle as μ varies in an exponentially small interval.

As μ grows the following types of canard cycles of System 3.1 exist, see Figure 3.8:

- (1) Canard cycles corresponding to singular cycles, which start at a point on S_a , pass through p_f , follow S_r , and jump back to the starting point on S_a .
- (2) Canard cycles corresponding to the singular cycle, which start at $p_* \in S_a$, pass through p_f , follow S_r until the point q , and jump back to $p_* \in S_a$.
- (3) Canard cycles corresponding to singular cycles, which start on S_a , pass through p_f , follow S_r , jump to the line L_A , jump to the line L_B , follow the slow flow on L_B downwards to the point q , and jump back to the point $p_* \in S_a$. This type of canards limits on the relaxation cycles corresponding to $\mu > 1$ considered in this paper.

Canard cycles of Type 1 are covered by the results in [71].

Canard cycles of Type 3 can be analyzed by combining results on canard points from [71] with the return mechanism discussed in this paper corresponding to the map $\Sigma_2 \rightarrow \Sigma_5$ (with an in a -direction suitably extended section Σ_2).

The analysis of intermediate canard cycles of Type 2 is more subtle and requires a more detailed analysis of the system from Section 3.5 obtained by blowing up the nilpotent point q , see Figure 3.11.

3.5. Passage of the nilpotent point q

Here we construct the transition map $\Pi_4 : R_4 \rightarrow \Sigma_5$ and prove Theorem 3.8. Since the construction of the transition map Π_4 is done in chart K_2 only, we omit the subscript $_2$ of the variables for the sake of readability. Hence, the governing equations are

$$(3.27) \quad \begin{aligned} a' &= -r(a + \varepsilon^2 a_2 - \varepsilon^2 \mu), \\ r' &= r(a + \varepsilon^2 a_2 - \varepsilon), \\ \varepsilon' &= -\varepsilon(a + \varepsilon^2 a - \varepsilon). \end{aligned}$$

We know from Section 3.2 (Lemma 3.1) that $q = (0, 0, 0)$ is an equilibrium of system (3.27) with a triple zero eigenvalue. To analyze this degenerate equilibrium we again use the blow-up method. We use the radial homogeneous blow-up

$$(3.28) \quad \begin{aligned} a &= \rho \bar{a}, \\ r &= \rho \bar{r}, \\ \varepsilon &= \rho \bar{\varepsilon}, \end{aligned}$$

where $(\bar{a}, \bar{r}, \bar{\varepsilon}) \in \mathbb{S}^2$ and $\rho \in [0, \rho_0]$ for ρ_0 sufficiently small, i.e., the origin is blown-up to a two-sphere, see Figure 3.10. The analysis of the blown-up vector field is

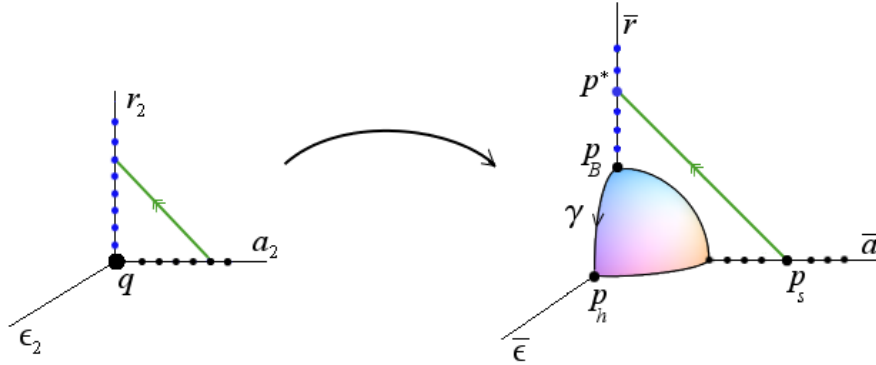


FIGURE 3.10. Blow-up transformation (3.28) for system (3.27).

again carried out in two charts \mathcal{K}_1 and \mathcal{K}_2 defined by setting $\bar{r} = 1$ and $\bar{\varepsilon} = 1$, respectively. The blow-up transformation is given by

$$(3.29) \quad a = \rho_1 a_1, \quad r = \rho_1, \quad \varepsilon = \rho_1 \varepsilon_1,$$

in chart \mathcal{K}_1 and by

$$(3.30) \quad a = \rho_2 a_2, \quad r = \rho_2 r_2, \quad \varepsilon = \rho_2$$

in chart \mathcal{K}_2 . The change of coordinates from \mathcal{K}_1 to \mathcal{K}_2 is given by

$$(3.31) \quad \begin{aligned} \rho_2 &= \varepsilon_1 \rho_1, \\ a_2 &= a_1 \varepsilon_1^{-1}, \\ r_2 &= \varepsilon_1^{-1}. \end{aligned}$$

The section Σ_4 from Subsection 3.3.4 written in chart \mathcal{K}_1 lies in the plane $\rho_1 = \delta$, similarly the section Σ_5 written in chart \mathcal{K}_2 lies in the plane $\rho_2 = \delta$.

The dynamics in chart \mathcal{K}_1 is governed by

$$(3.32) \quad \begin{aligned} a_1' &= -a_1 - a_1^2 + \varepsilon_1 a_1 + \rho_1 \varepsilon_1^2 \mu - \varepsilon_1^2 a_1 \rho_1^2 (a_1 + 1), \\ \rho_1' &= a_1 \rho_1 + \varepsilon_1^2 a_1 \rho_1^3 - \varepsilon_1 \rho_1, \\ \varepsilon_1' &= 2\varepsilon_1(\varepsilon_1 - a_1) - 2\rho_1^2 a_1 \varepsilon_1^3. \end{aligned}$$

We recover the line of steady states $L_B = \{(0, \rho_1, 0), \rho_1 \geq 0\}$ of system (3.27). We denote the steady state at $(0, 0, 0) \in L_B$ by p_B . Furthermore, the planes $\varepsilon_1 = 0$, $\rho_1 = 0$ and the ε_1 - and a_1 -axes are invariant under the flow (3.32).

In chart \mathcal{K}_1 the rectangle R_4 is defined by

$$R_4 = \{(a_1, \rho_1, \varepsilon_1) : a_1 \in [0, \tilde{\alpha}], \rho_1 = \delta, \varepsilon_1 \in [0, \tilde{\alpha}]\}.$$

LEMMA 3.3. *The following assertions hold for system (3.32):*

- (1) *The linearization of system (3.32) at the steady states in L_B has a stable eigenvalue -1 and a double zero eigenvalue. The associated stable and center eigenspaces are $E_b^s = (1, 0, 0)^T$ and $E_b^c = \text{span}\{(0, 0, 1)^T, (0, 1, 0)^T\}$.*
- (2) *There exists a two-dimensional center manifold \mathcal{M} at p_B which contains the line of steady states L_B and the invariant ε_1 -axis. In \mathcal{K}_1 the manifold is given as a graph $a_1 = h(\rho_1, \varepsilon_1) = \mu\rho_1\varepsilon_1^2 + O(\varepsilon_1^3\rho_1^5)$. The center manifold \mathcal{M} can be chosen to be the continuation of M from Lemma 3.2 by the flow.*
- (3) *The manifold \mathcal{M} is an attracting center manifold. All orbits starting from R_4 are exponentially attracted onto \mathcal{M} .*

PROOF. Assertion (1) follows from simple computations. Assertion (2) – (4) follows from center manifold theory [18], [46] applied at the point p_B which has gained an attracting direction due to the blow-up. \square

The dynamics in \mathcal{K}_2 is governed by

$$(3.33) \quad \begin{aligned} a_2' &= a_2^2 - a_2 - a_2 r_2 + r_2 \mu \rho_2 + a_2 \rho_2^2 (a_2 - r_2), \\ r_2' &= -2r_2 + 2a_2 r_2 + 2a_2 r_2 \rho_2^2, \\ \rho_2' &= \rho_2(1 - a_2) - \rho_2^3 a_2. \end{aligned}$$

The system has an equilibrium at the origin, which we denote by p_h . The planes $r_2 = 0$, $\rho_2 = 0$ and the a_2 -, r_2 - and ρ_2 -axes are invariant under the flow.

LEMMA 3.4. *The linearization at the equilibrium p_h is hyperbolic with the eigenvalues -1 , -2 and 1 with eigenvectors $(1, 0, 0)^T$, $(0, 1, 0)^T$ and $(0, 0, 1)^T$, respectively.*

This implies that there exists a heteroclinic orbit γ of the blown-up vector field on the sphere connecting p_B to p_h , which corresponds to the ε_1 -axis in \mathcal{K}_1 and to the r_2 -axis in \mathcal{K}_2 , see Figures 3.10 and 3.11. To prove Theorem 3.8 we have to study how orbits starting in R_4 pass the non-hyperbolic point p_B , follow the heteroclinic orbit across the sphere and exit close to the hyperbolic point p_h where they intersect Σ_5 by following the unstable $\bar{\varepsilon}$ -direction. It turns out that the behavior of all orbits is determined by the behavior of the continuation of the center manifold \mathcal{M} which attracts all other orbits.

To study the dynamics near p_B , we define the section Σ_{loc} in chart \mathcal{K}_1 by

$$\Sigma_{loc} = \{(a_1, \rho_1, \varepsilon_1) : a_1 \in [0, \alpha], \rho_1 \in [0, \delta], \varepsilon_1 = \alpha\}.$$

To study the dynamics near p_h , we define the section Σ_{in} in \mathcal{K}_2 by

$$\Sigma_{in} = \{(a_2, r_2, \rho_2) : a_2 \in [0, \alpha], r_2 = \alpha, \rho_2 \in [0, \delta]\}.$$

In \mathcal{K}_1 the section Σ_{in} lies in the plane $\varepsilon_1 = 1/\alpha$.

The transition map Π_4 will be obtained as the composition of a local transition map π_1 from R_4 to Σ_{loc} , a global transition map π_2 from Σ_{loc} to Σ_{in} and a local transition map π_3 from Σ_{in} to Σ_5 , see Figure 3.11.

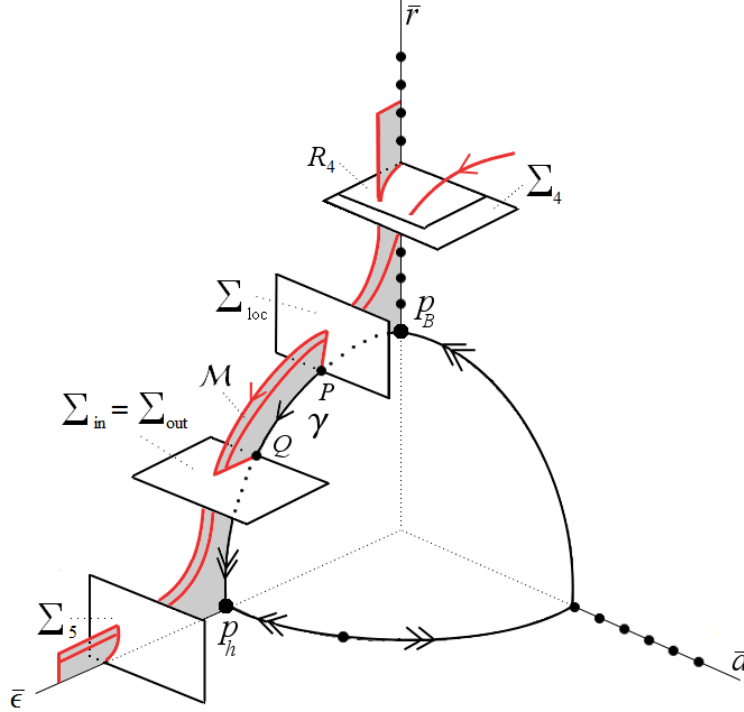


FIGURE 3.11. Blown-up phase space $\mathbb{S}^2 \times [0, \rho_0]$ for system (3.27): sections, slow manifold \mathcal{M} , and an orbit which is attracted to \mathcal{M} .

Analysis of π_1 . Here we work in chart \mathcal{K}_1 . At the point p_B the dynamics of system (3.32) is controlled by the attracting center manifold \mathcal{M} from Lemma 3.3 and we conclude the following.

LEMMA 3.5. *For δ and α sufficiently small the transition map $\pi_1 : R_4 \rightarrow \Sigma_{loc}$ is a smooth map with the properties:*

- (1) *The intersection of \mathcal{M} with Σ_{loc} is a smooth curve given by*

$$a_1 = \mu \rho_1 \alpha^2 + O(\alpha^3 \rho_1^5).$$

- (2) *Restricted to lines $\varepsilon_1 = \text{const.}$ the map π_1 is exponentially contracting with a rate e^{-c/ε_1} with a constant $c > 0$.*

Analysis of π_2 . We are still working in chart \mathcal{K}_1 . In the blown-up system the singular orbit Γ_0 intersects the section Σ_{loc} in the point $P = (0, 0, \alpha)$ and Σ_{in} in the point $Q = (0, 0, \frac{1}{\alpha})$, hence orbits starting in Σ_{loc} intersect Σ_{in} . More precisely, we have

LEMMA 3.6. *For δ and α sufficiently small the map $\pi_2 : \Sigma_{loc} \rightarrow \Sigma_{in}$ is a diffeomorphism. The intersection of the continuation of \mathcal{M} with Σ_{in} is a smooth curve with tangent vector $t_Q = (\sqrt{1/\alpha}, \sqrt{\alpha}, 0)^T$ at the point Q .*

PROOF. For δ and α sufficiently small all orbits starting in Σ_{loc} reach Σ_{in} in finite time hence π_2 is a diffeomorphism.

To have some information on the continuation of \mathcal{M} , we compute the evolution of its tangent space along the heteroclinic orbit γ . We parametrize γ by

$$(3.34) \quad \gamma = \{(0, 0, \varepsilon_1), \varepsilon_1 \in [0, \infty)\},$$

where $\varepsilon_1 = \alpha$ corresponds to the point $P \in \Sigma_{loc}$ and $\varepsilon_1 = \frac{1}{\alpha}$ corresponds to the point $Q \in \Sigma_{in}$. The variational equations along γ are

$$(3.35) \quad \begin{pmatrix} \delta a' \\ \delta \rho' \\ \delta \varepsilon' \end{pmatrix} = \begin{pmatrix} (\varepsilon_1 - 1) & \varepsilon_1^2 \mu & 0 \\ 0 & -\varepsilon_1 & 0 \\ -2\varepsilon_1 & 0 & 4\varepsilon_1 \end{pmatrix} \begin{pmatrix} \delta a \\ \delta \rho \\ \delta \varepsilon \end{pmatrix}$$

coupled to the equation

$$(3.36) \quad \varepsilon_1' = 2\varepsilon_1^2$$

for ε_1 along γ . Due to the invariance of the ε_1 -axis one tangent vector of \mathcal{M} is $(0, 0, 1)^T$. We conclude from Lemma 3.5 that the tangent vector of $\mathcal{M} \cap \Sigma_{loc}$ at the point $P = (0, 0, \alpha)$ is $t_P = (\mu\alpha^2, 1, 0)^T$. Note that the first two equations in (3.35) decouple from the third one. By solving the initial value problem

$$\delta a(\alpha) = \mu\alpha^2, \quad \delta \rho(\alpha) = 1, \quad \delta \varepsilon(\alpha) = 0$$

for (3.35) coupled to the equation (3.36) for $\varepsilon_1 \in [\alpha, \frac{1}{\alpha}]$ we obtain

$$(\delta a, \delta \rho, \delta \varepsilon)(\varepsilon_1) \approx (\sqrt{\varepsilon_1}, \frac{1}{\sqrt{\varepsilon_1}}, *),$$

where the third component $*$ is of no importance since $(0, 0, 1)^T$ is also tangent to \mathcal{M} . Evaluating this expression at $\varepsilon_1 = 1/\alpha$ finishes the proof of the lemma. \square

Analysis of π_3 . We now switch to chart \mathcal{K}_2 to study the transition map $\pi_3 : \Sigma_{in} \rightarrow \Sigma_5$ close to the hyperbolic equilibrium p_h from Lemma 3.4.

We rewrite system (3.33) as

$$(3.37) \quad \begin{aligned} a' &= -aF(a, r, \rho) + r(\mu\rho - a - a\rho^2), \\ r' &= -2rF(a, r, \rho), \\ \rho' &= \rho F(a, r, \rho), \end{aligned}$$

where $F(a, r, \rho) = 1 - a - a\rho^2$ and the subscript $_2$ of the variables is suppressed. In a small neighborhood of the origin the factor F does not vanish. Hence, we transform (3.37) by dividing out F to obtain

$$(3.38a) \quad a' = -a + \frac{r(\mu\rho - a - a\rho^2)}{1 - a - a\rho^2},$$

$$(3.38b) \quad r' = -2r,$$

$$(3.38c) \quad \rho' = \rho,$$

The origin is a hyperbolic equilibrium whose eigenvalues are $-1, -2, 1$. It is easy to see that all orbits starting in Σ_{in} with $\rho > 0$ exit through Σ_5 . Hence, the map π_3 is well defined and can be approximately described by the linearization. However, the eigenvalues are in resonance ($-1 = -2 + 1$), which indicates difficulties in finding a differentiable coordinate change that linearizes the vector field. Within the invariant plane $\rho = 0$ the eigenvalues are -1 and -2 therefore (3.38) can be linearized in the plane $\rho = 0$ by a smooth near identity transformation

$$(3.39) \quad a \rightarrow \Psi(\tilde{a}, r)$$

with $\Psi = \tilde{a} + h(\tilde{a}, r)$, see [108]. A computation shows that $h(\tilde{a}, r) = \frac{1}{2}\tilde{a}r + O(3)$. Under the transformation (3.39) system (3.38) becomes

$$(3.40a) \quad \tilde{a}' = -\tilde{a} + r\rho(\mu + H),$$

$$(3.40b) \quad r' = -2r,$$

$$(3.40c) \quad \rho' = \rho,$$

where $H = H(\tilde{a}, r, \rho) = \tilde{a}h_1 + rh_2 + \tilde{a}\rho h_3$ with bounded smooth functions h_1, h_2, h_3 . After these preliminary transformations we prove the following result.

LEMMA 3.7. *For δ and α sufficiently small the transition map $\pi_3 : \Sigma_{in} \rightarrow \Sigma_5$ for system (3.33) is a C^1 -map and has the form*

$$(3.41) \quad \pi_3(a_{in}, \alpha, \rho_{in}) = \begin{pmatrix} \tilde{\pi}_3(a_{in}, \rho_{in}) \\ \alpha(\frac{\rho_{in}}{\delta})^2 \\ \delta \end{pmatrix}$$

with $\tilde{\pi}_3(a_{in}, \rho_{in})$ given by

$$\tilde{\pi}_3(a_{in}, \rho_{in}) = \frac{\rho_{in}a_{in}}{\delta} - \mu\rho_{in}^2 \ln \rho_{in} + O(\rho_{in}^2).$$

PROOF. In the proof we use system (3.40) to construct the map π_3 . The transition time T needed for a point $(a_{in}, \alpha, \rho_{in}) \in \Sigma_{in}$ to reach Σ_5 under the flow of (3.40) satisfies

$$(3.42) \quad T = \ln\left(\frac{\delta}{\rho_{in}}\right).$$

We compute (ρ_{out}, a_{out}) as a function of $(\rho_{in}, a_{in}) \in \Sigma_{in}$. Substituting exact solutions of (3.40b) and (3.40c) into (3.40a) we obtain

$$(3.43) \quad \tilde{a}' = -\tilde{a} + \mu\alpha\rho_{in}e^{-t} + G,$$

where

$$G = \alpha\rho_{in}e^{-t}H(\alpha e^{-2t}, \rho_{in}e^t, \tilde{a}).$$

The above equation (3.43) is viewed as a small perturbation of

$$(3.44) \quad \tilde{a}'_0 = -\tilde{a}_0 + \mu\alpha\rho_{in}e^{-t}.$$

Equation (3.44) can be solved explicitly,

$$\tilde{a}_0(t) = a_{in}e^{-t} + \mu\alpha\rho_{in}te^{-t}.$$

Suppose the solution of (3.43) has the form

$$(3.45) \quad \tilde{a}(t) = a_{in}e^{-t} + \mu\alpha\rho_{in}te^{-t} + e^{-t}z,$$

where $z(0) = 0$. One gets the following equation for z

$$(3.46) \quad \begin{aligned} z'(t) = & \alpha \rho_{in} [(a_{in} e^{-t} + \mu \alpha \rho_{in} t e^{-t}) h_1 + \alpha e^{-2t} h_2 + (a_{in} \rho_{in} + \mu \alpha \rho_{in}^2 t) h_3] + \\ & + [\alpha \rho_{in} e^{-t} h_1 + \alpha \rho_{in}^2 h_3] z. \end{aligned}$$

We transform the equation (3.46) to the equivalent integral equation of the form (3.47)

$$\begin{aligned} z(T) = & \alpha \rho_{in} a_{in} \int_0^T e^{-t} h_1 dt + \mu \delta^2 \rho_{in}^2 \int_0^T t e^{-t} h_1 dt + \alpha^2 \rho_{in} \int_0^T e^{-2t} h_2 dt \\ & + a_{in} \alpha \rho_{in}^2 \int_0^T h_3 dt + \mu \rho_{in}^3 \alpha^2 \int_0^T t h_3 dt + \alpha \rho_{in} \int_0^T e^{-t} h_1 z dt + \alpha \rho_{in}^2 \int_0^T h_3 z dt. \end{aligned}$$

The bounds for the functions h_i , $i = 1, \dots, 3$ and $T = \ln \frac{\delta}{\rho_{in}}$ imply that the sum of the first five terms is of order $O(\rho_{in})$. Thus, we have

$$(3.48) \quad |z(T)| \leq O(\rho_{in}) + \alpha \rho_{in} K \int_0^T |z| dt$$

with a suitable constant $K > O$. Applying Gronwall's inequality to (3.48) yields to the following result

$$z = O(\rho_{in}).$$

Hence, we obtain

$$(3.49) \quad \tilde{a}(T) = \frac{\rho_{in} a_{in}}{\delta} - \frac{\mu \alpha \rho_{in}^2}{\delta} \ln\left(\frac{\rho_{in}}{\delta}\right) + O(\rho_{in}^2).$$

Finally, due to the corresponding inverse transformation $\tilde{a} = \tilde{\Psi}(a, r) = a + O(ar)$, the transition map is given by

$$\tilde{\pi}_3(a_{in}, \rho_{in}) = \frac{\rho_{in} a_{in}}{\delta} - \mu \rho_{in}^2 \ln \rho_{in} + O(\rho_{in}^2)$$

which implies the lemma. \square

PROOF OF THEOREM 3.8. Lemma 3.5, Lemma 3.6 and Lemma 3.7 imply all assertions of Theorem 3.8 except the tangency of the curve σ_5 with the line $r_2 = 0$.

In chart \mathcal{K}_2 the point Q is given by $(0, \alpha, 0)$ and the tangent vector t_Q of \mathcal{M} is given by $(\sqrt{\alpha}, 0, \frac{1}{\sqrt{\alpha}})^T$. By taking t_Q as a first order approximation of the curve $\mathcal{M} \cap \Sigma_{in}$ and applying the transition map 3.41 we obtain that σ_5 is tangent to $r_2 = 0$. \square

CHAPTER 4

Blowing-up the glycolytic oscillator

In this chapter a detailed geometric analysis of the Goldbeter-Lefever model

$$(4.1) \quad \begin{aligned} \rho\alpha' &= \mu - \phi(\alpha, \gamma), \\ \gamma' &= \lambda\phi(\alpha, \gamma) - \gamma, \end{aligned}$$

with

$$\phi(\alpha, \gamma) = \frac{\alpha^2(\gamma + 1)^2}{L + \alpha^2(\gamma + 1)^2},$$

is given. System (4.1) is a model of glycolytic oscillations with the variables α and γ being certain substrate and product concentrations and four positive parameters L , λ , μ , and ρ . As mentioned in the introduction, in suitably scaled variables the governing equations are a planar system of ordinary differential equations depending singularly on two small parameters ε and δ defined by (1.10) and (1.13), respectively.

In [101] it was argued that a limit cycle of relaxation type exists for $\varepsilon \ll \delta \ll 1$. The existence of this limit cycle is proven in this thesis by analyzing the problem in the spirit of geometric singular perturbation theory. The degeneracies of the limiting problem corresponding to $(\varepsilon, \delta) = (0, 0)$ are resolved by a novel variant of the blow-up method. It is shown that repeated blow-ups lead to a clear geometric picture of this fairly complicated two parameter multi-scale problem.

Chapter 4 is organized as follows. In Section 4.1 we discuss basic properties of the model, in particular, a preliminary slow-fast analysis is given. A more detailed analysis of three scaling regimes is performed in Section 4.2. In Section 4.3 the blow-up analysis is carried out and the existence of a periodic orbit of relaxation type is proven. We have included the discussion of the scaling regimes in Section 4.2 to emphasize that: i) in the blow-up approach to singular perturbation problems with non-hyperbolic critical manifolds results obtained by conventional scaling are recovered in the so-called rescaling charts and ii) matching of the non-overlapping rescaling charts is conveniently carried out in other charts, which are obtained in a natural way from the blow-up construction.

4.1. Scaling properties and singular limits

4.1.1. Basic properties and scaling. We begin by reproducing a numerical simulation of system (4.1) from [101] for the parameter values $L = 5 \times 10^6$, $\rho = 2.5$, $\lambda = 40$, $\mu = 0.15$. The results shown in Figure 4.1 indicate the existence of an attracting periodic solution of relaxation type.

Figure 4.1 illustrates the nullclines in the (α, γ) -plane. Note that in all figures the α -axis is drawn downwards since this leads to better visibility in later figures. Straightforward calculations in [101] prove the following properties. The condition $\lambda > 8$ guarantees that the γ nullcline is a folded curve with fold points B and D . For $\mu < 1$ the nullclines intersect just once in the unique equilibrium point of the

system. The steady state is unstable when it lies between the fold points B and D of the γ -nullcline. This is the situation where a limit cycle is expected to exist. For $\mu = 0.15$ we have this situation. The numerically computed attracting limit cycle is shown in Figure 4.1. The limit cycle is of relaxation type, i.e., the solution follows the left branch of the γ -nullcline until it reaches the fold point B , and from there the solution jumps to a point C on the right branch of the γ -nullcline, then follows the right branch until it reaches the fold point D , from where it jumps back to a point A on the left branch. Here we have followed the notation of [101], where more details can be found.

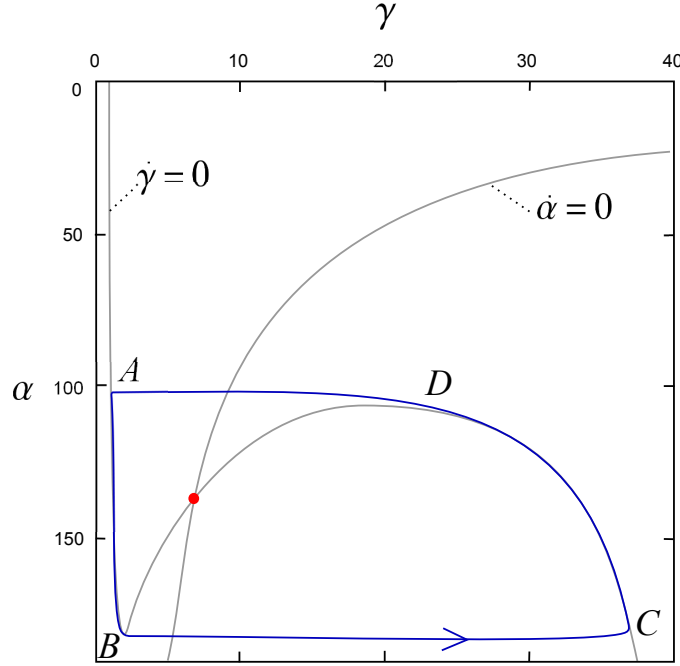


FIGURE 4.1. Nullclines and numerically computed limit cycle for $\mu = 0.15$, $L = 5 \times 10^6$, $\lambda = 40$.

Following [101] our analysis will be based on the assumption that L and λ are large, where L is larger than λ in the sense of condition (1.11). The scaling analysis in [101] is based on the following scaling properties of the points A , B , C , D with respect to L and λ . To leading order these points are

$$(4.2) \quad A \approx \left(\frac{2\sqrt{L}}{\lambda}, 1\right), \quad B \approx \left(\frac{1}{2}\sqrt{\frac{L}{\lambda}}, 1\right), \quad C \approx \left(\frac{1}{2}\sqrt{\frac{L}{\lambda}}, \lambda\right), \quad D \approx \left(\frac{2\sqrt{L}}{\lambda}, \frac{\lambda}{2}\right).$$

To simplify notation, we make the shift $\alpha = \hat{a}$, $\gamma = \hat{b} - 1$, which does not affect the validity of (4.2). Based on the orders of magnitude of B and C we introduce the scaling

$$(4.3) \quad \hat{a} = \sqrt{\frac{L}{\lambda}} a, \quad \hat{b} = \lambda b.$$

For the rest of the paper we set $\rho = 1$ and restrict our attention to the physically meaningful range of the variables $a, b \geq 0$. In these variables system (4.1) has the form

$$(4.4) \quad \begin{aligned} a' &= \varepsilon \left[\mu - \frac{a^2 b^2}{\delta^2 + a^2 b^2} \right], \\ b' &= \frac{a^2 b^2}{\delta^2 + a^2 b^2} - b + \delta^2, \end{aligned}$$

where ε and δ are defined by (1.10) and (1.13), respectively. For computational purposes we prefer to write system (4.4) in the equivalent polynomial form

$$(4.5) \quad \begin{aligned} a' &= \varepsilon [a^2 b^2 (\mu - 1) + \mu \delta^2], \\ b' &= a^2 b^2 (1 - b) + \delta^2 (a^2 b^2 - b + \delta^2). \end{aligned}$$

System (4.5) is obtained by multiplying the right-hand side of (4.4) by the non-vanishing factor $\delta^2 + a^2 b^2$, which leaves the orbits of the system unchanged. The resulting rescaled time variable is denoted by τ .

System (4.5) with ε small is in the standard form of slow-fast systems with slow variable a and fast variable b . By transforming to the slow time scale $t = \varepsilon \tau$ the equivalent system

$$(4.6) \quad \begin{aligned} \dot{a} &= a^2 b^2 (\mu - 1) + \mu \delta^2, \\ \varepsilon \dot{b} &= a^2 b^2 (1 - b) + \delta^2 (a^2 b^2 - b + \delta^2) \end{aligned}$$

is obtained, where the derivative is with respect to the slow time t .

4.1.2. Slow-fast analysis of classical relaxation oscillations for fixed $\delta > 0$. Setting $\varepsilon = 0$ in (4.5) and (4.6) defines two limiting systems: the layer problem

$$(4.7) \quad \begin{aligned} a' &= 0, \\ b' &= a^2 b^2 (1 - b) + \delta^2 (a^2 b^2 - b + \delta^2), \end{aligned}$$

and the reduced problem

$$(4.8) \quad \begin{aligned} \dot{a} &= a^2 b^2 (\mu - 1) + \mu \delta^2, \\ 0 &= a^2 b^2 (1 - b) + \delta^2 (a^2 b^2 - b + \delta^2). \end{aligned}$$

The equation

$$a^2 b^2 (1 - b) + \delta^2 (a^2 b^2 - b + \delta^2) = 0$$

defines the critical manifold S , which is of crucial importance for problems of this type, because it controls the slow and the fast dynamics as explained in the introduction.

Since S is precisely the γ -nullcline in the new variables, it is again a folded curve for $\delta < 1/\sqrt{8}$. The fold points of S are still denoted by B and D , respectively; see Figure 4.2. The points B and D divide S into an attracting left branch S_l , a repelling middle branch S_m , and an attracting right branch S_r , where attracting and repelling refer to the stability properties of points in S considered as steady states of the layer problem (4.7). Since the a -nullcline intersects S only once in the middle branch S_m with $\dot{a} > 0$ on the left of this nullcline, the variable a increases for the reduced flow on S_l and decreases on S_r . Hence, we obtain the following standard scenario of relaxation oscillations for fixed $\delta > 0$. A solution starting close to the point A is attracted by S_l , follows the reduced dynamics on S_l until it reaches the fold point B , jumps from the point B to the point $C \in S_r$, and follows the reduced dynamics on S_r until it reaches the fold point D from where it finally jumps back

to the point A . The closed curve consisting of the segment of S_l from A to B , the heteroclinic orbit of the layer problem (4.7) connecting B to C , the segment of S_r from C to D , and the heteroclinic orbit of the layer problem (4.7) connecting D to A is called a singular cycle Γ_0 .

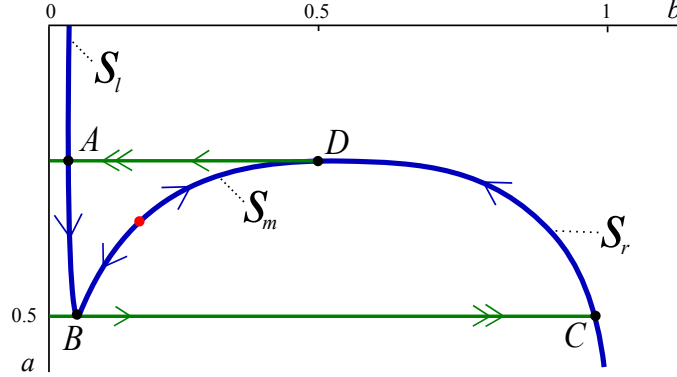


FIGURE 4.2. Critical manifold S and singular cycle Γ_0 .

The situation is essentially as in the classical Van der Pol oscillator [42], [81]. In these works and the references therein, problems of this type have been analyzed by the method of matched asymptotic expansions. The main difficulty in the analysis of relaxation oscillations is the analysis of the behavior of the solutions near the fold points B and D . During the last decade it became clear how to approach these problems in the framework of geometric singular perturbation theory by combining standard Fenichel theory [34] with the blow-up method [28], [71]. The relevant results from geometric singular perturbation theory and the treatment of fold points by the blow-up method are summarized in Chapter 2. Theorem 2.1 in [73] implies the existence of an attracting relaxation cycle of system (4.6) for fixed $\delta > 0$ and sufficiently small ε .

Our main interest will be the analysis of a certain limit, where ε and δ tend to zero simultaneously. For later reference we now change the notation for all the objects introduced in this section by explicitly adding the parameter δ ; i.e., the critical manifold is denoted S^δ , and the points defining the singular cycle Γ_0^δ are denoted by A^δ , B^δ , C^δ , and D^δ , where $\delta \in (0, 1/\sqrt{8})$. The above analysis for $\varepsilon \rightarrow 0$ for δ fixed is highly non-uniform with respect to δ . In particular, the geometry of the critical manifold S^δ depends singularly on δ for $\delta \rightarrow 0$.

4.1.3. The case ε, δ small. It turns out that the limit $(\varepsilon, \delta) \rightarrow (0, 0)$ for system (4.5) is more singular than the limit $\varepsilon \rightarrow 0$ in Subsection 4.1.2. In [101] it is argued that condition (1.11) is sufficient for the existence of a relaxation cycle. We will show that this condition indeed implies the existence of a relaxation cycle.

For $(\varepsilon, \delta) = (0, 0)$ system (4.5) has the simple form

$$(4.9) \quad \begin{aligned} a' &= 0, \\ b' &= a^2 b^2 (1 - b), \end{aligned}$$

which is the layer problem (4.7) with $\delta = 0$. This limiting problem is dynamically fairly degenerate as shown in the following. System (4.9) has a set of equilibria

defined by the equation $a^2b^2(1-b) = 0$, which we denote by S^0 . The critical manifold S^0 of (4.9) consists of the lines $a = 0$, $b = 0$, and $b = 1$, which we denote by l_b , l_a , and l_h , respectively. Since the zeros $a = 0$ and $b = 0$ have multiplicity two, the lines l_a and l_b are non-hyperbolic lines of equilibria, whereas the line l_h corresponding to the simple zero $b = 1$ is normally hyperbolic. The family of critical manifolds S^δ from Subsection 4.1.2 converges to (the more degenerate) critical manifold S^0 as $\delta \rightarrow 0$ in a singular way.

The lines of equilibria l_a and l_h are connected by heteroclinic orbits; i.e., an equilibrium $(a_0, 0) \in l_a$ is connected to the equilibrium $(a_0, 1) \in l_h$ by an orbit of the layer problem lying on the straight line $a = a_0$ (see Figure 4.3). This very degenerate situation allows us to define many singular cycles, consisting of segments of l_h , l_b , l_a , and one heteroclinic orbit of the layer problem. Fenichel theory applies near the normally hyperbolic line l_h , but we have no control of the behavior of the non-hyperbolic lines l_a and l_b for $(\varepsilon, \delta) \neq (0, 0)$.

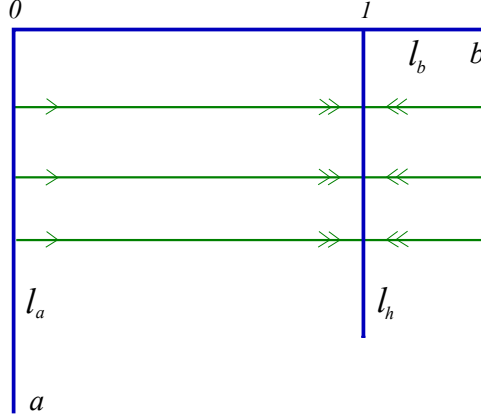


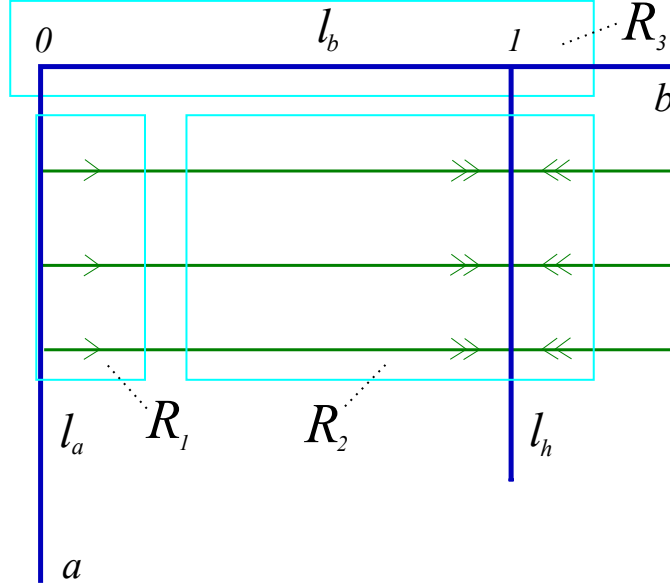
FIGURE 4.3. Critical manifold S^0 of system (4.7).

REMARK 4.1. *In view of the scaling properties (4.2) of the points A, B, C, D the collapse of the folded critical manifold S^δ of system (4.5) for $\delta > 0$ to the more singular “manifold” $S^0 = l_a \cup l_b \cup l_h$ for $\delta = 0$ is not surprising; i.e., roughly speaking, S_l^δ and the left half of S_m^δ are compressed onto l_a , the right half of S_m^δ and the part of S_r^δ corresponding to smaller values of a are compressed onto l_b , while the part of S_r^δ corresponding to larger values of a converges to the line l_h .*

4.2. Scaling regimes

The starting point of the analysis are the equations (4.5), where ε plays the role of a singular perturbation parameter causing the slow-fast structure, while δ affects mainly the shape of the critical manifold S^δ corresponding to $\varepsilon = 0$. For $\delta = 0$ essential parts of the sought limit cycle of system (4.5) are “hidden” in the non-hyperbolic lines l_a and l_b . To make these parts visible we use appropriate rescalings corresponding to the following regimes shown in Figure 4.4 as R_1 , R_2 , and R_3 :

- Regime 1, $a = O(1), b = O(\delta^2)$,
- Regime 2, $a = O(1), b = O(1)$,
- Regime 3, $a = O(\delta), b = O(1)$.

FIGURE 4.4. Scaling regimes R_1 , R_2 , and R_3 .

It will turn out that in Regime 3 the slow-fast structure persists only if the assumption $\varepsilon \ll \delta \ll 1$ is used. Anticipating this we will write

$$(4.10) \quad \varepsilon = \delta \tilde{\varepsilon}$$

in certain places, where $\tilde{\varepsilon} \geq 0$ is still considered as a small parameter.

4.2.1. Regime 1, $a = O(1), b = O(\delta^2)$. We introduce the scaling

$$(4.11) \quad a = a_1, \quad b = \delta^2 b_1.$$

In these variables system (4.5) has the form

$$(4.12) \quad \begin{aligned} a'_1 &= \varepsilon \delta^2 [\delta^2 a_1^2 b_1^2 (\mu - 1) + \mu], \\ \delta^2 b'_1 &= \delta^4 a_1^2 b_1^2 (1 - \delta^2 b_1) + \delta^2 (\delta^4 a_1^2 b_1^2 - \delta^2 b_1 + \delta^2). \end{aligned}$$

By rescaling time we cancel a factor of δ^2 on the right-hand side to obtain the equivalent system

$$(4.13) \quad \begin{aligned} a'_1 &= \varepsilon [\delta^2 a_1^2 b_1^2 (\mu - 1) + \mu], \\ b'_1 &= a_1^2 b_1^2 (1 - \delta^2 b_1) + \delta^2 a_1^2 b_1^2 - b_1 + 1. \end{aligned}$$

This system is a slow-fast system for ε small, which depends regularly on $\delta \in [0, \delta_0]$ for (a_1, b_1) bounded.

For $\varepsilon = 0$ we obtain a new layer problem depending on δ

$$(4.14) \quad \begin{aligned} a'_1 &= 0, \\ b'_1 &= a_1^2 b_1^2 (1 - \delta^2 b_1) + \delta^2 a_1^2 b_1^2 - b_1 + 1. \end{aligned}$$

By setting $\delta = 0$ problem (4.14) simplifies to

$$(4.15) \quad \begin{aligned} a'_1 &= 0, \\ b'_1 &= a_1^2 b_1^2 - b_1 + 1. \end{aligned}$$

The critical manifold S_1^0 of this system defined by $a_1^2 b_1^2 - b_1 + 1 = 0$ has an attracting branch $S_{l,1}^0$ corresponding to $b_1 < 2$, and a repelling part $S_{m,1}^0$ corresponding to $b_1 > 2$, which are separated by a fold point $B_1^0 = (1/2, 2)$. The branch $S_{m,1}^0$ is asymptotic to the b_1 -axis as $b_1 \rightarrow \infty$. An orbit which starts close to the b_1 -axis is rapidly attracted by $S_{l,1}^0$, follows the reduced dynamics until it reaches the fold point from where it jumps to the right along the orbit ω of the layer problem; see Figure 4.5. Thus, we have the situation of a jump point as described in Section 2.5 in Chapter 2. We specify Regime 1 by the conditions $a_1 \in [\alpha_1, 1]$ and $b_1 \in [0, \beta_1]$, with a small constant $\alpha_1 > 0$ and a large constant $\beta_1 > 0$. Regime 1 is shown as a rectangle in Figure 4.5. This gives precise meaning to the assertion that the original variables a, b satisfy $a = O(1)$ and $b = O(\delta^2)$ in Regime 1. On the domain

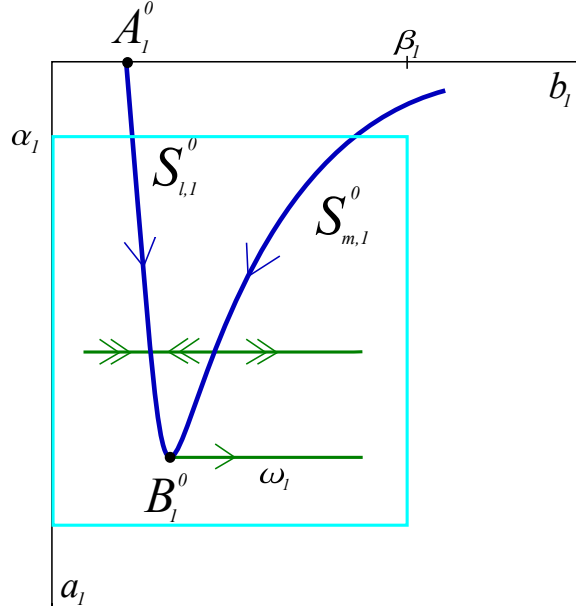


FIGURE 4.5. Critical manifold S_1^0 and fast dynamics in Regime 1.

under consideration, results for $\delta > 0$ follow by regular perturbation theory; i.e., system (4.14) has a folded critical manifold S_1^δ close to S_1^0 with similar dynamics (slow motion on the left branch $S_{l,1}^\delta$ and a fast jump from the point B_1^δ to the right). We conclude from the results described in Section 2.5 in Chapter 2 that the attracting critical manifolds $S_{l,1}^0$ and $S_{l,1}^\delta$ perturb smoothly to attracting slow invariant manifolds for small $\varepsilon > 0$.

REMARK 4.2. The slow manifold S_1^0 is the limit of parts of the rescaled slow manifolds S_l^δ and S_m^δ from Subsection 4.1.1 as $\delta \rightarrow 0$. The fold point B_1^0 corresponds to the fold point B^δ , and the point $A_1^0 = (0, 1)$ corresponds to the point A^δ . In some sense the fold point D^δ corresponds to $b_1 = \infty$ on $S_{m,1}^0$ in the limit $\delta \rightarrow 0$. Hence, the jump back from D^δ to A^δ in Figure 4.1 corresponds to the unbounded stable fiber of the point A_1^0 on the positive b_1 -axis, which is, however, not included in Regime 1 since perturbation methods do not apply there uniformly in (ε, δ) .

4.2.2. Regime 2, $a = O(1), b = O(1)$. In Regime 2 we consider system (4.5) away from the non-hyperbolic lines l_a and l_b , i.e., we consider $a \in [\alpha_2, 1]$ and $b \in [\beta_2, 2]$ with small constants $\alpha_2 > 0, \beta_2 > 0$. Setting $\varepsilon = 0$ in system (4.5) gives the layer problem (4.7). In this regime systems (4.5) and (4.7) depend regularly in δ . For $\delta = 0$ the layer problem (4.7) has the form

$$(4.16) \quad \begin{aligned} a' &= 0, \\ b' &= a^2 b^2 (1 - b). \end{aligned}$$

In the region under consideration the line $l_{h,2}$, defined by $b = 1$, is a normally hyperbolic attracting critical manifold. The reduced flow for system (4.8) on $l_{h,2}$ for $\delta = 0$ is governed by the equation

$$\dot{a} = a^2(\mu - 1);$$

hence, a decreases under the slow flow on $l_{h,2}$, see Figure 4.6.

For $\delta > 0$ the line $l_{h,2}$ perturbs regularly to a part of the normally hyperbolic attracting critical manifold S_r^δ with similar dynamics. Results for $\varepsilon > 0$ follow from standard Fenichel theory uniformly for small δ ; i.e., solutions starting on the left side of $l_{h,2}$ are rapidly attracted by the slow manifold corresponding to $l_{h,2}$ and follow the slow flow.

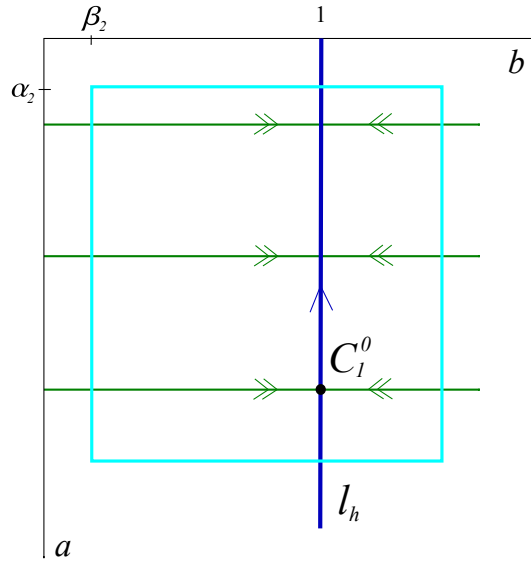


FIGURE 4.6. Critical manifold $l_{h,2}$ and fast dynamics in Regime 2.

REMARK 4.3. In the limit $\delta \rightarrow 0$ the line $l_{h,2}$ corresponds to the part of S_r^δ , where the variable a is large. The point $C_2^0 = (1/2, 1) \in l_{h,2}$ corresponds to the point $C^\delta \in S_r^\delta$. The fold point D^δ is not visible in this regime. Parts of the singular orbit connecting B_1^0 to C_2^0 are visible as the left side of the stable fiber of the point C_2^0 .

4.2.3. Regime 3, $a = O(\delta), b = O(1)$. We use (4.10) and rewrite system (4.5) as

$$(4.17) \quad \begin{aligned} a' &= \tilde{\varepsilon} \delta [a^2 b^2 (\mu - 1) + \mu \delta^2], \\ b' &= a^2 b^2 (1 - b) + \delta^2 (a^2 b^2 - b + \delta^2), \end{aligned}$$

where $\tilde{\varepsilon}$ causes the slow-fast structure, while δ mainly affects the shape of the critical manifold S^δ corresponding to $\tilde{\varepsilon} = 0$.

We use the scaling

$$(4.18) \quad a = \delta a_3, \quad b = b_3$$

with $a_3 \in [0, \alpha_3]$ and $b_3 \in [-0.1, 2]$, with a large constant $\alpha_3 > 0$. In these variables system (4.5) has the form

$$(4.19) \quad \begin{aligned} a'_3 &= \tilde{\varepsilon} [a_3^2 b_3^2 (\mu - 1) + \mu], \\ b'_3 &= a_3^2 b_3^2 (1 - b_3) - b_3 + \delta (a_3^2 b_3^2 + 1), \end{aligned}$$

where we have again divided out a factor δ ; i.e., the derivative is now with respect to the rescaled time variable $\delta\tau$. In the following system (4.19) is considered as a slow-fast system with $\tilde{\varepsilon}$ being a singular perturbation parameter, whereas δ acts as a regular perturbation parameter. This is the place where the condition (1.14) expressed in the form (4.10) is crucial. For $\delta = 0$ the layer problem, obtained from (4.19) by setting $\tilde{\varepsilon} = 0$, has the form

$$(4.20) \quad \begin{aligned} a'_3 &= 0, \\ b'_3 &= a_3^2 b_3^2 (1 - b_3) - b_3. \end{aligned}$$

The critical manifold S_3^0 of (4.20) is defined by the equation

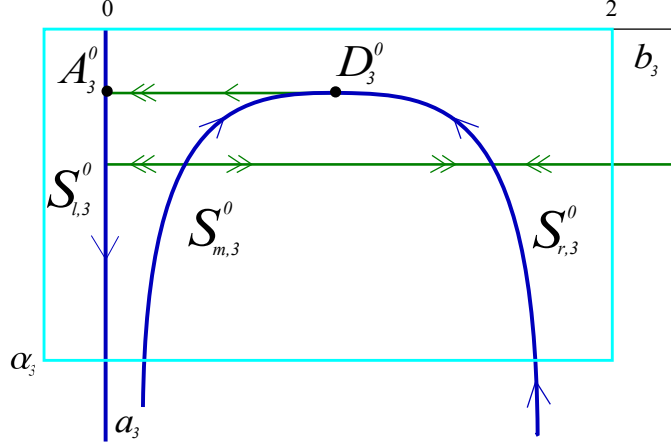
$$b_3 [a_3^2 b_3 (1 - b_3) - 1] = 0.$$

It consists of an attracting branch $S_{l,3}^0$ defined by $b_3 = 0$, and a repelling branch $S_{m,3}^0$ and an attracting branch $S_{r,3}^0$, which are the left and right branches of the curve

$$a_3 = \sqrt{\frac{1}{b_3(1 - b_3)}}$$

corresponding to $b_3 \in (0, 1/2)$ and $b_3 \in (1/2, 1)$, respectively. These branches are separated by the fold point $D_3^0 = (2, 1/2)$ corresponding to the point D^δ ; see Figure 4.7.

It is easy to see that D_3^0 is a jump point. Our main interest is in the singular orbit, which follows the slow flow on $S_{r,3}^0$ until it reaches the fold point D_3^0 from where it jumps to A_3^0 to follow the slow flow on $S_{l,3}^0$. Note that the fast jump from B_3^0 to C_3^0 is not visible in this regime. Since δ acts as a regular perturbation parameter in (4.19), we obtain a slightly perturbed critical manifold S_3^δ with branches $S_{l,3}^\delta$, $S_{m,3}^\delta$, $S_{r,3}^\delta$ and the fold point D_3^δ , which is still a jump point. As before these critical manifolds correspond to parts of the critical manifolds S_l^δ , S_m^δ , and S_r^δ from Subsection 4.1.2.

FIGURE 4.7. Critical manifold S_3^0 and fast dynamics in Regime 3.

Geometric singular perturbation theory is applicable in Regime 3 to obtain rigorous results for small $\tilde{\varepsilon} > 0$ uniformly in $\delta \geq 0$. In particular, we conclude from the results described in Section 2.5 in Chapter 2 that the attracting critical manifolds $S_{r,3}^0$ and $S_{r,3}^\delta$ perturb smoothly to attracting slow invariant manifolds for small $\varepsilon > 0$.

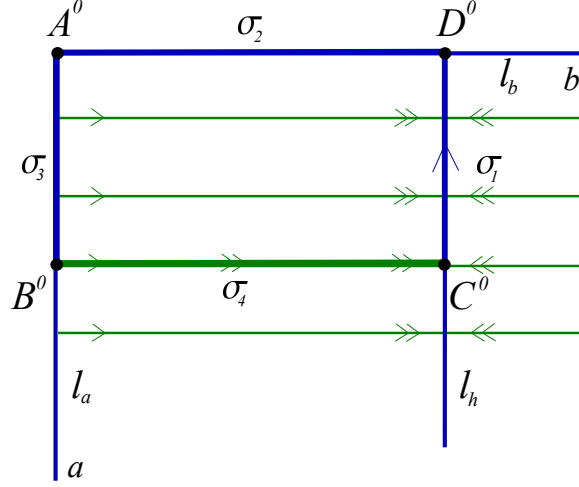
4.2.4. Singular cycles. Based on these results we now define the singular cycle Γ_0^0 of system (4.5) for $(\varepsilon, \delta) = (0, 0)$ as

$$(4.21) \quad \Gamma_0^0 := \sigma_1 \cup \sigma_2 \cup \sigma_3 \cup \sigma_4,$$

where σ_1 is the segment of the slow manifold l_h connecting the points $C^0 = (1/2, 1)$ and $D^0 = (0, 1)$, σ_2 is the segment of the slow manifold l_b connecting the point D^0 with the point $A^0 = (0, 0)$, σ_3 is the segment of the slow manifold l_a connecting the points A^0 to $B^0 = (1/2, 0)$, and σ_4 is the heteroclinic orbit of (4.7) connecting the point B^0 with the point C^0 . Keep in mind that all of Regime 1 collapses onto the non-hyperbolic line l_a , all of Regime 3 collapses onto the non-hyperbolic line l_b , and $\sigma_1, \sigma_2, \sigma_3$ are just sets of equilibria of system (4.9); see Figure 4.8.

The analysis in Regimes 1 – 3 suggests that Γ_0^0 is indeed a good candidate to obtain relaxation oscillations of the form described in Section 4.1 given approximately by slow motion from the point A^δ to B^δ , a fast jump from B^δ to C^δ , slow motion from C^δ to D^δ , and a final jump from D^δ to A^δ for $(\tilde{\varepsilon}, \delta)$ close to $(0, 0)$. The degeneracy of the singular cycle Γ_0^0 and of the non-hyperbolic slow manifolds l_a and l_b has been partially resolved by the scaling methods used in Regimes 1 and 2, respectively. However, uniform perturbation results are possible for Regimes 1 – 3 only in the way they were defined. Note that the domains in the (a, b) -plane corresponding to Regimes 1 – 3 do not overlap. Hence, the perturbation analysis of the singular cycle Γ_0^0 requires a detailed study of extending and matching the individual regimes.

This could possibly be carried out in the framework of classical matched asymptotic expansions, but the procedure would be much more complicated than

FIGURE 4.8. Critical manifold S^0 of system (4.7) and singular cycle Γ_0^0 .

for the — already complicated — case of classical relaxation oscillations. Circumventing these difficulties, the main goal of this work is to show that a geometric approach based on the blow-up method is well-suited to carry out the matching and to provide a comprehensive and clear picture of the global situation in this two-parameter singular perturbation problem.

Our main result is the following theorem.

THEOREM 4.1. *For $\mu < 1$ there exist $\delta_0 > 0$ and $\tilde{\varepsilon}_0 > 0$ such that system (4.5) has a unique attracting periodic orbit $\Gamma_\varepsilon^\delta$ for $0 < \delta \leq \delta_0$ and $0 < \varepsilon \leq \tilde{\varepsilon}_0 \delta$ with the following properties:*

- (1) $\Gamma_\varepsilon^\delta$ tends to Γ_0^δ as $\varepsilon \rightarrow 0$ for $\delta \in (0, \delta_0]$.
- (2) $\Gamma_\varepsilon^\delta$ tends to the singular cycle Γ_0^0 as $(\delta, \varepsilon) \rightarrow (0, 0)$.

PROOF. The assertions of the theorem will follow from Theorem 4.4 by setting $\varepsilon = \tilde{\varepsilon} \delta$ and by applying the blow-up transformations (4.23) and (4.34). \square

4.3. Blow-up analysis

In this section we carry out the blow-up analysis for (4.5). We start by rewriting system (4.5) with $\varepsilon = \tilde{\varepsilon} \delta$ (see (4.10)) as

$$\begin{aligned}
 (4.22) \quad a' &= \tilde{\varepsilon} \delta [a^2 b^2 (\mu - 1) + \mu \delta^2], \\
 b' &= a^2 b^2 (1 - b) + \delta^2 (a^2 b^2 - b + \delta^2), \\
 \delta' &= 0;
 \end{aligned}$$

i.e., we consider (4.22) as a three-dimensional vector field X_ε defined on \mathbb{R}^3 by treating the parameter δ as a variable, while $\tilde{\varepsilon}$ is the singular perturbation parameter causing the slow-fast structure. Obviously, all planes $\delta = \text{const.}$ are invariant for system (4.22). The family of critical manifolds S^δ , $\delta \in [0, \delta_0]$, from Section 4.1.1 and Section 4.2 is now viewed as a two-dimensional critical manifold S . For $\delta > 0$ the critical manifold S has a folded structure, i.e., $S = S_l \cup S_m \cup S_r$ with folds along the curves $F_B := \{(B^\delta, \delta) : \delta \in [0, \delta_0]\}$ and $F_D := \{(D^\delta, \delta) : \delta \in [0, \delta_0]\}$. On the plane

$\delta = 0$ the critical manifold S limits on $S^0 \times \{0\}$ with $S^0 = l_a \cup l_b \cup l_h$. For δ bounded away from zero the results on the existence of slow manifolds and relaxation cycles from Section 4.1.2 can be readily interpreted for analogous two-dimensional objects obtained by adding the δ direction.

It turns out that the main task is to analyze the dynamics close to the degenerate lines $l_a \cup \{0\}$ and $l_b \cup \{0\}$, where for $\tilde{\varepsilon} = 0$ the linearization of system (4.22) at points of $l_a \cup \{0\}$ and $l_b \cup \{0\}$ has a triple zero eigenvalue. This will be achieved by a cylindrical blow-up of the line $l_b \cup \{0\}$ followed by a cylindrical blow-up of the line $l_a \cup \{0\}$, which leads to a desingularization of the extended system (4.22) at $\delta = 0$. Roughly speaking, the non-hyperbolic lines l_a and l_b will be blown-up to cylinders by introducing suitable polar-like coordinates in the directions transverse to the lines. We will see that the blow-up procedure is able to resolve the degeneracies of the original problem. In particular, the critical manifold S of system (4.22) will be blown-up to a critical manifold \bar{S} , which is normally hyperbolic away from the fold curves.

The analysis of the blown-up problem will be carried out in charts $K_1 - K_4$ introduced below. We use the following notation: any object O of the extended system (4.22) is denoted as \bar{O} for the blown-up problem, and by O_i in chart K_i , $i = 1, \dots, 4$. It will turn out that the charts K_1 and K_3 correspond to the scaling Regimes 1 and 3, respectively, and that scaling Regime 2 is covered by parts of chart K_2 (and also by parts of K_4). We will see that chart K_2 and parts of K_4 provide sufficient overlap to match Regimes 1 – 3. We will be able to identify a singular cycle $\bar{\Gamma}_0^0$ of the blown-up system with improved hyperbolicity and transversality properties. Once the correct singular cycle has been found the proof of Theorem 4.1 on the existence of the relaxation cycle can be based on well-established methods from geometric singular perturbation theory.

4.3.1. Blow-up of the non-hyperbolic line $l_b \times \{0\}$. We define the blow-up transformation of the non-hyperbolic line of steady states $l_b \times \{0\}$ by

$$(4.23) \quad \begin{aligned} a &= r\bar{a}, \\ b &= \bar{b}, \\ \delta &= r\bar{\delta} \end{aligned}$$

with $(\bar{a}, \bar{\delta}, r, \bar{b}) \in \mathbb{S}^1 \times \mathbb{R} \times \mathbb{R}$. The line $l_b \times \{0\}$ corresponding to $r = 0$ is blown-up to the cylinder $Z_b := \mathbb{S}^1 \times \{0\} \times \mathbb{R}$, see Figure 4.9.

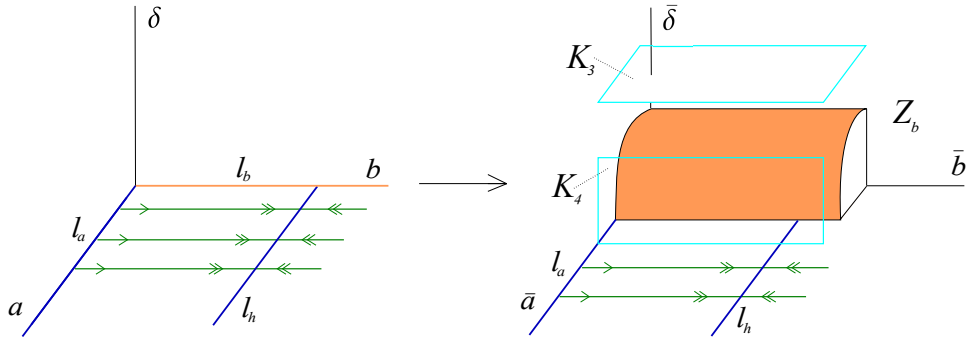


FIGURE 4.9. Blow-up of the non-hyperbolic line $l_b \times \{0\}$.

The vector field (4.22) induces a vector field on the blown-up space $\mathbb{S}^1 \times \mathbb{R} \times \mathbb{R}$. Since the cylinder Z_b is constructed as the blow-up of a line of equilibria, the blown-up vector field vanishes on the cylinder. To obtain a non-trivial flow on the cylinder, the blown-up vector field must be divided by a suitable power of r . Note that $\delta = 0$ in the original system corresponds to either $\bar{\delta} = 0$ or $r = 0$; thus, the dynamics of the blown-up system in the plane $\bar{\delta} = 0$ and on the cylinder Z_b is particularly important.

The blown-up vector field is analyzed in charts K_3, K_4 defined by setting $\bar{\delta} = 1, \bar{a} = 1$, respectively, in the blow-up transformation (4.23); again, see Figure 4.9. Thus, chart K_3 covers the whole upper part of the cylinder corresponding to $\bar{\delta} > 0$, while K_4 covers its front side corresponding to $\bar{a} > 0$. In chart K_3 the blow-up transformation is given by

$$(4.24) \quad a = r_3 a_3, \quad b = b_3, \quad \delta = r_3$$

and in chart K_4 the blow-up transformation is given by

$$(4.25) \quad a = r_4, \quad b = b_4, \quad \delta = r_4 \delta_4.$$

Dynamics in K_3 . Since $r_3 = \delta$, the transformation (4.24) is precisely the scaling transformation (4.18) used in Regime 3. Thus, K_3 is identical to Regime 3. Hence, system (4.22) written in K_3 has the form

$$(4.26) \quad \begin{aligned} a'_3 &= \tilde{\varepsilon}[a_3^2 b_3^2 (\mu - 1) + \mu], \\ b'_3 &= a_3^2 b_3^2 (1 - b_3) - b_3 + r_3 (a_3^2 b_3^2 + 1), \\ r'_3 &= 0, \end{aligned}$$

which is precisely system (4.19) with $\delta = r_3$ and additional equation $r'_3 = 0$. As before $'$ denotes the derivative with respect to the rescaled time scale $r_3 \tau$. System (4.26) is the same as system (4.19); i.e., K_3 corresponds to Regime 3. In this chart the cylinder Z_b corresponds to the plane $r_3 = 0$. Thus, the geometric singular perturbation analysis of Regime 3 with respect to $\tilde{\varepsilon}$ is valid on compact domains. The relevant dynamics on the cylinder is as shown in Figure 4.7.

Dynamics in K_4 . Inserting (4.25) into system (4.22) gives a system of differential equations for r_4, b_4, δ_4 . We obtain

$$(4.27) \quad \begin{aligned} r'_4 &= \tilde{\varepsilon} r_4^3 \delta_4 [b_4^2 (\mu - 1) + \mu \delta_4^2], \\ b'_4 &= r_4^2 [b_4^2 (1 - b_4) + \delta_4^2 (r_4^2 b_4^2 - b_4 + r_4^2 \delta_4^2)], \\ \delta'_4 &= -\tilde{\varepsilon} r_4^2 \delta_4^2 [b_4^2 (\mu - 1) + \mu \delta_4^2]. \end{aligned}$$

By dividing out a factor r_4^2 , we obtain the (partially desingularized) blown-up system

$$(4.28) \quad \begin{aligned} r'_4 &= \tilde{\varepsilon} r_4 \delta_4 [b_4^2 (\mu - 1) + \mu \delta_4^2], \\ b'_4 &= b_4^2 (1 - b_4) + \delta_4^2 (r_4^2 b_4^2 - b_4 + r_4^2 \delta_4^2), \\ \delta'_4 &= -\tilde{\varepsilon} \delta_4^2 [b_4^2 (\mu - 1) + \mu \delta_4^2]. \end{aligned}$$

The derivative in (4.28) is with respect to a rescaled time variable τ_4 . The plane $r_4 = 0$, which corresponds to the cylinder Z_b , and the plane $\delta_4 = 0$ are both invariant under the flow of (4.28). System (4.28) is a singularly perturbed system with slow variables r_4, δ_4 , fast variable b_4 , and singular perturbation parameter $\tilde{\varepsilon}$.

Setting $\tilde{\varepsilon} = 0$ gives the layer problem

$$(4.29) \quad \begin{aligned} r'_4 &= 0, \\ b'_4 &= b_4^2(1 - b_4) + \delta_4^2(r_4^2 b_4^2 - b_4 + r_4^2 \delta_4^2), \\ \delta'_4 &= 0. \end{aligned}$$

The surface defined by

$$(4.30) \quad b_4^2(1 - b_4) + \delta_4^2(r_4^2 b_4^2 - b_4 + r_4^2 \delta_4^2) = 0$$

is denoted by S_4 , since it corresponds to the critical manifold S of system (4.22). Instead of analyzing the equation defining S_4 directly, it is instructive to restrict one's attention to the invariant planes $r_4 = 0$ and $\delta_4 = 0$ of system (4.28).

In the invariant plane $r_4 = 0$ the dynamics is governed by

$$(4.31) \quad \begin{aligned} b'_4 &= b_4^2(1 - b_4) - \delta_4^2 b_4, \\ \delta'_4 &= -\tilde{\varepsilon} \delta_4^2 [b_4^2(\mu - 1) + \mu \delta_4]. \end{aligned}$$

This system is the standard form of slow-fast systems with respect to the small parameter $\tilde{\varepsilon}$, i.e., with slow variable δ_4 and fast variable b_4 . Setting $\tilde{\varepsilon} = 0$ gives the layer problem

$$(4.32) \quad \begin{aligned} b'_4 &= b_4^2(1 - b_4) - \delta_4^2 b_4, \\ \delta'_4 &= 0. \end{aligned}$$

The critical manifold \hat{S}_4 of system (4.32), defined by the equation

$$b_4[b_4(1 - b_4) - \delta_4^2] = 0,$$

consists of the invariant line $b_4 = 0$, denoted by $\hat{S}_{l,4}$, a branch $\hat{S}_{m,4}$, and a branch $\hat{S}_{4,r}$, which are given by

$$\delta_4 = \sqrt{b_4(1 - b_4)}$$

with $b_4 \in [0, 1/2)$ and $b_4 \in (1/2, 1]$, respectively, see Figure 5.15. Obviously, $\hat{S}_{l,4}$, $\hat{S}_{m,4}$, $\hat{S}_{r,4}$ are the branches of the intersection of S_4 with the plane $r_4 = 0$. $\hat{S}_{m,4}$ and $\hat{S}_{r,4}$ are separated by the fold point $D_4^0 = (1/2, 1/2)$. $\hat{S}_{l,4}$ and $\hat{S}_{m,4}$ intersect in the non-hyperbolic point $(0, 0)$. The branch $\hat{S}_{r,4}$ is attracting for the flow in $r_4 = 0$. Similarly, away from the origin the line $\hat{S}_{l,4}$ is attracting, while the branch $\hat{S}_{m,4}$ is repelling. The variable δ_4 increases for the slow flow on $\hat{S}_{r,4}$, while it decreases for the slow flow on $\hat{S}_{l,4}$. Hence, the fold point D_4^0 is a jump point from where a fast jump to the point $A_4^0 = (0, 1/2) \in \hat{S}_{l,4}$ takes place. Note that the origin is still a degenerate steady state of system (4.32).

REMARK 4.4. *The relevant dynamics in chart K_3 takes place in the region $a_3 \geq 1$. Since this region is covered by chart K_4 , chart K_3 is not explicitly needed in our analysis; i.e., the critical manifold S_3^0 corresponds to the parts of \hat{S}_4 with $\delta_4 \geq 1/\alpha_3$ (compare Figure 4.5 with Figure 5.15). Furthermore, the parts of \hat{S}_4 with $\delta_4 \in [0, 1/\alpha_3]$ correspond to the unbounded branches of S_3^0 corresponding to $a_3 \geq \alpha_3$, which had to be excluded from the analysis in Regime 3.*

REMARK 4.5. *It is an important property of the blow-up method that all results which are obtained in the scaling regimes are recovered in some charts, i.e., here in chart K_3 . The power of the blow-up method comes from the fact that other charts, i.e., here chart K_4 , provide a compactification of the unbounded domains in the scaling regimes, where perturbation methods were not applicable.*

In the invariant plane $\delta_4 = 0$ the dynamics is governed by

$$(4.33) \quad \begin{aligned} r_4' &= 0, \\ b_4' &= b_4^2(1 - b_4). \end{aligned}$$

The equilibria of this system are the line $b_4 = 0$ and the line $b_4 = 1$, which we denote by $l_{a,4}$ and $\check{S}_{r,4}$, respectively. Clearly, $l_{a,4}$ and $\check{S}_{r,4}$ are the intersections of S_4 with the plane $\delta_4 = 0$. The curves $\hat{S}_{l,4}$ and $\hat{S}_{m,4}$ meet at the point $\check{q}_4 = (0, 1, 0)$. Similarly, the curves $\hat{S}_{l,4}$, $\hat{S}_{m,4}$ and $l_{a,4}$ intersect in the origin, see Figure 4.10.

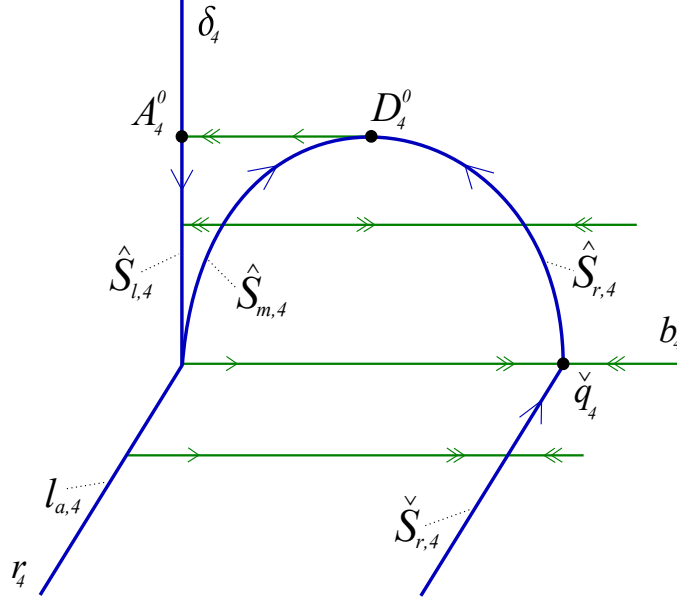


FIGURE 4.10. Dynamics of system (4.28) in $r_4 = 0$ and $\delta_4 = 0$.

From the above discussion we conclude with the following lemma.

LEMMA 4.1. *The critical manifold S_4 described by (4.30) has the following properties at least for r_4 or δ_4 small:*

- (1) S_4 is smooth away from the line $l_{a,4}$.
- (2) S_4 has a folded structure, i.e., $S_4 = S_{l,4} \cup l_{a,4} \cup S_{m,4} \cup F_{D,4} \cup S_{r,4}$, where $S_{m,4}$ and $S_{r,4}$ are separated by the fold curve $F_{D,4}$ while the branches $S_{l,4}$ and $S_{m,4}$ intersect cusp-like along $l_{a,4}$. The branches $S_{l,4}$ and $S_{r,4}$ are attracting and $S_{m,4}$ is repelling for the layer problem (4.29).
- (3) The branch $S_{r,4}$ limits on $\hat{S}_{r,4}$ for $r_4 = 0$ and on $\check{S}_{r,4}$ for $\delta_4 = 0$. Similarly, $S_{m,4}$ limits on $\hat{S}_{m,4}$ for $r_4 = 0$ and on $l_{a,4}$ for $\delta_4 = 0$. $S_{l,4}$ limits on $\hat{S}_{l,4}$ for $r_4 = 0$ and on $l_{a,4}$ for $\delta_4 = 0$. The fold curve $F_{D,4}$ limits on D_4^0 (see Figure 4.10).

PROOF. Outside a neighborhood of the line $l_{a,4}$ the assertions of the lemma follow from the implicit function theorem and the structural stability of folds. The properties of the critical manifold S_4 close to the line $l_{a,4}$ will be proved in Subsection 4.3.2. \square

Summing up, the singular relaxation cycle $\Gamma_{0,4}^0$ in chart K_4 consists of slow motion along the branch $\hat{S}_{r,4}$, followed by slow motion along $\hat{S}_{r,4}$ from the point \tilde{q}_4 to the fold point D_4^0 , a fast jump from the point D_4^0 to the point A_4^0 , and slow motion along the branch $\hat{S}_{l,4}$ from the point A_4^0 to the origin, followed by (not yet analyzed) slow motion along the line $l_{a,4}$; see Figure 4.10. Since the linearization of system (4.28) at points in the line $l_{a,4}$ has a triple zero eigenvalue for $\tilde{\varepsilon} = 0$, the line $l_{a,4}$ is still degenerate. The geometry of the critical manifold S_4 and the dynamics in a neighborhood of the line $l_{a,4}$ will be studied by means of a further blow-up in the following.

4.3.2. Blow-up of the non-hyperbolic line $l_{a,4}$. To study the dynamics of system (4.28) close to the non-hyperbolic line $l_{a,4}$, we introduce the blow-up transformation

$$(4.34) \quad \begin{aligned} r_4 &= \bar{r}, \\ b_4 &= \rho^2 \bar{b}, \\ \delta_4 &= \rho \bar{\delta} \end{aligned}$$

with $(\bar{b}, \bar{\delta}, \rho, \bar{r}) \in \mathbb{S}^1 \times \mathbb{R} \times \mathbb{R}$. By this construction the line $l_{a,4}$ is blown-up to the cylinder $Z_a := \mathbb{S}^1 \times \{0\} \times \mathbb{R}$; see Figure 4.11.

The vector field (4.28) induces a vector field on the blown-up space $\mathbb{S}^1 \times \mathbb{R} \times \mathbb{R}$, which again leaves the cylinder Z_a invariant. The analysis of this blown-up vector field is performed in local charts K_1, K_2 , which are defined by setting $\bar{\delta} = 1$, $\bar{b} = 1$, respectively, in the blow-up transformation (4.34). Chart K_1 covers the upper part of the cylinder Z_a corresponding to $\bar{\delta} > 0$, while K_2 covers its front side corresponding to $\bar{b} > 0$. In chart K_1 the blow-up transformation is given by

$$(4.35) \quad r_4 = r_1, \quad b_4 = \rho_1^2 b_1, \quad \delta_4 = \rho_1,$$

and in chart K_2 the blow-up transformation is given by

$$(4.36) \quad r_4 = r_2, \quad b_4 = \rho_2^2, \quad \delta_4 = \rho_2 \delta_2.$$

Dynamics in K_1 . By inserting the transformation (4.35) into system (4.28) and dividing out a factor of ρ_1^2 , we obtain the final desingularized blown-up system

$$(4.37) \quad \begin{aligned} r_1' &= \tilde{\varepsilon} r_1 \rho_1 [\rho_1^2 b_1^2 (\mu - 1) + \mu], \\ b_1' &= 2\tilde{\varepsilon} \rho_1 [\rho_1^2 b_1^2 (\mu - 1) + \mu] + b_1^2 (1 - \rho_1^2 b_1) + \rho_1^2 r_1^2 b_1^2 - b_1 + r_1^2, \\ \rho_1' &= -\tilde{\varepsilon} \rho_1^2 [\rho_1^2 b_1^2 (\mu - 1) + \mu]. \end{aligned}$$

System (4.37) is a singularly perturbed system with slow variables r_1, ρ_1 , fast variable b_1 , singular perturbation parameter $\tilde{\varepsilon}$, and the layer problem

$$(4.38) \quad \begin{aligned} r_1' &= 0, \\ b_1' &= b_1^2 (1 - \rho_1^2 b_1) + \rho_1^2 r_1^2 b_1^2 - b_1 + r_1^2, \\ \rho_1' &= 0. \end{aligned}$$

The layer problem (4.38) has a two-dimensional critical manifold S_1 described by the equation

$$(4.39) \quad b_1^2 (1 - \rho_1^2 b_1) + \rho_1^2 r_1^2 b_1^2 - b_1 + r_1^2 = 0.$$

As before, we first restrict our attention to the invariant planes, namely, the plane $r_1 = 0$, which corresponds to a region in the front of the cylinder Z_b of the first blow-up, and the plane $\rho_1 = 0$ corresponding to the cylinder Z_a .

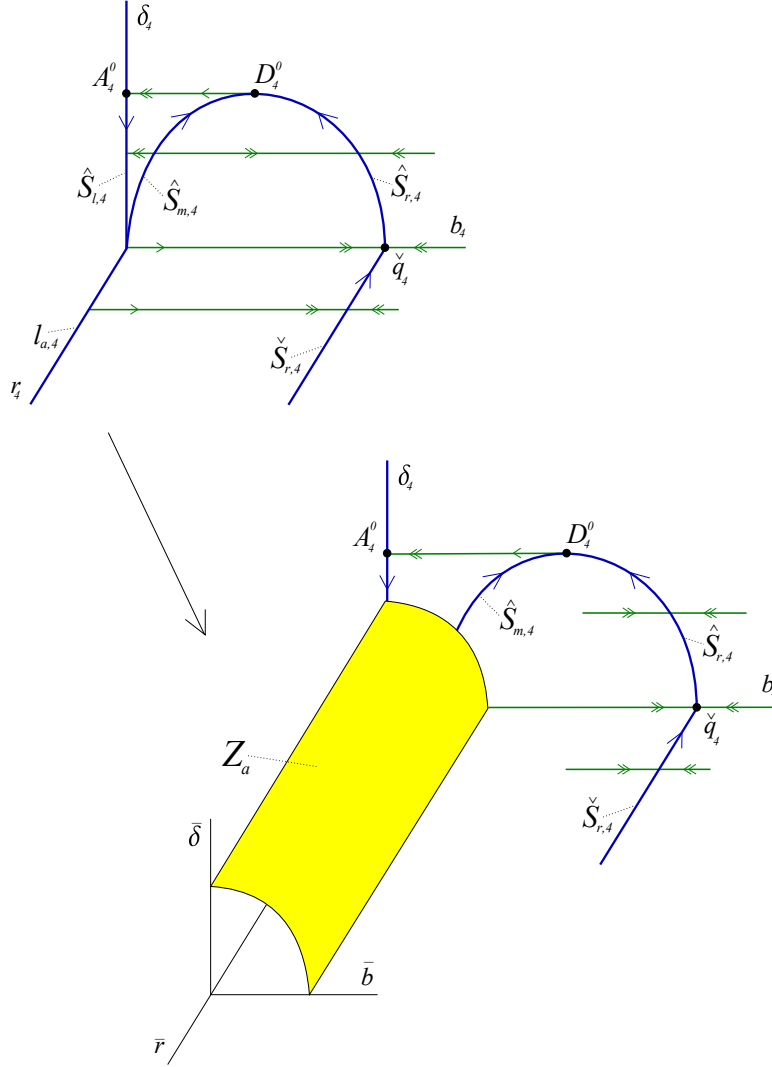


FIGURE 4.11. Blow-up transformation (4.34) for system (4.28).

In the invariant plane $r_1 = 0$ the dynamics is governed by

$$\begin{aligned}
 (4.40) \quad b_1' &= 2\tilde{\varepsilon}\rho_1[\rho_1^2 b_1^2(\mu - 1) + \mu] + b_1^2(1 - \rho_1^2 b_1) - b_1, \\
 \rho_1' &= -\tilde{\varepsilon}\rho_1^2[\rho_1^2 b_1^2(\mu - 1 + \mu)],
 \end{aligned}$$

which is a slow-fast system with singular perturbation parameter $\tilde{\varepsilon}$, fast variable b_1 and slow variable ρ_1 . The corresponding layer problem ($\tilde{\varepsilon} = 0$) has the form

$$\begin{aligned}
 (4.41) \quad b_1' &= b_1^2(1 - \rho_1^2 b_1) - b_1, \\
 \rho_1' &= 0.
 \end{aligned}$$

The corresponding critical manifold \hat{S}_1 , defined by the equation

$$b_1[b_1(1 - \rho_1^2 b_1) - 1] = 0,$$

consists of a stable branch $\hat{S}_{l,1}$ with $b_1 = 0$, and an unstable branch $\hat{S}_{m,1}$ and a stable branch $\hat{S}_{r,1}$ given by $\rho_1 = \sqrt{\frac{1}{b_1} - \frac{1}{b_1^2}}$ with $b_1 \in [1, 2)$ and $b_1 \in (2, \infty)$, respectively. The fold point $D_1^0 = (2, 1/2)$ separates the branches $\hat{S}_{m,1}$ and $\hat{S}_{r,1}$; see Figure 4.12. Again, $\hat{S}_{l,1}$, $\hat{S}_{m,1}$ and $\hat{S}_{r,1}$ are the branches of the intersection of S_1 with the plane $r_1 = 0$.

REMARK 4.6. *The configuration in the plane $r_1 = 0$ of chart K_1 is a desingularized version of the configuration in the plane $r_4 = 0$ of chart K_4 . The degenerate equilibrium at the origin of system (4.32) has been blown-up to the line $\rho_1 = 0$ (which is in fact the circle $\mathbb{S}^1 \times \{0\} \times \{0\}$ on the cylinder of the second blow-up). The branches $\hat{S}_{l,1}$ and $\hat{S}_{m,1}$, which intersected in chart K_4 , have been separated and are attracting and repelling, respectively. Their endpoints in the plane $r_1 = 0$ are denoted by $\hat{p}_1 = (0, 0)$ and $\hat{q}_1 = (1, 0)$.*

In the invariant plane $\rho_1 = 0$ system (4.37) reduces to

$$(4.42) \quad \begin{aligned} r_1' &= 0, \\ b_1' &= b_1^2 - b_1 + r_1^2. \end{aligned}$$

The equilibria of system (4.42) are given by the curve $r_1 = \sqrt{b_1 - b_1^2}$. This curve, denoted by \check{S}_1 , consists of a stable branch $\check{S}_{l,1}$ corresponding to $b_1 \in [0, 1/2)$, a repelling branch $\check{S}_{m,1}$ corresponding to $b_1 \in (1/2, 1]$, and the fold point $B_1^0 = (1/2, 1/2)$; see Figure 4.12. Clearly, $\check{S}_{l,1}$ and $\check{S}_{m,1}$ are the branches of the intersection of S_1 with the plane $\rho_1 = 0$.

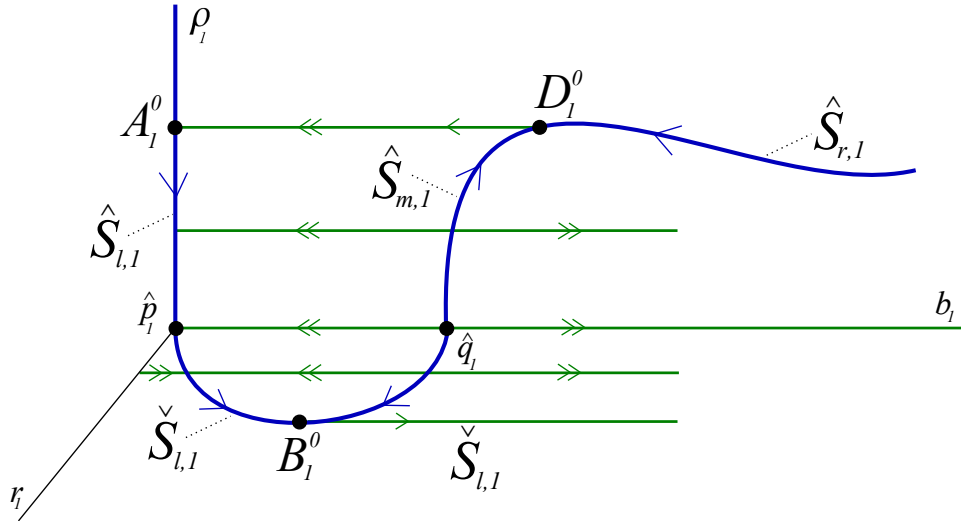


FIGURE 4.12. Dynamics in K_1 .

REMARK 4.7. *Chart K_1 covers essentially Regime 1. In particular, the manifold \check{S}_1 described above is precisely the critical manifold S_1^0 of system (4.13) from Regime 1.*

REMARK 4.8. Note that for $\rho_1 = 0$ the reduced (slow) vector fields with respect to $\tilde{\varepsilon}$ on $\tilde{S}_{l,1}$ and $\tilde{S}_{m,1}$ (on the corresponding slow manifolds) vanish identically. Hence, the fold point B_1^0 is not a jump point. This apparent difficulty is in some sense an artefact caused by setting $\varepsilon = \tilde{\varepsilon}\delta$, which is needed in Regime 3, but not in Regime 1, see also the proof of Lemma 4.6.

As before we conclude with the following lemma.

LEMMA 4.2. The critical manifold S_1 defined by (4.39) has the following properties at least for r_1 or ρ_1 small:

- (1) S_1 is smooth.
- (2) S_1 has a folded structure, i.e., $S_1 = S_{l,1} \cup F_{B,1} \cup S_{m,1} \cup F_{D,1} \cup S_{r,1}$, where $S_{l,1}$ and $S_{r,1}$ are attracting and $S_{m,1}$ is repelling for the layer problem (4.38). The branches $S_{l,1}$ and $S_{m,1}$ are separated by the fold curve $F_{B,1}$, while $S_{m,1}$ and $S_{r,1}$ are separated by the fold curve $F_{D,1}$.
- (3) The branch $S_{l,1}$ limits on $\hat{S}_{l,1}$ for $r_4 = 0$ and on $\tilde{S}_{l,1}$ for $\rho_1 = 0$. Similarly, $S_{m,1}$ limits on $\hat{S}_{m,1}$ for $r_1 = 0$ and on $\tilde{S}_{m,1}$ for $\rho_1 = 0$. $S_{r,1}$ limits on $\hat{S}_{r,1}$ for $r_1 = 0$. The fold curve $F_{D,1}$ limits on D_1^0 , and the fold curve $F_{B,1}$ limits on B_1^0 (see Figure 4.12).

Summing up, the singular relaxation cycle $\Gamma_{0,1}^0$ in chart K_1 follows the slow dynamics along the branch $\hat{S}_{r,1}$ to the fold point D_1^0 , the fast orbit from the point D_1^0 to the point A_1^0 , and the branch $S_{l,1}$ from the point A_1^0 to the point B_1^0 through the point \hat{p}_1 , and finally jumps to the right from the point B_1^0 . To see how the singular orbit continues for large b_1 , we have to switch to chart K_2 .

Dynamics in K_2 . By inserting transformation (4.36) into system (4.28) and dividing out a factor of ρ_2^2 , we obtain the final desingularized blown-up system written in chart K_2

$$\begin{aligned}
 (4.43) \quad r'_2 &= \tilde{\varepsilon} r_2 \rho_2 \delta_2 [\rho_2^2 (\mu - 1) + \mu \delta_2^2], \\
 \rho'_2 &= \frac{1}{2} \rho_2 [1 - \rho_2^2 + \delta_2^2 (r_2^2 \rho_2^2 - 1 + r_2^2 \delta_2^2)], \\
 \delta'_2 &= -\tilde{\varepsilon} \rho_2 \delta_2^2 [\rho_2^2 (\mu - 1) + \mu \delta_2^2] - \frac{1}{2} \delta_2 [1 - \rho_2^2 + \delta_2^2 (r_2^2 \rho_2^2 - 1 + r_2^2 \delta_2^2)].
 \end{aligned}$$

System (4.43) is a singularly perturbed system with singular perturbation parameter $\tilde{\varepsilon}$. Setting $\tilde{\varepsilon} = 0$ gives the layer problem

$$\begin{aligned}
 (4.44) \quad r'_2 &= 0, \\
 \rho'_2 &= \frac{1}{2} \rho_2 [1 - \rho_2^2 + \delta_2^2 (r_2^2 \rho_2^2 - 1 + r_2^2 \delta_2^2)], \\
 \delta'_2 &= -\frac{1}{2} \delta_2 [1 - \rho_2^2 + \delta_2^2 (r_2^2 \rho_2^2 - 1 + r_2^2 \delta_2^2)].
 \end{aligned}$$

The layer problem (4.44) has a 2-dimensional critical manifold S_2 described by the equation

$$(4.45) \quad 1 - \rho_2^2 + \delta_2^2 (r_2^2 \rho_2^2 - 1 + r_2^2 \delta_2^2) = 0.$$

Additionally, there exists a line of equilibria l_2 defined by $\delta_2 = 0, \rho_2 = 0$, i.e. l_2 is the r_2 -axis.

REMARK 4.9. All of the critical manifold S_2 has already been covered in chart K_1 and K_4 . The following discussion of S_2 is included just for completeness. The important dynamics occurs close to the line l_2 , which is not visible in other charts

and provides the so far missing overlap between chart K_1 and K_4 (i.e., Regime 1 and 3).

REMARK 4.10. Note that away from S_2 , ρ_2 and δ_2 are fast variables. This shows that system (4.43) is not in the standard form (2.6) of slow-fast systems. However, Fenichel theory applies in this more general situation as well. Since we focus on the dynamics close to the line l_2 , we do not give further details.

The planes $r_2 = 0$, $\rho_2 = 0$, and $\delta_2 = 0$ are invariant under the flow of (4.43). The plane $r_2 = 0$ corresponds to a region in the front of the cylinder Z_b of the first blow-up, while the plane $\rho_2 = 0$ corresponds to the front side of the cylinder Z_a of the second blow-up, see Figure 4.13.

In the invariant plane $\rho_2 = 0$ system (4.43) reduces to the system

$$(4.46) \quad \begin{aligned} r_2' &= 0, \\ \delta_2' &= -\frac{1}{2}\delta_2[1 + r_2^2\delta_2^4 - \delta_2^2]. \end{aligned}$$

The line l_2 is attracting for this system. Again, the equation $1 + r_2^2\delta_2^4 - \delta_2^2 = 0$ defines a folded curve \check{S}_2 of equilibria. The fold point B_2^0 separates \check{S}_2 into an attracting branch $\check{S}_{l,2}$ and a repelling branch $\check{S}_{m,2}$; see Figure 4.13. Clearly, $\check{S}_{l,2}$ corresponds to the curve $\check{S}_{l,1}$, and $\check{S}_{m,2}$ corresponds to the curve $\check{S}_{m,1}$ from chart K_1 .

In the invariant plane $\delta_2 = 0$ system (4.43) has the form

$$(4.47) \quad \begin{aligned} \rho_2' &= \frac{1}{2}\rho_2(1 - \rho_2^2), \\ r_2' &= 0. \end{aligned}$$

The line $\check{S}_{r,2}$ defined by $\rho_2 = 1$ and the line l_2 are the lines of equilibria. The situation in the plane $\delta_2 = 0$ is similar to the situation in the plane $\delta_4 = 0$ in chart K_4 , with the only difference being that the non-hyperbolic line $l_{a,4}$ from chart K_4 has been replaced by the hyperbolic line l_2 due to the second blow-up (4.34). Within $\delta_2 = 0$ the line l_2 is repelling, and the line $\check{S}_{r,2}$ is attracting.

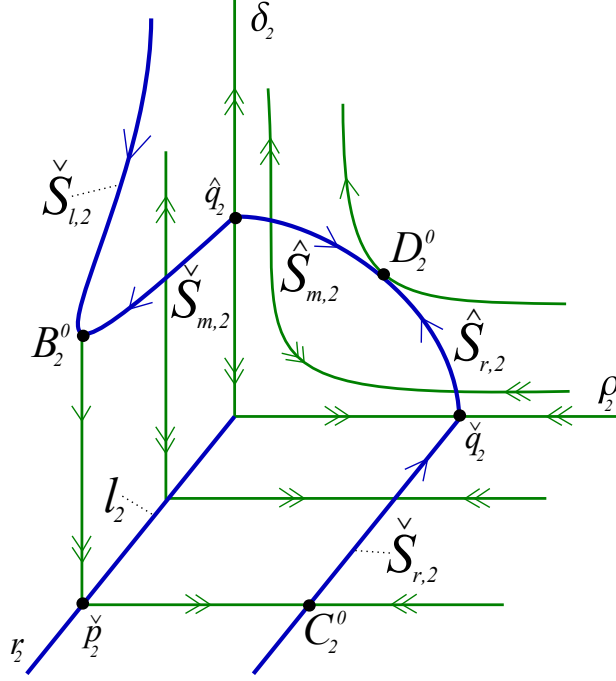
The dynamics in the plane $r_2 = 0$ can be analyzed similarly and turns out to be consistent with results obtained in charts K_1 and K_4 . Since this part of phase space is already covered by charts K_1 and K_4 , we omit more details. We find a curve of equilibria connecting the point \check{q}_2 to the point \hat{q}_2 , which consists of an attracting branch $\hat{S}_{r,2}$ and a repelling branch $\hat{S}_{m,2}$ separated by a fold point D_2^0 ; see Figure 4.13.

As before we conclude with the following lemmas.

LEMMA 4.3. *The critical manifold S_2 defined by (4.45) has the following properties if at least one of the variables r_2 , ρ_2 , or δ_2 is small:*

- (1) S_2 is smooth.
- (2) S_2 is a folded surface, i.e., $S_2 = S_{l,2} \cup S_{m,2} \cup S_{r,2}$ with fold curves $F_{B,2}$ and $F_{D,2}$, where $S_{l,2}$ and $S_{m,2}$ are attracting and $S_{r,2}$ is repelling for the layer problem (4.44).
- (3) The branch $S_{l,2}$ limits on $\check{S}_{l,2}$ for $\rho_2 = 0$. The branch $S_{m,2}$ limits on $\check{S}_{m,2}$ for $\rho_2 = 0$ and on $\hat{S}_{l,2}$ for $r_2 = 0$. Similarly, $S_{r,2}$ limits on $\hat{S}_{r,2}$ for $r_2 = 0$ and on $\check{S}_{r,2}$ for $\delta_2 = 0$. The fold curve $F_{B,2}$ limits on B_2^0 , and $F_{D,2}$ limits on D_2^0 (see Figure 4.13).

LEMMA 4.4. *The line l_2 considered as a line of equilibria of system (4.43) is of saddle-type. Its stable manifold lies in the plane $\rho_2 = 0$, and its unstable manifold lies in the plane $r_2 = 0$.*

FIGURE 4.13. Dynamics in K_2 .

Summing up, we obtain the following description of the singular relaxation cycle in chart K_2 . From the fold point B_2^0 there is a fast jump to the point $\check{p}_2 = (1/2, 0, 0) \in l_2$, then a fast jump to the point $C_2^0 = (1/2, 1, 0)$, followed by slow motion along $\check{S}_{r,2}$ to the point D_2^0 from where another fast jump takes place.

4.3.3. Properties of the blown-up system. The geometry of the blown-up space \bar{M} after the two consecutive blow-ups (4.23) and (4.34) is shown schematically in Figure 4.14. Recall that first the line l_b is blown-up to the cylinder Z_b , shown in the back of the figure. In the second blow-up (4.34) the line l_a (actually a part of its pre-image under the first blow-up) is blown-up to the cylinder Z_a , shown in the front of the figure. The vector field $X_{\tilde{\varepsilon}}$ on $M = \mathbb{R}^3$ corresponding to system (4.22) induces the blown-up vector field $\bar{X}_{\tilde{\varepsilon}}$ on the blown-up space \bar{M} , which has been analyzed in detail in the individual charts. Recall that the blow-up construction resolves the degeneracy of the critical manifold S at $\delta = 0$, while $\tilde{\varepsilon}$ still acts as a singular perturbation parameter in the vector field $\bar{X}_{\tilde{\varepsilon}}$. The equation $\delta' = 0$ from system (4.22) implies that the blown-up phase space has an invariant foliation corresponding to constant values of δ . The singular leaf corresponding to $\delta = 0$ is the union of the cylinders Z_b , Z_a and the plane Δ , where the plane Δ is defined by setting $\bar{\delta} = 0$ in (4.34); see Figure 4.14.

These properties imply that the vector field \bar{X}_0 restricted to $Z_b \cup Z_a \cup \Delta$ provides the unperturbed dynamics corresponding to $(\tilde{\varepsilon}, \delta) = (0, 0)$. In particular, we will be able to identify the singular cycle $\bar{\Gamma}_0^0 \subset Z_b \cup Z_a \cup \Delta$. The analysis in the individual charts K_4 , K_1 and K_2 implies the following results, see also Figure 4.14.

THEOREM 4.2. *The blown-up vector field \bar{X}_0 on \bar{M} has the following properties:*

- (1) *There exists a smooth two-dimensional critical manifold \bar{S} with a folded structure, i.e.,*

$$\bar{S} = \bar{S}_l \cup \bar{F}_B \cup \bar{S}_m \cup \bar{F}_D \cup \bar{S}_r,$$

where \bar{S}_l and \bar{S}_r are attracting, and \bar{S}_m is repelling. The attracting branches of S are separated from the repelling branch S_m by the fold curves F_B and F_D .

- (2) *There exists a singular orbit $\bar{\Gamma}_0^0$ of relaxation type, defined by*

$$\bar{\Gamma}_0^0 = \omega_1 \cup \omega_2 \cup \omega_3 \cup \omega_4 \cup \omega_5 \cup \omega_6 \cup \omega_7$$

with a fast jump from \bar{B}^0 to $\check{p} \in l$ along a heteroclinic orbit ω_1 on Z_a , a fast jump from \check{p} to the point $\bar{C}^0 \in S_r$ along a heteroclinic orbit ω_2 in the plane $\Delta = 0$, a segment ω_3 of \bar{S}_r from the point \bar{C}^0 to the point \check{q} in the plane $\delta = 0$, a segment ω_4 of \bar{S}_r from the point \check{q} to the fold point \bar{D}^0 on Z_b , a fast jump from the fold point \bar{D}^0 to the point $\bar{A}^0 \in \bar{S}_l$ along a heteroclinic orbit ω_5 on the cylinder Z_b , a segment ω_6 of \bar{S}_l from \bar{A}^0 to the point \hat{p} on the cylinder Z_b , and a final segment ω_7 of \bar{S}_l from the point \hat{p} to the fold point \bar{B}^0 on the cylinder Z_a .

- (3) *Within each leaf $\delta = \text{const.}$ there exists a singular cycle $\bar{\Gamma}_0^\delta$ for $\delta \in (0, \delta_0]$ for δ_0 small following the slow flow on \bar{S}_r and \bar{S}_l with jumps at the fold curves \bar{F}_B and \bar{F}_D , which limits on $\bar{\Gamma}_0^0$ as $\delta \rightarrow 0$.*

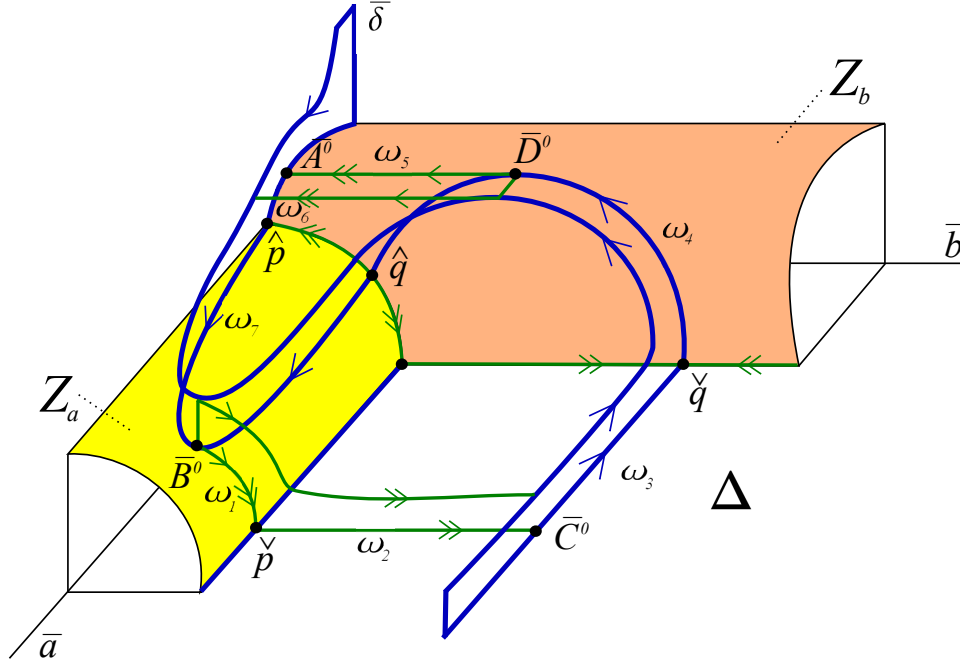


FIGURE 4.14. Geometry of the blown-up space, critical manifold \bar{S} , and singular cycles $\bar{\Gamma}_0^\delta$.

REMARK 4.11. *The singular behavior of the fold-shaped critical manifold S^δ of system (4.7) for $\delta \rightarrow 0$ (with the degenerate critical manifold S^0 of system (4.9) for $\delta = 0$) has been desingularized such that its branched structure is visible again. Intuitively, our blow-up construction prevents the non-uniform collapse of the critical manifold S^δ onto the degenerate manifold S^0 ; see Remark 4.1.*

Similarly, the non-uniform behavior of the singular cycle Γ_0^δ for system (4.5) as $\delta \rightarrow 0$ has been resolved in the blown-up problem.

In this global picture of the critical manifold \bar{S} we recover all the results from the scaling Regimes 1 – 3. In addition, compact neighborhoods of the intersections $Z_b \cap \Delta$, $Z_a \cap \Delta$, and $Z_b \cap Z_a$ cover the unbounded domains of the scaling regimes, which cannot be analyzed perturbatively. We will see that smoothness and hyperbolicity properties of the blown-up vector field \bar{X}_ε , $\varepsilon \in [0, \tilde{\varepsilon}_0]$, permit us a perturbation analysis in these neighborhoods, which allows to match the regimes. A first result in this direction is that the attracting slow manifolds from Regimes 1 – 3 fit together smoothly as parts of global attracting slow manifolds.

THEOREM 4.3. *There exists $\tilde{\varepsilon}_0 > 0$ such that the blown-up vector field \bar{X}_ε has smooth attracting slow manifolds $\bar{S}_{l,\varepsilon}$ and $\bar{S}_{r,\varepsilon}$ for $\varepsilon \in [0, \tilde{\varepsilon}_0]$.*

PROOF. The result follows from Fenichel theory [34], [61] applied to normally hyperbolic parts of the critical manifolds \bar{S}_r and \bar{S}_l . \square

REMARK 4.12. *In the following we will assume that the slow manifolds have been extended beyond the fold lines \bar{F}_B and \bar{F}_D by the flow corresponding to the blown-up vector field \bar{X}_ε . Refer to Section 2.5 in Chapter 2 and [111] for this standard procedure.*

4.3.4. Poincaré map and existence of limit cycles. To prove Theorem 4.1, we analyze a Poincaré map defined in a neighborhood of the singular cycle $\bar{\Gamma}_0^0$. We will show that within each leaf $\delta = \text{const.}$ the Poincaré map is a strong contraction for ε small and has an attracting fixed point corresponding to the limit cycle.

To construct the Poincaré map for the vector field \bar{X}_ε , we choose sections Σ , Σ_a , and Σ_b , as shown in Figure 4.15, i.e.,

$$\begin{aligned} \Sigma &\text{ is transversal to the heteroclinic orbit } \omega_2, \\ \Sigma_b &\text{ is transversal to the heteroclinic orbit } \omega_5, \\ \Sigma_a &\text{ is transversal to the heteroclinic orbit } \omega_1. \end{aligned}$$

The sections will be defined more precisely later, where the Poincaré map is considered in the individual charts. In the following we outline the construction of the Poincaré map.

The Poincaré map will be obtained as the composition of three maps. All orbits starting in Σ approach $\bar{S}_{r,\varepsilon}$, follow the slow flow along $\bar{S}_{r,\varepsilon}$, pass the non-hyperbolic fold curve \bar{F}_D , and follow the heteroclinic orbit ω_5 to intersect Σ_b . This defines the map

$$\Pi_1 : \Sigma \rightarrow \Sigma_b.$$

Similarly, all orbits starting in Σ_b approach $\bar{S}_{l,\varepsilon}$, follow the slow flow along $\bar{S}_{l,\varepsilon}$ until they pass the non-hyperbolic fold curve \bar{F}_B , and follow the heteroclinic orbit ω_1 to intersect Σ_a . This defines the map

$$\Pi_2 : \Sigma_b \rightarrow \Sigma_a.$$

The map

$$\Pi_3 : \Sigma_a \rightarrow \Sigma$$

describes how orbits pass through a neighborhood of the hyperbolic line l . The Poincaré map $\Pi : \Sigma \rightarrow \Sigma$ is defined as

$$\Pi = \Pi_3 \circ \Pi_2 \circ \Pi_1.$$

The construction of the transition map Π_1 is carried out in chart K_4 , whereas the construction of the transition maps Π_2 and Π_3 is carried out in the charts K_1 and K_2 , respectively.

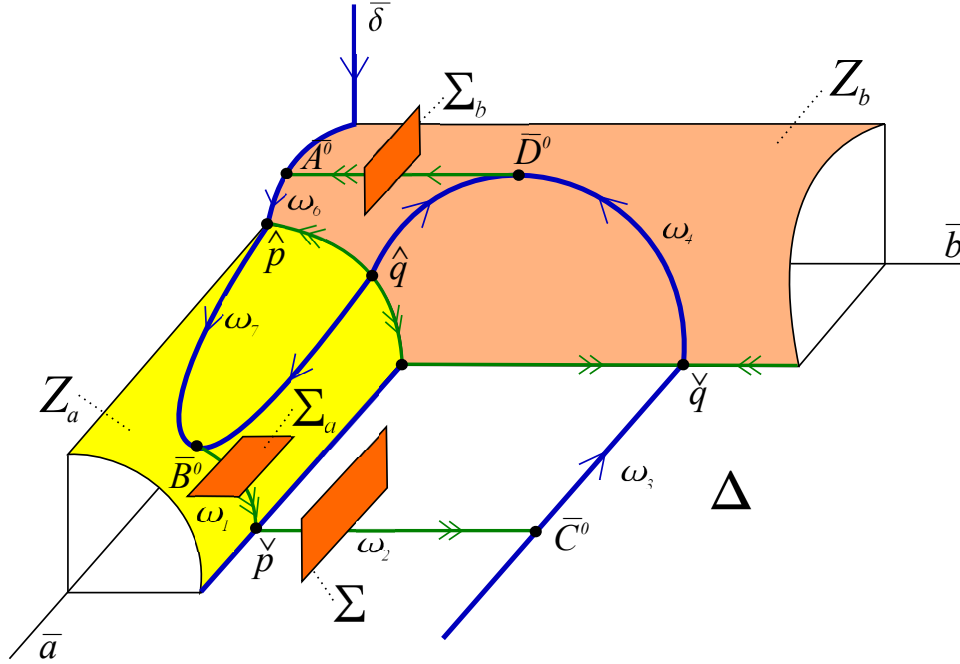
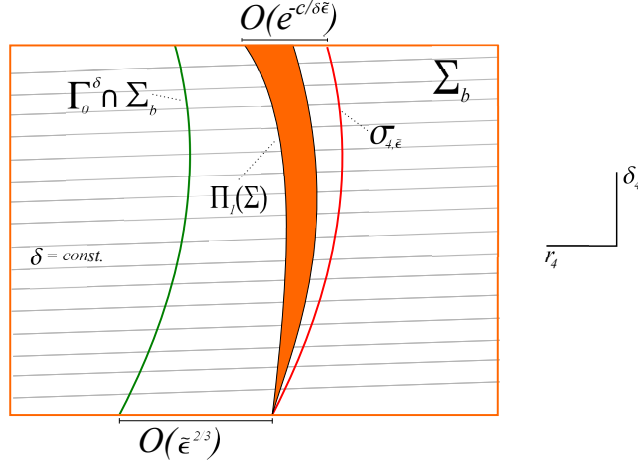


FIGURE 4.15. Sections for the Poincaré map.

The transition map Π_1 . The section Σ is defined in chart K_4 by the conditions $b_4 = 1/2$, r_4 close to $1/2$, and $|\delta_4|$ small. Similarly, the section Σ_b is defined by the conditions $b_4 = 1/4$, δ_4 close to $1/2$, and $|r_4|$ small. Note that the invariant leaves $\delta = \text{const.}$ correspond to $\delta = \delta_4 r_4$; hence, these leaves are given by $\delta_4 \approx 2\delta$ in Σ and $r_4 \approx 2\delta$ in Σ_b , respectively.

LEMMA 4.5. *The transition map $\Pi_1 : \Sigma \rightarrow \Sigma_b$ is well defined for $\tilde{\varepsilon}$ small enough. There exists a constant $c > 0$ such that the map Π_1 restricted to a leaf $\delta = \text{const.}$ is a contraction with a contraction rate $e^{-c/\delta\tilde{\varepsilon}}$.*

PROOF. All orbits starting in Σ are attracted by the extended slow manifold $\bar{S}_{r,\tilde{\varepsilon}}$ at the exponential rate stated above. The results in [71], [111] on the behavior of slow manifolds near generic folds imply that the intersection of $\bar{S}_{r,\tilde{\varepsilon}}$ with Σ_b is a curve $\sigma_{4,\tilde{\varepsilon}}$, which is $O(\tilde{\varepsilon}^{2/3})$ close to the curve given by $\bar{\Gamma}_0^\delta \cap \Sigma_b$ with δ small. Hence, all of Σ is mapped to a thin wedge exponentially close to $\sigma_{4,\tilde{\varepsilon}}$; see Figure 4.16. \square

FIGURE 4.16. Image of the section Σ under the transition map Π_1 .

REMARK 4.13. *The above proof is carried out in chart K_4 , in which the blown-up vector field is three-dimensional. However, the region corresponding to the fold curve is also covered by chart K_3 , i.e., Regime 3. The governing equations (4.19) in Regime 3 are a family of singularly perturbed planar vector fields depending regularly on the parameter δ . Therefore, the description of the passage of the fold point can be also based on the results for the planar singularly perturbed fold in [71]. Although these two points of view are equivalent, the latter is useful in obtaining a more detailed description. For the analysis of the fold curve in chart K_4 one has to use the results of [111] for folds in \mathbb{R}^3 .*

The transition map Π_2 . The transition map Π_2 is studied in chart K_1 . The transformation from chart K_4 to chart K_1 is carried out according to equations (4.35). Hence, the section Σ_b is now given by $\rho_1^2 b_1 = 1/2$ with ρ_1 close to $1/2$ and r_1 small. Because of $\delta = \rho_1 r_1$, the invariant leaves $\delta = \text{const.}$ are given by $r_1 \approx 2\delta$ in Σ_b . We define the section Σ_a by $b_1 = 1$, r_1 close to $1/2$, and ρ_1 small. Because of $\delta = \rho_1 r_1$, the invariant leaves $\delta = \text{const.}$ are given by $\rho_1 \approx 2\delta$ in Σ_a .

LEMMA 4.6. *The transition map $\Pi_2 : \Sigma_b \rightarrow \Sigma_a$ is well defined for $\tilde{\varepsilon}$ small enough. There exists a constant $c > 0$ such that the map Π_2 restricted to a leaf $\delta = \text{const.}$ is a contraction with a contraction rate $e^{-c/\delta\tilde{\varepsilon}}$.*

PROOF. All orbits starting in Σ_b are attracted by the extended slow manifold $\bar{S}_{l,\tilde{\varepsilon}}$ at the exponential rate stated above. The intersection of $\bar{S}_{l,\tilde{\varepsilon}}$ with Σ_a is a curve $\sigma_{1,\tilde{\varepsilon}}$. Hence, all of Σ_b is mapped to an exponentially thin wedge close to $\sigma_{1,\tilde{\varepsilon}}$. Note that the results in [71], [111] do not apply directly to system (4.37); however, the dynamics close to the fold curve $F_{B,1}$ can also be described in Regime 1, which is a family of planar singularly perturbed folds with singular perturbation parameter ε parameterized by δ , where the results of [71] apply. This shows further that within a leaf $\delta = \text{const.}$ the curve $\sigma_{1,\tilde{\varepsilon}}$ is $O(\varepsilon^{2/3}) = O(\delta^{2/3}\tilde{\varepsilon}^{2/3})$ close to the point $\bar{\Gamma}_0^\delta \cap \Sigma_a$. \square

The transition map Π_3 . The transition map Π_3 is studied in chart K_2 . The transformation from chart K_1 to chart K_2 is carried out according to

$$(4.48) \quad r_2 = r_1, \quad \delta_2 = b_1^{-1/2}, \quad \rho_2 = b_1^{1/2} \rho_1.$$

The section Σ_a written in chart K_2 is given by the conditions $\delta_2 = 1$, r_2 close to $1/2$, and ρ_2 small. The invariant leaves $\delta = \text{const.}$ in Σ_a are now described by $\rho_2 \approx 2\delta$. The transformation from chart K_4 to chart K_2 is carried out according to

$$(4.49) \quad r_2 = r_4, \quad \rho_2 = b_4^{1/2}, \quad \delta_2 = \delta_4 b_4^{-1/2}.$$

Hence, the section Σ is now given by $\rho_2 = 1/\sqrt{2}$, r_2 close to $1/2$, and δ_2 small. The invariant leaves $\delta = \text{const.}$ in Σ are now described by $\delta_2 \approx 2\sqrt{2}\delta$.

REMARK 4.14. *In order to guarantee that Π_3 maps Σ_a into Σ the size of the section Σ in the direction of r_2 (which is equal to r_4) has to be chosen slightly larger than the size of the section Σ_a in the direction of r_2 .*

LEMMA 4.7. *The transition map*

$$\Pi_3 : \Sigma_a \rightarrow \Sigma, \quad (r_{2,in}, \rho_{2,in}, 1) \mapsto (r_{2,out}, 1/\sqrt{2}, \delta_{2,out})$$

is well defined for $\tilde{\varepsilon}$ small and $\delta \in [0, \delta_0]$ for δ_0 small enough. The map Π_3 is essentially a small translation in r_2 -direction, i.e.,

$$r_{2,out} = r_{2,in} + O(\tilde{\varepsilon}\delta \ln(1/\delta)).$$

Restricted to a leaf $\delta = \text{const.}$, the map is at most weakly (algebraically) expanding.

PROOF. By dividing the vector field (4.43) by the non-vanishing factor

$$\frac{1}{2}\rho_2[1 - \rho_2^2 + \delta_2^2(r_2^2\rho_2^2 - 1 + r_2^2\rho_2\delta_2^2)],$$

we rewrite the system as

$$(4.50) \quad \begin{aligned} r_2' &= \tilde{\varepsilon}r_2\rho_2\delta_2 R(r_2, \rho_2, \delta_2), \\ \rho_2' &= \rho_2, \\ \delta_2' &= -\delta_2 + \tilde{\varepsilon}r_2\rho_2\delta_2 R(r_2, \rho_2, \delta_2) \end{aligned}$$

with a smooth function $R(r_2, \rho_2, \delta_2)$, which is $O(1)$ in the domain of interest. We consider this system as a perturbation of the linear system

$$(4.51) \quad \begin{aligned} r_2' &= 0, \\ \rho_2' &= \rho_2, \\ \delta_2' &= -\delta_2. \end{aligned}$$

A short computation shows that the transition time T , which a solution starting in Σ_a needs to reach the section Σ , is

$$T = O(\ln \frac{1}{\delta}),$$

where we have used that $\delta = r_2\rho_2\delta_2$. The assertions of the lemma follow. \square

This completes the construction and analysis of the Poincaré map Π and allows us to prove the existence of limit cycles for $\tilde{\varepsilon}$ small.

THEOREM 4.4. *For $\mu < 1$ there exist $\delta_0 > 0$ and $\tilde{\varepsilon}_0 > 0$ such that the blown-up vector field $\bar{X}_{\tilde{\varepsilon}}$ has a unique family of attracting periodic orbits $\bar{\Gamma}_{\tilde{\varepsilon}}^{\delta}$ for $0 < \delta \leq \delta_0$ and $0 < \tilde{\varepsilon} \leq \tilde{\varepsilon}_0$ with the properties*

- (1) $\bar{\Gamma}_\varepsilon^\delta$ tends to $\bar{\Gamma}_0^\delta$ as $\tilde{\varepsilon} \rightarrow 0$ uniformly for $\delta \in (0, \delta_0]$,
(2) $\bar{\Gamma}_\varepsilon^\delta$ tends to the singular cycle $\bar{\Gamma}_0^0$ as $(\tilde{\varepsilon}, \delta) \rightarrow (0, 0)$.

PROOF. We conclude from Lemmas 4.5, 4.6, and 4.7 that there exist $\delta_0 > 0$ and $\tilde{\varepsilon}_0 > 0$ such that the Poincaré map $\Pi : \Sigma \rightarrow \Sigma$ is well defined for $\delta \in [0, \delta_0]$ and $\tilde{\varepsilon} \in [0, \tilde{\varepsilon}_0]$. Restricted to a leaf $\delta = \text{const.}$, i.e., $\delta = \delta_4 r_4$ with $r_4 \approx 1/2$, the map Π is a contraction with contraction rate $e^{-c/\delta\tilde{\varepsilon}}$ for some constant $c > 0$. The contraction mapping theorem implies the existence of a unique fixed point $\gamma_\varepsilon^\delta$ corresponding to the limit cycle $\bar{\Gamma}_\varepsilon^\delta$.

The point $\gamma_\varepsilon^\delta$ is $O(e^{-c/\delta\tilde{\varepsilon}})$ close to the curve $\bar{S}_{l,\tilde{\varepsilon}} \cap \Sigma$. The proofs of Lemmas 4.6 and 4.7 imply that within a leaf $\delta = \text{const.}$, the curve $\bar{S}_{l,\tilde{\varepsilon}} \cap \Sigma$ is $O(\delta^{2/3}\tilde{\varepsilon}^{2/3})$ close to the point $\bar{\Gamma}_0^\delta \cap \Sigma$; see Figure 4.17. The assertions of the theorem follow. \square

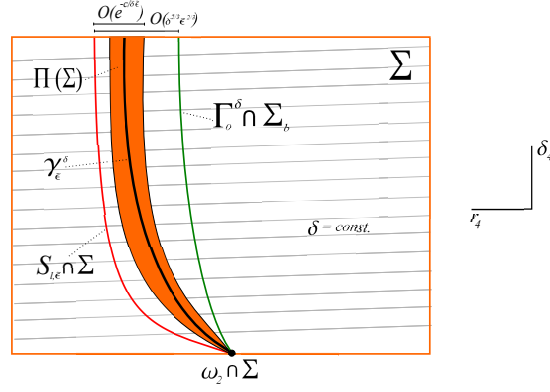


FIGURE 4.17. Image of the section Σ under the Poincaré map Π .

REMARK 4.15. By setting $\varepsilon = \tilde{\varepsilon}\delta$ and by applying the blow-up transformations (4.23) and (4.34), the limit cycles $\bar{\Gamma}_\varepsilon^\delta$ become the limit cycles $\Gamma_\varepsilon^\delta$ of the original system (4.5). Thus, the proof of Theorem 4.1 also is completed.

CHAPTER 5

A new type of relaxation oscillations in a model of the mitotic oscillator

This chapter is devoted to a geometric analysis of a new type of relaxation oscillations in an enzyme reaction. We are concerned with the model presented in the introduction, i.e., system (1.16) describing at the molecular level the mitosis part of the cell division cycle in eukaryotes. So far this model has been studied only numerically [33]. In this thesis we rewrite the model as a three-dimensional singularly perturbed system and analyze its dynamics in the spirit of geometric singular perturbation theory. Relaxation oscillations of a new type arise from the phenomenon of a delayed exchange of stability, which occurs at non-hyperbolic lines along which branches of the two-dimensional critical manifold intersect. This novel type of relaxation oscillations is studied by means of several blow-up transformations. Our results extend and complete the study presented in [33].

Chapter 5 is organized as follows. In Section 5.1 we discuss the oscillatory behavior of the model and present its slow-fast analysis. In Section 5.2 we carry out the blow-up analysis. The main result, i.e., the existence of an attracting periodic orbit, is proved in Section 5.3.

5.1. Slow-fast analysis of the mitotic oscillator

5.1.1. Basic properties and sustained oscillations. We begin by analyzing system (1.16) for the parameters that were employed in [40]. Namely, the chosen parameter values are $k_d = 0.25$, $v_i = 0.25$, $K_c = 0.5$, $K_d = 0$, $V_{M1} = 3$, $V_2 = 1.5$, $V_{M3} = 1$, $V_4 = 0.7$, $v_d = 0.25$, $k_j = 10^{-3}$, $j = 1, \dots, 4$, for which system (1.16) has the form

$$\begin{aligned}
 \frac{dX}{d\tau} &= M \frac{1-X}{\varepsilon+1-X} - \frac{7}{10} \frac{X}{\varepsilon+X}, \\
 \frac{dM}{d\tau} &= \frac{6C}{1+2C} \frac{1-M}{\varepsilon+1-M} - \frac{3}{2} \frac{M}{\varepsilon+M}, \\
 \frac{dC}{d\tau} &= \frac{1}{4}(1-X-C)
 \end{aligned}
 \tag{5.1}$$

with $\varepsilon := k_j$, $j = 1, \dots, 4$. We restrict our attention to the physically meaningful range of the variables $X \geq 0$, $M \geq 0$, and $C \geq 0$, and refer to the introduction for the specification and a more detailed explanation of the variables and the parameters.

Providing $\varepsilon \ll 1$ the following switching behavior emerges, see Figure 5.1. Given a low cyclin concentration, this value increases at a constant rate, while M and X stay low (close to 0). Once the variable C passes the activation threshold value $C^* \approx 0.5$, the variable M increases sharply (up to 1). As soon as M exceeds the

threshold $M^* \approx 0.7$, X is activated and also increases sharply (up to 1). This in turn triggers the degradation of the cyclin and therefore C , M , and X drop rapidly; in particular, first M decreases and once it drops below the threshold $M^* \approx 0.7$, cyclin protease X is inactivated. Consequently, both M and X return to low values, while the level of C may rise again. This proceeds in a periodic manner and results in the generation of the limit cycle type oscillations, see Figure 5.1 and Figure 5.2, where a numerical simulation of (5.1) and the corresponding limit cycle in the phase space are shown.

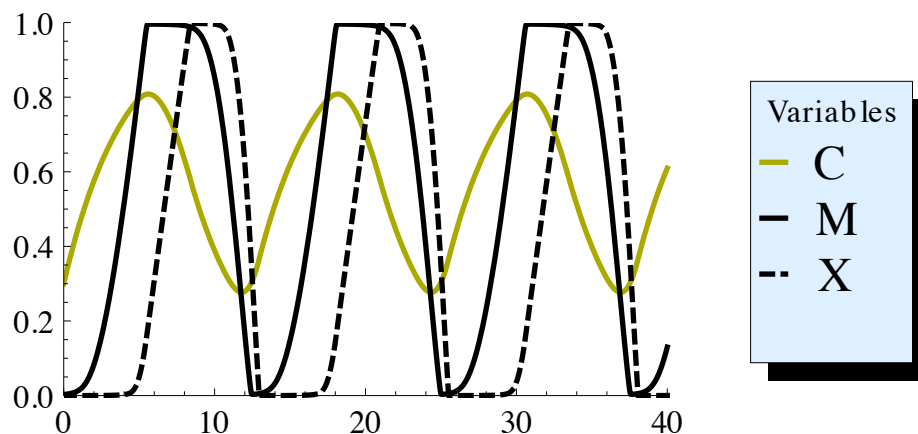


FIGURE 5.1. Oscillatory activity of the mitotic cyclin C , cyclin dependent kinase M , and cyclin protease X .

In [39] the behavior illustrated above of the limit-cycle oscillations for progressively larger values of V_{M1} and V_2 (V_2/V_{M1} fixed) was shown to persist, only if the Michaelis constants ε are small. However, in [33] the authors investigated the observed oscillations only numerically and judged the full system (5.1) as to be too complicated for the phase space analysis. Therefore, they decided to simplify the problem by applying the quasi-steady-state approximation for one of the dependent variables. Consequently, they demonstrated that the resulting reduced two-variable system did not exhibit limit-cycle oscillations. By introducing a rather complicated rescaling, a new QSSA-reduced system was found. However, this two-variable limit did not allow to recover sustained oscillatory behavior of the full model.

To understand the enzyme kinetics for small concentrations of C , M , and X , we apply singular perturbation theory. Our work extends and completes the study of Erneux and Goldbeter [33]. By carrying out a detailed geometric analysis of the full system (5.2), we will show that it indeed exhibits an interesting type of oscillations, as shown in Figure 5.1.

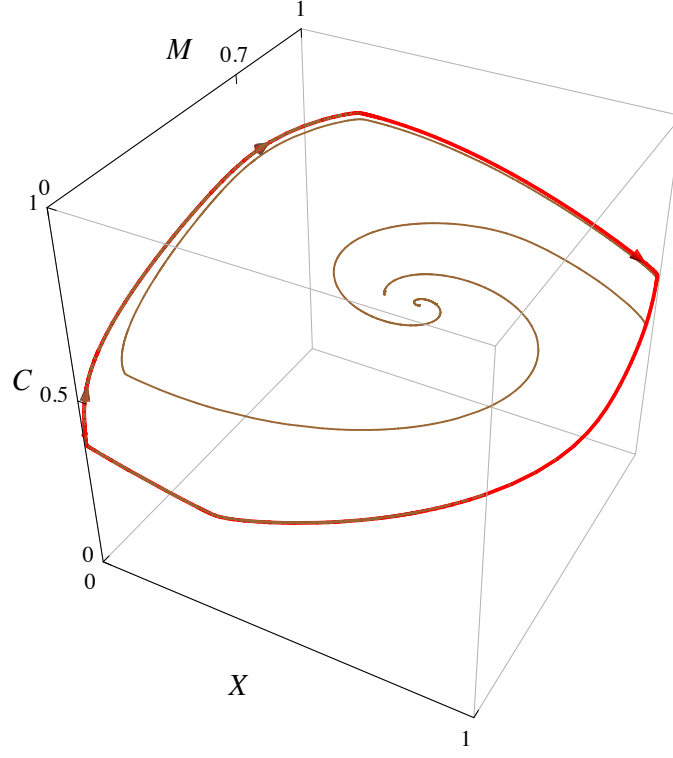


FIGURE 5.2. Numerically computed limit cycle (shown in red) for $k_d = 0.25, v_i = 0.25, K_c = 0.5, K_d = 0, V_{M1} = 3, V_2 = 1.5, V_{M3} = 1, V_4 = 0.7, v_d = 0.25, k_j = 10^{-3}, j = 1, \dots, 4$, and two orbits attracted onto it (shown in brown).

5.1.2. Slow-fast structure. A starting point of our geometric singular perturbation analysis is the following system

$$\begin{aligned}
 \frac{dX}{d\tau} &= [M(1-X)(\varepsilon+X) - \frac{7}{10}X(\varepsilon+1-X)]F_\varepsilon(M), \\
 \frac{dM}{d\tau} &= \left[\frac{6C}{1+2C}(1-M)(\varepsilon+M) - \frac{3}{2}M(\varepsilon+1-M) \right] F_\varepsilon(X), \\
 \frac{dC}{d\tau} &= \frac{1}{4}(1-X-C)F_\varepsilon(X, M),
 \end{aligned}
 \tag{5.2}$$

which is obtained by multiplying the right hand side of (5.1) by the factor $F_\varepsilon(X, M)$ such that

$$\begin{aligned}
 F_\varepsilon(X, M) &= F_\varepsilon(X)F_\varepsilon(M), \\
 F_\varepsilon(X) &= (\varepsilon+1-X)(\varepsilon+X), \\
 F_\varepsilon(M) &= (\varepsilon+1-M)(\varepsilon+M).
 \end{aligned}
 \tag{5.3}$$

This amounts to a space-dependent rescaling of time, but leaves the phase portrait unchanged. Moreover, it brings the kinetic equations of the mitotic oscillator into an

equivalent polynomial form. The derivative in (5.2) is with respect to the resulting rescaled time variable, which we still denote by τ .

REMARK 5.1. *We emphasize here once more that systems (5.1) and (5.2) have the same phase portraits, but they have different time-scales, i.e., the dynamics of system (5.1) happens on just one time scale, whereas due to the multiplication trick, it will turn out that the dynamics of system (5.2) is multiple-time-scale. Thus, it is important to note that the existence result (Theorem 5.3) applies to both systems, however, the whole upcoming discussion on slow-fast time scales refers only to system (5.2).*

The parameter $\varepsilon > 0$ representing the Michaelis constants is very small and acts in system (5.2) as a singular perturbation parameter. System (5.2) is, however, not written in standard form of slow-fast systems, where the slow and fast variables are distinguished a priori. More precisely, in system (5.2) in the corresponding limiting problem for $\varepsilon = 0$ none of the three variables become constants. In the $\varepsilon = 0$ sub-system given by

$$(5.4) \quad \begin{aligned} \frac{dX}{d\tau} &= \left(M - \frac{7}{10}\right) F_0(X, M), \\ \frac{dM}{d\tau} &= \left(\frac{6C}{1+2C} - \frac{3}{2}\right) F_0(X, M), \\ \frac{dC}{d\tau} &= \frac{1}{4}(1 - X - C)F_0(X, M) \end{aligned}$$

with

$$F_0(X, M) = (1 - M)(1 - X)MX,$$

all the three variables evolve on the fast time scale τ . In the following we will call system (5.4) the layer problem.

In the next subsections, following the standard singular perturbation approach, we analyze system (5.2) in the singular limit $\varepsilon = 0$, i.e., the fast and slow dynamics of the layer problem and the corresponding reduced system.

5.1.3. Fast dynamics. The equations

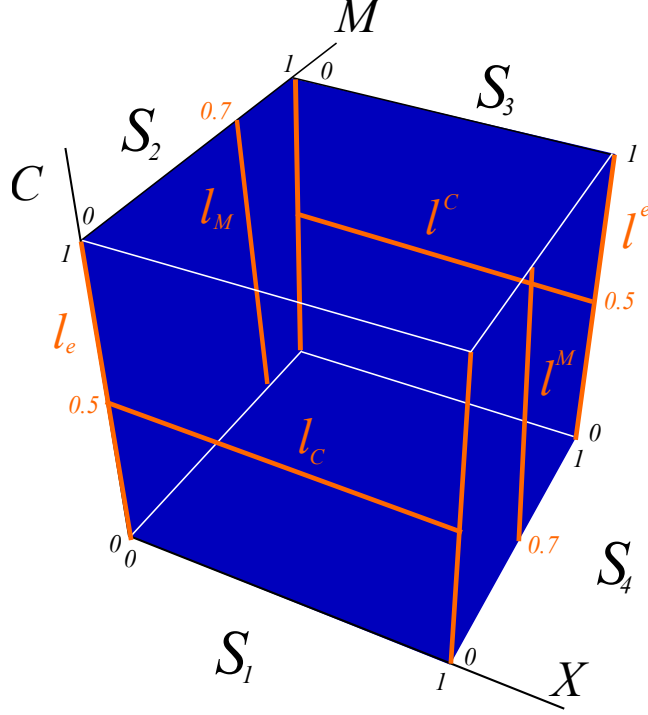
$$\begin{aligned} \left(M - \frac{7}{10}\right)(1 - M)(1 - X)MX &= 0, \\ \left(\frac{6C}{1+2C} - \frac{3}{2}\right)(1 - M)(1 - X)MX &= 0, \\ \frac{1}{4}(1 - X - C)(1 - M)(1 - X)MX &= 0 \end{aligned}$$

define the critical manifold S of the steady states of the layer problem (5.4). The critical manifold S consists of four planes, defined by $M = 0$, $X = 0$, $M = 1$, $X = 1$, which we denote by S^1 , S^2 , S^3 , S^4 , respectively, and the equilibrium point $(X, M, C) = (0.5, 0.7, 0.5)$ denoted by p . Hence,

$$S = S^1 \cup S^2 \cup S^3 \cup S^4 \cup p.$$

REMARK 5.2. *The equilibrium point p plays no role in the analysis; however, we include it for completeness.*

REMARK 5.3. *Recall that our attention is restricted to the physically meaningful range of the variables $X \geq 0$, $M \geq 0$, and $C \geq 0$.*

FIGURE 5.3. Critical manifold S and non-hyperbolic lines.

The planes intersect along four non-hyperbolic lines, where an exchange of stability occurs. Two of them are of particular interest, i.e., the non-hyperbolic edge along which the planes S^1 and S^2 intersect, and the non-hyperbolic edge, which is the intersection of the planes S^3 and S^4 . We denote them by l_e and l^e , respectively. In addition, each of the planes changes its stability at another non-hyperbolic line given by $C = 0.5$, $M = 0.7$, $C = 0.5$, and $M = 0.7$, respectively, denoted by l_C , l_M , l^C , and l^M ; see Figure 5.3. We summarize the stability properties of points in S in the following lemma.

LEMMA 5.1. *The layer problem (5.4) has the following properties:*

- S^1 is attracting for $C < 0.5$ and repelling for $C > 0.5$.
- S^2 is attracting for $M < 0.7$ and repelling for $M > 0.7$.
- S^3 is attracting for $C > 0.5$ and repelling for $C < 0.5$.
- S^4 is attracting for $M > 0.7$ and repelling for $M < 0.7$.
- Equilibrium p is of saddle-focus type.

PROOF. Computations. For instance, the linearization of system (5.4) at the steady state p has one real negative eigenvalue and a pair of complex conjugated eigenvalues. The real eigenvalue ($\lambda_1 = -0.8$) is with the sign opposite to the sign of

the real part of the complex conjugated eigenvalues ($\lambda_{2,3} = 0, 28 \pm 0, 6i$), therefore the steady state p is of saddle-focus type. \square

REMARK 5.4. We denote the attracting (repelling) part of S^i by S_a^i (S_r^i) for $i = 1, \dots, 4$.

From Theorem 2.1 presented in Chapter 2 we conclude that normally hyperbolic parts of S persist under ε -perturbation as slow manifolds.

5.1.4. Slow dynamics. Any compact subset of the critical manifold S that does not contain the non-hyperbolic lines is normally hyperbolic. To such normally hyperbolic parts of S (away from the edges and away from the non-hyperbolic lines l_C, l_M, l^C, l^M , respectively), Fenichel theory applies [34]. In particular, the theory implies that these parts perturb to slow manifolds, which lie within $O(\varepsilon)$ of S . More precisely, we have

THEOREM 5.1. For small $\delta > 0$ there exist $\varepsilon_0 > 0$ and smooth functions $h_\varepsilon^1(X, C)$ and $h_\varepsilon^3(X, C)$ defined on $I_a := [\delta, 1 - \delta] \times [\delta, \frac{1}{2} - \delta]$ and $I_r := [\delta, 1 - \delta] \times [\frac{1}{2} + \delta, 1 - \delta]$, respectively, such that the graphs

$$\begin{aligned} S_{a,\varepsilon}^1 &= \{(X, M, C) : M = h_\varepsilon^1(X, C), (X, C) \in I_a\}, \\ S_{r,\varepsilon}^1 &= \{(X, M, C) : M = h_\varepsilon^1(X, C), (X, C) \in I_r\}, \\ S_{a,\varepsilon}^3 &= \{(X, M, C) : M = 1 + h_\varepsilon^3(X, C), (X, C) \in I_r\}, \\ S_{r,\varepsilon}^3 &= \{(X, M, C) : M = 1 + h_\varepsilon^3(X, C), (X, C) \in I_a\} \end{aligned}$$

are locally invariant attracting, respectively repelling, slow manifolds of system (5.2) for $\varepsilon \in (0, \varepsilon_0]$. The functions have the expansions

$$\begin{aligned} h_\varepsilon^1(X, C) &= \frac{-4C}{2C-1}\varepsilon + O(\varepsilon^2), \\ h_\varepsilon^3(X, C) &= \frac{1+2C}{1-2C}\varepsilon + O(\varepsilon^2). \end{aligned}$$

PROOF. The above expansions are obtained by plugging the expansion of $h_\varepsilon^j, j = 1, 3$ in powers of ε into (5.2) and comparing coefficients of powers of ε . \square

Similarly, normally hyperbolic pieces of the planes $X = 0, X = 1$ perturb to smooth locally invariant attracting (repelling) two-dimensional slow manifolds.

THEOREM 5.2. For small $\delta > 0$ there exist $\varepsilon_0 > 0$ and smooth functions $h_\varepsilon^2(M, C)$ and $h_\varepsilon^4(M, C)$ defined on $J_a := [\delta, 0.7 - \delta] \times [\delta, 1 - \delta]$ and $J_r := [0.7 + \delta, 1 - \delta] \times [\delta, 1 - \delta]$, respectively, such that the graphs

$$\begin{aligned} S_{a,\varepsilon}^2 &= \{(X, M, C) : X = h_\varepsilon^2(M, C), (M, C) \in J_a\}, \\ S_{r,\varepsilon}^2 &= \{(X, M, C) : X = h_\varepsilon^2(M, C), (M, C) \in J_r\}, \\ S_{a,\varepsilon}^4 &= \{(X, M, C) : X = 1 + h_\varepsilon^4(M, C), (M, C) \in J_r\}, \\ S_{r,\varepsilon}^4 &= \{(X, M, C) : X = 1 + h_\varepsilon^4(M, C), (M, C) \in J_a\} \end{aligned}$$

are locally invariant attracting, respectively repelling slow manifolds of system (5.2) for $\varepsilon \in (0, \varepsilon_0]$. The functions have the expansions

$$\begin{aligned} h_\varepsilon^2(M, C) &= \frac{M}{0.7-M}\varepsilon + O(\varepsilon^2), \\ h_\varepsilon^4(M, C) &= \frac{0.7}{0.7-M}\varepsilon + O(\varepsilon^2). \end{aligned}$$

PROOF. The above expansions are obtained by plugging the expansion of $h_\varepsilon^j, j = 2, 4$ in powers of ε into (5.2) and comparing coefficients of powers of ε . \square

Finally, the equations governing the slow dynamics on the critical manifold S are found by first substituting the functions $h_\varepsilon^j, j = 1, \dots, 4$ into (5.2), then transforming to the slow time variable $t = \varepsilon\tau$, and setting $\varepsilon = 0$. We now analyze the reduced flows in each of the planes.

Reduced flow on S^1 . The dynamics of the reduced system on S^1 , i.e., on the plane $M = 0$, is governed by

$$\begin{aligned} \dot{X} &= \frac{7X(1-X)(6C+3)}{10(6C-3)}, \\ \dot{C} &= \frac{(1-X-C)(X-1)X(6C+3)}{4(6C-3)}, \end{aligned} \quad (5.5)$$

where \cdot denotes differentiation with respect to the slow variable t .

System (5.5) is singular at the line $C = 0.5$, i.e., the flow is not defined there. The lines $X = 0$ and $X = 1$, shown in blue in Figure 5.4, are lines of equilibria. The line $X = 0$ is attracting for $C < 0.5$ and repelling for $C > 0.5$, whereas the line $X = 1$ is repelling for $C < 0.5$ and attracting for $C > 0.5$, see Figure 5.4.

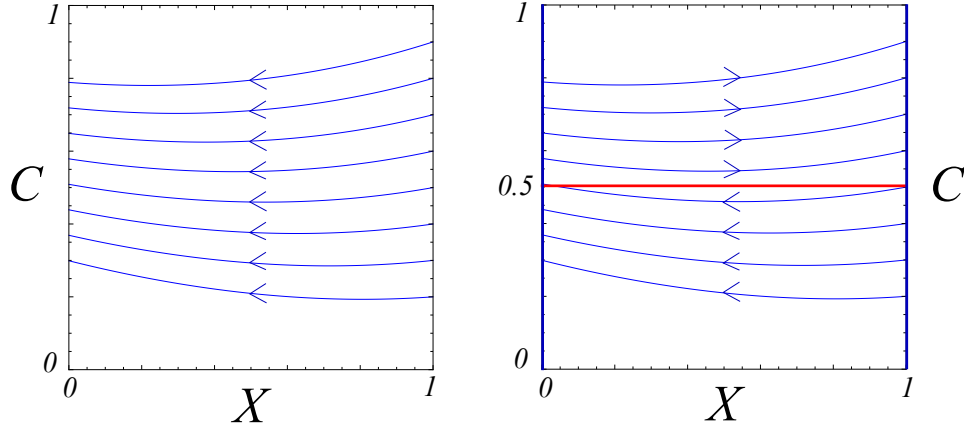


FIGURE 5.4. Reduced flow on the critical manifold S^1 (on the right) and its desingularized version (on the left).

REMARK 5.5. *Note that the lines $X = 0$ and $X = 1$ of equilibria of system (5.5) are artefacts of the multiplication trick (5.3), and are not lines of equilibria of system (5.1).*

Since the standard existence and uniqueness result for ODEs do not hold at $C = 0.5$, to study the phase portrait of the reduced system in more detail, we rescale the time in (5.5) by the factor $\frac{(6C-3)}{(6C+3)(X-1)X}$. We obtain the desingularized system

$$\begin{aligned} \dot{X} &= -\frac{7}{10}, \\ \dot{C} &= \frac{1}{4}(1-X-C). \end{aligned} \quad (5.6)$$

Systems (5.5) and (5.6) have the same phase portraits on the lower part of the plane $M = 0$, i.e., for $C < 0.5$. On the upper part, for $C > 0.5$, we must reverse time in the phase portrait of system (5.6) in order to obtain the phase portrait of the reduced system (5.5), see Figure 5.4. Such a desingularization of system (5.5) leads to the cancellation of the singularity and the reduced flow passes through the line $C = 0.5$.

REMARK 5.6. *Note that for $C < 0.5$ systems (5.5) and (5.6) have qualitatively the same dynamics. More precisely, the vector field (5.6) is C^∞ -equivalent, but not C^∞ -conjugate to the original vector field (5.5). This is no problem as we are not interested in precise time-estimation along the orbits. For $C > 0.5$ the orientation is not preserved, i.e., the direction of motion along orbits must be changed due to the time reparameterization by a decreasing function in t . We refer to [16] and [116] for a background on conjugacies and equivalences of vector fields, and time reparameterization of flows.*

Recall that the critical manifold S^1 is attracting for $C < 0.5$. Hence, for our purposes it suffices to study the flow of system (5.5) in the lower part of the $M = 0$ plane, away from the line l_C , and away from the lines of equilibria, which are non-hyperbolic for the layer problem (5.4). Thus, it suffices to study the flow of system (5.6) for $C < 0.5$. The equations in (5.6) are decoupled and integrable. Note that X acts as a time in (5.6), hence the equation for C is non-autonomous, but linear in C . Consequently, the flow of (5.6) is contracting in C . Since the slow flow on S_ε^2 is a regular perturbation of the reduced flow, we conclude that the contraction property of the slow flow also holds for $\varepsilon > 0$, i.e., the slow flow on $S_{a,\varepsilon}^1$ is contracting C .

Reduced flow on S^2 . On the plane $X = 0$ the dynamics is governed by

$$\begin{aligned} \dot{M} &= \frac{(6C-3)M(1-M)}{2(2C+1)(0.7-M)}, \\ \dot{C} &= \frac{(1-C)(1-M)M}{4(0.7-M)}. \end{aligned} \quad (5.7)$$

System (5.7) has two lines of equilibria, i.e., $M = 0$ and $M = 1$, and is singular at $M = 0.7$. The lines of equilibria are attracting for $C < 0.5$ and repelling for $C > 0.5$. To understand better the dynamics of the reduced system (5.7) (especially, close to the line $M = 0.7$), we divide out the factor $\frac{M(M-1)}{M-0.7}$, and obtain

$$\begin{aligned} \dot{M} &= \frac{(6C-3)}{2(2C+1)}, \\ \dot{C} &= \frac{1}{4}(1-C). \end{aligned} \quad (5.8)$$

Systems (5.7) and (5.8) have the same phase portraits for $M < 0.7$, see Figure 5.5. The phase portrait of the reduced system (5.7) on S_r^2 is obtained by changing the direction of the flow in Figure 5.5 for $M > 0.7$.

REMARK 5.7. *Note that for $C > 0.5$ the reduced flow on S^2 is directed towards the line $M = 0.7$. Hence, orbits on S_a^2 and S_r^2 reach the line l_M in finite forward time and are forced to jump. This phenomenon is studied in detail in Subsection 5.2.2.*

Similarly, the reduced flows on the $M = 1$ and $X = 1$ planes have been analyzed.

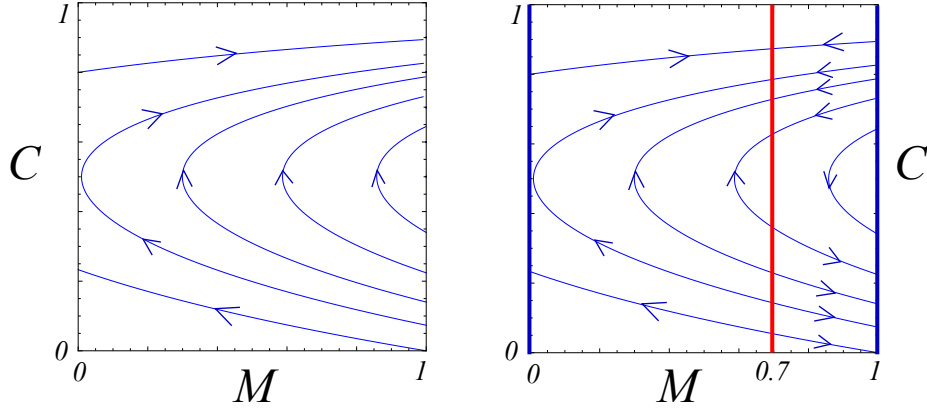


FIGURE 5.5. Reduced flow on the critical manifold S^2 (on the right) and its desingularized version (on the left).

5.1.5. Singular cycle. One goal of the analysis of system (5.2) in the singular limit $\varepsilon = 0$ is to identify a singular cycle, i.e., a closed curve consisting of alternating segments of the critical manifold S and orbits of the layer problem. Note, however, that just from inspection of the layer problem and the reduced problems, it is not clear how to define a singular cycle, which would be a good candidate to obtain relaxation oscillations. The reason for this is that at the moment we have no valid description of the dynamics close to the edges l_e nor l^e . Moreover, we need to understand better the dynamics of system (5.2) in a neighbourhood of the non-hyperbolic lines l_M and l^M .

A full description of the dynamics will be obtained by carrying out the blow-up analysis presented in Section 5.2. By combining these results, we define in anticipation the following singular cycle Γ_0 of system (5.2) for $\varepsilon = 0$, half of which consists of

- (1) slow motion in the attracting part of S^1 (the plane $M = 0$) towards the (non-hyperbolic) edge l_e ,
- (2) very slow drift along the edge l_e ,
- (3) slow motion in the attracting part of S^2 (the plane $X = 0$) to a point p_f on the non-hyperbolic line l_M ,
- (4) a fast jump from p_f to the attracting part of S^3 (the plane $M = 1$).

More precisely, we distinguish the following points (see Figure 5.6 and Figure 5.7): $q_e = (0, 0, \frac{1}{2}) \in l_e$, $p_f \in l_M$, $p_3 \in P(l_M) \subset S_a^3$, $p^{en} \in l^e$, $q^e = (1, 1, \frac{1}{2}) \in l^e$, $p^f \in l^M$, $p_1 \in P(l^M) \subset S_a^1$, and $p_{en} \in l_e$, where $P(l_M)$ and $P(l^M)$ denote the projections along the fast fibers of the lines l_M and l^M on the attracting branches of S^3 and S^1 , respectively. It will turn out that the points $p_f \in l_M$ and $p^f \in l^M$ are jump points and we will assume that the reduced flows on S^1 and S^3 are transverse to the projection curves $P(l^M)$ and $P(l_M)$ at the points p_1 and p_3 , respectively.

This transversality condition¹ clearly holds, but is not checked since it is beyond our scope to find precisely the coordinates of the points p_1 and p_3 .

The other points we describe by introducing the following notation: ω_1 is a segment of S_a^2 from q_e to p_f , ω_2 is the heteroclinic orbit of system (5.4) from p_f to p_3 , ω_3 is a segment of S_a^3 from p_3 to p^{en} , ω_4 is a segment of l^e from p^{en} to q^e , ω_5 is a segment of S_a^4 from q^e to p^f , ω_6 is the heteroclinic orbit of (5.4) from p^f to p_1 , ω_7 is a segment of S_a^1 from p_1 to p_{en} ; finally, ω_8 is a segment of l_e from p_{en} to q_e .

We define the singular cycle Γ_0 of system (5.2) for $\varepsilon = 0$ as

$$(5.9) \quad \Gamma_0 := \omega_1 \cup \omega_2 \cup \omega_3 \cup \omega_4 \cup \omega_5 \cup \omega_6 \cup \omega_7 \cup \omega_8.$$

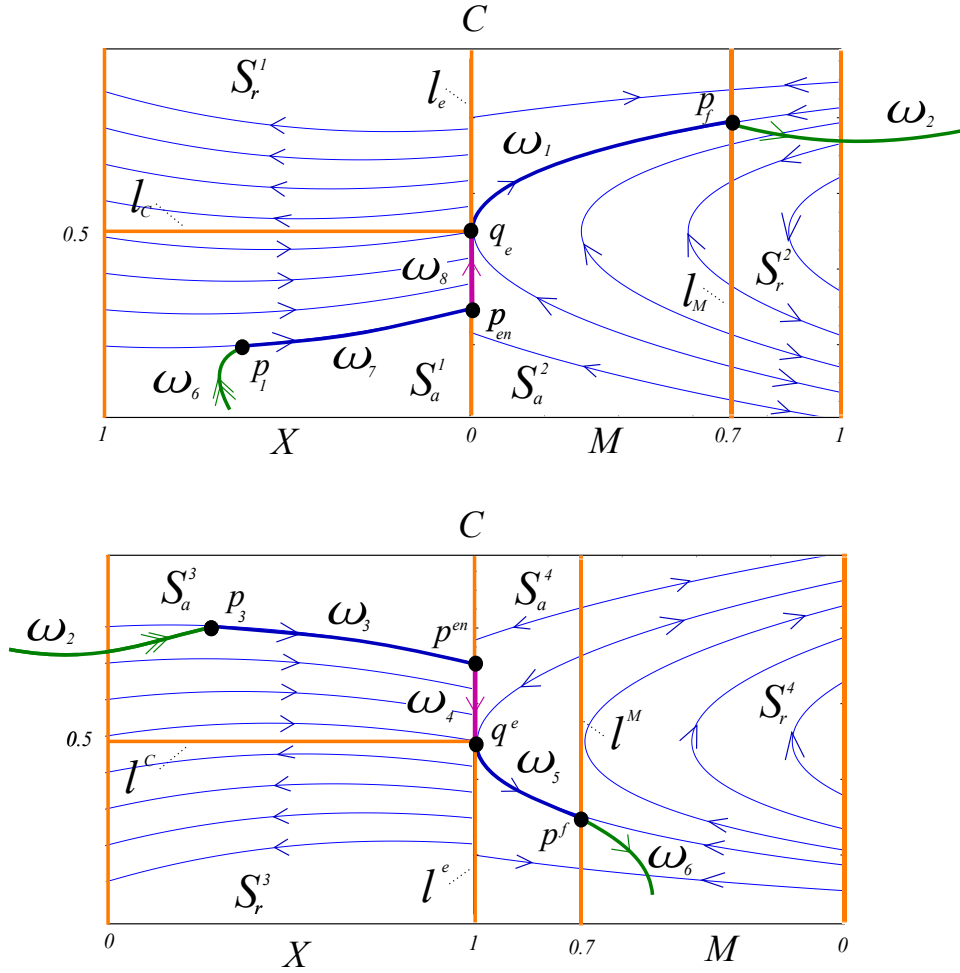


FIGURE 5.6. Reduced flows and singular cycle Γ_0 .

¹The dynamics of systems for which the transversality condition fails is more complicated. We refer to [49] where the existence of chaotic attractors of relaxation oscillators is studied.

REMARK 5.8. Note that starting at the point $q_e = (0, 0, \frac{1}{2})$ guarantees that Γ_0 defined as (5.9) is unique. Alternatively, a starting point to define Γ_0 could be the point $q^e = (1, 1, \frac{1}{2}) \in l^e$.

REMARK 5.9. The upper picture in Figure 5.6 shows the planes $M = 0$ and $X = 0$ intersecting along the edge l_e , whereas in the lower picture the planes $M = 1$ and $X = 1$, which intersect along the edge l^e , are shown. Both pictures show in blue the corresponding reduced flows on S^1 , S^2 , S^3 , and S^4 , respectively; the components of the singular cycle Γ_0 are drawn as thick curves. Namely, in blue two types of solutions of the reduced problems are drawn, i.e., connecting the points of the projection curves $P(l^M)$ and $P(l_M)$ and the points on the edges l_e and l^e , and connecting the points on the edges l_e and l^e and the jump points; these slow solutions are connected by fast fibers, shown in green, from l_M and l^M to $P(l_M)$ and $P(l^M)$, respectively; double green arrows indicate hyperbolic behavior of the layer problem, while non-hyperbolic behavior of the layer problem is indicated by a single green arrow. In contrast to singular cycles in standard slow-fast systems, the slow drifts along the edges shown in purple, which separate the slow motions, are new components of Γ_0 and have been discovered due to the blow-up analysis presented in Section 5.2.1. In Figure 5.7 the singular cycle Γ_0 is shown in \mathbb{R}^3 .

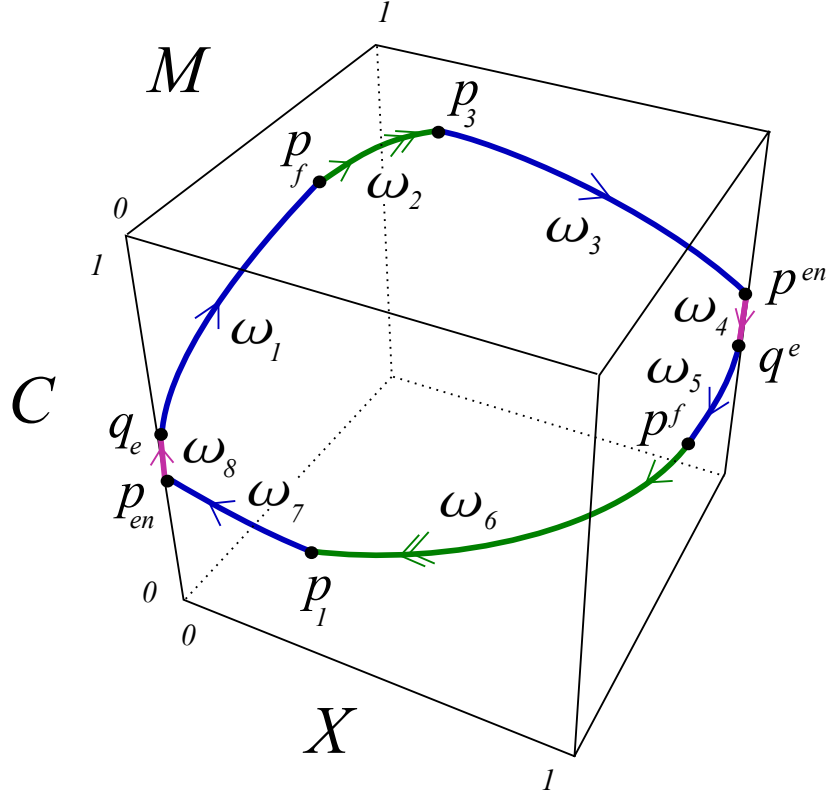


FIGURE 5.7. Singular cycle Γ_0 in \mathbb{R}^3 .

In fact, such identified Γ_0 will be shown to persist in the form of a relaxation cycle of system (5.2) under small singular ε -perturbation. Our main result is the following.

THEOREM 5.3. *The existence of the singular cycle Γ_0 with the specific properties described above implies that for ε sufficiently small there exists a unique attracting periodic orbit Γ_ε of system (5.2), and hence of the equivalent system (5.1), which tends to the singular cycle Γ_0 for $\varepsilon \rightarrow 0$.*

The proof of Theorem 5.3 is given in several steps in the following subsections, which will be then summarized in Section 5.3. Here we briefly present our strategy.

We carry out the proof in a geometric way based on the blow-up technique. The blow-up analysis in the next section starts by performing suitably defined blow-ups of the non-hyperbolic edge l_e and the non-hyperbolic line l_M . We will work exclusively with the blown-up systems and analyze their dynamics.

To show that the existence of Γ_0 implies the existence of a relaxation orbit Γ_ε of system (5.2), we construct a local Poincaré map, half of which is the composition of three different intermediate maps. Two of these maps are constructed for the blown-up systems, i.e., the maps Π_e and Π_f , and describe the dynamics near the non-hyperbolic edge l_e and the non-hyperbolic line l_M , respectively. The third map describes a contraction onto the attracting slow manifolds $S_{a,\varepsilon}^1$.

Finally, we will show that within each leaf $\varepsilon = \text{const.}$ the Poincaré map is a strong contraction and has an attracting fixed point corresponding to the limit cycle.

REMARK 5.10. *We do not present the results for the other two blow-ups, i.e., the edge l^e and the line l^M . The analysis is analogous and for this reason we only show how to construct one half of the return map.*

5.2. Blow-up analysis

In this section we carry out the blow-up analysis for system (5.2). We focus our attention on the dynamics close to the edge l_e and on the dynamics in the plane $X = 0$ close to the non-hyperbolic line l_M . We first perform a blow-up of the non-hyperbolic edge l_e , and then we blow-up the non-hyperbolic line l_M . For this purpose we rewrite system (5.2) as

$$\begin{aligned}
 \frac{dX}{d\tau} &= [M(1-X)(\varepsilon+X) - \frac{7}{10}X(\varepsilon+1-X)]F_\varepsilon(M), \\
 (5.10) \quad \frac{dM}{d\tau} &= \left[\frac{6C}{1+2C}(1-M)(\varepsilon+M) - \frac{3}{2}M(\varepsilon+1-M) \right] F_\varepsilon(X), \\
 \frac{dC}{d\tau} &= \frac{1}{4}(1-X-C)F_\varepsilon(X, M), \\
 \frac{d\varepsilon}{d\tau} &= 0,
 \end{aligned}$$

where as before $F_\varepsilon(M) = (\varepsilon+1-M)(\varepsilon+M)$, $F_\varepsilon(X) = (\varepsilon+1-X)(\varepsilon+X)$, and $F_\varepsilon(X, M) = F_\varepsilon(X)F_\varepsilon(M)$. System (5.10) is considered as a four-dimensional vector field on \mathbb{R}^4 by treating the parameter ε as a variable dependent on τ .

5.2.1. Local analysis close to the non-hyperbolic edge l_e . We investigate the transition of the flow of (5.1) near the edge l_e . We concentrate on the attracting part of S^1 , i.e., S_a^1 and analyze the behaviour of the slow manifold $S_{a,\varepsilon}^1$ together with nearby solutions as they pass near the edge l_e . An exchange of stability behavior is expected to occur, i.e., a transition from slow motion along $S_{a,\varepsilon}^1$ to slow motion along $S_{a,\varepsilon}^2$. Instead, we observe a new phenomenon, which we call a *delayed exchange of stability*. We will see that a slow motion-to-slow motion transition is delayed due to a very slow drift, which occurs almost along the C -axis.

A numerical simulation of the dynamics for $\varepsilon > 0$ close to the edge l_e is shown in Figure 5.8. A drift almost the C -axis is observed for all trajectories starting close to the edge with different initial conditions with $C < 0.5$. This new phenomenon motivated much of our interest in this problem.

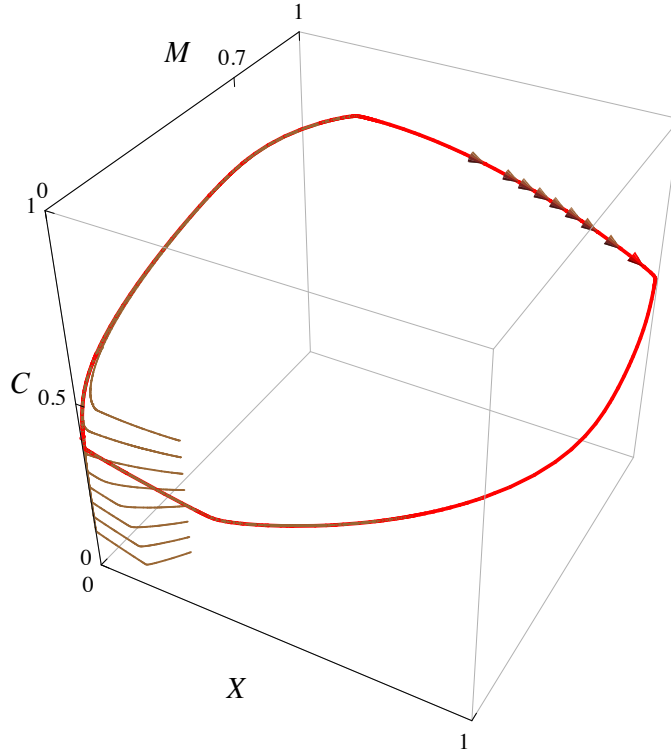


FIGURE 5.8. Numerical simulations of the flow of system (5.2) illustrating a drift almost along the C -axis. Limit cycle Γ_ε is shown in red, while several trajectories attracted to Γ_ε are drawn in brown.

In the singular limit $\varepsilon = 0$ the delayed exchange of stability phenomenon is schematically illustrated in Figure 5.9. For a better visibility of the dynamics, it is drawn as a planar picture and viewed from inside the unit cube. Hence, the $M = 0$ plane is on the left, while the plane $X = 0$ is on the right. Recall that the critical manifold S^1 and the attracting part of the critical manifold S^2 intersect along the non-hyperbolic edge l_e shown in orange; the corresponding slow dynamics is shown

in blue. A solution, which follows the reduced flow on S_a^1 (shown as a thick blue curve), reaches the edge l_e and then, surprisingly, the slow flow pushes it up, and a very slow drift along the edge occurs (shown in purple). When the value $C = 0.5$ is reached, the solution is repelled and follows the reduced flow in the attracting part of S^2 , i.e., in the plane $X = 0$.

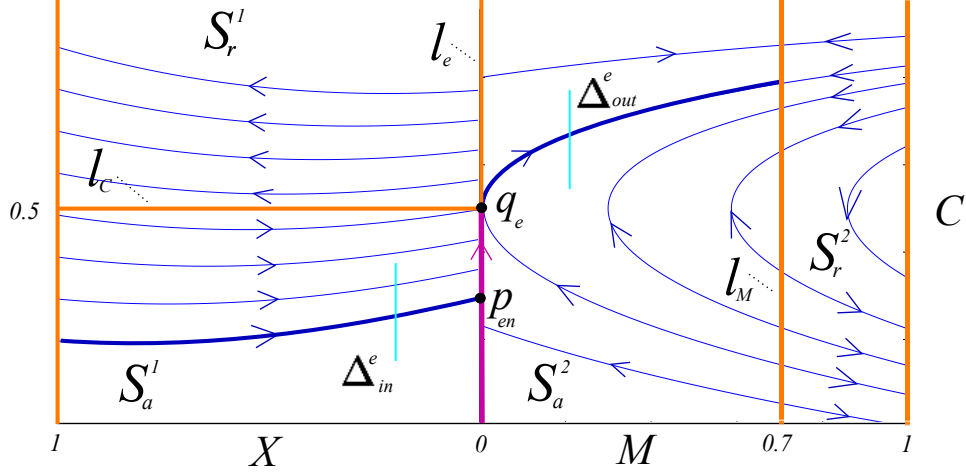


FIGURE 5.9. Delayed exchange of stability at the non-hyperbolic edge l_e .

The behavior of the solutions close to the edge will be studied in this section systematically by the blow-up method. In fact, we will prove Theorem 5.4, which is the main result in the study of this phenomenon. More precisely, let Δ_{in}^e and Δ_{out}^e be two sections transverse to S_a^1 and S_a^2 , respectively, and defined as

$$\Delta_{in}^e = \{(\delta, M, C) : (M, C) \in L_1\}, \quad \Delta_{out}^e = \{(X, \delta, C) : (X, C) \in L_2\},$$

for small $\delta > 0$ and suitable rectangles L_1, L_2 . Note that these sections are two dimensional objects and Figure 5.9 shows their projections onto the planes $M = 0$ and $X = 0$, respectively. Let π_e be a transition map from Δ_{in}^e to Δ_{out}^e induced by the flow of (5.2). We have the following result.

THEOREM 5.4. *For system (5.2) there exist δ and $\varepsilon_0 > 0$ such that for $\varepsilon \in (0, \varepsilon_0]$:*

- (1) *The intersection of manifold $S_{a,\varepsilon}^1$ and Δ_{out}^e is a curve of exponentially small length lying close to a point $(X(\varepsilon), \delta, C(\varepsilon))$.*
- (2) *The image of Δ_{in}^e is a two-dimensional domain of exponentially small width containing the curve $S_{a,\varepsilon}^1 \cap \Delta_{out}^e$.*
- (3) *The transition map π_e is an exponential contraction with a rate $O(e^{-c/\varepsilon})$, where c is a positive constant.*

REMARK 5.11. *The proof of Theorem 5.4 based on blowing up the edge l_e will be given at the end of this section. The point $(X(\varepsilon), \delta, C(\varepsilon)) \in \Delta_{out}^e$ is the intersection point of Δ_{out}^e and a certain one-dimensional fully attracting slow manifold, which is visible only in the blown-up coordinates.*

We now turn to the blow-up analysis.

Blow-up of the non-hyperbolic edge $l_e \times \{0\}$. Note that for the extended system (5.10) the line $l_e \times \{0\}$ is a set of equilibria, at which the linearization of the system has a quadruple zero eigenvalue. Thus, the construction of the slow manifold, as an ε -section of an attracting three-dimensional center-like manifold W_a^c of the extended system (5.10) corresponding to S_a^1 , fails close to the edge l_e . To overcome these degeneracies, we define the blow-up transformation of the non-hyperbolic line of steady states $l_e \times \{0\}$ by

$$(5.11) \quad \begin{aligned} X &= r\bar{X}, \\ M &= r\bar{M}, \\ \varepsilon &= r\bar{\varepsilon}, \\ C &= \bar{C} \end{aligned}$$

with $(\bar{X}, \bar{M}, \bar{\varepsilon}, r, \bar{C}) \in \mathbb{S}^2 \times \mathbb{R} \times \mathbb{R}$. More precisely, we consider the blow-up trans-

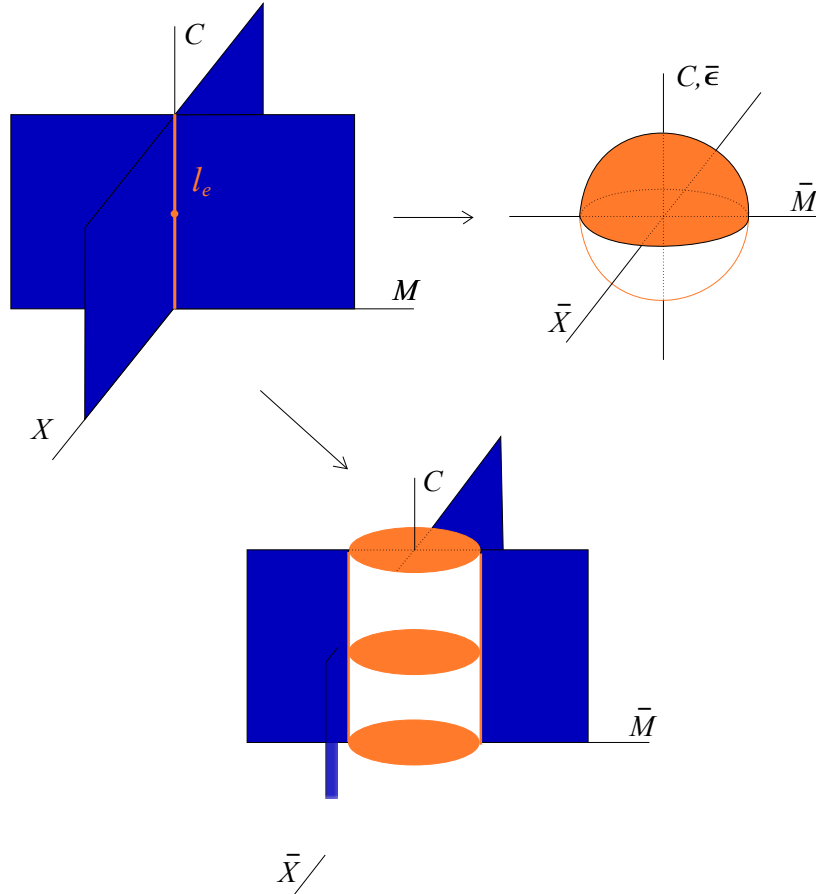


FIGURE 5.10. Blow-up transformation of the non-hyperbolic edge l_e . For C fixed each point $(0, 0, C) \in l_e$ is blown-up to a sphere.

formation (5.11) as a mapping

$$\Phi_e : \mathbb{S}^2 \times \mathbb{R}^2 \rightarrow \mathbb{R}^4,$$

which for $r > 0$ is a diffeomorphism and for $r = 0$ is singular, i.e., the edge $l_e \times \{0\}$ corresponding to $r = 0$ is blown-up to the manifold $Z := \mathbb{S}^2 \times \{0\} \times \mathbb{R}$. For C fixed each point $(0, 0, C) \in l_e$ is blown-up to a sphere, see Figure 5.10.

The blown-up vector field is analyzed in charts K_1 , K_2 , and K_3 , which cover the part of the manifold Z corresponding to $\bar{X} \geq 0$, $\bar{\varepsilon} \geq 0$, and $\bar{M} \geq 0$, respectively. More precisely, we define the charts by setting $\bar{X} = 1$, $\bar{\varepsilon} = 1$, and $\bar{M} = 1$ in the blow-up transformation (5.11). Hence, the local coordinates of charts K_1 , K_2 , and K_3 are given by

$$(5.12) \quad X = r_1, \quad M = r_1 M_1, \quad \varepsilon = r_1 \varepsilon_1, \quad C = C_1,$$

$$(5.13) \quad X = \varepsilon X_2, \quad M = \varepsilon M_2, \quad \varepsilon = r_2, \quad C = C_2,$$

$$(5.14) \quad X = r_3 X_3, \quad M = r_3, \quad \varepsilon = r_3 \varepsilon_3, \quad C = C_3.$$

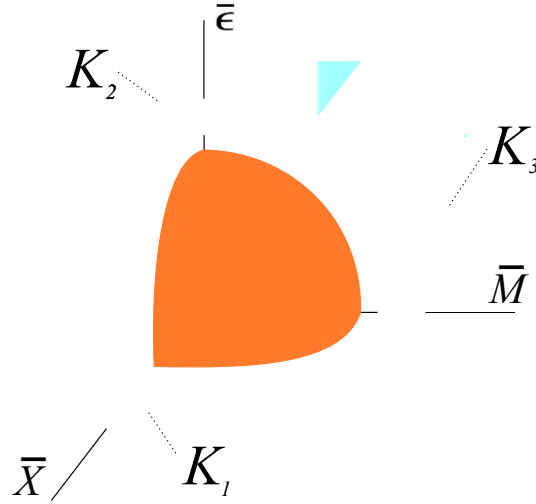


FIGURE 5.11. Local charts covering the sphere for C fixed. Chart K_1 covers the region corresponding to $\bar{X} \geq 0$, chart K_2 covers the upper part of the sphere, and chart K_3 the region corresponding to $\bar{M} \geq 0$.

To obtain the systems of equations written in the coordinates of K_1 , K_2 , and K_3 , we first insert (5.12) – (5.14) into system (5.10), respectively. Note that the resulting systems are well defined on $\{r = 0\}$, however, have trivial flows. It is possible to desingularize these flows by dividing out the common factors (a suitable power of r), which results in a rescaling of time. Consequently, the desingularized systems have nontrivial dynamics for $r = 0$.

Thus, the dynamics in K_1 is governed by

$$\begin{aligned}
 r'_1 &= r_1 f(r_1, M_1, \varepsilon_1), \\
 M'_1 &= \left[\frac{6C_1}{1+2C_1} (1 - r_1 M_1) (\varepsilon_1 + M_1) - \frac{3}{2} M_1 (r_1 \varepsilon_1 + 1 - r_1 M_1) \right] g(r_1, \varepsilon_1) \\
 (5.15) \quad &- M_1 f(r_1, M_1, \varepsilon_1), \\
 C'_1 &= \frac{1}{4} r_1 (1 - r_1 - C_1) (r_1 \varepsilon_1 + 1 - r_1 M_1) (\varepsilon_1 + M_1) g(r_1, \varepsilon_1), \\
 \varepsilon'_1 &= -\varepsilon_1 f(r_1, M_1, \varepsilon_1),
 \end{aligned}$$

with the function $g(r_1, \varepsilon_1) = (\varepsilon_1 + 1 - r_1)(\varepsilon_1 + 1)$ and $f(r_1, M_1, \varepsilon_1)$ given by

$$f(r_1, M_1, \varepsilon_1) = [r_1 M_1 (1 - r_1) (\varepsilon_1 + 1) - \frac{7}{10} (r_1 \varepsilon_1 + 1 - r_1)] (r_1 \varepsilon_1 + 1 - r_1 M_1) (\varepsilon_1 + M_1).$$

In chart K_2 system (5.10) has the form

$$\begin{aligned}
 X'_2 &= -\frac{7}{10} X_2 (1 + M_2) + O(\varepsilon), \\
 (5.16) \quad M'_2 &= \left[\frac{6C_2}{2C_2+1} (1 + M_2) - \frac{3}{2} M_2 \right] (1 + X_2) + O(\varepsilon), \\
 C'_2 &= \frac{1}{4} (1 - C_2) (1 + M_2) (1 + X_2) \varepsilon + O(\varepsilon^2),
 \end{aligned}$$

and in the coordinates of chart K_3 it is given by

$$\begin{aligned}
 X'_3 &= (1 - r_3 \varepsilon_3) (r_3 \varepsilon_3 + 1 - r_3) (\varepsilon_3 + 1) (\varepsilon_3 + X_3) r_3 + \\
 &- \left[\frac{7}{10} (r_3 \varepsilon_3 + 1 - r_3) + \frac{6C_3}{2C_3+1} (1 - r_3) (\varepsilon_3 + X_3) \right] X_3 (\varepsilon_3 + 1) + \\
 &+ \frac{3}{2} X_3 (r_3 \varepsilon_3 + 1 - r_3) (\varepsilon_3 + X_3), \\
 (5.17) \quad r'_3 &= \left[\frac{6C_3}{2C_3+1} (1 - r_3) (\varepsilon_3 + 1) - \frac{3}{2} (r_3 \varepsilon_3 + 1 - r_3) \right] (\varepsilon_3 + X_3) r_3, \\
 C'_3 &= \frac{1}{4} (1 - r_3 X_3 - C_3) (r_3 \varepsilon_3 + 1 - r_3) (\varepsilon_3 + 1) (\varepsilon_3 + X_3) r_3, \\
 \varepsilon'_3 &= \left[\frac{3}{2} (r_3 \varepsilon_3 + 1 - r_3) - \frac{6C_3}{2C_3+1} (1 - r_3) (1 + \varepsilon_3) \right] (\varepsilon_3 + X_3) \varepsilon_3.
 \end{aligned}$$

We emphasize once more that the derivatives in (5.15) – (5.17) are with respect to the rescaled fast time scales $\tau_i, i = 1, 2, 3$, respectively, due to the desingularization of the blown-up vector field.

To understand the flow of (5.10) near the non-hyperbolic edge l_e , we analyze systems (5.15) – (5.17). Note that system (5.16) is a family of vector fields with parameter ε (since $r'_2 = \varepsilon' = 0$), whereas in charts K_1 and K_3 the variables r_1 and r_3 have become dynamic variables; therefore, systems (5.15) and (5.17) are four-dimensional. To connect the flow between the charts on their overlap, we use the following coordinate change relations.

LEMMA 5.2. *The changes of coordinates κ_{ij} from chart K_i to $K_j, i, j = 1, 2, 3$, are given by*

$$(5.18) \quad \kappa_{12} : X_2 = \varepsilon_1^{-1}, \quad r_2 = r_1 \varepsilon_1, \quad M_2 = \frac{M_1}{\varepsilon_1}, \quad C_2 = C_1.$$

$$(5.19) \quad \kappa_{23} : X_3 = \frac{X_2}{M_2}, \quad r_3 = r_2 M_2, \quad \varepsilon_3 = M_2^{-1}, \quad C_3 = C_2.$$

By κ_{ji} we denote the inverse transformations, i.e., from chart K_j to $K_i, i, j = 1, 2, 3$.

REMARK 5.12. We use the following notation: any object P of the extended system (5.10) is denoted as \bar{P} for the blown-up problem, and by P_i in chart K_i , $i = 1, 2, 3$.

In the following we will construct a transition map $\Pi_e : \Sigma_{in}^e \rightarrow \Sigma_{out}^e$ induced by the blown-up vector field, where the sections Σ_{in}^e and Σ_{out}^e are transversal to the attracting branches of the critical manifold S (see Figure 5.12), and will be defined more precisely in specific charts. The transition map Π_e will be used to prove Theorem 5.4.

Recall that the equation $\varepsilon' = 0$ from system (5.10) implies that the blown-up phase space has an invariant foliation corresponding to constant values of ε . In particular, the singular leaf corresponding to $\varepsilon = 0$ is the union of the manifold Z and the region defined by setting $\bar{\varepsilon} = 0$ in (5.11). At the end of this section we will show that restricted to such leafs the map Π_e induced by the blown-up vector field is a strong contraction.

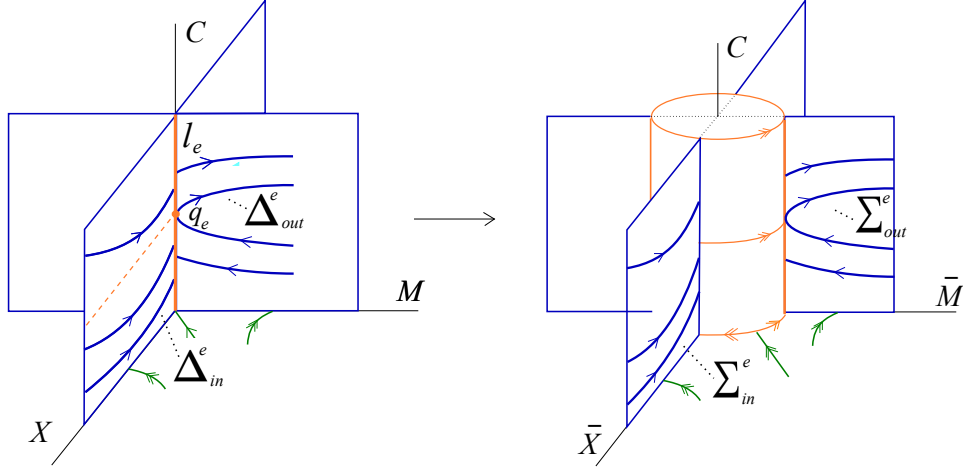


FIGURE 5.12. Sections and blow-up of the non-hyperbolic edge l_e .

The map Π_e will be the composition of three local maps Π_i , which in turn are constructed in charts K_i , $i = 1, 2, 3$, respectively, i.e.,

$$\Pi_e = \Pi_3 \circ \kappa_{2,3} \circ \Pi_2 \circ \kappa_{1,2} \circ \Pi_1.$$

In chart K_1 we will find the extension of the slow manifold $S_{a,\varepsilon}^1$ and see that the transition in K_1 is described by a certain three-dimensional center manifold and its foliation. Next, we will analyze how the continuation of the slow manifold $S_{a,\varepsilon}^1$ can be further extended in other charts. In chart K_2 , we will see that the map Π_2 is an exponential contraction due to the existence of a one-dimensional attracting slow manifold, see Figure 5.13. This one-dimensional slow manifold plays a very special role in the analysis. It will lead the continuation of the slow manifold $S_{a,\varepsilon}^1$ across the cylinder. In chart K_3 we will see that there exists the so-called exit point. We will analyze how the extension of the one-dimensional slow manifold found from chart K_2 exits near this point. Since the exit point is nilpotent, the construction of the transition map Π_3 is more complicated and requires a second-blow-up procedure.

In order not to interrupt the main argument, we present the blow-up of the exit point in Section 5.4 at the end of this chapter. We will see that the contraction gained in chart K_2 is not lost during the passage of the exit point.

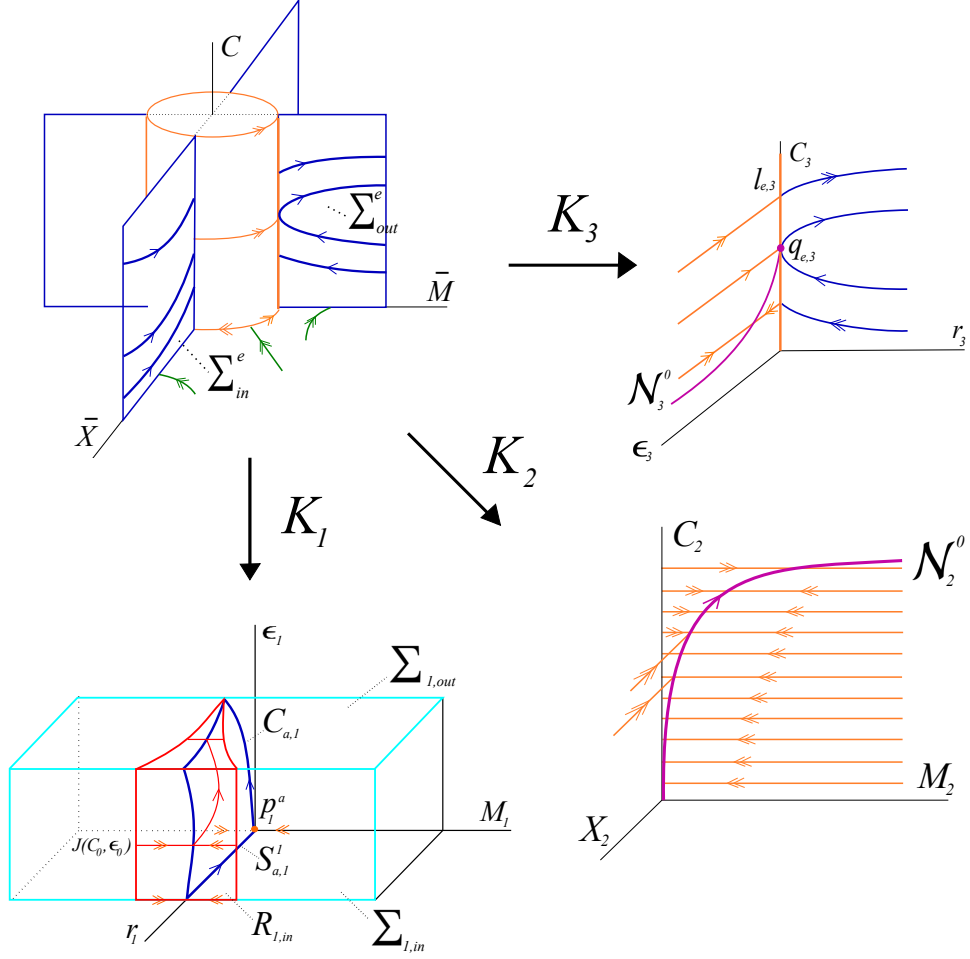


FIGURE 5.13. The flow of (5.10) in the blown-up coordinates.

We now turn to the analysis in the individual charts, which will provide us with the pictures illustrated in anticipation in Figure 5.13.

Analysis in chart K_1 . We start with system (5.15). This system has two invariant hyperplanes, which organize the dynamics in chart K_1 ; namely, the hyperplane $r_1 = 0$ and $\varepsilon_1 = 0$. The $r_1 = 0$ hyperplane corresponds to the manifold Z ,

whereas the hyperplane $\varepsilon_1 = 0$ to the region in front of it. The intersection of these invariant hyperplanes is the (M_1, C_1) -plane, in which the dynamics is governed by

$$(5.20) \quad \begin{aligned} M_1' &= [\frac{6C_1-3}{2(1+2C_1)}]M_1 + \frac{7}{10}M_1^2, \\ C_1' &= 0. \end{aligned}$$

For each $C_1 < \frac{1}{2}$ fixed there are two hyperbolic equilibria $p_1^a = (0, 0, C_1, 0)$ and $p_1^r = (0, \frac{15}{7} \frac{1-2C_1}{1+2C_1}, C_1, 0)$. For the flow in the (M_1, C_1) -plane point p_1^a is attracting, while point p_1^r is repelling. For $C_1 = \frac{1}{2}$ these two points collide at a non-hyperbolic point $(0, 0, \frac{1}{2}, 0)$.

In the invariant hyperplane $\varepsilon_1 = 0$ the dynamics is governed by

$$(5.21) \quad \begin{aligned} r_1' &= r_1 M_1 (r_1 M_1 - \frac{7}{10})(1 - r_1)(1 - r_1 M_1), \\ M_1' &= M_1 (1 - r_1)(1 - r_1 M_1) [\frac{6C_1}{1+2C_1} - \frac{3}{2} - r_1 M_1^2 + \frac{7}{10} M_1], \\ C_1' &= \frac{1}{4} r_1 M_1 (1 - r_1 - C_1)(1 - r_1)(1 - r_1 M_1). \end{aligned}$$

The plane $M_1 = 0$ is a normally hyperbolic plane of equilibria of system (5.21), which we denote by $S_{a,1}^1$. For $0 \leq r_1 < 1$ and $0 \leq C_1 < \frac{1}{2}$ the nonzero eigenvalue along $S_{a,1}^1$ is stable. In particular, the C_1 -axis contained in $S_{a,1}^1$ is attracting for the flow in the $r_1 = 0$ plane. We denote it by $l_{e,1}$ since it corresponds to the non-hyperbolic edge l_e ; however, we have gained normal hyperbolicity due to the blow-up. Furthermore, the curve defined by

$$r_1 = 0, \quad M_1 = -\frac{15}{7} \frac{2C_1 - 1}{2C_1 + 1}$$

is a curve of saddle-type equilibria for system (5.15). We denote it by \mathcal{N}_1^r , see Figure 5.14.

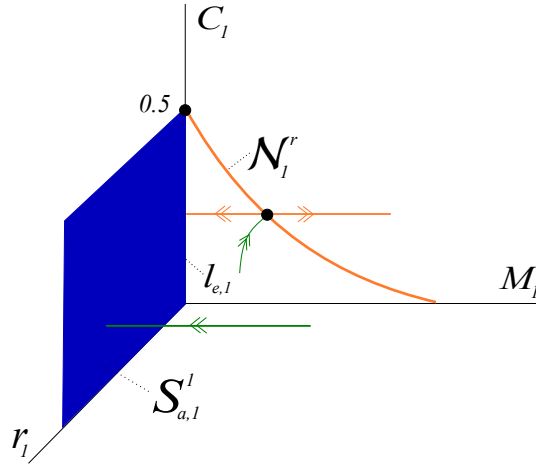


FIGURE 5.14. Equilibria of system (5.15) in the invariant hyperplane $\varepsilon_1 = 0$.

REMARK 5.13. Note that the plane $S_{a,1}^1$ corresponds to the critical manifold S^1 , i.e., the plane $M = 0$.

REMARK 5.14. *The curve of equilibria \mathcal{N}_1^r corresponds to the incoming fast fiber, i.e., these equilibria are the points on the manifold Z , where stable fibers of the layer problem (5.4) end. However, they do not play an important role in the analysis, we mention them for completeness.*

In the invariant hyperplane $r_1 = 0$ system (5.15) reduces to

$$(5.22) \quad \begin{aligned} C_1' &= 0, \\ M_1' &= \left[\frac{6C_1}{1+2C_1}(\varepsilon_1 + M_1) - \frac{3}{2}M_1 \right](\varepsilon_1 + 1) + \frac{7}{10}M_1(\varepsilon_1 + M_1), \\ \varepsilon_1' &= \frac{7}{10}\varepsilon_1(\varepsilon_1 + M_1). \end{aligned}$$

We recover the line $l_{e,1}$ and the curve \mathcal{N}_1^r , see Figure 5.15 (shown in blue and orange, respectively). The Jacobian matrix at the points in $l_{e,1}$ is

$$\begin{pmatrix} \frac{6C_1-3}{2(2C_1+1)} & \frac{6C_1}{2C_1+1} \\ 0 & 0 \end{pmatrix},$$

i.e., the C_1 -axis is attracting for the flow in the $\varepsilon_1 = 0$ plane ($0 \leq C_1 < \frac{1}{2}$). However, we obtain one additional zero eigenvalue due to the equation for ε_1 . This implies the existence of a two-dimensional center manifold $\mathcal{C}_{a,1}$ with center directions $(C_1, M_1, \varepsilon_1) = (1, 0, 0)$ and $(0, -1, \frac{4C_1}{2C_1-1})$. For $C_1 < \frac{1}{2}$ the curve of equilibria \mathcal{N}_1^r is normally hyperbolic.

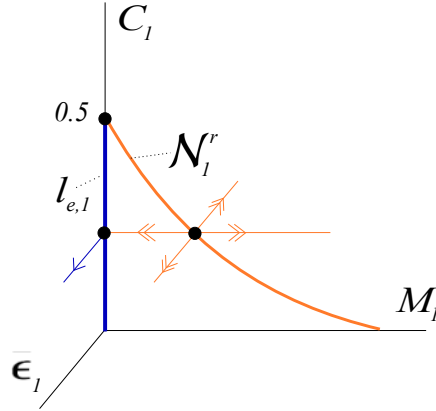


FIGURE 5.15. Equilibria of system (5.15) in the invariant hyperplane $r_1 = 0$.

REMARK 5.15. *In chart K_1 the center manifold $\mathcal{C}_{a,1}$ plays the most important role in the analysis since on the blown-up manifold it can be considered as the extension of the critical manifold $S_{a,1}^1$.*

We summarize the analysis in the invariant hyperplanes with the following lemmas.

LEMMA 5.3. *System (5.15) has the following manifolds of equilibria*

$$\mathcal{N}_1^r = \{(r_1, M_1, C_1, \varepsilon_1) : r_1 = 0, \quad M_1 = -\frac{15}{7} \frac{2C_1-1}{2C_1+1}, \quad C_1 \in [0, \frac{1}{2}], \quad \varepsilon_1 = 0\}$$

and the plane $S_{a,1}^1$, which contains the line $l_{e,1}$.

LEMMA 5.4. *For system (5.15) the following assertions hold.*

- (1) *The linearization of system (5.15) at the steady states of $S_{a,1}^1$ has the following real eigenvalues*
 - (a) $\lambda_1 = \frac{6C_1-3}{2(2C_1+1)}(1-r_1)$ *with eigenvector $(0, 1, 0, 0)^T$. For $r_1 = 0$ it corresponds to the flow in the invariant (M_1, C_1) -plane.*
 - (b) *double $\lambda_2 = 0$ with eigenvectors tangent to the $M_1 = 0$ plane.*
 - (c) $\lambda_3 = 0$ *with the eigenvector $(0, -1, 0, \frac{4C_1}{2C_1-1})$ corresponding to the center direction in the invariant hyperplane $r_1 = 0$.*
- (2) *For ρ_1, ρ_2 sufficiently small there exists a three-dimensional center manifold $W_{a,1}^c$ of the line $l_{e,1}$, which contains the plane of equilibria $S_{a,1}^1$ and the center manifold $C_{a,1}$. The manifold $W_{a,1}^c$ is attracting and in a set D_1*

$$D_1 = \{(r_1, M_1, C_1, \varepsilon_1) : 0 \leq r_1 \leq \delta, 0 \leq \varepsilon_1 \leq \alpha_1, C_1 \in I_1\}$$
is given as a graph

$$M_1 = h_{a,1}(r_1, C_1, \varepsilon_1),$$

where I_1 is a suitable interval. In particular, at a point $p_{a,1} \in l_{e,1}$ such that $C_0 \in I_1$ the function $h_{a,1}(r_1, C_1, \varepsilon_1)$ has the expansion

$$(5.23) \quad h_{a,1}(r_1, C_0, \varepsilon_1) = -\frac{4C_0}{2C_0-1}\varepsilon_1 + O(2).$$

- (3) *There exists $c_1 < \frac{3-6C_0}{2(2C_0+1)}$ such that the orbits near the center manifold $W_{a,1}^c$ are attracted to $W_{a,1}^c$ by an exponential rate of order $O(e^{-c_1 t_1})$.*

PROOF. The first assertion follows from calculations. The last two assertions follow from center manifold theory [18], [46], applied at a point $p_{a,1} \in l_{e,1}$, which has gained an attracting direction due to the blow-up. \square

REMARK 5.16. *The manifold $W_{a,1}^c$ corresponds to the slow manifold $S_{a,\varepsilon}^1$ described in Theorem 5.1. Recall that Fenichel theory implies the existence of an attracting center-like manifold W_a^c of the extended system (5.10) for sufficiently small ε . The slow manifold $S_{a,\varepsilon}^1$ is obtained as a section $\varepsilon = \text{const.}$ of W_a^c . In chart K_1 this center manifold is given by (5.23).*

Thus, in chart K_1 we are mainly interested in understanding the dynamics near the center manifold $W_{a,1}^c$ as it corresponds to the neighborhood of the attracting slow manifold $S_{a,\varepsilon}^1$ of system (5.2). Let $\delta > 0$, $\alpha_1 > 0$ and β_1 be small constants. We define two sections $\Sigma_{1,in}$ and $\Sigma_{1,out}$, and a rectangle $R_{1,in}$ by

$$\begin{aligned} \Sigma_{1,in} &= \{(r_1, M_1, C_1, \varepsilon_1) \in D_1 : r_1 = \delta\}, \\ \Sigma_{1,out} &= \{(r_1, M_1, C_1, \varepsilon_1) \in D_1 : \varepsilon_1 = \alpha_1\}, \\ R_{1,in} &= \{(r_1, M_1, C_1, \varepsilon_1) \in D_1 : r_1 = \delta, |M_1| \leq \beta_1\}. \end{aligned}$$

Note that with this choice of δ , α_1 and β_1 the following relations hold

$$R_{1,in} \subset \Sigma_{1,in}, \quad \Sigma_{1,in} \subset \Delta_{in}^e.$$

Moreover, we can choose the constants such that the intersection of the center manifold $W_{a,1}^c$ with the section $\Sigma_{1,in}$ lies in $R_{1,in}$, i.e., $W_{a,1}^c \cap \Sigma_{1,in} \subset R_{1,in}$.

REMARK 5.17. *The invariant leaves $\varepsilon = \text{const.}$ are given by $\varepsilon_1 = \frac{\varepsilon}{\delta}$ in $\Sigma_{1,in}$ and by $r_1 = \frac{\varepsilon}{\alpha_1}$ in $\Sigma_{1,out}$ due to the relation $\varepsilon = r_1 \varepsilon_1$.*

Our goal is to construct the transition map $\Pi_1 : \Sigma_{1,in} \rightarrow \Sigma_{1,out}$ defined by the flow of (5.15). We are interested how solutions starting in $R_{1,in} \subset \Sigma_{1,in}$ near the center manifold $W_{a,1}^c$ reach the section $\Sigma_{1,out}$. Therefore, we first look at the evolution of the C_1 variable in the three-dimensional center manifold $W_{a,1}^c$ of the line $l_{e,1}$, i.e., our goal is to estimate $C_{1,out} \in \Sigma_{1,out}$ for a given $(r_{1,in}, C_{1,in}, \varepsilon_{1,in}) \in \Sigma_{1,in}$. For this purpose we substitute $M_1 = h_{a,1}(r_1, C_1, \varepsilon_1)$ into system (5.15) and rescale time to obtain the flow on the center manifold. Namely, we get

$$(5.24) \quad \begin{aligned} r_1' &= -r_1, \\ C_1' &= \frac{5}{14}(1 - r_1 - C_1)(O(r_1) + O(r_1\varepsilon_1)), \\ \varepsilon_1' &= \varepsilon_1. \end{aligned}$$

Note that the derivative in system (5.24) is with respect to a rescaled time scale s_1 .

Consider a solution $(r_1(s_1), C_1(s_1), \varepsilon_1(s_1))$ of (5.24), which satisfies

$$(5.25) \quad \begin{aligned} r_1(0) &= \delta & r_1(T_s) &= r_{1,out} \\ C_1(0) &= C_{1,in} & C_1(T_s) &= C_{1,out} \\ \varepsilon_1(0) &= \varepsilon_{1,in} & \varepsilon_1(T_s) &= \alpha_1. \end{aligned}$$

The formulas $\varepsilon_1(s_1) = \varepsilon_{1,in} \exp(s_1)$ and $r_1(s_1) = \delta \exp(-s_1)$ imply that the transition time T_s , i.e., time needed for a point $(\delta, C_{1,in}, \varepsilon_{1,in}) \in \Sigma_{1,in}$ to reach $\Sigma_{1,out}$ under the flow of (5.24), is given by

$$(5.26) \quad T_s = \ln \frac{\alpha_1}{\varepsilon_{1,in}}.$$

By integrating the equation

$$C_1' = \frac{5}{14}(1 - \delta e^{-s_1} - C_1)(\delta e^{-s_1} O(1) + \delta \varepsilon_{1,in} O(1)),$$

we estimate the evolution of C_1 , i.e., we get

$$(5.27) \quad C_1(s_1) = C_{1,in} e^{-\frac{5}{14}\delta(-e^{-s_1} + s_1\varepsilon_{1,in})} - \frac{5}{14}\delta e^{-\frac{5}{14}\delta(-e^{-s_1} + s_1\varepsilon_{1,in})} f(s_1),$$

where $f(s_1)$ is given by

$$f(s_1) = \int e^{-2s_1 + \frac{5}{14}\delta(-e^{-s_1} + \varepsilon_{1,in}s_1)} (-e^{s_1} + \delta)(1 + e^{s_1}\varepsilon_{1,in}) ds_1.$$

We therefore obtain that

$$(5.28) \quad C_1(T_s) = C_{1,out} =: F_1(\delta, C_{1,in}, \varepsilon_{1,in})$$

with

$$F_1(\delta, C_{1,in}, 0) = -\frac{9}{5} + C_{1,in}$$

describing the flow on $S_{a,1}$ from $\Sigma_{1,in}$ to the $l_{e,1}$ -axis. In the original variables $F_1(\delta, C_{1,in}, 0)$ corresponds to the reduced flow from Σ_{in} to the non-hyperbolic edge l_e .

REMARK 5.18. *We note that due to the complicated formula (5.27), the estimate (5.28) for $C_{1,out} \in \Sigma_{1,out}$ is imprecise, but it does still allow us to construct the transition map Π_1 . Moreover, as it will turn out in chart K_2 , it is not necessary to quantify this estimate.*

We summarize the obtained results in Theorem 5.5 and illustrate them in Figure 5.16, which shows the geometry and dynamics in chart K_1 projected to the hyperplane $C_1 = \text{const.}$.

THEOREM 5.5. *For system (5.15) the transition map $\Pi_1 : R_{1,in} \rightarrow \Sigma_{1,out}$ is well-defined for δ, α_1 small enough, and sufficiently small $R_{1,in} \subset \Sigma_{1,in}$, and has the following properties*

- (1) $\Pi_1(R_{1,in}) \subset \Sigma_{1,out}$ is a three-dimensional wedge-like region in $\Sigma_{1,out}$, i.e., for fixed $c > \frac{6C_0-3}{2(2C_0+1)}$ there exists a constant $\tilde{K} = \tilde{K}(c, \delta, \alpha_1, \beta_1)$ such that for $\varepsilon_0 \in (0, \alpha_1]$, $C_0 \in I_1$, the image $\Pi_1(J(C_0, \varepsilon_0))$ is a line in $W_{a,1}^c \cap \Sigma_{1,out}$, whose length is bounded by $\tilde{K}e^{-cT}$, where

$$T = O(1/\varepsilon_1).$$

- (2) The transition map Π_1 is given by

$$(5.29) \quad \Pi_1 \begin{pmatrix} \delta \\ M_1 \\ C_1 \\ \varepsilon_1 \end{pmatrix} = \begin{pmatrix} \frac{\delta}{\alpha_1} \varepsilon_1 \\ h_{a,1}^{out}(\frac{\delta}{\alpha_1} \varepsilon_1, F_1(\delta, C_1, \varepsilon_1), \alpha_1) \\ F_1(\delta, C_1, \varepsilon_1) \\ \alpha_1 \end{pmatrix} + \begin{pmatrix} 0 \\ \psi(M_1, C_1, \varepsilon_1) \\ 0 \\ 0 \end{pmatrix}$$

with $h_{a,1}^{out}(\frac{\delta}{\alpha_1} \varepsilon_1, F_1(\delta, C_1, \varepsilon_1), \alpha_1) = O(\varepsilon_1)$ and the exponentially small function $\psi(M_1, C_1, \varepsilon_1)$.

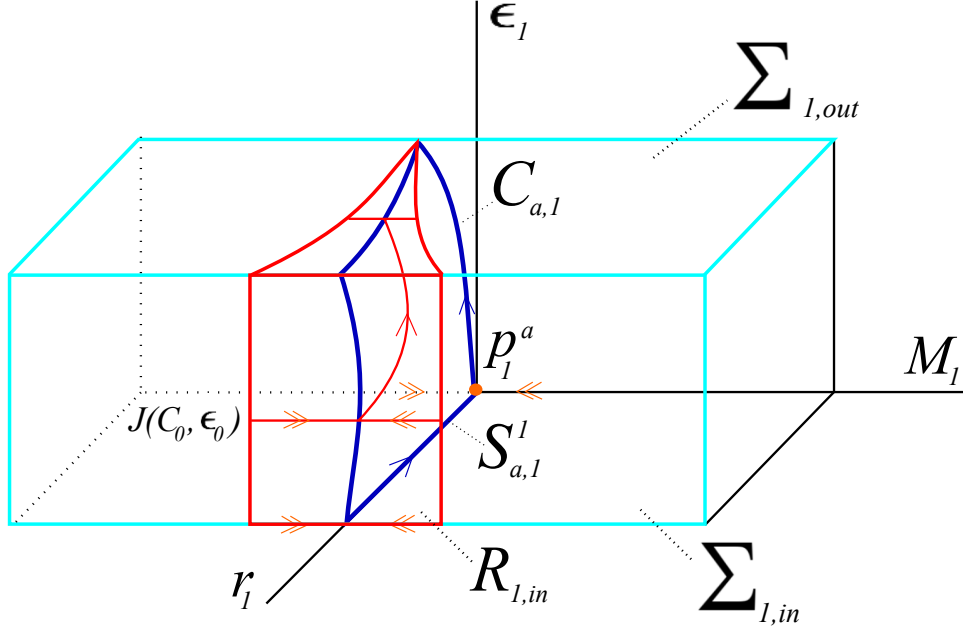


FIGURE 5.16. Dynamics in chart K_1 projected to $C_1 = \text{const.}$

Let $\sigma_{1,out}$ denote a surface formed by the intersection of $\Sigma_{1,out}$ with the center manifold $W_{a,1}^c$. Note that $\sigma_{1,out}$ is described by the first term in the right hand side of (5.29) and as $\varepsilon_1 \rightarrow 0$, $\Pi_1(\delta, M_1, C_1, \varepsilon_1)$ converges to the intersection curve of $\Sigma_{1,out}$ and $C_{a,1}$; see Figure 5.16, where the situation projected to $C_1 = \text{const.}$ is shown.

Summing up, from the analysis in chart K_1 we see that the behavior of all orbits starting in $\Sigma_{1,in}$ is determined by the continuation of the slow manifold $S_{a,1}^1$.

Analysis in chart K_2 . System (5.16) is a slow-fast system with respect to ε , i.e., C_2 is the slow variable, X_2 and M_2 are the fast variables, and $'$ denotes differentiation with respect to the fast time scale τ_2 . By transforming to the slow time scale $t_2 = \varepsilon\tau_2$, we obtain the equivalent slow system

$$\begin{aligned} \varepsilon \dot{X}_2 &= -\frac{7}{10}X_2(1+M_2) + O(\varepsilon), \\ (5.30) \quad \varepsilon \dot{M}_2 &= [\frac{6C_2}{2C_2+1}(1+M_2) - \frac{3}{2}M_2](1+X_2) + O(\varepsilon), \\ \dot{C}_2 &= \frac{1}{4}(1-C_2)(1+M_2)(1+X_2) + O(\varepsilon). \end{aligned}$$

The derivative in (5.30) is now with respect to t_2 .

REMARK 5.19. *In this chart the variables M_2 and X_2 vary on the same time scale, whereas the variable C_2 on a slower time scale. This reflects the fact that in system (5.2) the variable C_2 is no longer fast close to the non-hyperbolic edge l_e .*

Setting $\varepsilon = 0$ in (5.16) gives the layer problem

$$\begin{aligned} X_2' &= -\frac{7}{10}X_2(1+M_2), \\ (5.31) \quad M_2' &= [\frac{6C_2}{2C_2+1}(1+M_2) - \frac{3}{2}M_2](1+X_2), \\ C_2' &= 0. \end{aligned}$$

The corresponding critical manifold, which we denote by \mathcal{N}_2^0 , can be taken as any compact subset of

$$\left\{ -\frac{7}{10}X_2(1+M_2) = 0, \quad [\frac{6C_2}{2C_2+1}(1+M_2) - \frac{3}{2}M_2](1+X_2) = 0 \right\},$$

i.e., it is a curve of equilibria given by $X_2 = 0, M_2 = -\frac{4C_2}{2C_2-1}$, shown in purple in Figure 5.17. The critical manifold \mathcal{N}_2^0 is fully attracting. In particular, for C_2 -fixed, each point $q_2^a = (0, -\frac{4C_2}{2C_2-1}, C_2)$ is a stable node.

Setting $\varepsilon = 0$ in (5.30) defines the reduced problem

$$\begin{aligned} 0 &= -\frac{7}{10}X_2(1+M_2), \\ (5.32) \quad 0 &= [\frac{6C_2}{2C_2+1}(1+M_2) - \frac{3}{2}M_2](1+X_2), \\ \dot{C}_2 &= \frac{1}{4}(1-C_2)(1+M_2)(1+X_2). \end{aligned}$$

The dynamics of the reduced problem (5.32) on the critical manifold \mathcal{N}_2^0 is obtained by substituting $M_2 = -\frac{4C_2}{2C_2-1}$ and $X_2 = 0$ into the third equation of system (5.32). This gives the equation

$$(5.33) \quad \dot{C}_2 = \frac{1}{4}(C_2 - 1)\left(\frac{2C_2 + 1}{2C_2 - 1}\right).$$

Hence, C_2 increases under the slow flow on \mathcal{N}_2^0 , as shown in Figure 5.17. To see what happens at $C_2 = \frac{1}{2}$, one must switch to chart K_3 , since the slow flow is not defined for $C_2 = \frac{1}{2}$.

A description of the dynamics for $0 < \varepsilon \ll 1$ in chart K_2 can be given by Fenichel theory, which implies the existence of a slow manifold $\mathcal{N}_2^\varepsilon$ that is a perturbation of \mathcal{N}_2^0 , i.e., lies within $O(\varepsilon)$ of \mathcal{N}_2^0 . We have

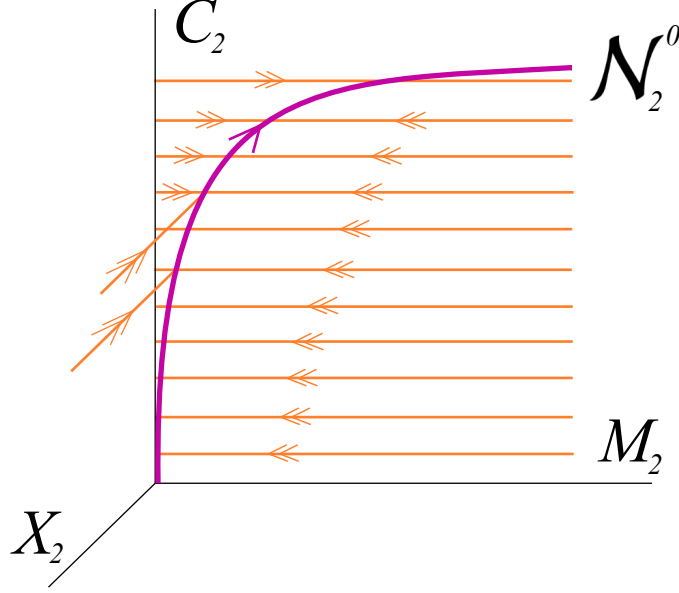


FIGURE 5.17. Critical manifold \mathcal{N}_2^0 , fast and slow dynamics in chart K_2 .

THEOREM 5.6. *For a suitable interval I_2 there exists ε_0 such that for $\varepsilon \in (0, \varepsilon_0]$ there exists a smooth locally invariant attracting one-dimensional slow manifold $\mathcal{N}_2^\varepsilon$ given by the equations*

$$(5.34) \quad (X_2, M_2) = h(C_2) = \left(0, -\frac{4C_2}{2C_2 - 1}\right) + O(\varepsilon), \quad C_2 \in I_2.$$

REMARK 5.20. *The description of the dynamics governed in chart K_2 helps us understand the kinetics and mitotic events that happen for small concentrations of *cdc2* kinase M and cyclin protease X . A slow accumulation of cyclin C results from the fact that a solution starting close to the slow manifold $\mathcal{N}_2^\varepsilon$, i.e., with a low value of cyclin and M , X close to zero, is rapidly attracted by the slow manifold $\mathcal{N}_2^\varepsilon$ and follows the slow flow along it. Hence, the value of C continues to increase.*

REMARK 5.21. *The situation corresponding to the activation of *cdc2* kinase M , i.e., when the cyclin level reaches the threshold value $C \approx 0.5$, is best seen in chart K_3 .*

We now construct a local transition map Π_2 . Recall that the outgoing section $\Sigma_{1,out}$ in chart K_1 is mapped by the diffeomorphism κ_{12} to the incoming section of chart K_2 , i.e., section $\Sigma_{2,in}$ is defined by

$$\Sigma_{2,in} := \{(X_2, M_2, C_2, \varepsilon) : X_2 = \frac{1}{\alpha_1}, \quad M_2 \in [0, \beta_2], \quad C_2 \in I_2, \quad \varepsilon \in [0, \alpha_2]\}$$

with the invariant leaves $\varepsilon = \text{const.}$, $\beta_2 = \beta_1/\alpha_1$, $\delta > 0$ small, $\alpha_2 = \delta\alpha_1$, and a suitable interval I_2 . We define the outgoing section $\Sigma_{2,out}$ in chart K_2 by

$$\Sigma_{2,out} := \{(X_2, M_2, C_2, \varepsilon) : X_2 \in [0, 1/\alpha_1], \quad M_2 = \beta_2, \quad C_2 \in I_2, \quad \varepsilon \in [0, \alpha_2]\}.$$

REMARK 5.22. *Recall that $\Pi_1(R_{1,in})$ is a three-dimensional wedge-like region in $\Sigma_{1,out}$, and $\sigma_{1,out}$ is a surface formed by the intersection of $W_{a,1}^c \cap \Sigma_{1,out}$. Since κ_{12}*

is a diffeomorphism restricted to $\Sigma_{1,out}$, $\kappa_{12}(\Pi_1(R_{1,in}))$ is also a wedge-like region in $\Sigma_{2,in}$ around the surface $\kappa_{12} \circ \Pi_1(R_{1,in} \cap W_{a,1}^c)$. Let $\sigma_{2,in}$ denote the image of $\sigma_{1,out}$ under the map κ_{12} .

The transition map $\Pi_2 : \Sigma_{2,in} \rightarrow \Sigma_{2,out}$ is described by the Fenichel theory. All orbits starting from $(\frac{1}{\alpha_1}, M_{2,in}, C_{2,in}, \varepsilon) \in \Sigma_{2,in}$ are attracted by the slow manifold $\mathcal{N}_2^\varepsilon$, follow the slow dynamics along $\mathcal{N}_2^\varepsilon$, and after a while cross the section $\Sigma_{2,out}$ transversally.

THEOREM 5.7. *For $\alpha_1 > 0$ there exists α_2 small enough such that the following assertions hold.*

(1) *The transition map*

$$\Pi_2 : \Sigma_{2,in} \rightarrow \Sigma_{2,out}, \quad \left(\frac{1}{\alpha_1}, C_{2,in}, M_{2,in}, \varepsilon\right) \mapsto (X_{2,out}, \beta_2, C_{2,out}, \varepsilon)$$

is well-defined. Restricted to slices $\varepsilon = \text{const.}$ in $\Sigma_{2,in}$ the map is contracting with a rate $e^{-c/\varepsilon}$, where $c > 0$.

(2) *The intersection of $\mathcal{N}_2^\varepsilon$ with $\Sigma_{2,out}$ is a smooth curve denoted by $\eta_{2,out}$.*

(3) *The image $\Pi_2(\Sigma_{2,in})$ is an exponentially thin wedge lying exponentially close to the curve $\eta_{2,out}$.*

REMARK 5.23. *Note that for ε -fixed, the intersection of the slow manifold $\mathcal{N}_2^\varepsilon$ with $\Sigma_{2,out}$, i.e., the curve $\eta_{2,out}$ is just a point, and the incoming section $\Sigma_{2,in}$ is mapped into an interval lying exponentially close to this point.*

Summing up, the importance of the slow manifold $\mathcal{N}_2^\varepsilon$ and its strongly contracting properties is that it “leads” the incoming continuation of the slow manifold $S_{a,\varepsilon}^1$ through chart K_2 , i.e., across the cylinder to a certain exit point, which will be visible in chart K_3 . Hence, it is of our interest to see how this slow manifold further extends in K_3 .

Analysis in chart K_3 . We switch to chart K_3 , where the dynamics is governed by system (5.17). Again we start with the analysis in the invariant hyperplanes, namely the hyperplane $\varepsilon_3 = 0$ and $r_3 = 0$. Their intersection is the (X_3, C_3) -plane, which is also invariant and the dynamics there is described by

$$(5.35) \quad \begin{aligned} X_3' &= \frac{3-6C_3}{2(2C_3+1)} X_3^2 - \frac{7}{10} X_3, \\ C_3' &= 0. \end{aligned}$$

For each $C_3 < 0.5$ there are two hyperbolic equilibria $p_3^a = (0, 0, C_3, 0)$ and $p_3^r = (\frac{7}{15} \frac{1+2C_3}{1-2C_3}, 0, C_3, 0)$. The point p_3^a is attracting for the flow in the (X_3, C_3) -plane, whereas the point p_3^r is repelling.

REMARK 5.24. *Note that for $C_3 = 1/2$ the point p_3^r goes to infinity and is no longer visible in chart K_3 .*

In the invariant hyperplane $\varepsilon_3 = 0$ the dynamics is governed by

$$(5.36) \quad \begin{aligned} X_3' &= [(r_3 - \frac{7}{10}) - X_3(\frac{6C_3}{2C_3+1} - \frac{3}{2})](1 - r_3)X_3, \\ r_3' &= [\frac{6C_3}{2C_3+1} - \frac{3}{2}](1 - r_3)X_3r_3, \\ C_3' &= \frac{1}{4}(1 - r_3X_3 - C_3)(1 - r_3)X_3r_3. \end{aligned}$$

The equilibria of this system are the $X_3 = 0$ plane denoted by S_3^2 and the curve of equilibria given by $X_3 = \frac{7}{15} \frac{1+2C_3}{1-2C_3}$, which we denote by \mathcal{N}_3^r . The change of the stability of the points in S_3^2 occurs at $r_3 = \frac{7}{10}$, i.e., for $r_3 < \frac{7}{10}$ the points are attracting while for $r_3 > \frac{7}{10}$ the points are repelling. We denote the attracting and repelling part by $S_{a,3}^2$ and by $S_{r,3}^2$, respectively. The attracting part $S_{a,3}^2$ emanates from the C_3 -axis, which we denote by $l_{e,3}$. The line $l_{e,3}$ is also attracting for the flow in the $r_3 = 0$ plane. The curve \mathcal{N}_3^r is of saddle type and recovered from chart K_1 , i.e., it is the image of the curve \mathcal{N}_1^r from chart K_1 under the transformation κ_{13} , see Figures 5.14 and 5.18. This also explains the notation.

REMARK 5.25. *The curve \mathcal{N}_3^r is mentioned just for completeness as it plays no important role in chart K_3 .*

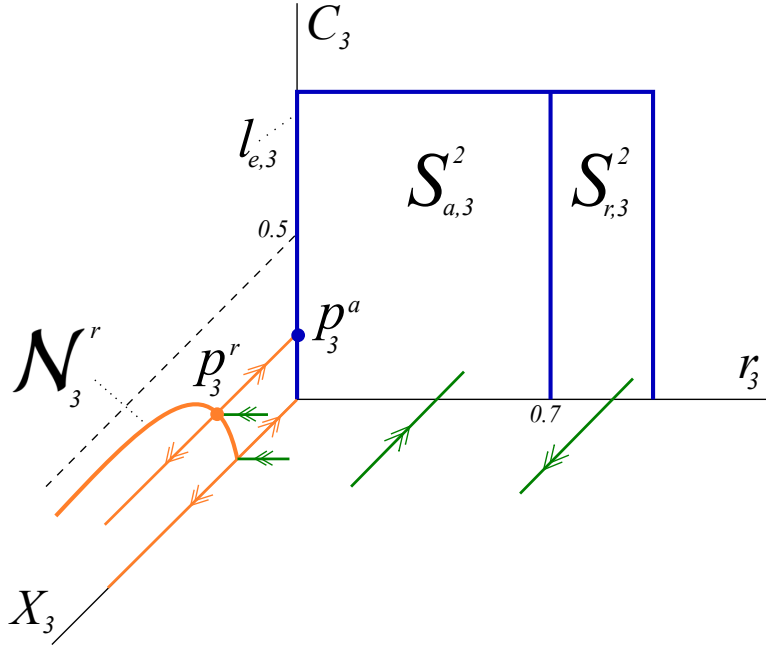


FIGURE 5.18. Dynamics of system (5.17) in the invariant hyperplane $\varepsilon_3 = 0$.

For $r_3 = 0$ system (5.17) reduces to

$$\begin{aligned}
 (5.37) \quad C_3' &= 0, \\
 X_3' &= [-(\frac{7}{10} + \frac{6C_3}{2C_3+1}(\varepsilon_3 + X_3))(\varepsilon_3 + 1) + \frac{3}{2}(\varepsilon_3 + X_3)]X_3, \\
 \varepsilon_3' &= [\frac{3}{2} - \frac{6C_3}{2C_3+1}(1 + \varepsilon_3)](\varepsilon_3 + X_3)\varepsilon_3.
 \end{aligned}$$

The curves of equilibria of (5.37) are shown in Figure 5.19. We recover the curve \mathcal{N}_3^r and the line $l_{e,3}$. In addition, we find one more curve of equilibria, which is precisely the critical manifold \mathcal{N}_2^0 found in chart K_2 , i.e., the curve \mathcal{N}_3^0 is the image of the critical manifold \mathcal{N}_2^0 under the transformation κ_{23} given by (5.19). The curve \mathcal{N}_3^0 is fully attracting. Note, however, that at $C_3 = \frac{1}{2}$ the curve \mathcal{N}_3^0 intersects the line $l_{e,3}$ at the non-hyperbolic point, which we denote by $q_{e,3} = (\frac{1}{2}, 0, 0)$.

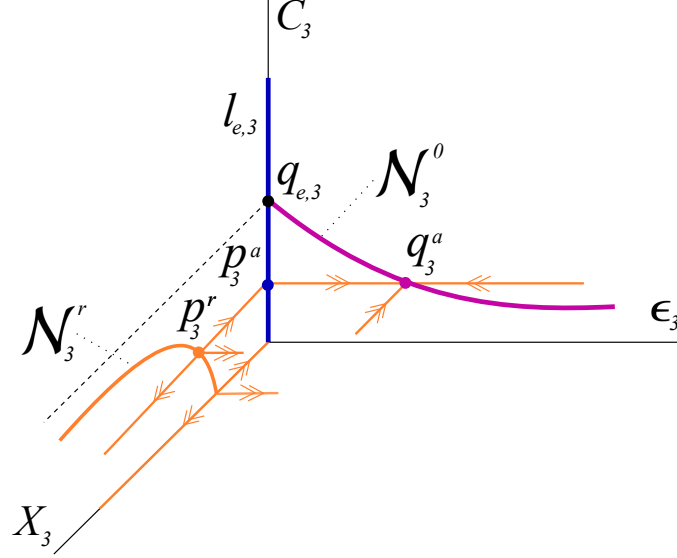


FIGURE 5.19. Dynamics of system (5.17) in the invariant hyperplane $r_3 = 0$.

REMARK 5.26. Note that the attracting manifold \mathcal{N}_2^0 , which was unbounded in chart K_2 , has been compactified in chart K_3 , see Figure 5.17 and 5.19. Thus, what happens when $C_2 \rightarrow \frac{1}{2}$ in chart K_2 is now visible in chart K_3 precisely at $C_3 = \frac{1}{2}$.

REMARK 5.27. Recall that in the original problem, the variable C activates *cdc2* kinase M once the activation threshold value ≈ 0.5 is passed. This activation corresponds to the passage of the non-hyperbolic point $q_{e,3}$ in chart K_3 and will be further studied by means of a blow-up.

From the analysis in the invariant hyperplanes we conclude with the following lemmas.

LEMMA 5.5. System (5.17) has two one-dimensional manifolds of equilibria

$$\mathcal{N}_3^0 = \{(X_3, r_3, C_3, \epsilon_3) : X_3 = 0, r_3 = 0, C_3 \in (0, \frac{1}{2}], \epsilon_3 = \frac{1-2C_3}{4C_3}\},$$

$$\mathcal{N}_3^r = \{(X_3, r_3, C_3, \epsilon_3) : X_3 = \frac{7}{15} \frac{1+2C_3}{1-2C_3}, r_3 = 0, C_3 \in [0, \frac{1}{2}), \epsilon_3 = 0\},$$

and the plane S_3^2 , which emanates from the line $l_{e,3}$.

LEMMA 5.6. For system (5.17) the following assertions hold.

- (1) The equilibria of system (5.17) in \mathcal{N}_3^0 with $C_3 < \frac{1}{2}$ have
 - (a) a two-dimensional stable manifold corresponding to negative eigenvalues.
 - (b) a two-dimensional center manifold corresponding to a double zero eigenvalue.
- (2) The linearization at equilibria in S_3^2 is
 - (a) hyperbolic for $r \neq \frac{7}{10}$ with the eigenvalue $(r - \frac{7}{10})(1 - r)$.
 - (b) non-hyperbolic for $r = \frac{7}{10}$.

- (3) The linearization of (5.17) at the steady states in the line $l_{e,3}$ has a stable eigenvalue $-\frac{7}{10}$ and a triple zero eigenvalue. There exists a three-dimensional center manifold $W_{a,3}^c$ at the point $(0, 0, C_3, 0) \in l_{e,3}$. In chart K_3 close to $C_3 = \frac{1}{2}$, the center manifold $W_{a,3}^c$ is given as a graph

$$(5.38) \quad X_3 = \varepsilon_3 r_3 \left(\frac{10}{7} + O(\varepsilon_3 r_3) \right).$$

In chart K_3 our main goal is to describe the flow of (5.17) close to the line $l_{e,3}$. More precisely, we will analyze the dynamics close to the exit point $q_{e,3} \in l_{e,3}$. Recall that in chart K_2 we have found the slow manifold $\mathcal{N}_2^\varepsilon$, which is one-dimensional and fully attracting. To find out how the extension of this manifold and nearby orbits pass the point $q_{e,3}$, we restrict attention to the following sets

$$\begin{aligned} D_{in} &= \{(X_3, r_3, C_3, \varepsilon_3) : 0 \leq r_3 \leq \delta, \quad 0 \leq C_3 \leq \frac{1}{2}, \quad 0 \leq \varepsilon_3 \leq \beta_3\}, \\ D_{out} &= \{(X_3, r_3, C_3, \varepsilon_3) : 0 \leq r_3 \leq \delta, \quad \frac{1}{2} \leq C_3 \leq 1, \quad 0 \leq \varepsilon_3 \leq \beta_3\}, \end{aligned}$$

and define two sections

$$\begin{aligned} \Sigma_{3,in} &= \{(X_3, r_3, C_3, \varepsilon_3) \in D_{in} : \varepsilon_3 = \beta_3\}, \\ \Sigma_{3,out} &= \{(X_3, r_3, C_3, \varepsilon_3) \in D_{out} : r_3 = \delta\}, \end{aligned}$$

where $\beta_3 = \beta_2^{-1}$ due to (5.19). Let Π_3 be a transition map from $\Sigma_{3,in}$ to $\Sigma_{3,out}$ induced by the flow of (5.17). As a first step to construct the map Π_3 , we reduce system (5.17) to its center manifold $W_{a,3}^c$ and discuss the structure of the system governing the dynamics on $W_{a,3}^c$.

By inserting (5.38) into system (5.17) and re-scaling time by dividing out the common factor $\varepsilon_3(1 + \frac{10}{7}r_3 + O(\varepsilon_3^2 r_3^2))$, we obtain the flow on the center manifold

$$(5.39) \quad \begin{aligned} r_3' &= r_3 F(r_3, C_3, \varepsilon_3), \\ C_3' &= \frac{1}{4} r_3 G(r_3, C_3, \varepsilon_3), \\ \varepsilon_3' &= -\varepsilon_3 F(r_3, C_3, \varepsilon_3), \end{aligned}$$

where the functions $G(r_3, C_3, \varepsilon_3)$ and $F(r_3, C_3, \varepsilon_3)$ are given by

$$\begin{aligned} G(r_3, C_3, \varepsilon_3) &= \left(1 - \frac{10}{7}\varepsilon_3 r_3^2 - C + O(\varepsilon_3^2 r_3^2)\right)(r_3 \varepsilon_3 + 1 - r_3)(\varepsilon_3 + 1), \\ F(r_3, C_3, \varepsilon_3) &= \frac{6C_3}{1 + 2C_3}(1 - r_3)(\varepsilon_3 + 1) - \frac{3}{2}(r_3 \varepsilon_3 + 1 - r_3). \end{aligned}$$

The derivative in (5.39) is with respect to the rescale time scale denoted by s_3 . The plane $r_3 = 0$ and $\varepsilon_3 = 0$ are invariant for system (5.39).

In the invariant plane $r_3 = 0$ system (5.39) simplifies to

$$\begin{aligned} C_3' &= 0, \\ \varepsilon_3' &= -\varepsilon_3 \left(\frac{6C_3}{1+2C_3}(\varepsilon_3 + 1) - \frac{3}{2} \right). \end{aligned}$$

We recover the curve of equilibria \mathcal{N}_3^0 and the line of equilibria $l_{e,3}$, see Figure 5.20. The curve is attracting for the flow in $r_3 = 0$, whereas the line $l_{e,3}$ is attracting for $C_3 > \frac{1}{2}$ and repelling for $C_3 < \frac{1}{2}$. The point $(0, \frac{1}{2}, 0) \in l_{e,3}$ is degenerate.

In the invariant plane $\varepsilon_3 = 0$ the governing equations are

$$\begin{aligned} r_3' &= r_3(1 - r_3) \left[\frac{6C_3}{1+2C_3} - \frac{3}{2} \right], \\ C_3' &= \frac{1}{4} r_3(1 - C)(1 - r_3). \end{aligned}$$

For the flow in the plane $\varepsilon_3 = 0$, the line $l_{e,3}$ is attracting for $C_3 < \frac{1}{2}$ and repelling otherwise. In addition, the flow meets the line $l_{e,3}$ with a quadratic tangency at $(0, \frac{1}{2}, 0) \in l_{e,3}$, see Figure 5.20.

REMARK 5.28. *Note that the dynamics in the invariant plane $\varepsilon_3 = 0$ corresponds to the reduced flow on S_a^2 in the original system, compare Figure 5.5 with Figure 5.20.*

LEMMA 5.7. *For system (5.39) the following assertions hold.*

- (1) *The curve \mathcal{N}_3^0 of equilibria of system (5.39) has a one-dimensional stable manifold and a two-dimensional center manifold.*
- (2) *The linearization of system (5.39) at the points in $l_{e,3}$ is*

$$\begin{pmatrix} 0 & 0 & 0 \\ 0 & \frac{6C_3}{1+2C_3} - \frac{3}{2} & 0 \\ 0 & 0 & \frac{3}{2} - \frac{6C_3}{1+2C_3} \end{pmatrix}.$$

- (3) *The point $q_{e,3}$ is nilpotent.*

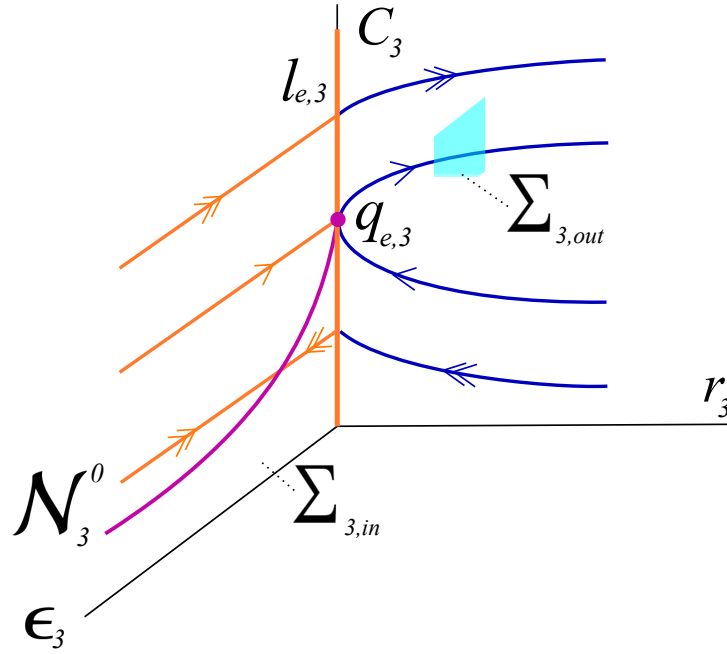


FIGURE 5.20. Dynamics of system (5.39).

Recall that our goal is to construct the map $\Pi_3 : \Sigma_{3,in} \rightarrow \Sigma_{3,out}$. Note that in the $(r_3, C_3, \varepsilon_3)$ -coordinates, $\Sigma_{3,in}$ is transverse to \mathcal{N}_3^0 , whereas $\Sigma_{3,out}$ is transverse to the parabolas' branches with $C_3 > \frac{1}{2}$ in the $\varepsilon_3 = 0$ plane. From the analysis of the dynamics on $W_{a,3}^c$, we see that the construction of the transition map Π_3 is a bit more complicated due to the existence of the nilpotent point $q_{e,3}$. To describe the transition map induced by the flow of (5.39) from $\Sigma_{3,in}$ to $\Sigma_{3,out}$, a blow-up of the point $q_{e,3}$ is required. In order not to interrupt the main argument, we present this blow-up procedure in Section 5.4, which led to the following result.

THEOREM 5.8. *Let $\tilde{R} \subset \Sigma_{3,in}$ be a small rectangle centered at the intersection point $\mathcal{N}_3^0 \cap \Sigma_{3,in}$. For δ small enough the transition map $\tilde{\Pi}_3 : \tilde{R} \rightarrow \Sigma_{3,out}$ induced by the flow of (5.39) is a well-defined map with the following properties:*

- (1) *The continuation of \mathcal{N}_3^0 by the flow intersects $\Sigma_{3,out}$ in a curve denoted by $\eta_{3,out}$.*
- (2) *Restricted to lines $r_3 = \text{const.}$ in \tilde{R} , the map is contracting with a rate e^{-c_3/r_3} with $c_3 > 0$.*
- (3) *The image $\tilde{\Pi}_3(\tilde{R})$ is an exponentially thin wedge containing the curve $\eta_{3,out}$.*

From the above analysis, we conclude that the transition map $\Pi_3 : \Sigma_{3,in} \rightarrow \Sigma_{3,out}$ induced by the flow of (5.17) is at most algebraically expanding. In particular, this means that the contraction gained in K_2 is not lost during the passage of the exit $q_{e,3}$. We have the following result.

THEOREM 5.9. *The transition map $\Pi_3 : \Sigma_{3,in} \rightarrow \Sigma_{3,out}$ defined by the flow of system (5.17) is given by*

$$\Pi_3 \begin{pmatrix} X_3 \\ r_3 \\ C_3 \\ \beta_3 \end{pmatrix} = \begin{pmatrix} g^{out}(\delta, C_{3,out}, \varepsilon_{3,out}) + \Psi_3(X_3, r_3, C_3) \\ \delta \\ C_{3,out}(\varepsilon_{3,out}) \\ \varepsilon_{3,out} \end{pmatrix},$$

where g^{out} describes the center manifold $W_{a,3}^c$ and $C_{3,out}(\varepsilon_{3,out})$ describes the curve $\eta_{3,out} \subset \Sigma_{3,out}$ formed by the intersection of \mathcal{N}_3^0 with $\Sigma_{3,out}$.

REMARK 5.29. *Note that it was beyond our scope to obtain the asymptotics for $C_{3,out}$. In fact, due to the complicated structure of the systems governing the dynamics in K_3 , it is a non-trivial task.*

Phase portrait of the blown-up vector field and proof of Theorem 5.4.

The vector field on \mathbb{R}^4 corresponding to system (5.10) induces the blown-up vector field on the blown-up space, which has been analyzed in detail in the individual charts $K_1 - K_3$. The established results provide us with the following picture of the dynamics of the blown-up vector field, see Figure 5.21.

Recall that the planes $X = 0$ and $M = 0$ intersect along the non-hyperbolic line l_e , which due to the blow-up has been replaced by the cylinder shown in orange. The flow on the center manifolds $W_{a,1}^c$ found in chart K_1 in the $\varepsilon_1 = 0$ plane and the flow on $W_{a,3}^c$ found in chart K_3 in the $\varepsilon_3 = 0$ plane are shown in blue. Recall that these flows correspond to the reduced flows on $M = 0$ and $X = 0$, respectively. Hence, the orbits $\bar{\omega}_7$ and $\bar{\omega}_1$ correspond to the orbits ω_7 and ω_1 , respectively, compare Figure 5.6 and Figure 5.21.

In chart K_2 covering the interior of the cylinder we have found the slow manifold. This manifold is fully attracting and explains the slow drift taking place almost along the C -axis in the original problem, i.e., all orbits are attracted onto the slow manifold and follow the slow flow on it upwards. Thus, due to the blow-up the singular cycle Γ_0 defined as (5.9) has been replaced by the more complicated singular cycle $\bar{\Gamma}_0$ with improved hyperbolicity properties, again compare Figure 5.6 and Figure 5.21. More precisely, the segment ω_8 of l_e in Figure 5.6 corresponds now to the connection between the points \bar{p}_{en} and \bar{q}_e , which consists of two pieces: the thick orange orbit and the slow motion along \mathcal{N}^0 shown in purple, see Figure 5.21.

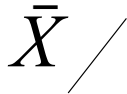


FIGURE 5.21. Geometry of the blown-up space and singular cycle $\bar{\Gamma}_0$.

Based on the results from the blow-up analysis of (5.2), we finally prove Theorem 5.4. The proof is given by combining the results obtained for the local transition maps Π_1 , Π_2 , and Π_3 , which describe the evolution of the center manifold $W_{a,1}^c$ and the rectangle $R_{1,in}$ under the flow of the blown-up vector field.

PROOF OF THEOREM 5.4. The assertions of Theorem 5.4 follow by constructing the map π_e for $\varepsilon > 0$ as

$$(5.40) \quad \pi_e = \Phi_e \circ \Pi_e \circ \Phi_e^{-1},$$

where Φ_e is given by (5.11), Φ_e^{-1} is the corresponding blow-down transformation, and the map Π_e is a transition map from $\Sigma_{1,in}$ to $\Sigma_{3,out}$ for the flow induced by the blown-up vector field on Z . More precisely, the map Π_e is given by

$$\Pi_e = \Pi_3 \circ \kappa_{23} \circ \Pi_2 \circ \kappa_{12} \circ \Pi_1.$$

Recall that the transition map Π_1 constructed in chart K_1 is described by the attracting center manifold and its foliation, and the map Π_1 is contracting M_1 with the rate $O(e^{-c/\varepsilon_1})$. The transition map Π_2 is a strong contraction in both (M_2, C_2) due to the existence of the fully attracting one-dimensional slow manifold. This contraction is not lost in K_3 , in particular during the passage through the exit point $q_{e,3}$ since the map Π_3 is at most algebraically expanding.

We now analyze $\Pi_e(W_{a,1}^c \cap R_{1,in})$. It follows from Theorem 5.5, Theorem 5.7, and Theorem 5.9 that $\Pi_e(W_{a,1}^c \cap R_{1,in})$ is a curve of exponentially small length lying close to the point

$$\{(X_3(\varepsilon_3), \delta, C_3(\varepsilon_3), \varepsilon_3) : \varepsilon_3 \in [0, \beta_3]\},$$

formed by the intersection of the continuation of the slow manifold $\mathcal{N}_2^\varepsilon$ with $\Sigma_{3,out}$. Moreover, from Theorem 5.5, Theorem 5.7, Theorem 5.9, and the fact that κ_{12} and κ_{23} are diffeomorphisms, we conclude that $\Pi_e(R_{1,in})$ is a two-dimensional region of width of $O(e^{-c/\varepsilon_1})$ around $\Pi_e(W_{a,1}^c \cap R_{1,in})$. Recall that $\varepsilon = \delta\varepsilon_1 = \delta\varepsilon_3$ is a constant of motion for the flow of the blown-up vector field. Therefore, lines $\varepsilon_1 = \varepsilon/\delta$ in $\Sigma_{1,in}$ are mapped to lines $\varepsilon_3 = \varepsilon/\delta$ in $\Sigma_{3,out}$. Restricted to such leaves, the map Π_e is a contraction with contraction rate $O(e^{-c/\varepsilon_1})$ for some $c > 0$.

Finally, the transition π_e is given by (5.40) with $\Delta_{in}^\varepsilon = \Phi_{e,1}(R_{1,in})$, where $\Phi_{e,1}$ is the directional blow-up given by (5.12), and by this construction the assertions of Theorem 5.4 follow. □

5.2.2. Local analysis close to the non-hyperbolic line l_M . In this subsection we study the dynamics of system (5.2) close to the non-hyperbolic line l_M . Recall that this line splits the critical manifold S^2 at $M = 0.7$ into the attracting branch S_a^2 with $M < 0.7$, and the repelling branch S_r^2 with $M > 0.7$. It will turn out that the points $p \in l_M$ are jump points, i.e., system (5.2) close to l_M can be viewed as a straightened regular fold in \mathbb{R}^3 [111]. More precisely, the reduced flows near the line l_M are directed towards the line, hence the solutions following the reduced flow in the attracting part S_a^2 reach the line in finite forward time. From there the solutions jump almost parallel to the unstable fibers, i.e., the system switches from the slow to the fast dynamics; see Figure 5.22, where a jump phenomenon is schematically illustrated.

Due to Fenichel, the attracting (repelling) manifold S_a^2 (S_r^2) perturbs smoothly to a locally invariant slow manifold $S_{a,\varepsilon}^2$ ($S_{r,\varepsilon}^2$). To investigate the behaviour of the slow manifold $S_{a,\varepsilon}^2$ as it passes the line $M = 0.7$, we construct a transition map

$$\pi_f : \Delta_{in}^f \rightarrow \Delta_{out}^f,$$

where for $\delta > 0$ small and suitable rectangles \tilde{L}_1, \tilde{L}_2

$$\Delta_{in}^f = \{(X, \delta, C) : (X, C) \in \tilde{L}_1\}, \quad \Delta_{out}^f = \{(\delta, M, C) : (M, C) \in \tilde{L}_2\}$$

are two sections transverse to S_a^2 and the fast fibers, respectively.

It turns out that the situation close to l_M is as encountered in [111]. Thus, the results for folds in \mathbb{R}^3 apply to the analysis of the dynamics close to the line l_M . We therefore sketch the construction of the map π_f noting that many of the details, in particular, the estimates of the contraction rates are as in [111]. In fact, based on [111], the following theorem holds for system (5.2).

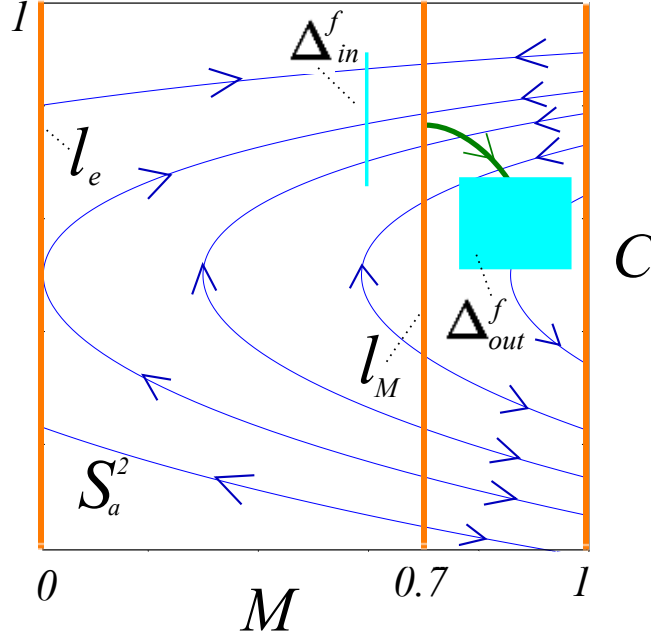


FIGURE 5.22. Jump phenomenon at the line l_M .

THEOREM 5.10. *For system (5.2) there exist $\delta > 0$ and $\varepsilon_0 > 0$ such that for $\varepsilon \in (0, \varepsilon_0]$:*

- (1) *The manifold $S_{a,\varepsilon}^2$ intersects Δ_{out}^f in a smooth curve, which is a graph, i.e.,*

$$M_{out} = h^{out}(C^{out}, \varepsilon), \quad C \in I^{out},$$

where I^{out} is a suitable interval. Moreover, $h^{out}(C, \varepsilon) = O(\varepsilon^{2/3})$.

- (2) *The section Δ_{in}^f is mapped to an exponentially thin strip around $S_{a,\varepsilon}^2 \cap \Delta_{out}^f$, i.e., its width in M -direction is $O(e^{-c/\varepsilon})$, where c is a positive constant.*

- (3) *The map $\pi_f : \Delta_{in}^f \rightarrow \Delta_{out}^f$ has the form*

$$(5.41) \quad \pi_f \begin{pmatrix} X \\ \delta \\ C \end{pmatrix} = \begin{pmatrix} \delta \\ \pi_f^M(X, C, \varepsilon) \\ \pi_f^C(X, C, \varepsilon) \end{pmatrix},$$

where

$$\pi_f^M(X, C, \varepsilon) = h^{out}(\pi_f^C(X, C, \varepsilon), \varepsilon) + \Psi_f(X, C, \varepsilon),$$

$$\pi_f^C(X, C, \varepsilon) = G_{f,0} + O(\varepsilon \ln \varepsilon),$$

and the function $\Psi_f(X, C, \varepsilon)$ is exponentially small. The function $G_{f,0}$ is induced by the reduced flow on S_a^2 from Δ_{in}^f to the line l_M .

REMARK 5.30. Note that the jump phenomenon at the line l_M explains the activation of protease kinase X , i.e., when $cdc2$ kinase M crosses the threshold value ≈ 0.7 , X is activated and increases up to 1. This sharp increase occurs during the jump from the manifold S_a^2 to the attracting branch of S^3 .

PROOF. The assertions of the theorem follow by applying to system (5.10) the following blow-up transformation

$$(5.42) \quad \begin{aligned} X &= r^2 \bar{X} \\ M &= \frac{7}{10} + r \bar{M}, \\ C &= \bar{C}, \\ \varepsilon &= r^3 \bar{\varepsilon} \end{aligned}$$

with $(\bar{X}, \bar{M}, \bar{\varepsilon}, r, \bar{C}) \in \mathbb{S}^2 \times \mathbb{R} \times \mathbb{R}$, and taking $\pi_f := \Phi_f \circ \Pi_f \circ \Phi_f^{-1}$, where Φ_f is given by (5.42) and Φ_f^{-1} is the corresponding blow-down transformation. The map Π_f is a transition map constructed for the blown-up system and its construction is analogous to the one presented in [111]. We briefly sketch this construction by presenting the analysis of the blown-up vector field performed in local charts \mathcal{K}_1 , \mathcal{K}_2 , and \mathcal{K}_3 .

The charts are defined by setting $\bar{M} = -1$, $\bar{\varepsilon} = 1$, and $\bar{X} = 1$, respectively, in the blow-up transformation (5.42). Hence, the coordinates of the corresponding charts are

$$(5.43) \quad X = r_1^2 X_1, \quad M = \frac{7}{10} - r_1, \quad C = C_1, \quad \varepsilon = r_1^3 \varepsilon_1.$$

$$(5.44) \quad X = r_2^2 X_2, \quad M = \frac{7}{10} + r_2 M_2, \quad C = C_2, \quad \varepsilon = r_2^3,$$

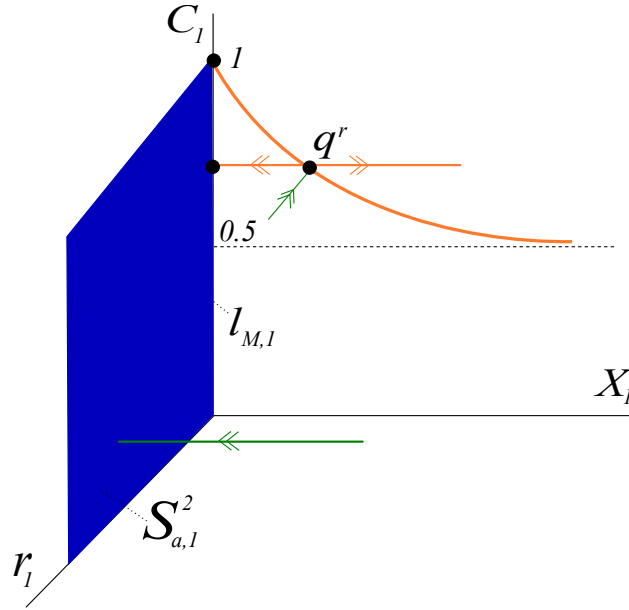
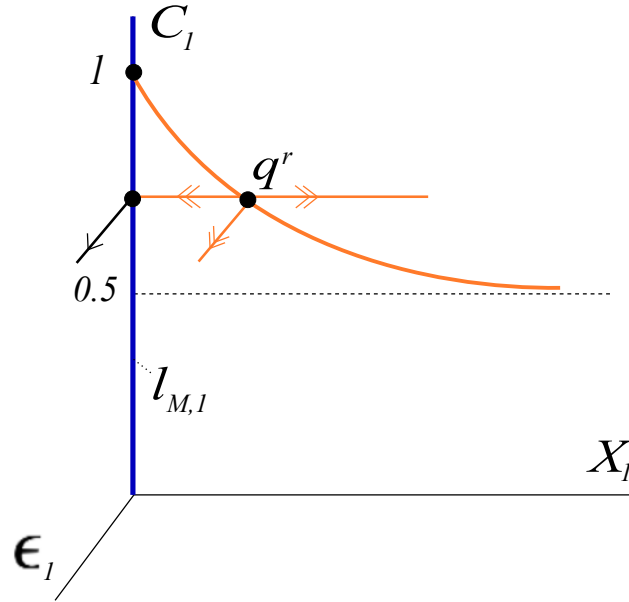
$$(5.45) \quad X = r_3^2, \quad M = \frac{7}{10} + r_3 M_3, \quad C = C_3, \quad \varepsilon = r_3^3 \varepsilon_3.$$

In what follows we restrict our attention to the relevant parts of the dynamics, i.e., for $C > 0.5$, and to the attracting objects found in the analysis. First the dynamics in chart \mathcal{K}_1 is analyzed. We will see how the critical manifold S_a^2 can be extended on the cylinder. Then, it will be further studied in chart \mathcal{K}_2 , where a special orbit leads the manifold across the upper part of $\mathbb{S}^2 \times [0, r_0]$. Finally, in chart \mathcal{K}_3 , we will see how solutions take off in the direction of the fast flow.

Dynamics in chart \mathcal{K}_1 . The desingularized equations in chart \mathcal{K}_1 have the form

$$(5.46) \quad \begin{aligned} X_1' &= \frac{7}{10} \varepsilon_1 - X_1 + 3X_1^2 \frac{2C_1 - 1}{1 + 2C_1} + O(r_1), \\ r_1' &= \frac{3}{2} r_1 X_1 \frac{1 - 2C_1}{1 + 2C_1} + O(r_1^2), \\ C_1' &= \frac{1}{4} r_1 (1 - C_1) X_1 + O(r_1^2), \\ \varepsilon_1 &= \frac{9}{2} \varepsilon_1 X_1 \frac{2C_1 - 1}{1 + 2C_1} + O(r_1). \end{aligned}$$

The hyperplanes $r_1 = 0$ and $\varepsilon_1 = 0$ are invariant for (5.46). The results obtained from the analysis in these hyperplanes are illustrated in Figure 5.23 and Figure 5.24, and lead to the following lemmas.

FIGURE 5.23. Dynamics of system (5.46) in the hyperplane $\varepsilon_1 = 0$.FIGURE 5.24. Dynamics of system (5.46) in the hyperplane $r_1 = 0$.

LEMMA 5.8. *System (5.46) has a curve of hyperbolic equilibria defined by the equations $r_1 = 0$, $X_1 = \frac{1}{3} \frac{2C_1+1}{2C_1-1}$, and a normally hyperbolic plane $S_{a,1}^2$ of equilibria given by $C_1 = 0$, $r_1 = 0$ that contains the C_1 -axis.*

LEMMA 5.9. *The C_1 -axis denoted by $l_{M,1}$ is a line of non-hyperbolic equilibria of system (5.46). More precisely, the linearization of (5.46) at $p \in l_{M,1}$ has a triple zero eigenvalue and the non-zero eigenvalue equal to -1 .*

REMARK 5.31. *Note that the curve lies in the plane $r_1 = 0$, which corresponds to the cylinder; hence, the points q_1^r in the curve correspond to the points, where stable fibers of the layer problem end on the cylinder. The plane $S_{a,1}^2$ corresponds to the attracting critical manifold S_a^2 .*

The most important object in chart \mathcal{K}_1 is introduced in lemma below.

LEMMA 5.10. *There exists an attracting three-dimensional center manifold $\mathcal{W}_{a,1}^c$ of the line of equilibria $l_{M,1}$, which in a set*

$$D = \{(X_1, r_1, C_1, \varepsilon_1) : 0 \leq r_1 \leq \delta, \quad 0 \leq \varepsilon \leq \delta, \quad C \in (0.5, 1]\}$$

is given as a graph

$$(5.47) \quad X_1 = \tilde{h}_{a,1}(r_1, C_1, \varepsilon_1)$$

with $\tilde{h}_{a,1}(r_1, C_1, \varepsilon_1) = \frac{7}{10}\varepsilon_1 + O(2)$. Furthermore, there exists a stable invariant foliation with base $\mathcal{W}_{a,1}^c$ and one-dimensional fibers along which the contraction is stronger than $e^{-c\tau_1}$ for c any positive constant.

By substituting (5.47) into system (5.46) and rescaling time, the flow on $\mathcal{W}_{a,1}^c$ is obtained. Namely,

$$(5.48) \quad \begin{aligned} C_1' &= \frac{1}{4}r_1(1 - C_1) + O(r_1^2), \\ r_1' &= \frac{3}{2}r_1 \frac{1-2C_1}{1+2C_1} + O(r_1^2), \\ \varepsilon_1' &= -\frac{9}{2}\varepsilon_1 \frac{1-2C_1}{1+2C_1} + O(r_1\varepsilon_1). \end{aligned}$$

A local transition map, induced by the flow of (5.46) between suitably defined two sections, can be constructed by taking into account the properties of system (5.48) and the attracting manifold $\mathcal{W}_{a,1}^c$ itself. The contraction rate for such a map is as in [111].

REMARK 5.32. *Note that in the invariant plane $\varepsilon_1 = 0$ system (5.48) reduces to a planar system, which in the original variables describes the reduced flow on S_a^2 .*

Dynamics in chart \mathcal{K}_2 . The blown-up system in chart \mathcal{K}_2 is given by

$$(5.49) \quad \begin{aligned} X_2' &= \frac{7}{10} + M_2 X_2 + O(\varepsilon), \\ M_2' &= \left(\frac{6C_2}{2C_2+1} - \frac{3}{2} \right) X_2 + O(\varepsilon), \\ C_2' &= \frac{1}{4}(1 - C_2)X_2\varepsilon, \end{aligned}$$

which is a slow-fast system with respect to ε , i.e., the variable C_2 is slow, while the variables X_2 and M_2 are fast. Note, however, that there is no slow manifold in the rescaling chart, since for $\varepsilon = 0$ the resulting equations have no equilibria. Namely, setting $\varepsilon = 0$ in (5.49) gives the system

$$(5.50) \quad \begin{aligned} X_2' &= \frac{7}{10} + M_2 X_2, \\ M_2' &= \left(\frac{6C_2}{2C_2+1} - \frac{3}{2} \right) X_2, \\ C_2' &= 0 \end{aligned}$$

with the following properties (see Figure 5.25):

- (1) the half plane $X_2 > 0$ is positively invariant under the flow (5.50),

- (2) for $C_2 > 0.5$ the constant factor $\frac{6C_2-3}{2(1+2C_2)}$ is positive, hence $M_2, X_2 \rightarrow \infty$.

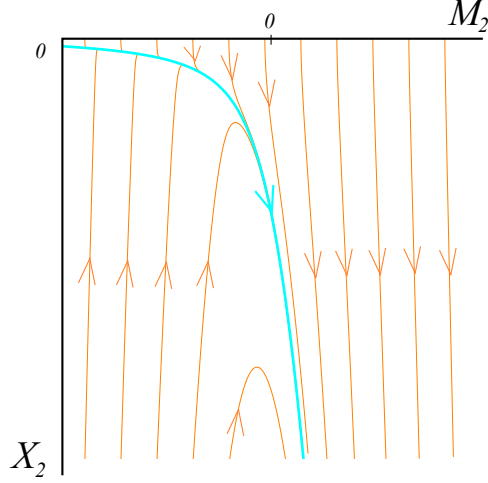


FIGURE 5.25. Dynamics of system (5.50) in the rescaling chart \mathcal{K}_2 .

From this we expect that the continuation of the critical manifold S_a^2 onto the sphere (as a center manifold) described in the rescaling chart will lie in the half plane $X_2 > 0$. Furthermore, the continuation of the critical manifold will exit the sphere at a hyperbolic exit point with $\bar{X} > 0$ and $\bar{M} > 0$. Figure 5.26 illustrates

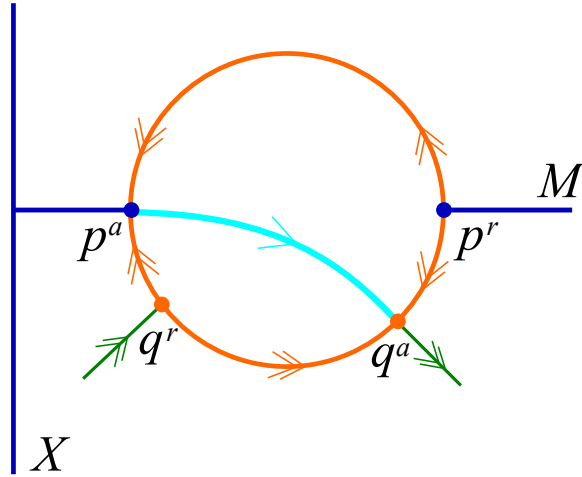


FIGURE 5.26. Compactification phase portrait on \mathbb{S}^2 .

the compactification phase portrait in the rescaling chart in the interior of a circle $X_2^2 + M_2^2 = 1$ in the (X_2, M_2) - coordinate system. The critical manifold $X = 0$ with $M < 0.7$ corresponds to the point $p^a = (-1, 0)$, the critical manifold $X = 0$

with $M > 0.7$ corresponds to the point $p^r = (1, 0)$. There are two more equilibria on the circle $q^r = (M_{in}, X_{in})$ with $M_{in} < 0$ and $X_{in} > 0$ where a stable fiber of the layer problem ends and $q^a = (M_{out}, X_{out})$ with $M_{out} > 0$ and $X_{out} > 0$ where an unstable fiber of the layer problem starts. A unique orbit γ connecting p^a to q^a is shown in light blue. Our expectations are confirmed by the analysis in chart \mathcal{K}_3 .

Dynamics in \mathcal{K}_3 . The desingularized form of system (5.10) in \mathcal{K}_3 is given by

$$\begin{aligned}
 (5.51) \quad C'_3 &= \frac{1}{4}(1 - C_3)r_3 + O(r_3^2), \\
 r'_3 &= \frac{1}{2}(M_3 + \frac{7}{10}\varepsilon_3)r_3 + O(r_3^2), \\
 M'_3 &= \frac{6C_3}{1+2C_3} - \frac{3}{2} - \frac{1}{2}M_3[(M_3 + \frac{7}{10}\varepsilon_3)] + O(r_3), \\
 \varepsilon_3 &= -\frac{3}{2}\varepsilon_3(M_3 + \frac{7}{10}\varepsilon_3) + O(r_3).
 \end{aligned}$$

System (5.51) has a folded curve of equilibria defined by

$$(5.52) \quad r_3 = 0, \quad \varepsilon_3 = 0, \quad M_3 = \mp \sqrt{\frac{6C_3 - 3}{1 + 2C_3}}.$$

It consists of two branches separated by a fold point. For the flow in the invariant hyperplane $r_3 = 0$ the left branch consists of unstable equilibria, whereas the equilibria on the right branch are stable. For the flow in $\varepsilon_3 = 0$ the left branch is attracting, while the right branch is repelling. These points correspond to the points where the stable fibers of the layer problem end and start on the cylinder, respectively. Note that the eigenvalues of the linearization of (5.51) at points in the right branch are in resonance, as is the case in [111]. Hence, one can apply a similar analysis to theirs to prove the occurrence of logarithmic (switchback) terms in a local transition map defined for suitable sections in \mathcal{K}_3 .

The analysis of the dynamics in each chart leads to Figure 5.27, which shows the geometry of the blown-up space.

Finally, the transition map Π_f is defined as

$$(5.53) \quad \Pi_f = \pi_3 \circ \iota_{23} \circ \pi_2 \circ \iota_{12} \circ \pi_1,$$

where π_i is a transition map constructed in chart \mathcal{K}_i , $i = 1, 2, 3$, and ι_{ij} denotes the appropriate change of coordinates from chart \mathcal{K}_i to chart \mathcal{K}_j , $i, j = 1, 2, 3$, respectively. \square

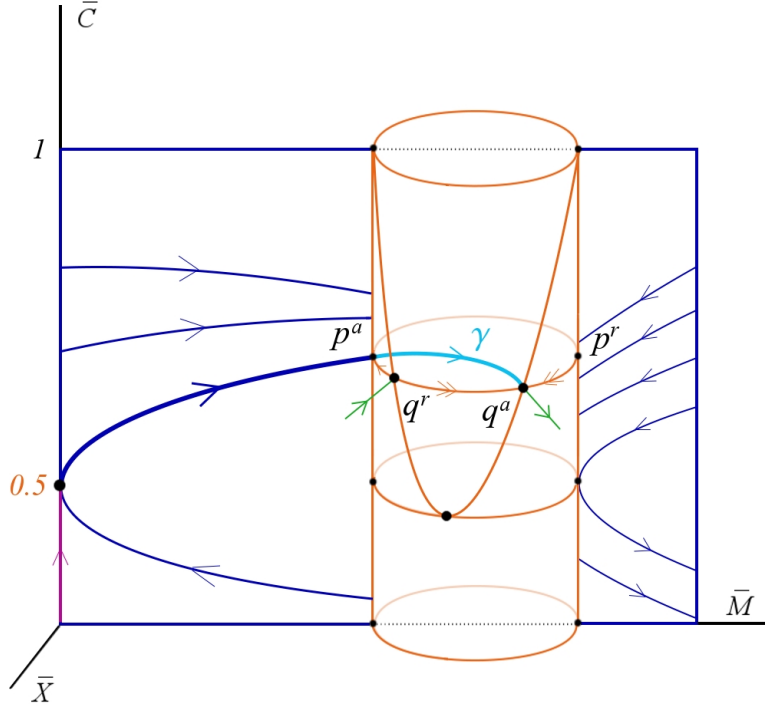


FIGURE 5.27. Dynamics of the blown-up system.

5.3. Proof of the main result

In this section we prove Theorem 5.3. Recall that the blow-up constructions presented in Section 5.2 provide us with a detailed description of the dynamics close to the edge l_e and the line l_M . Based on these results we have identified in anticipation the singular cycle Γ_0 as described in Section 5.1.5, i.e.,

$$\Gamma_0 = \omega_1 \cup \omega_2 \cup \omega_3 \cup \omega_4 \cup \omega_5 \cup \omega_6 \cup \omega_7 \cup \omega_8,$$

where ω_i , $i = 1, 3, 5, 7$ are slow motions in the attracting parts of the critical manifold S , ω_i , $i = 2, 6$ are the heteroclinic orbits of the layer problem (5.4), and ω_i , $i = 4, 8$ denote the slow drifts along the edges l_e and l^e , respectively.

In the following we will construct and analyze a Poincaré map defined in a neighborhood of the singular cycle Γ_0 and show that within each leaf $\varepsilon = \text{const.}$ the map is a strong contraction.

PROOF OF THEOREM 5.3. We start by choosing four sections Δ , Δ_{in}^e , Δ_{out}^e , and Δ_{out}^f , as shown in Figure 5.28, i.e.,

- Δ — transverse to ω_6 and close to S^1 ,
- Δ_{in}^e — transverse to $\omega_7 \subset S^1$ and close to the edge l_e ,
- Δ_{out}^e — transverse to $\omega_1 \subset S^2$ and close to the edge l_e ,
- Δ_{out}^f — transverse to ω_2 and close to the line l_M .

More precisely, we define the sections as

$$\begin{aligned}\Delta &:= \{(\tilde{\delta}, M, C) : (M, C) \in L\}, \\ \Delta_{in}^e &:= \{(\delta, M, C) : (M, C) \in L_1\}, \\ \Delta_{out}^e &:= \{(X, \delta, C) : (X, C) \in L_2\}, \\ \Delta_{out}^f &:= \{(\delta, M, C) : (M, C) \in \tilde{L}_2\},\end{aligned}$$

where $0.5 < \tilde{\delta} < 1$, $\delta > 0$, and L , L_1 , L_2 , and \tilde{L}_2 are suitable rectangles. Note that

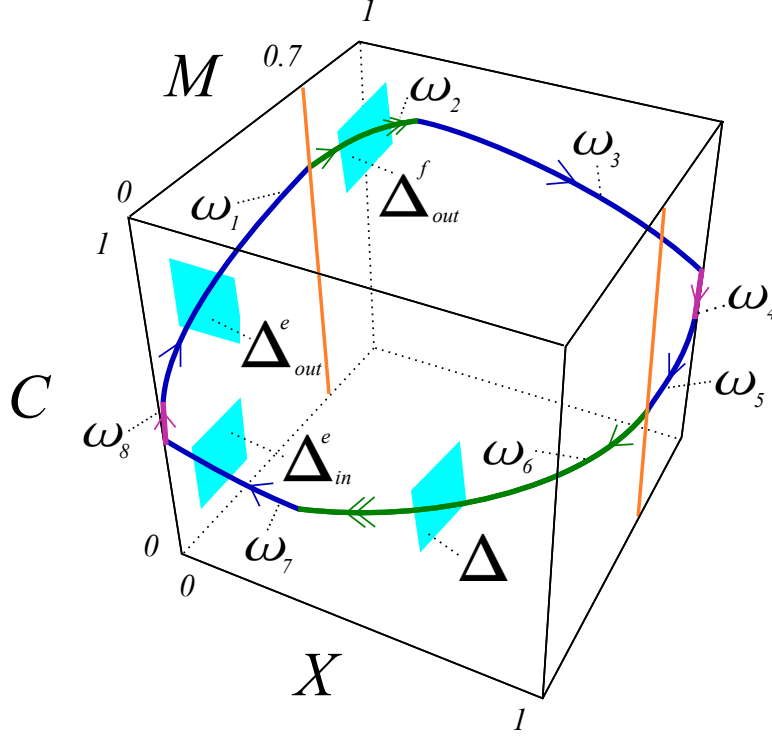


FIGURE 5.28. Singular cycle Γ_0 and sections for the Poincaré map.

the sections Δ_{in}^e , Δ_{out}^e , and Δ_{out}^f have been already defined in Section 5.2, where we described the dynamics close to the edge l_e and the line l_M . Moreover, these sections are transversal to the singular cycle Γ_0 independently of ε and can be made small enough.

The first half of the Poincaré map is defined as the composition of three maps:

$$\begin{aligned}\pi_a : \Delta &\rightarrow \Delta_{in}^e && \text{— contraction onto the slow manifold } S_{a,\varepsilon}^1, \\ \pi_e : \Delta_{in}^e &\rightarrow \Delta_{out}^e && \text{— passage of the edge } l_e, \\ \pi_f : \Delta_{out}^e &\rightarrow \Delta_{out}^f && \text{— passage of the line } l_M.\end{aligned}$$

We start with discussing the map π_a . Recall that the slow manifold $S_{a,\varepsilon}^1$ is given as a graph over (M, C) . All orbits starting in Δ approach $S_{a,\varepsilon}^1$, follow the slow flow along $S_{a,\varepsilon}^1$ and intersect Δ_{in}^e . The intersection of the slow manifold $S_{a,\varepsilon}^1$ with Δ_{in}^e is a graph $M = h^1(C, \varepsilon)$. We choose local coordinates in Δ_{in}^e such that the slow

manifold becomes the C -axis. Recall that $P(l^M) \subset S_a^1$ denotes the projection along the fast fibers of the line l^M on the attracting branch S_a^1 . Under the assumption that the reduced flow on S_a^1 is transversal to the curve $P(l^M) \subset S_a^1$ and that there exists the hyperbolic singular orbit Γ_0 , the map $\pi_a : \Delta \rightarrow \Delta_{in}^e$ is well-defined. More precisely, π_a induced by system (5.2) is given by

$$(5.54) \quad \pi_a \begin{pmatrix} M \\ C \end{pmatrix} = \begin{pmatrix} \pi_a^M(M, C, \varepsilon) \\ \pi_a^C(M, C, \varepsilon) \end{pmatrix}$$

with $\Pi_a^M(M, C, \varepsilon)$ exponentially small, and $\Pi_a^C(M, C, \varepsilon) = G_{S_a,0}(C) + O(\varepsilon)$, where $G_{S_a,0}$ is induced by the reduced flow on the critical manifold S_a^1 between the base point on $P(l^M)$ and Δ_{in}^e . Remember that the slow flow on $S_{a,\varepsilon}^1$ is contracting C . Hence, the map π_a is a strong contraction described by Fenichel theory.

Recall that the blow-up analysis presented in Section 5.2 led to the local results for the transition maps π_e and π_f , i.e., Theorem 5.4 and Theorem 5.10. More precisely, Theorem 5.4 implies that for $\delta > 0$ and sufficiently small rectangle L_1 , the map π_e is well-defined and there exists a constant $c > 0$ such that the map π_e restricted to a leaf $\varepsilon = \text{const.}$ is a contraction with a contraction rate $e^{-c/\varepsilon}$. For $\delta > 0$ there exists a sufficiently small rectangle L_2 such that the map π_f is well-defined. Theorem 5.10 implies that the map π_f is exponentially contracting in X -direction, and the derivative of π_f with respect to C stays bounded.

By taking the incoming section Δ_{in}^f from Theorem 5.10 as the outgoing section Δ_{out}^e from Theorem 5.4, we conclude that there exists $\varepsilon_0 > 0$ such that the first half of the Poincaré map $\Pi : \Delta \rightarrow \Delta_{out}^f$ given by

$$\Pi = \pi_f \circ \pi_e \circ \pi_a$$

is well-defined for $\varepsilon \in (0, \varepsilon_0]$. For $\varepsilon > 0$ the map Π is a diffeomorphism. In a similar way a map from Δ_{out}^f to Δ can be constructed and its analysis is analogous to the one we have presented. Hence, the full Poincaré map from Δ to Δ is well-defined for $\varepsilon \in (0, \varepsilon_0]$ and for $\varepsilon > 0$ is smooth. Based on the contracting properties of the maps π_a , π_e , and π_f , we conclude that $\Pi(\Delta) \subset \Delta$, and Π is a contraction with a fixed point. From the contracting mapping theorem the existence of a unique relaxation orbit of system (5.2) close to the singular cycle Γ_0 for sufficiently small ε follows. \square

5.4. Dynamics near the exit point $q_{e,3}$

Here we describe the dynamics of system (5.17) in chart K_3 close to the exit point $q_{e,3}$ and prove Theorem 5.8. We will construct the transition map $\tilde{\Pi}_3 : \tilde{R}_3 \rightarrow \Sigma_{3,out}$ induced by the flow of system (5.39), i.e.,

$$(5.55) \quad \begin{aligned} r' &= rF(r, C, \varepsilon), \\ C' &= \frac{1}{4}rG(r, C, \varepsilon), \\ \varepsilon' &= -\varepsilon F(r, C, \varepsilon), \end{aligned}$$

with the functions $F(r, C, \varepsilon)$ and $G(r, C, \varepsilon)$ given by

$$\begin{aligned} F(r, C, \varepsilon) &= \frac{6C}{1+2C}(1-r)(\varepsilon+1) - \frac{3}{2}(r\varepsilon+1-r), \\ G(r, C, \varepsilon) &= (1 - \frac{10}{7}\varepsilon r^2 - C + O(\varepsilon^2 r^2))(r\varepsilon+1-r)(\varepsilon+1). \end{aligned}$$

Note that here we have omitted the subscript $_3$ of the variables for the sake of readability. Recall that $q_{e,3} = (0, \frac{1}{2}, 0)$ is an equilibrium of system (5.55), which is the intersection point of the line $l_{e,3}$ and the attracting manifold \mathcal{N}_3^0 , see Figure 5.29. From Lemma 5.7 we know that this point is nilpotent. To analyze how the attracting manifold \mathcal{N}_3^0 extends beyond this point, we again use the blow-up method.

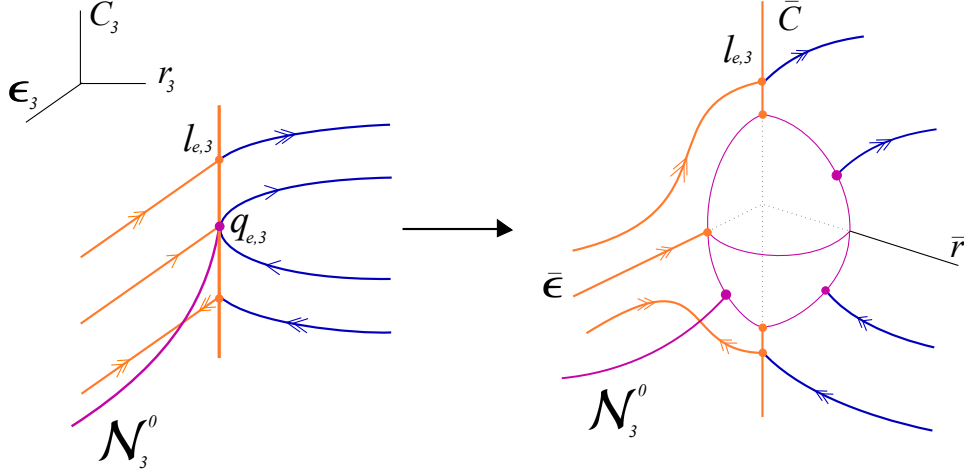


FIGURE 5.29. Blow-up of the point $q_{e,3}$.

We apply to system (5.55) the following blow-up transformation

$$(5.56) \quad \begin{aligned} r &= \rho^2 \bar{r}, \\ C &= \rho \bar{C} + \frac{1}{2}, \\ \varepsilon &= \rho \bar{\varepsilon} \end{aligned}$$

with $\bar{r}^2 + \bar{C}^2 + \bar{\varepsilon}^2 = 1$ and $\rho \in [0, \rho_0]$ for ρ_0 sufficiently small. Thus, the point $q_{e,3} = (0, \frac{1}{2}, 0)$ is shifted to the origin and blown-up to a sphere, see Figure 5.29.

We now briefly discuss the analysis of the blown-up vector field in two charts K_{en} and K_{ex} defined by setting $\bar{\varepsilon} = 1$ and $\bar{r} = 1$, respectively. The blow-up transformation in chart K_{en} is given by

$$(5.57) \quad r = \rho_1^2 r_1, \quad C = \rho_1 C_1 + \frac{1}{2}, \quad \varepsilon = \rho_1,$$

while in chart K_{ex} it has the form

$$(5.58) \quad r = \rho_2^2, \quad C = \rho_2 C_2 + \frac{1}{2}, \quad \varepsilon = \rho_2 \varepsilon_2.$$

First we will analyze in chart K_{en} how trajectories enter a neighborhood of the origin. The exit through the neighborhood is analyzed in chart K_{ex} , which covers the part of the sphere corresponding to $\bar{r} > 0$.

The dynamics in chart K_{en} is governed by

$$(5.59) \quad \begin{aligned} r_1' &= \frac{9}{2} r_1 \tilde{F}(r_1, C_1, \rho_1), \\ C_1' &= \frac{3}{2} C_1 \tilde{F}(r_1, C_1, \rho_1) + \frac{1}{4} r_1 (1 + \rho_1 C_1) G(r_1, C_1, \rho_1), \\ \rho_1' &= -\frac{3}{2} \rho_1 \tilde{F}(r_1, C_1, \rho_1), \end{aligned}$$

where

$$\begin{aligned}\tilde{F}(r_1, C_1, \rho_1) &= 1 + C_1 + 2\rho_1 C_1 + O(r_1 \rho_1^2), \\ G(r_1, C_1, \rho_1) &= \frac{1}{2} + \frac{1}{2}\rho_1 - \rho_1 C_1 - \rho_1^2 C_1 + O(r_1 \rho_1^2).\end{aligned}$$

The derivative in (5.59) is with respect to the rescaled time scale τ_{en} . In the invariant plane $r_1 = 0$ we recover the attracting curve of equilibria \mathcal{N}_3^0 of system (5.39), i.e., in chart K_{en} the curve is defined by the equation $1 + C_1 + 2\rho_1 C_1 = 0$ and denoted by \mathcal{N}_{en} . The curve \mathcal{N}_{en} meets the C_1 -axis at the point $p_{in} = (0, -1, 0)$. In addition, system (5.59) has an equilibrium at the origin.

LEMMA 5.11. *The following assertions hold for system (5.59).*

- (1) *The equilibrium at the origin is a saddle with eigenvalues $\frac{9}{2}, \frac{3}{2}, -\frac{3}{2}$.*
- (2) *The point $p_{in} \in \mathcal{N}_{en}$ has a one-dimensional stable eigenspace and a two-dimensional center eigenspace.*

The second assertion of Lemma 5.11 implies the existence of an attracting two-dimensional center manifold N^c at p_{in} . In a suitable set the center manifold N^c is given as a graph $C_1 = h(r_1, \rho_1)$. Furthermore, there exists a stable foliation with the base N^c and one-dimensional fibers. For any $c > -\frac{3}{2}$ the orbits near the center manifold N^c are attracted to N^c by an exponential rate of order $O(e^{-c\tau_{en}})$.

Hence, we conclude that the dynamics close to p_{in} is controlled by the attracting center manifold N^c , which is the continuation of \mathcal{N}_3^0 . Consequently, an appropriately defined local transition map induced by the flow of (5.59) and restricted to lines $r_1 = \text{const.}$ is a contraction with a rate e^{-c_{en}/r_1} , $c_{en} > 0$.

The governing equations in chart K_{ex} are

$$\begin{aligned}\rho_2' &= \frac{3}{4}\rho_2 \tilde{F}(\rho_2, C_2, \varepsilon_2), \\ (5.60) \quad C_2' &= -\frac{3}{4}C_2 \tilde{F}(\rho_2, C_2, \varepsilon_2) + \frac{1}{4}(1 + \rho_2 C_2)G(\rho_2, C_2, \varepsilon_2), \\ \varepsilon_2' &= -\frac{9}{4}\varepsilon_2 \tilde{F}(\rho_2, C_2, \varepsilon_2),\end{aligned}$$

where

$$\begin{aligned}\tilde{F}(\rho_2, C_2, \varepsilon_2) &= \varepsilon_2 + C_2 + O(\rho_2^2 \varepsilon_2) + O(\rho_2^2 C_2), \\ G(\rho_2, C_2, \varepsilon_2) &= \frac{1}{2} - \frac{1}{2}\rho_2 \varepsilon_2 - \frac{1}{2}\rho_2^2 - \rho_2 C_2 + O(\rho_2^2 C_2, \rho_2 \varepsilon_2 C_2).\end{aligned}$$

The planes $\rho_2 = 0$ and $\varepsilon_2 = 0$ are both invariant under the flow of (5.60). System (5.60) has two equilibria on the C_2 -axis, namely $q_{out} = (0, \frac{\sqrt{6}}{6}, 0)$ and $q = (0, -\frac{\sqrt{6}}{6}, 0)$. The point q has a two-dimensional unstable eigenspace and a one-dimensional stable eigenspace. The point q_{out} is a saddle with resonant eigenvalues

$$\frac{\sqrt{6}}{8}, -\frac{\sqrt{6}}{4}, -\frac{3\sqrt{6}}{8}.$$

Using the analysis in K_{en} and K_{ex} we prove the following result, see Figure 5.30.

LEMMA 5.12. *There exists a connection from $p_{in} \in K_{en}$ to $q_{out} \in K_{ex}$.*

PROOF. To prove the lemma, we look at the dynamics on the sphere. Note that in chart K_{en} this corresponds to the invariant plane $\rho_1 = 0$, while in K_{ex} to the invariant plane $\rho_2 = 0$. In K_{en} for $\rho_1 = 0$ system (5.59) reduces to

$$(5.61) \quad \begin{aligned} r_1' &= \frac{9}{2}r_1(1 + C_1), \\ C_1' &= \frac{3}{2}C_1(1 + C_1) + \frac{1}{8}r_1. \end{aligned}$$

Note that the region $r_1 > 0$, $C_1 > -1$ is positively invariant under the flow of (5.61), hence $r_1, C_1 \rightarrow \infty$.

In chart K_{ex} in the invariant plane $\rho_2 = 0$ the dynamics is governed by

$$(5.62) \quad \begin{aligned} C_2' &= -\frac{3}{4}C_2(C_2 + \varepsilon_2) + \frac{1}{8}, \\ \varepsilon_2' &= -\frac{9}{4}\varepsilon_2(C_2 + \varepsilon_2). \end{aligned}$$

Note that system (5.61) and (5.62) have no equilibria nor limit cycles away from the C_1 - and C_2 -axis, respectively. The statement follows from the Poincaré - Bendixon theorem. \square

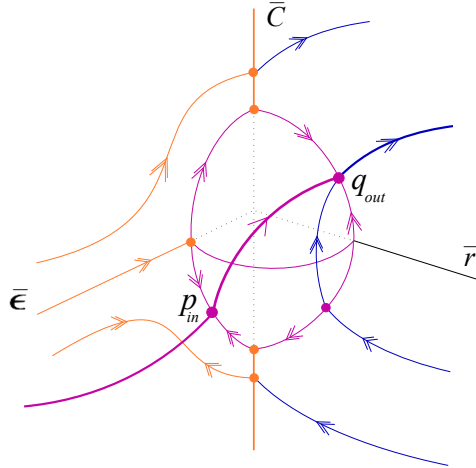


FIGURE 5.30. Blow-up of the point $q_{e,3}$.

PROOF OF THEOREM 5.8. Recall that the incoming section $\Sigma_{3,in}$ is contained in the $\rho_1 = \text{const.}$ plane in chart K_{en} and transversal to the manifold \mathcal{N}_{en} , while the outgoing section $\Sigma_{3,out}$ is contained in the $r_2 = \text{const.}$ plane in chart K_{ex} . All orbits starting from a suitable rectangle $\tilde{R} \subset \Sigma_{3,in}$ pass the non-hyperbolic point p_{in} . Lemma 5.11 implies that the local transition is described by the attracting center manifold N^c and its foliation. Lemma 5.12 implies that the trajectories, which leave chart K_{en} , follow the flow across the sphere and exit near the point q_{out} . In particular, the continuation of manifold \mathcal{N}_{en} intersects the outgoing section $\Sigma_{3,out}$ as a curve. Note that the global transition across the sphere involves no significant expansion (or in other words, the amount of expansion is negligible). Similarly, no expansion is incurred during the transition close to q_{out} , however, there is occurrence of logarithmic terms due to the resonant eigenvalues. This implies all the assertions of Theorem 5.8. \square

Bibliography

- [1] O.D. ANOSOVA, *On Invariant Manifolds in Singularly Perturbed Systems*, Journal of Dynamical and Control Systems, (5) 1999, pp. 501–507.
- [2] V. I. ARNOLD, *Encyclopedia of mathematical sciences: Dynamical Systems V*, Springer-Verlag, Berlin/New York, 1994.
- [3] D. K. ARROWSMITH AND C. M. PLACE, *An introduction to dynamical systems / D.K. Arrowsmith*, Cambridge, New York, Cambridge University Press, 1990.
- [4] S. M. BAER AND T. ERNEUX, *Singular Hopf Bifurcation to Relaxation Oscillations I*, SIAM Journal on Applied Mathematics, (46) 1986, pp. 721–739.
- [5] S. M. BAER AND T. ERNEUX, *Singular Hopf Bifurcation to Relaxation Oscillations II*, SIAM Journal on Applied Mathematics, (52) 1992, pp. 1651–1664.
- [6] E. BENOÎT, *Chasse au canard. II. Tunnels-entonnoirs-peignes. (French) [Duck hunt. II. Tunnels-funnels-combs]*, Collect. Math., (32) 1981, pp. 77–97.
- [7] E. BENOÎT AND J. CALLOT, *Chasse au canard. IV. Annexe numérique. (French) [Duck hunt. IV. Numerical appendix]*, Collect. Math., (32) 1981, pp. 115–119.
- [8] R. BERTRAM, A. SHERMAN, AND L. S. SATIN, *Metabolic and electrical oscillations: partners in controlling pulsatile insulin secretion*, American journal of physiology. Endocrinology and metabolism, 293 (2007), pp. E890–900.
- [9] B. BRAAKSMA, *Singular Hopf bifurcation in systems with fast and slow variables*, J. Nonlinear Sci., (8) 1998, pp. 457–490.
- [10] M. BRONS, M. KRUPA AND M. WECHSELBERGER, *Mixed mode oscillations due to the generalized canard phenomenon*, in “Bifurcation Theory and Spatio-Temporal Pattern Formation,” Amer. Math. Soc., 2006, pp. 39–63.
- [11] M. BRUNELLA AND M. MIARI, *Topological equivalence of a plane vector field with its principal part defined through Newton polyhedra*, J. Differential Equations, (85) 1990, pp. 338–366.
- [12] J. CALLOT, *Chasse au canard. III. Les canards ont la vie brève. (French) [Duck hunt. III. Ducks have a short life]*, Collect. Math., (32) 1981, pp. 99–114.
- [13] J. CARR, *Applications of centre manifold theory*, New York, Springer-Verlag, 1981.
- [14] B. CESSAC AND M. SAMUELIDES, *From neuron to neural networks dynamics*, Eur. Phys. J. Special Topics, (142) 2007, pp. 7–88.
- [15] B. CHANCE, K. PYE, AND J. HIGGINS, *Waveform generation by enzymatic oscillators*, IEEE Spectrum, (4) 1967, pp. 79–86.
- [16] C. CHICONE, *Ordinary Differential Equations with Applications*, New York, NY : Springer Science+Business Media, Inc., 2006.
- [17] H. F. CHOU, N. BERMAN, AND E. IPP, *Oscillations of lactate released from islets of Langerhans: evidence for oscillatory glycolysis in beta-cells*, Am. J. Physiol., (262) 1992, pp. E800–E805.
- [18] S. N. CHOW, C. LI AND D. WANG, *“Normal Forms and Bifurcation of Planar Vector Fields”*, Cambridge University Press, Cambridge, 1994.
- [19] G.B. COOK, P. GRAY, D. G. KNAPP, AND S. K. SCOT, *Bimolecular Routes to Cubic Auto-catalysis*, J. Phys. Chem., (93) 1989, pp. 2749–2155.
- [20] H. CROISIER, *Continuation and bifurcation analyses of a periodically forced slow-fast system*, PhD thesis, Académie Wallonie-Europe Université de Liège Faculté des Sciences, 2009.
- [21] P. DE MAESSCHALCK AND F. DUMORTIER, *Canard solutions at non-generic turning points*, Trans. Amer. Math. Soc., 358 (2006), pp. 2291–2334.
- [22] Z. DENKOWSKA AND R. ROUSSARIE, *A method of desingularization for analytic two-dimensional vector field families*, Bol. Soc. Braz. Math., (22) 1991, pp. 93–126.

- [23] M. DESROCHES, B. KRAUSKOPF AND H. M. OSINGA, *The geometry of mixed-mode oscillations in the Olsen model for the Peroxidase-Oxidase reaction*, Discrete and Continuous Dynamical Systems - Series S, (2) 2009, pp. 807–827.
- [24] M. DESROCHES, J. GUCKENHEIMER, B. KRAUSKOPF, C. KUEHN, H. M. OSINGA, AND M. WECHSELBERGER, *Mixed-mode oscillations with multiple time scales*, to appear in SIAM Review (2011).
- [25] F. DIENER AND M. DIENER, *Chasse au canard. I. Les canards. (French) [Duck hunt. I. The ducks]*, Collect. Math., (32) 1981, pp. 37–74.
- [26] F. DIENER AND M. DIENER, *Nonstandard Analysis in Practice*, Springer-Verlag, Berlin/New York, 1995.
- [27] F. DUMORTIER, *Techniques in the theory of local bifurcations: blow-up, normal forms, nilpotent bifurcations, singular perturbations*, NATO Adv. Sci. Inst. Ser. C Math. Phys. Sci., Kluwer Acad. Publ., Dordrecht, (408) 1993, pp. 19–73.
- [28] F. DUMORTIER AND R. ROUSSARIE, *Canard cycles and center manifolds*, Mem. Amer. Math. Soc., Providence, (577) 1996.
- [29] F. DUMORTIER AND R. ROUSSARIE, *Geometric singular perturbation theory beyond normal hyperbolicity*, Multiple-time-scale dynamical systems, The IMA Volumes in Mathematics and its Applications, (122) 2000, pp. 29–64.
- [30] F. DUMORTIER AND R. ROUSSARIE, *Multiple canard cycles in generalized Li-Åñnard equations*, J. Differential Equations, (174) 2001, pp. 1–29.
- [31] F. DUMORTIER, N. POPOVIC, AND T. J. KAPER, *The critical wave speed for the Fisher-Kolmogorov-Petrovskii-Piscounov equation with cut-off*, Nonlinearity, (20) 2007, pp. 855–877.
- [32] J. ELDERING, *Persistence of noncompact Normally Hyperbolic Invariant Manifolds*, SIAM DS 2011 poster.
- [33] T. ERNEUX AND A. GOLDBETER, *Rescue of the quasi-steady state approximation in a model for oscillations in an enzymatic cascade*, SIAM J. Appl. Math., (67) 2006, pp. 305–320.
- [34] N. FENICHEL, *Geometric singular perturbation theory*, J. Differential Equations, (31) 1979, pp. 53–98.
- [35] E. H. FLACH AND S. SCHNELL, *On the use and abuse of the Quasi-Steady-State Approximation*, IEE Proceedings Systems Biology, (153) 2006, pp. 187–191.
- [36] L. K. FORBES AND C. A. HOLMES, *Limit-cycle behaviour in a model chemical reaction: the cubic autocatalator*, Journal of Engineering Mathematics, (24) 1990, pp. 179–189.
- [37] B. R. FRENKEL, *Control of reduced diphosphopyridine nucleotide oscillations in beef heart extracts. I. Effects of modifiers of phosphofructokinase activity*, Arch. Biochem. Biophys., (125) 1968, pp. 151–156.
- [38] A. FRIEDMAN, *Tutorials in mathematical biosciences 3. cell cycle, proliferation, and cancer*, New York, NY Springer, 2006.
- [39] A. GOLDBETER, *A minimal cascade model for the mitotic oscillator involving cyclin and cdc2 kinase*, Proc. Natl. Acad. Sci. USA, (88) 1991, pp. 9107–9111.
- [40] A. GOLDBETER, *Biochemical Oscillations and Cellular Rhythms: The Molecular Bases of Periodic and Chaotic Behaviour*, Cambridge University Press, Cambridge, 1996.
- [41] A. GOLDBETER AND R. LEFEVER, *Dissipative structures for an allosteric model. Application to glycolytic oscillations*, Biophysical journal, (12) 1972, pp. 1302–15.
- [42] J. GRASMAN, *Asymptotic Methods for Relaxation Oscillations and Applications*, Springer, New York, 1987.
- [43] B. F. GRAY, M. J. ROBERTS AND J. H. MERKIN, *The cubic autocatalator: The influence of the quadratic autocatalytic and the uncatalysed reactions*, Journal of Engineering Mathematics, (22) 1988, pp. 267–284.
- [44] B. F. GRAY AND R. A. THURAISINGHAM, *The cubic autocatalator: the influence of degenerate singularities in a closed system*, Journal of Engineering Mathematics, (23) 1989, pp. 283–293.
- [45] P. GRAY AND S. K. SCOTT, *A New Model for Oscillatory Behaviour in Closed Systems: The Autocatalator*, Berichte der Bunsengesellschaft fuer physikalische Chemie, (90) 1986, pp. 985–996.
- [46] J. GUCKENHEIMER AND P. HOLMES, *Nonlinear Oscillations, Dynamical Systems, and Bifurcations of Vector Fields*, Springer, New York, 1983.
- [47] J. GUCKENHEIMER, *Singular Hopf Bifurcation in Systems with Two Slow Variables*, SIAM J. Appl. Dyn. Syst., (7) 2008, pp. 1355–1377.

- [48] J. GUCKENHEIMER AND CH. SCHEPER, *A Geometric Model for Mixed-Mode Oscillations in a Chemical System*, SIAM J. Appl. Dyn. Syst., (10) 2011, pp. 92–128.
- [49] J. GUCKENHEIMER, M. WECHSELBERGER AND L-S. YOUNG, *Chaotic attractors of relaxation oscillators*, Nonlinearity, (19) 2006, pp. 701–720.
- [50] I. GUCWA AND P. SZMOLYAN, *Geometric singular perturbation analysis of an Autocatalator model*, Discrete and Continuous Dynamical Systems - Series S, 2 (2009), pp. 783–806.
- [51] G. HEK, *Geometric singular perturbation theory in biological practice*, J. Math. Biol., (60) 2010, pp. 347–386.
- [52] B. HESS, *The glycolytic oscillator*, The Journal of experimental biology, 81 (1979), pp. 7–14.
- [53] J. HIGGINS, *A chemical mechanism for oscillation of glycolytic intermediates in yeast cells*, Proc. Natl. Acad. Sci. USA, 51 (1964), pp. 989–994.
- [54] M. W. HIRSCH AND S. SMALE, *Differential equations, dynamical systems, and linear algebra*, San Diego, Academic Press, 1974.
- [55] M. W. HIRSCH, C. C. PUGH, AND M. SHUB, *Invariant Manifolds*, Bull. Amer. Math. Soc., (76) 1970, pp. 1015–1019.
- [56] A. HUBER AND P. SZMOLYAN, *Geometric singular perturbation analysis of the Yamada model*, SIAM J. Appl. Dyn. Syst., 4 (2005), pp. 607–648.
- [57] T. HUNT, *Protein synthesis, proteolysis, and cell cycle transitions*, Nobel lecture, http://www.nobelprize.org/nobel_prizes/medicine/laureates/2001/hunt-lecture.pdf, 2001.
- [58] S.B. HSU AND J. SHI, *Relaxation oscillation profile of limit cycle in predator-prey system*, Discrete and Continuous Dynamical Systems Series B, (11) 2009, pp. 893–911.
- [59] K. K. IBSEN AND K. W. SCHILLER, *Oscillations of nucleotides and glycolytic intermediates in aerobic suspensions of Ehrlich ascites tumor cells*, Biochem. Biophys. Acta, (131) 1967, pp. 405–407.
- [60] E. M. IZHIKEVICH, *Dynamical Systems in Neuroscience: The Geometry of Excitability and Bursting*, The MIT Press, 2007.
- [61] C.K.R.T. JONES, *Geometric singular perturbation theory*, Springer Lecture Notes in Mathematics, Berlin, 1609 (1995), pp. 44–120.
- [62] T. J. KAPER, *An introduction to geometric methods and dynamical systems theory for singular perturbation problems, analyzing multiscale phenomena using singular perturbation methods*, Proc. Sympos. Appl. Math., (56) 1999, pp. 85–131.
- [63] A. KATOK, ANATOLE AND B. HASSELBLATT, *Introduction to the modern theory of dynamical systems*, Cambridge [u. a.], Cambridge University Press, 1996.
- [64] S. A. KAUFFMAN, *At home in the universe : the search for laws of self-organization and complexity*, New York, Oxford University Press, 1995.
- [65] J. P. KEENER, J. SNEYD, *Mathematical Physiology*, New York, Springer, 1998.
- [66] J. KEVORKIAN AND J. D. COLE, *Multiple scale and singular perturbation methods*, Applied Mathematical Sciences, 114. Springer-Verlag, New York, 1996.
- [67] I. KOSIUK AND P. SZMOLYAN, *Geometric Desingularization in Slow-Fast Systems with Application to the Glycolytic Oscillations Model*, AIP Conf. Proc., (1281) 2010, pp. 235–238.
- [68] I. KOSIUK AND P. SZMOLYAN, *Scaling in Singular Perturbation Problems: Blowing Up a Relaxation Oscillator*, SIAM J. Appl. Dyn. Syst., 10 (2011), pp. 1307–1343.
- [69] M. KRUPA, N. POPOVIC, AND N. KOPELL, *Mixed-mode oscillations in three time-scale systems: a prototypical example*, SIAM J. Appl. Dyn. Syst., 7 (2008), pp. 361–420.
- [70] M. KRUPA, N. POPOVIĆ, N. KOPELL AND H. G. ROTSTEIN, *Mixed-mode oscillations in a three time-scale model for the dopaminergic neuron*, Chaos, (18) 2008, pp. 015106–015106-19.
- [71] M. KRUPA AND P. SZMOLYAN, *Extending geometric singular perturbation theory to non-hyperbolic points-fold and canard points in two dimensions*, SIAM J. Math. Analysis, 33 (2001), pp. 286–314.
- [72] M. KRUPA AND P. SZMOLYAN, *Extending slow manifolds near transcritical and pitchfork singularities*, Nonlinearity, 14 (2001), pp. 1473–1491.
- [73] M. KRUPA AND P. SZMOLYAN, *Relaxation oscillation and canard explosion*, J. Differential Equations, 174 (2001), pp. 312–368.
- [74] P. A. LAGERSTROM, *Matched asymptotic expansions: Ideas and techniques*, Springer-Verlag, Berlin/New York, 1988.
- [75] S. LEFSCHETZ, *Differential equations : geometric theory*, New York, Dover Publications, 1977.
- [76] J. D. MEISS, *Differential dynamical systems*, Philadelphia, PA : Society for Industrial and Applied Mathematics, 2007.

- [77] J. H. MERKIN, D. J. NEEDHAM AND S. K. SCOTT, *On the structural stability of a simple pooled chemical system*, Journal of Engineering Mathematics, (21) 1987, pp. 115–127.
- [78] A. MILIK, “*Mixed-Mode Oscillations in Chemical Systems*”, Ph.D thesis, Vienna University of Technology, 1996.
- [79] A. MILIK AND P. SZMOLYAN, *Multiple time scales and canards in a chemical oscillator*, in “Multiple-time-scale Dynamical Systems (Minneapolis, MN, 1997)”, IMA Vol. Math. Appl., Springer, New York, (122) 2001, pp. 117–140.
- [80] A. MILIK, P. SZMOLYAN, H. LÖFFELMANN AND E. GRÖLLER, *Geometry of Mixed-Mode Oscillations in the 3-D Autocatalator*, Internat. J. Bifurcations and Chaos, (8) 1998, pp. 505–519.
- [81] E.F. MISHCHENKO AND N.KH. ROZOV, *Differential Equations with Small Parameters and Relaxation Oscillations*, Plenum Press, New York, 1980.
- [82] E.F. MISHCHENKO, YU. S. KOLESOV, A. YU. KOLESOV, AND N.KH. ROZOV *Asymptotic methods in singularly perturbed systems*, New York : Consultants Bureau, 1994.
- [83] D. O. MORGAN, *The cell cycle : principles of control*, London : New Science Press, Corby : Oxford University Press ; Sunderland, Mass. : Sinauer Associates, 2007.
- [84] J. D. MURRAY, *Mathematical biology 1. An introduction*, New York, Springer, 2001.
- [85] B. NOVAK AND J.J. TYSON, *Quantitative Analysis of a Molecular Model of Mitotic Control in Fission Yeast*, J. Theor. Biol., (173) 1995, pp. 283–305.
- [86] B. NOVAK AND J.J. TYSON, *Modeling the control of DNA replication in fission yeast*, Proc. Natl. Acad. Sci. USA, (94) 1997, pp. 9147–9152.
- [87] B. NOVAK, A. CSIKASZ-NAGY, B. GYORFFY, K. CHEN, AND J. J. TYSON, *Mathematical model of the fission yeast cell cycle with checkpoint controls at the G1/S, G2/M and metaphase/anaphase transitions*, Biophysical Chemistry, (72) 1998, pp. 185–200.
- [88] P. NURSE, *A Long Twentieth Century of the Cell Cycle and Beyond*, Cell, 100 (2000), pp. 71–78.
- [89] P. NURSE, *Cyclin dependent kinases and cell cycle control*, Nobel lecture, http://www.nobelprize.org/nobel_prizes/medicine/laureates/2001/nurse-lecture.pdf, 2001.
- [90] R. E. O’MALLEY, *Introduction to singular perturbations*, Academic Press, New York, 1974.
- [91] B. O’ROURKE, B.M. RAMZA, AND E. MARBAN, *Oscillations of membrane current and excitability driven by metabolic oscillations in heart cells*, Science, (265) 1994, pp. 962–966.
- [92] L. PERKO, *Differential equations and dynamical systems*, New York, NY Springer, 2001.
- [93] V. PETROV, S. K. SCOTT AND K. SHOWALTER, *Mixed-mode oscillations in chemical systems*, Journal of Chemical Physics, (97) 1992, pp. 6191–6198.
- [94] N. POPOVIC, *A geometric analysis of logarithmic switchback phenomena*, J. Phys.: Conf. Ser., (22) 1995, pp. 164–173.
- [95] N. POPOVIC AND P. SZMOLYAN, *A geometric analysis of the Lagerstrom model problem*, J. Differential Equations, 199 (2004), pp. 290–325.
- [96] S. RINALDI, *Laura and Petrarch: An Intriguing Case of Cyclical Love Dynamics*, SIAM J. Appl. Math., (58) 1998, pp. 1205–1221.
- [97] S. RINALDI AND M. SCHEFFER, *Geometric Analysis of Ecological Models with Slow and Fast Processes*, Ecosystems, (3) 2000, pp. 507–521.
- [98] S. K. SCOTT, “*Chemical Chaos. International Series of Monographs on Chemistry*” Oxford University Press, New York, (24) 1991.
- [99] S. K. SCOTT, *Oscillations, waves, and chaos in chemical kinetics*, Oxford University Press, 1994.
- [100] S. SCHECTER AND P. SZMOLYAN, *Persistence of rarefactions under Dafermos regularization: blow-up and an exchange lemma for gain-of-stability turning points*, SIAM J. Applied Dynamical Systems, Vol. 8, Issue 3 (2009), pp. 822–853.
- [101] L. SEGEL AND A. GOLDBETER, *Scaling in biochemical kinetics: dissection of a relaxation oscillator*, J. Math. Biol., 32 (1994), pp. 147–160.
- [102] E. SEL’KOV, *Self-oscillations in glycolysis. 1. A simple kinetic model*, Eur. J. Biochem., 4 (1968), pp. 79–86.
- [103] L.P. SHIL’NIKOV, A. L. SHIL’NIKOV, D. V. TURAEV, AND L. O. CHUA, *Methods of qualitative theory in nonlinear dynamics. Part I*, Singapore, River Edge, NJ : World Scientific, 1998.
- [104] L.P. SHIL’NIKOV, A. L. SHIL’NIKOV, D. V. TURAEV, AND L. O. CHUA, *Methods of qualitative theory in nonlinear dynamics. Part II*, Singapore, World Scientific, 2001.
- [105] A. SLAVOVA, *Nonlinear singularly perturbed systems of differential equations: A survey*, Mathematical Problems in Engineering, (1) 1995, pp. 275–301.

- [106] P. SMOLEN, *A model for glycolytic oscillations based on skeletal muscle phosphofructokinase kinetics*, Journal of theoretical biology, 174 (1995), pp. 137–48.
- [107] S. STERNBERG, *Local Contractions and a Theorem of Poincaré*, Amer. J. Math., (79) 1957, pp. 809–824.
- [108] S. STERNBERG, *On the structure of local homeomorphisms of euclidean n -space II*, Amer. J. Math., (80) 1958, pp. 623–631.
- [109] A. SVEICZER, J. J. TYSON, AND B. NOVAK, *Modelling the fission yeast cell cycle*, Brief. Funct. Genomic Proteomic., (2) 2004, pp. 298–307.
- [110] P. SZMOLYAN AND M. WECHSELBERGER, *Canards in \mathbb{R}^3* , J. Differential Equations, (177) 2001, pp. 419–453.
- [111] P. SZMOLYAN AND M. WECHSELBERGER, *Relaxation oscillations in \mathbb{R}^3* , J. Differential Equations, (200) 2004, pp. 69–104.
- [112] F. TAKENS, *Partially hyperbolic fixed points*, Topology, (10) 1971, pp. 133–147.
- [113] J.J. TYSON, *Modeling the cell division cycle: cdc2 and cyclin interactions*, Proc. Natl. Acad. Sci. USA, (88) 1991, pp. 7328–7332.
- [114] J. J. TYSON, K. CHEN, B. NOVAK, *Network dynamics and cell physiology*, Nat. Rev. Mol. Cell Biol., (2) 2001, pp. 908–16.
- [115] M. WECHSELBERGER, *Existence and bifurcation of canards in \mathbb{R}^3 in the case of a folded node*, SIAM J. Appl. Dyn. Syst., (4) 2005, pp. 101–139.
- [116] S. WIGGINS, *Normally hyperbolic invariant manifolds in dynamical systems*, New York, Springer-Verlag, 1994.
- [117] S. WIGGINS, *Introduction to applied nonlinear dynamical systems and chaos*, New York, Springer, 2003.
- [118] B. VAN DER POL, *On relaxation oscillations*, Philosophical Magazine, (7) 1926, pp. 978–992.
- [119] B. VAN DER POL, *The nonlinear theory of electric oscillations*, Proc. IRE, (22) 1934, pp. 1051–1086.
- [120] B. VAN DER POL AND J. VAN DER MARK, *The heartbeat considered as a relaxation oscillation, and an electrical model of the heart*, The London, Edinburgh, and Dublin Philosophical Magazine and Journal of Science, (6) 1928, pp. 763–775.
- [121] S. VAN GILS, M. KRUPA, AND P. SZMOLYAN, *Asymptotic expansions using blow-up*, Z. Angew. Math. Phys., 56 (2005), pp. 369–397.
- [122] W. G. XU AND Q. S. LI, *The dimensionlessness of chemical kinetic equation*, Journal of Mathematical Chemistry, (31) 2002, pp. 237–250.

Veröffentlichungen und Vorträge

(Publications and Talks)

Begutachtete Artikel (Publications)

- I.Kosiuk, P. Szmolyan, *Scaling in Singular Perturbation Problems: Blowing Up a Relaxation Oscillator*, SIAM J. Appl. Dyn. Syst., 10 (2011), pp. 1307–1343.
- I.Kosiuk, P. Szmolyan, *Geometric Desingularization in Slow-Fast Systems with Application to the Glycolytic Oscillations Model*, AIP Conf. Proc., 1281 (2010), pp. 235–238.
- I. Gucwa, P. Szmolyan *Geometric singular perturbation analysis of an autocalototor model*, Discrete and Continuous Dynamical Systems Series S, 2 (2009), pp. 783–806.
- N.N. Bogoliubov (Jr.), A.K. Prykarpatski, I. Gucwa and J. Golenia, *Analytical properties of an Ostrovsky-Whitham type dynamical system for a relaxing medium with spatial memory and its integrable regularization*, Preprint IC/2007/109, The Abdus Salam International Center for Theoretical Physics, Trieste, Italy.

Vorträge (Talks)

- November 2011* 13th International EMBL PhD Symposium
Heidelberg, Germany
contributed talk: *Early mitotic events on a cylinder:
blow-up of the cell cycle engine*
- August 2011* EQUADIFF 2011, Loughborough, UK
invited talk: *Delayed exchange of stability and
relaxation oscillations of a new type in an enzyme reaction*
(Singular perturbation theory session)
- May 2011* SIAM Conference on Applications of Dynamical Systems
Snowbird, Utah, USA
contributed talk: *A New Type of Relaxation Oscillations
in a Model for an Enzyme Reaction*

- December 2010* The ANR Analyse Non Linaire Application aux Rythmes du Vivant meeting, La Rochelle, France
invited talk: *A new type of relaxation oscillations in a model for enzyme reactions*
- September 2010* 8th International Conference of Numerical Analysis and Applied Mathematics, Rhodes, Greece
invited talk: *Geometric desingularization in slow-fast systems with application to the glycolytic oscillator*
(Third Symposium on Recent Trends in the Numerical Solution of Differential Equations)
- May 2010* 8th AIMS International Conference on Dynamical Systems, Differential Equations and Applications, Dresden, Germany
invited talk: *A new type of relaxation oscillations in a model for the mitotic oscillator*
(Special Session on Singular Perturbations)
- May 2010* 2nd International Workshop-School
CHAOS and DYNAMICS in BIOLOGICAL NETWORKS
Institut d'Etudes Scientifiques de Cargese - Corsica (France)
contributed talk: *Geometric analysis of a singularly perturbed glycolytic oscillator*
- January 2010* University of Sydney, Australia
invited seminar talk: *Blow-up analysis of an autocatalator model*
- September 2009* Dynamics of Systems Biology Conference, Aberdeen, Scotland
contributed talk: *Blow-up analysis of glycolytic relaxation oscillations*
- September 2009* Dynamics Days Europe Conference, Göttingen, Germany
contributed talk: *Blow-up analysis of glycolytic relaxation oscillations*
- July 2009* WK Summer Camp, Weissensee, Austria
contributed talk: *Geometric desingularization in slow-fast systems: non-uniform collapse of a folded critical manifold*

Short CV

Name	Ilona Kosiuk
Date of Birth	11.08.1983
10/2008 –	PhD student at MPI MiS Scientific advisor Prof. Dr. Jürgen Jost Member of the International Max Planck Research School Mathematics in the Sciences (IMPRS MIS) PhD student at the University of Leipzig, Germany
10/2007 – 09/2008	PhD student at Vienna University of Technology, Austria Scientific advisor Ao. Univ. Prof. Dr. Peter Szmolyan Member of the Wissenschaftskolleg (WK) <i>Differential Equation Models in Science and Engineering</i>
2002 – 2007	Master of Science degree in Mathematics at AGH University of Science and Technology Cracow, Poland

Angaben zur Person

Name	Ilona Kosiuk
Geburtsdatum	11.08.1983
2002 – 2007	Mathematikstudium AGH Universität Krakau, Polen
10/2007 – 09/2008	Doktorandin an der TU Wien Wien, Österreich Betreuer Ao. Univ. Prof. Dr. Peter Szmolyan Mitglied des Wissenschaftskollegs <i>Differential Equation Models in Science and Engineering</i>
seit 10/2008	Doktorandin am Max-Planck-Institut für Mathematik in den Naturwissenschaften in Leipzig Betreuer Prof. Dr. Jürgen Jost IMPRS-Mitglied

Bibliographische Daten

Relaxation oscillations in slow-fast systems beyond the standard form

Ilona Kosiuk

Universität Leipzig, Dissertation, 2012

125 Seiten, 64 Abbildungen, 122 Referenzen, S-Nummer 2

Selbstständigkeitserklärung

Hiermit erkläre ich, die vorliegende Dissertation selbständig und ohne unzulässige fremde Hilfe angefertigt zu haben. Ich habe keine anderen als die angeführten Quellen und Hilfsmittel benutzt und sämtliche Textstellen, die wörtlich oder sinngemäß aus veröffentlichten oder unveröffentlichten Schriften entnommen wurden, und alle Angaben, die auf mündlichen Auskünften beruhen, als solche kenntlich gemacht. Ebenfalls sind alle von anderen Personen bereitgestellten Materialien oder erbrachten Dienstleistungen als solche gekennzeichnet.

Leipzig, den 27. November 2012

.....
(Ilona Kosiuk)